University of Mohamed Boudiaf - M'sila

FACULTY OF TECHNOLOGY

DEPARTMENT OF MECHANICAL ENGINEERING

Serial number : ……

Registration number : **D.CM/3C/04/21**

Thesis

Presented for the graduation of:

DOCTORAT LMD

Sector: Mechanical Engineering

Option: Mechanical Construction

THEME

Study of the machinability and mechanical behavior of a bio composite material reinforced with lignocellulosic fibers

Presented by

Riyadh Benyettou

Supported on: 09 / 05 / 2024

Examining Committee Members:

First & Family Name	Grade	Establishment	Quality
Moussa Zaoui	Professor	Univ. Of M'sila	President
Salah Amroune	Professor	Univ. Of M'sila	Supervisor
Mohamed Slamani	Professor	Univ. Of M'sila	Co-Supervisor
Noureddine Menasri	Professor	Univ. Of M'sila	Examiner
Rabah Boubaaya	MCA	Univ of Bordj Bou Arreridj	Examiner
Mokhtar Djendel	MCA	Univ of Bordj Bou Arreridj	Examiner

Academic year : 2023/2024

Publications & Conferences

Publications:

- Amroune, Salah, Ahmed Belaadi, Moussa Zaoui, Noureddine Menaseri, Barhm Mohamad, Khalissa Saada, and **Riyadh Benyettou**. (2021). Manufacturing of rapid prototypes of mechanical parts using reverse engineering and 3D Printing. ***Journal of the Serbian Society for Computational Mechanics***/Vol 15 (2):1-10.
- **Riyadh Benyettou**, Salah Amroune, Slamani Mohamed, Yasemin Seki & Alain Dufresne (2022) Experimental Investigation of the Absorption Behavior of Date Palm Fiber Reinforced Iso-Polyester Composites: Artificial Neuron Network (ANN) Modeling, ***Journal of Natural Fibers***, 19:17, 15902-15918, DOI: 10.1080/15440478.2022.2136323
- **Riyadh Benyettou**, Salah Amroune, Mohamed Slamani, Yasemin Seki, Alain Dufresne, Mohammad Jawaid, Salman Alamery, Assessment of induced delamination drilling of natural fiber reinforced composites: a statistical analysis, ***Journal of Materials Research and Technology***,Volume 21,2022,Pages 131-152,ISSN 2238 7854,https://doi.org/10.1016/j.jmrt.2022.08.161.
- **BENYETTOU, R.**, et al., INVESTIGATION OF MACHINABILITY OF BIOCOMPOSITES: MODELING AND ANN OPTIMIZATION. ***ACADEMIC JOURNAL OF MANUFACTURING ENGINEERING***, 2023. 21(1).
- **Benyettou, R.**, S. Amroune, M. Slamani, K. Saada, H. Fouad, M. Jawaid, and S. Sikdar, Modelling and optimization of the absorption rate of date palm fiber reinforced composite using response surface methodology. ***Alexandria Engineering Journal***, 2023. 79: p. 545-555.DOI: https://doi.org/10.1016/j.aej.2023.08.042.
- Saada, Khalissa, Moussa Zaoui, Salah Amroune, **Riyadh Benyettou**, Amina Hechaichi, Mohammad Jawaid, Mohamed Hashem, and Imran Uddin. (2024). Exploring tensile properties of bio composites reinforced date palm fibers using experimental and Modelling Approaches. ***Materials Chemistry and Physics*** 314:128810. doi: https://doi.org/10.1016/j.matchemphys.2023.128810.

Conferences

- Participation in **"1st National Conference on the Foundations and Methods of Scientific Research on December 13/14, 2021at M'sila/Algeria"** Under the title: "*Review: Numerical and experimental study of the machining of bio composites*"
- Participation in **"1st International Conference on Innovative Academic Studies on 10-13 September in 2022 at Konya/Turkey**". Under the title:" *Surface method (RSM) and artificial neural networks (ANN) for modeling tensile mechanical of natural fibers*".
- Participation in "**1st International Conference on Innovative Academic Studies on 10-13 September in 2022 at Konya/Turkey**". Under the title:" *Numerical study of mechanical properties and crack propagation in a 2024 T3 Aluminum plate*".
- Participation in "**2nd International Conference on Engineering and Applied Natural Sciences on 15-18 October in 2022 at Konya/Turkey**". Under the title:" *The effect of the meshing technique on cracking and its extension in a bio composite plate*".
- Participation in "**2nd International Conference on Engineering and Applied Natural Sciences on 15-18 October in 2022 at Konya/Turkey**". Under the title:" *The effect of fiber orientation on the thermo mechanical properties of bio composites*"**.**
- Participation in "**2nd International Conference on Engineering and Applied Natural Sciences on 15-18 October in 2022 at Konya/Turkey**". Under the title:" *Analysis of the effect of cutting conditions for circularity and cylindricity errors for drilling bio composites*".
- Participation in "**2nd International Seminar on Industrial Engineering and Applied Mathematics (Isieam'22) In Skikda (Algeria), October 23 & 24th, 2022"**. Under the title:" *Investigation of machinability of biocomposites reinforced by natural fibers: artificial neuron network (ANN)".*
- Participation in "**2nd International Seminar on Industrial Engineering and Applied Mathematics (Isieam'22) In Skikda (Algeria), October 23 & 24th, 2022"**. Under the title:" *Study and numerical simulation of the stress intensity factor of cracked plates".*
- Participation in "**1st National Seminar on Artificial Intelligence in Community Service in M'Sila (Algeria), April 16 & 19th, 2023**". Under the title : " *EXPLORATION DE L'UTILISATION DE RÉSEAUX DE NEURONES ARTIFICIELS (ANN) DANS LA RÉSOLUTION DE PROBLÈME MÉCANIQUE* ".

Acknowledgments

الحمد لله

Embarking on and completing this doctoral thesis has been a transformative experience marked by personal and academic development. I extend my gratitude to those instrumental in making this endeavor possible, with special thanks to **Pr. Salah Amroune** and **Pr. Mohamed Slamani**, the advisors, for their steadfast support and guidance. Working under their supervision has been a fortunate and enriching experience, and their unwavering dedication throughout this journey has been invaluable.

I extend my heartfelt appreciation to **Pr. Zaoui Moussa**, a professor at the University of M'sila, for graciously accepting the role of presiding over the thesis committee. I also extend my thanks to **Pr. Noureddine Menasri**, a Professor at the University of M'sila, for his evaluation of this work. My gratitude further extends to **Dr. Rabah Boubaaya**, a doctor at the University of Mohamed Bachir el Ibrahimi in Bordj Bou Arreridj, for his willingness to evaluate this work. Additionally, I would like to express my thanks to **Dr. Mokhtar Djendel**, a doctor at the University of Mohamed Bachir el Ibrahimi in Bordj Bou Arreridj, for his thoughtful assessment of the research.

I'd like to express my gratitude to **Pr. Mansour Rokbi**, the head of the mechanical engineering department at the University of M'sila for his invaluable support during my doctoral pursuit. I'd also like to express my gratitude to **Pr. Mohammad Jawaid** a Professor at University Putra Malaysia and **Mr. Belkacem Aoufi**, Assistant Engineer at the University of M'sila, as well as to **Mr. Laifa Fakerdien**, **Mr. Tarek Bidi**, and **Mr. Hassan Mokrani** company manager Alger precision, **Mr. Nabil Boutaleb**,and **Mr. Leulmi Rabah** company manager LORN Chemicals Algiers.

I deeply appreciate the academic environment and collaborative opportunities fostered by my colleagues and fellow researchers at the University of M'sila. Their support has been instrumental in the advancement of this research. I am particularly thankful to **my family** for their steadfast encouragement; their unwavering support has been my anchor through the trials of this academic pursuit. Additionally, I extend my gratitude to all my friends, both near and far, with special recognition to **Khalil Zouaoui** and **Aymen Asseli**, Ph.D. students, and **Ayoub Touil**, **Khalil Khalfa**, childhood friends, for their unwavering support and motivation.

Contents

List of Figures

List of Tables

Nomenclature

MMCs	Metal Matrix Composites
CMCs	Ceramic Matrix Composites
PMCs	Polymer Matrix Composites
GFRP	Glass Fiber-Reinforced Composites
CFRP	Carbon Fiber-Reinforced Composites
AFRP	Aramid Fiber-Reinforced Composites
PP	Polypropylene
ANN	Artificial Neural Networks
RSM	Response Surface Methodology
DPFPs	Date palm fiber/Iso-polyester composites
DPFP40	Date palm fiber/Iso-polyester composites with a 40% fiber rate
PFPEs	Palm fiber powder/epoxy composites
UD	Unidirectional stacking
C	Cross-stacking
DPF	Date palm fibers
Mt	The relative water absorption
D	The diffusion coefficient
HSS-TITAN	High-speed steel drill bit with a TiN protective layer
HSS-CARBIDE	High-speed steel drill bit with a carbide drill bit
HSS-SUPER	Super high-speed steel drill bit
CMM	Coordinate Measuring Machine
PCA	Principal component analysis
FEM	Fnite element method
PSO	Particle swarm optimization
F_d	The delamination factor
DOE	Design of Experiments
ANOVA	Analysis of Variance
S/N	The signal-to-noise ratio
HFRP	Hybrid fiber-reinforced polymer
CFRP	Carbon fiber-reinforced polymer
MMCs	Metal-based composites
G FRP	Glass fiber-reinforced polymer
NFRCs	Natural Fiber Reinforced Composites
MSE	Mean Squared Error
R	Correlation coefficient

Abstract

The thesis conducted a comprehensive examination of the physical properties of newly manufactured Date Palm Fiber/ Iso polyester composites (DPFPs) in three different configurations: unidirectional (UD) and cross-linked (C), with layer numbers ranging from 2 to 4. Moreover, it explored the mechanical behavior and the machinability of two recently developed biocomposites: DPFP40 (Date Palm Fiber/ Iso polyester), characterized by a 40% by-weight fiber reinforcement, and PFPEs (palm fiber powder/epoxy) featuring an 18% by-weight fiber reinforcement. The examination of drilling behavior of these bio composites yields crucial insights into specific mechanical properties. This analysis considers factors such as assessing the final surface quality of drilled holes to understand the biocomposite's reaction to cutting forces, as well as investigating the impact of various drilling parameters including spindle speed, feed rate, materials and point angles of drill bits. These investigations aid in optimizing machining conditions to enhance overall mechanical performance of developed biocomposites. The study focused on DPFPs' water absorption behavior across different water types and examined DPFP40 and PFPEs drilling behaviors under various cutting conditions. Three optimization and modeling methods, including Artificial Neural Networks (ANN), Response Surface Methodology (RSM), and the Taguchi approach, were developed for predictive capabilities. A water absorption study revealed a linear correlation between absorption rates and fiber content. DPFP40 drilling analysis indicated optimal parameters for delamination, circularity, and cylindricity errors of drilled holes. ANN and RSM models demonstrated excellent alignment with experimental data. PFPEs drilling characteristics were assessed, highlighting the impact of feed rate, spindle speed, and drill point angle on circularity and cylindricity errors of drilled holes. ANN and Taguchi models accurately predicted experimental results, providing valuable insights for improving the machinability of Natural Fiber Reinforced Composites (NFRCs) in lightweight structural applications across various industries.

Résumé

Cette thèse a réalisé une analyse approfondie des propriétés physiques des bio composites nouvellement élaborés (Fibres de Palmier Dattier / Iso polyester) (DPFP) selon trois configurations distinctes : unidirectionnelle (UD) et réticulée (C), avec un nombre de couches variant de 2 à 4. Par ailleurs, elle a examiné le comportement mécanique et l'usinabilité de deux biocomposites récemment mis au point : le DPFP40 (Date Palm Fiber/ Iso polyester), caractérisé par un renforcement de fibres de 40 % en poids, et les PFPEs (Poudre de Fibres de Palme/Epoxy) présentant un renforcement de fibres de 18 % en poids. L'examen du comportement au perçage de ces biocomposites offre des informations cruciales sur des propriétés mécaniques spécifiques.

Cette analyse prend en compte des facteurs tels que l'évaluation de la qualité de surface finale des trous percés pour comprendre la réaction du biocomposite aux forces de coupe, ainsi que l'étude de l'impact de divers paramètres de perçage, notamment la vitesse de broche, la vitesse d'avance, les matériaux et les angles de pointe des forets. Ces investigations permettent d'optimiser les conditions d'usinage pour améliorer les performances mécaniques globales des biocomposites développés. L'étude s'est concentrée sur le comportement d'absorption d'eau de DPFPs selon différents types d'eau et a examiné les comportements de perçage de DPFP40 et PFPEs dans diverses conditions de coupe. Trois méthodes d'optimisation et de modélisation, dont les Réseaux de Neurones Artificiels (ANN), la Méthodologie de Surface de Réponse (RSM) et l'approche Taguchi, ont été développées pour des capacités prédictives. Une étude sur l'absorption d'eau a révélé une corrélation linéaire entre les taux d'absorption et le taux de fibres. L'analyse du perçage de DPFP40 a indiqué des paramètres optimaux pour le facteur délamination et les erreurs de circularité et de cylindricité des trous percées. Les modèles ANN et RSM ont montré une excellente concordance avec les données expérimentales. Les caractéristiques de perçage de PFPEs ont été évaluées, mettant en évidence l'impact de la vitesse d'avance, la vitesse de broche et de la pointe d'angle de foret sur les erreurs de circularité et de cylindricité des trous percées. Les modèles ANN et Taguchi ont prédit avec précision les résultats expérimentaux, offrant des perspectives précieuses pour améliorer l'usinabilité des composites renforcés de fibres naturelles (NFRCs) dans des applications structurelles légères à travers diverses industries.

ملخص

أجرت هذه الأطروحة فحصًا شاملاً للخصائص الفيزيائية لمركبات ألياف نخيل التمر/ ايزو بوليستير (DPFPs) المصنعة حديثًا في ثلاثة تكوينات مختلفة: أحادية الاتجاه (UD) ومترابطة (C)، مع أرقام طبقات تتراوح من 2 إلى 4. علاوة على ذلك، استكشفت هذه الأطروحة السلوك الميكانيكي و إمكانية تصنيع نوعين من المركبات الحيوية التي تم تطويرها مؤخرًا: DPFP40 (ألياف نخيل التمر/ ايزو بوليستير)، التي تتميز بتقوية الألياف بنسبة 40% بالوزن، وPFPEs (مسحوق ألياف النخيل/الإيبوكسي) التي تتميز بتعزيز الألياف بنسبة 18% بالوزن. يوفر فحص سلوك الثقب لهذه المركبات الحيوية معلومات مهمة عن الخواص الميكانيكية المحددة. يأخذ هذا التحليل في الاعتبار عوامل مثل تقييم جودة السطح النهائية للثقوب لفهم استجابة المركب الحيوي لقوى القطع، بالإضافة إلى دراسة تأثير معلمات الثقب المختلفة، بما في ذلك سرعة المغزل، ومعدل التغذية ومواد وزوايا نقطة الثقب. تتيح هذه التحقيقات تحسين ظروف التشغيل لتحسين الأداء الميكانيكي العام للمركبات الحيوية المطورة. ركزت الدراسة على سلوك امتصاص الماء لـ DPFPs عبر أنواع المياه المختلفة وفحصت سلوكيات ثقب DPFP40 وPFPE في ظل ظروف القطع المختلفة. تم تطوير ثلاث طرق للتحسين والنمذجة، بما في ذلك الشبكات العصبية الاصطناعية (ANN)، ومنهجية سطح الاستجابة (RSM)، ونهج تاجوتشي، من أجل القدرات التنبؤية. كشفت دراسة امتصاص الماء عن وجود علاقة خطية بين معدلات الامتصاص ومحتوى الألياف. أشار تحليل ثقب DPFP40 إلى المعلمات المثالية لعامل التصفيح والأخطاء الدائرية والأسطوانية للثقوب المحفورة. أظهرت نماذج ANN وRSM توافقًا ممتازًا مع البيانات التجريبية. تم تقييم خصائص ثقب PFPEs، مع تسليط الضوء على تأثير معدل التغذية، وسرعة المغزل، وزاوية نقطة الحفر على أخطاء الدائرية

والأسطوانية. تنبأ نموذجا ANN وTaguchi بالنتائج التجريبية بدقة، مما يوفر رؤى قيمة لتحسين إمكانية تصنيع المركبات المقواة بالألياف الطبيعية (NFRCs) في التطبيقات الهيكلية خفيفة الوزن عبر مختلف الصناعات.

General introduction

Composite materials reinforced with natural fibers, such as banana, kenaf, flax, jute, hemp, sisal, coir, curauá, Strelitzia reginae, and palm, have garnered considerable attention in recent years due to their environmentally friendly characteristics and potential for lightweight structural applications across various industries[1]. These industries encompass shipbuilding, aviation, automotive, rail transport, and high-performance construction materials like partitions, suspended ceilings, furniture, decorative items, kitchenware, and decking. These natural fiber composites offer significant advantages, including biodegradability, cost-effectiveness, and mechanical properties comparable to synthetic fiber-reinforced alternatives. However, they also present several drawbacks, including susceptibility to moisture absorption, variability in mechanical properties due to natural fiber heterogeneity, and vulnerability to microbial degradation[2].

Palm fibers, as versatile natural materials, find widespread applications in various contexts. These fibers are abundantly available in tropical and subtropical regions globally. Notably, Algeria possesses substantial renewable natural resources, with date palms standing out among them. The oases in southern Algeria boast over 19 million date palms, producing more than 750 varieties of dates[3].

Date palms exhibit a fibrous structure, encompassing five types of fibers: leaf fibers in the peduncle, peduncle stem fiber, brush stem fibers, wood fibers in the trunk, and surface fibers around the trunk. Palm fibers possess key characteristics that enhance their versatility and usefulness. These fibers are known for their high tensile strength, low density, and excellent flexibility, making them well-suited for diverse applications, including handicrafts, traditional construction, and, more recently, as reinforcements in composite materials. Moreover, palm fibers are recognized for their environmentally friendly attributes, being both biodegradable and derived from renewable resources. The exploration and utilization of palm fibers, especially in regions like Algeria, hold significant potential for promoting sustainable development and fostering eco-friendly practices[4].

Problematic

Conventional materials utilized in manufacturing processes frequently entail non-renewable resources and impose considerable environmental footprints. Consequently, there's an escalating demand for sustainable substitutes. Bio-composite materials, fortified with lignocellulosic fibers, have surfaced as environmentally conscious alternatives. Nevertheless, there's a requisite for a thorough investigation into their machinability and mechanical characteristics. It's imperative to comprehend the interactions of these materials with diverse machining methods and the resultant mechanical attributes. Tackling these facets is paramount for the seamless integration of bio-composites into industrial settings.

Objective

The main goal of this thesis is to conduct a comprehensive examination of the machinability , physical and mechanical characteristics of a bio-composite material reinforced with date palm fiber. The specific objectives encompass:

- Investigation of Absorption Behavior: This involves evaluating factors such as water uptake rate, diffusion coefficient, and fiber porosity.
- Assessment of Machinability: Evaluation of circularity, cylindricity errors, and delamination, especially under varied cutting conditions employed during the drilling process.
- Study of Mechanical Behavior: Understanding how these properties are influenced by factors like fiber orientation, fiber content, and manufacturing processes.
- The ultimate aim is to propose strategies for optimizing machining processes and material composition to enhance both machinability and mechanical performance. This may entail adjusting fiber content, exploring different fiber treatments, or modifying machining parameters.

Thesis Layout

The initial chapter offers a broad overview of composite materials, delving into their classification according to the matrix material and types of reinforcement. Additionally, it includes an exploration of various plant fibers and their unique physical and mechanical properties. Towards the end of this chapter, a literature review is provided, focusing on absorption behavior and the potential for bio composite manufacturing.

In the second chapter, the equipment and techniques utilized for sample production in this study, along with the experimental tests such as absorption and drilling tests, are detailed. Additionally, the chapter covers methods for analysis and optimization, specifically focusing on artificial neural networks (ANN), response surface methodology (RSM), and the Taguchi method.

In the third chapter, the focus is on presenting findings and discussions related to the absorption behavior of (date palm fibers/iso-polyester) composites. This covers various aspects, including the rate of water absorption, the diffusion coefficient of DPFPs, and the evaluation of porosity in palm fibers.

In the fourth chapter, the focus is on presenting the machining performance of bio composites, along with findings and discussions regarding the drilling behavior of DPFP40 and PFPEs. This includes examining aspects like delamination, as well as circularity and cylindricity errors observed in the holes of DPFP40 and PFPEs.

The conclusive fifth chapter highlights three methods of analysis, optimization, and modelization, specifically artificial neural networks (ANN), response surface methodology (RSM), and the Taguchi method. These methods were employed to analyze and predict the physical and mechanical characteristics of the palm fiber-reinforced bio composites developed in this study.

This thesis culminates with a comprehensive conclusion summarizing the key findings derived from the experimental tests.

Chapter I

Composite Materials - Overview and Literature Review

I . Chapter I: Composite Materials - Overview and Literature Review

I.1 Introduction

The initial chapter embarks on a comprehensive examination of composite materials, centering on their diverse classifications, properties, applications, and manufacturing processes. It commences by tracing the historical evolution of material utilization, spanning from ancient civilizations to the contemporary era, accentuating pivotal milestones in material history and the transition towards sustainable alternatives like biocomposites. Emphasis is placed on the significance of natural fiber reinforced composites in various industries, underscoring their environmentally friendly nature and versatile properties. This chapter also delves into the physical and mechanical attributes of palm fiber, shedding light on its distinctive qualities that position it as an outstanding material for a range of applications. Furthermore, it investigates experimental inquiries and scrutinizes the outcomes of prior research on composite materials, encompassing studies on water absorption properties ,the machinability , and drilling parameters related to these composites, underscoring the importance of comprehending and optimizing these variables to enhance overall performance and efficiency.

I.2 History of materials use

Certainly, the history of human material usage spans thousands of years. One of the earliest instances of such utilization can be traced back to the Stone Age when our forebears commenced carving stones to fashion their inaugural tools. This era, recognized as the Paleolithic era, is distinguished by the utilization of natural materials like stone, wood, bone, and horn. The Neolithic period marked a pivotal shift in material expertise. Human endeavors in domesticating plants and animals emerged, leading to the rise of agriculture and animal husbandry. This transformation also resulted in a broader utilization of materials such as pottery, fired clay, and copper craftsmanship for the creation of tools and practical items[5].

The Bronze Age ushered in a significant era in material evolution with the extensive use of metals, particularly copper and tin. This period witnessed the development of bronze tools and weapons, notable for their durability and heightened strength compared to preceding materials. The subsequent Iron Age introduced a new epoch where iron and steel found widespread application in the manufacturing of tools, weaponry, and structures. This substantial reliance on metals endured through ancient, medieval, and modern civilizations[6].

While the widespread use of metals in the contemporary era has yielded numerous advantages, it has also spawned several drawbacks, prompting concerns in environmental, social, and economic domains. These drawbacks include the depletion of natural resources, the

environmental impact of mining, greenhouse gas emissions, and the issue of electronic waste[7]. To mitigate these challenges, the discovery of bio composites has emerged as a viable solution. Bio composites, being hybrid materials, serve as a sustainable alternative to conventional composites derived from non-renewable raw materials. The development of bio composites in recent years has experienced noteworthy growth, fueled by the escalating demand for environmentally friendly solutions and the quest for more sustainable materials across various industries. A diverse array of materials has been observed, encompassing widely prevalent composite products to high-performance composites distinguished by unique mechanical and thermal characteristics [8]. As a result, current research is dedicated to comprehending the nature and classifications of these materials and addressing their distinctive mechanical attributes.

I.3 Composite materials

A composite material strategically combines two or more distinct materials, usually a matrix and a reinforcement, to maximize the individual advantages of each component (refer to **Figure I-1**)[9, 10]. The selection of these components is done meticulously to form a material that demonstrates synergistic properties surpassing those of the individual materials. The matrix, frequently composed of a polymer, serves as a cohesive element, whereas the reinforcement, such as fibers or particles, amplifies the mechanical properties of the composite material. These materials are utilized across diverse industries because of their lightweight characteristics, strength, and adaptability to specific applications[11-13].

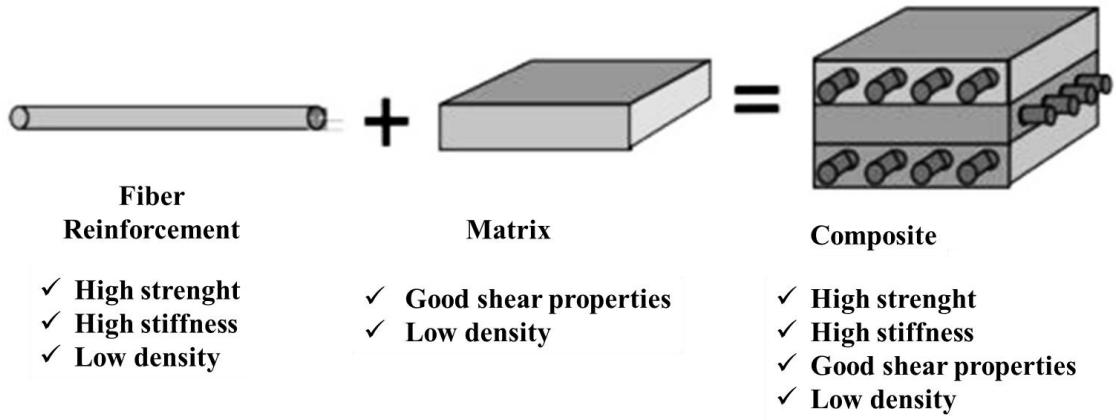

Figure I-1: Composite materials[14].

I.4 Classification of Composite Materials

I.4.1 Classification based on the Matrix Material

I.4.1.1 Metal Matrix Composites (MMCs)

MMCs utilize metals such as aluminum or magnesium as the matrix, strengthened with ceramic particles or carbide fibers (refer to **Figure I-2**). These composites exhibit remarkable attributes, including a high strength-to-weight ratio, enhanced wear resistance, high-temperature stability, thermal conductivity, customizable properties, corrosion resistance, and improved fatigue resistance[15-17]. Despite their numerous advantages, Metal Matrix Composites face associated challenges, such as processing complexity, high costs, anisotropic properties, limited ductility, and waste generation[18, 19].

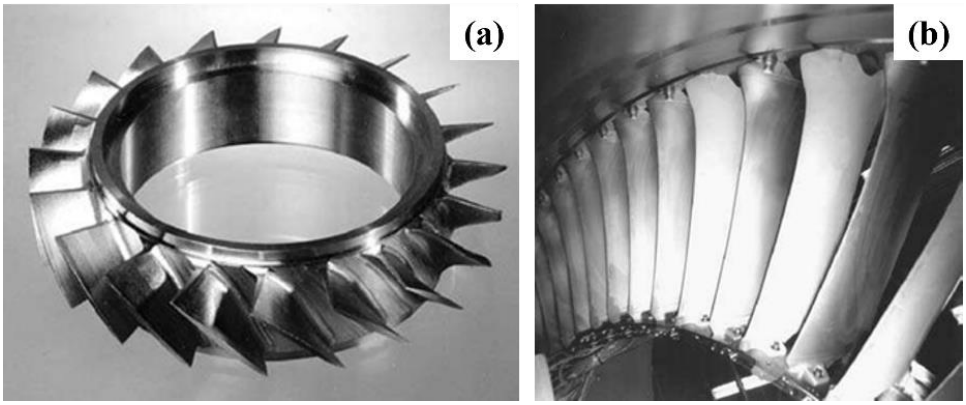

Figure I-2: a) demonstration bling featuring a titanium metal matrix composite. b) vanes made of aluminum metal matrix composite in non-structural positions for fan outlet guide valve[20].

I.4.1.2 Ceramic Matrix Composites (CMCs)

CMCs involve ceramic matrices, like silicon nitride, reinforced with ceramic fibers such as alumina (refer to **Figure I-3**). These composites are renowned for their exceptional resistance to elevated temperatures and harsh environments. The advantages of CMCs encompass high-temperature resistance, chemical resistance, low thermal expansion, and electrical insulation. However, challenges such as brittleness, high costs, and limited ductility pose difficulties in their manufacturing[21, 22].

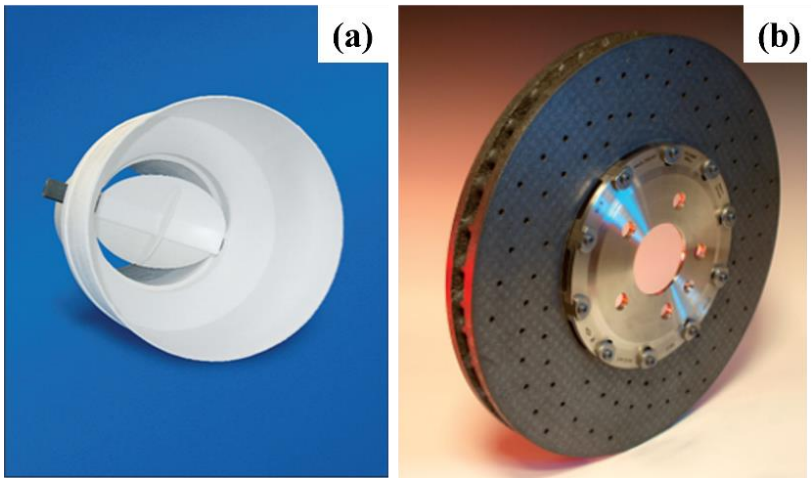

Figure I-3: a) Ox/Ox CMCs hot gas valve employed for regulating gas flow in gas-fired furnace, b) The brake disk, crafted from C/SiC CMCs [23].

I.4.1.3 Polymer Matrix Composites (PMCs)

PMCs use polymers like epoxy resins, polyester, or polyethylene as the matrix, reinforced with fibers of glass, carbon, or aramid (see **Figure I-4**). PMCs showcase excellent features, including a lightweight, high strength-to-weight ratio, design flexibility, corrosion resistance, fatigue resistance, damping properties, thermal insulation, cost-effective manufacturing, electrical insulation, and versatility. These advantages have resulted in the widespread adoption of polymer matrix composites across various industries, including aerospace, automotive, construction, sports equipment, and consumer goods[24-26].

Figure I-4: Polymer Matrix Composites[27].

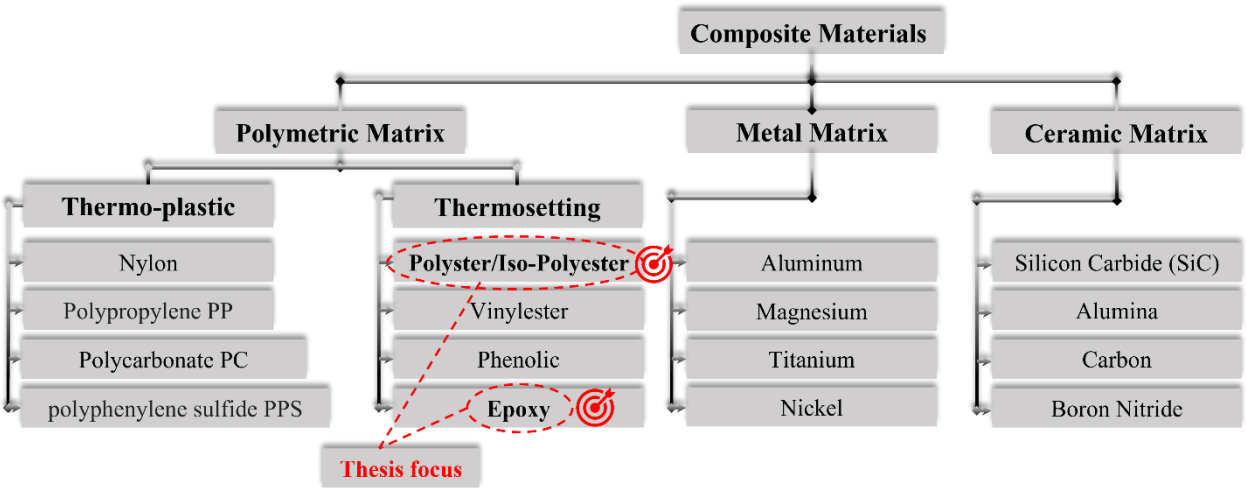

Figure I-5: Classification of composite materials according to the matrix material.

This project focuses on the realm of polymer matrix composites, specifically on thermosetting resins, namely Iso-polyester and epoxy (refer to **Figure I-5**). The following provides an in-depth explanation of these two matrix materials.

I.4.1.3.1 Polyester / Iso-Polyester resin

I.4.1.3.1.1 Definition

Polyester resin, derived from petroleum and consisting of esterified monomers such as terephthalic acid and glycol, undergoes chemical reactions to form three-dimensional bonds, resulting in a robust and rigid structure. Widely utilized in composite manufacturing [28], these composites, also referred to as polyester matrix composites, are created by blending polyester resin with glass fibers, producing resilient and versatile materials (see **Figures I-6** and **I-7**). This combination forms a strong matrix, imparting outstanding mechanical properties to the composites and making them suitable for various applications in industrial and construction sectors [29, 30]. (Refer to **Figure I-6**). on other hand. Iso-polyester resin, an advanced formulation within the polyester resin family, exhibits distinct characteristics that set it apart from conventional polyester resin. The key feature of iso-polyester resin lies in the incorporation of isophthalic acid during its production, contributing to enhanced chemical resistance, increased durability, and improved resistance to water absorption. This makes iso-polyester resin particularly suitable for applications where exposure to harsh environments or corrosive substances is a concern[31, 32].

Figure I-6: Polyester resin.

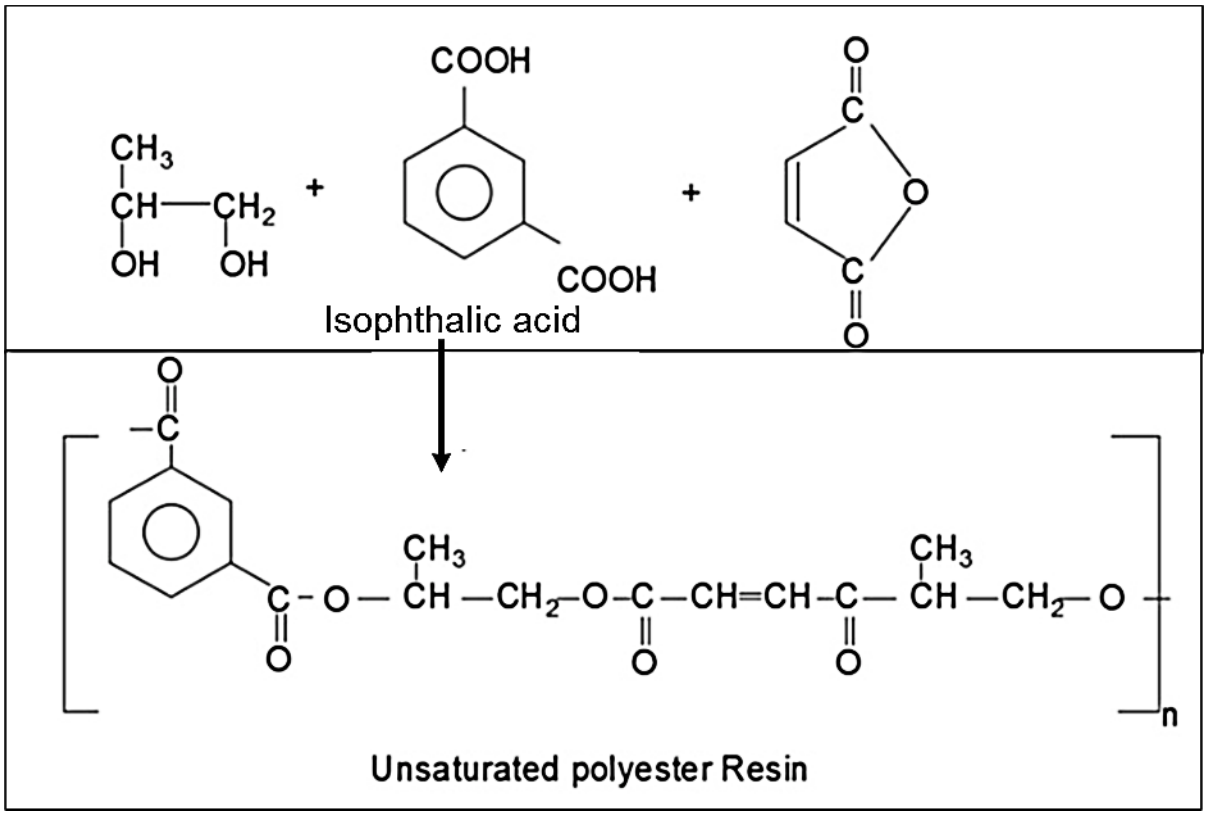

Figure I-7: Chemical structure of polyester resin[33].

I.4.1.3.1.2 The upsides of polyester resin

The polyester resin provides numerous advantages that position it as a preferred option in composite manufacturing. Its cost-effectiveness makes it an economical choice, and its ease of fabrication benefits from its relatively low viscosity, aiding in the impregnation of reinforcing fibers[34, 35]. Its exceptional fiber adhesion effectively reinforces composite structures, ensuring

both lightweight characteristics and versatility, which are particularly advantageous for applications necessitating lightweight materials, such as those in the marine and aerospace sectors[36, 37]. polyester resin demonstrates satisfactory chemical resistance. Moreover, polyester resin displays acceptable chemical resistance. In contrast to regular polyester resin, iso-polyester resin outperforms in terms of both chemical and moisture resistance. Although polyester resin is economical and user-friendly, it might exhibit greater vulnerability to chemical degradation and water absorption when juxtaposed with iso-polyester resin. while its diverse formulations allow for the customization of mechanical properties as required[38]. Moreover, these composites offer weather resistance and durability, leading to their utilization across various industries including construction, automotive, and boat manufacturing[39]. Additionally, with its electrical insulation properties, polyester resin meets the specific requirements of certain electrical applications[40].

I.4.1.3.1.3 The downsides of polyester resin

Despite the numerous advantages it presents, polyester resin has certain drawbacks that need to be considered during its use. Among these, one can mention its sensitivity to moisture, which can lead to progressive deterioration of the material over time. Additionally, the relatively limited thermal resistance of polyester resin restricts its use in applications subjected to high temperatures[41]. Another important consideration is its vulnerability to ultraviolet (UV) rays, which can result in discoloration and deterioration of the surface of composites exposed to prolonged sunlight[42]. Furthermore, polyester resin may emit potential volatile organic compounds (VOCs) during the curing process, raising environmental and safety concerns[43]. Due to its petroleum-derived composition, it is also important to note that polyester resin is not considered an entirely eco-friendly option, which can be a limiting factor in the context of growing concerns related to sustainability. In summary, while offering many advantages, it is essential to take these specific drawbacks into account to judiciously choose its use in various applications.

I.4.1.3.2 Epoxy resin

I.4.1.3.2.1 Definition

An epoxy resin is a thermosetting polymer, which means it is a plastic material that hardens when heated. It is composed of epoxy monomers, also known as epoxides, which chemically react to form three-dimensional bonds when exposed to a hardener or cross-linking agent (refer to **Figure I-9).** This cross-linking process creates a solid, strong, and durable structure[44, 45].(**Figure I-8**)

Figure I-8: Epoxy resin with Hardener.

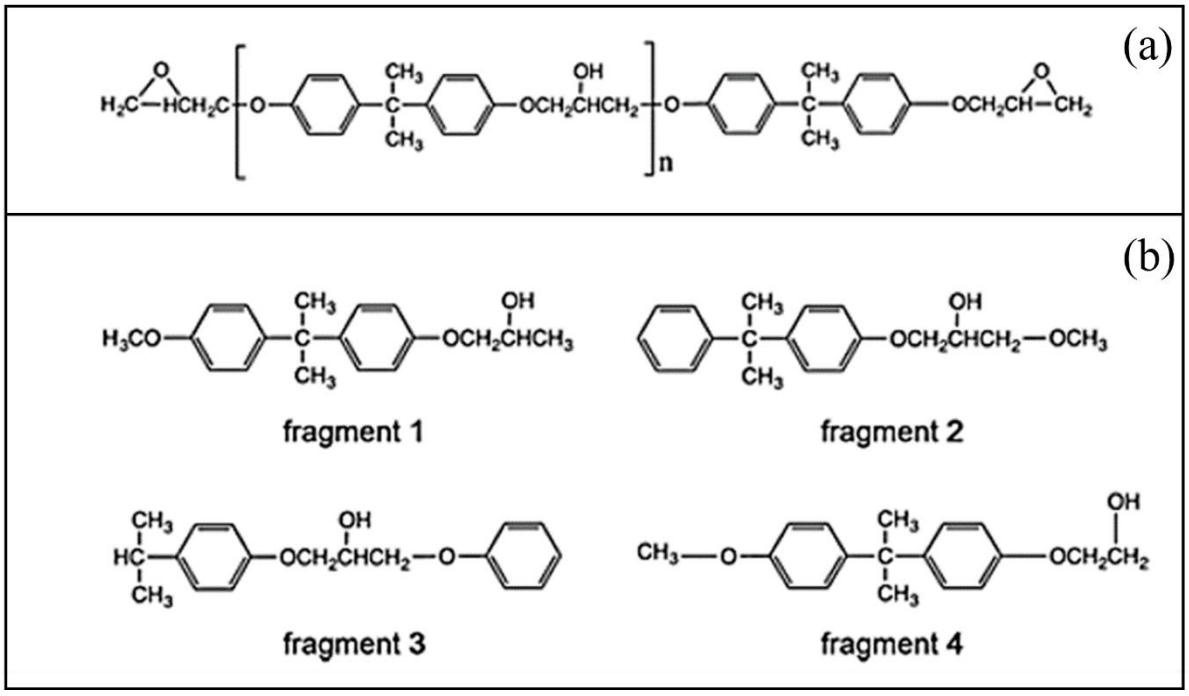

Figure I-9: The chemical structure of (a) epoxy resin and (b) its molecular fragments[46].

I.4.1.3.2.2 The upsides of epoxy resin

Epoxy resin provides a diverse array of benefits, establishing itself as a versatile material extensively employed across various applications. The controlled polymerization process, initiated by a hardener, facilitates the formation of robust and rigid structures with outstanding adhesion on a multitude of surfaces, such as metal, wood, glass, and diverse plastics, ensuring considerable

versatility[47]. Another noteworthy advantage of epoxy resin lies in its exceptional mechanical resistance, imparting extraordinary toughness to manufactured objects and structures, rendering them resilient to stress, impacts, and everyday wear and tear[48, 49]. Furthermore, its outstanding chemical resistance allows it to endure exposure to various corrosive substances without undergoing degradation, proving suitable for environments with demanding chemical conditions. Additionally, its superior thermal resistance qualifies it for diverse applications, ranging from industrial floor coatings and surfboards to electronic components. In summary, epoxy resin distinguishes itself through its exceptional properties, positioning it as a preferred material for a broad spectrum of applications[50-52].

I.4.1.3.2.3 The downsides of polyester resin

Despite its numerous advantages, epoxy resin presents certain disadvantages that require careful consideration. Firstly, the curing process can be temperature-sensitive, requiring specific conditions to ensure proper polymerization. Additionally, epoxy resin may be prone to the formation of air bubbles during mixing and application, compromising the structural integrity of the final material[53, 54]. Another aspect to consider is the potential toxicity of the chemical components used in epoxy resin, raising health and safety concerns, especially when used in poorly ventilated environments[55]. Moreover, epoxy resin may exhibit sensitivity to ultraviolet (UV) rays, leading to discoloration and deterioration when exposed to prolonged direct sunlight[56]. Lastly, the relatively high cost of epoxy resin can be a limiting factor in certain applications, necessitating a careful evaluation of the benefits versus the costs. In summary, while epoxy resin offers excellent performance, it is essential to consider these potential drawbacks for judicious use in various contexts.

I.4.2 Classification based on reinforcement types

I.4.2.1 Classification of composites based on the architecture or arrangement of the fiber reinforcement within the matrix

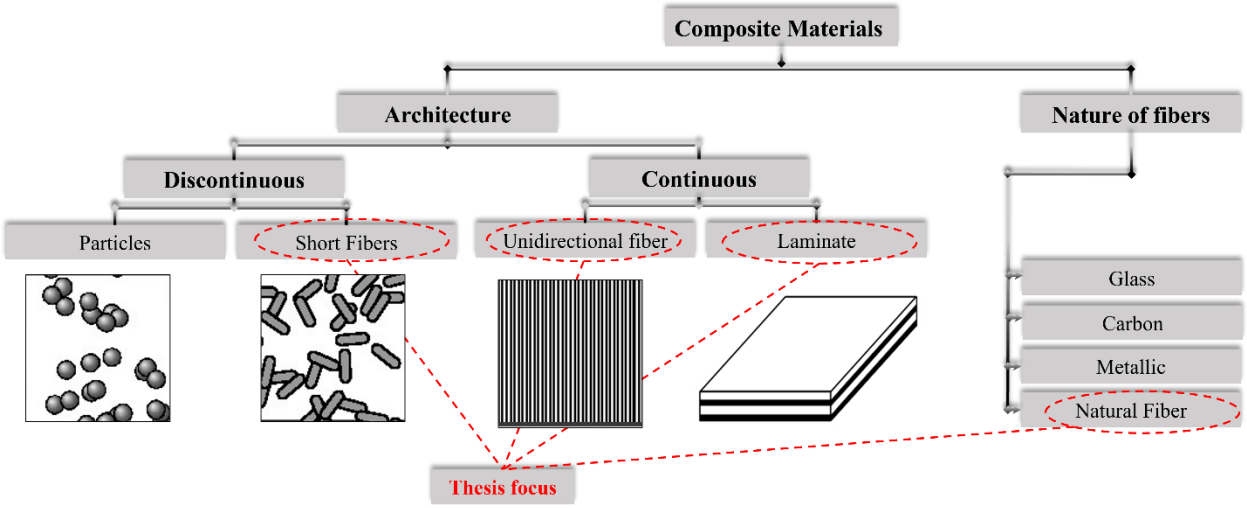

Figure I-10: Classification of composite materials according to the reinforcement types.

I.4.2.1.1 Continuous Fiber-Reinforced Composites:

These composites feature reinforcing fibers that extend continuously throughout the matrix (refer to **Figure I-10**), delivering heightened strength, stiffness, and durability of the composite. The seamless alignment of fibers enables efficient load transfer and enhances resistance against deformation and fractures. This type of composite is widely utilized in diverse industries such as aerospace, automotive, and construction, leveraging its exceptional mechanical properties to contribute to the creation of lightweight and high-performance structures[57-59].

Continuous fiber-reinforced composites can be segmented into two categories: unidirectional fibers and laminated fibers. These configurations offer tailored solutions to address distinct engineering requirements in continuous fiber-reinforced composites, allowing for the optimization of material properties according to the intended application[60].

I.4.2.1.1.1 Unidirectional fibers

Unidirectional fibers within Continuous Fiber-Reinforced Composites denote fibers aligned in a singular direction within the matrix (refer to **Figure I-11c**). In this configuration, the fibers run parallel, imparting exceptional strength along the designated direction. Unidirectional composites prove advantageous in applications where robust load-bearing capabilities are crucial, leveraging the inherent strength of the aligned fibers[61-63].

I.4.2.1.1.2 Laminate fibers

laminate fibers in Continuous Fiber-Reinforced Composites entail the stacking of multiple sheets or plies of fibers oriented in diverse directions within the matrix (refer to **Figure I-11d**). This deliberate arrangement enhances the overall mechanical properties of the composite, with each layer contributing unique strengths. Through the amalgamation of fibers with distinct orientations, laminate composites achieve a harmonious blend of strength, stiffness, and flexibility, rendering them versatile for diverse applications[64-66].

I.4.2.1.2 Discontinuous Fiber-Reinforced Composites

Discontinuous Fiber-Reinforced Composites feature the integration of short fibers or discontinuous reinforcements within a matrix. In contrast to continuous fibers that span the composite's entire length, these short fibers are dispersed unevenly. The matrix, responsible for securing the fibers, may consist of polymers, metals, ceramics, or other materials[67]. They can be segmented into two categories: Particles and Short Fibers (refer to **Figure I-10**):

I.4.2.1.2.1 Particles

Particles are defined as diminutive, solid, and distinct components scattered within the composite matrix (refer to **Figure I-11a**). These particles may consist of diverse materials, including ceramics, metals, or polymers[68]. Introducing particles into the matrix yields various advantages, such as heightened stiffness, dimensional stability, enhanced wear resistance, and improved thermal or electrical conductivity[69]. The arrangement of particles in the matrix is frequently irregular, contributing to distinctive material attributes tailored to specific applications[70, 71].

I.4.2.1.2.2 Short Fibers

Short fibers, being of shorter length than continuous fibers, are scattered within the matrix to fortify and enhance the mechanical properties of the composite (refer to **Figure I-11b**). These fibers may be crafted from materials like glass, carbon, or aramid. Despite not extending continuously throughout the material, short fibers nonetheless enhance strength, stiffness, and impact resistance[69]. The orientation and arrangement of short fibers within the matrix are critical factors that influence the overall performance of the composite. Short fiber reinforcement proves especially beneficial in applications where cost-effectiveness and ease of processing are key considerations[71].

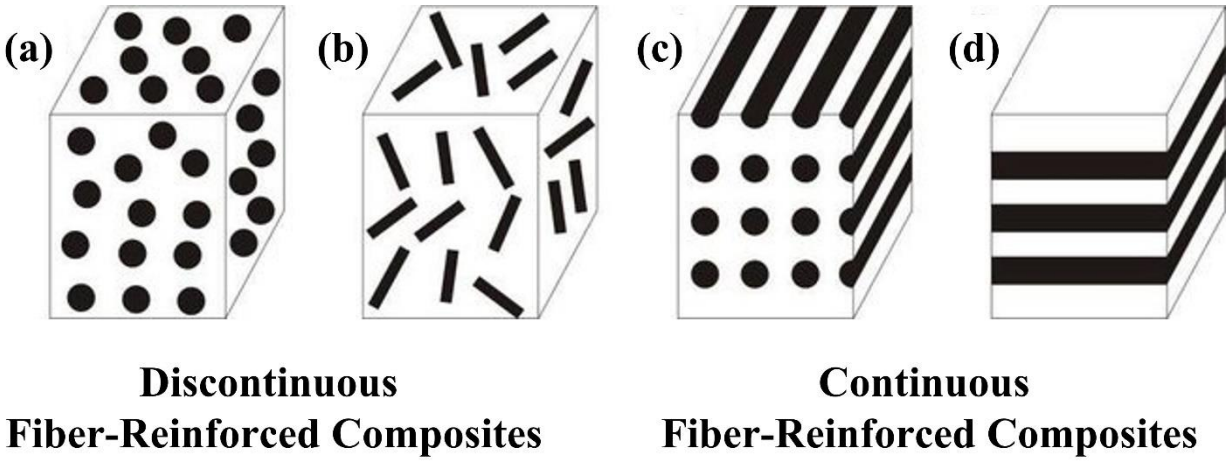

Figure I-11: Schematic representation of the arrangement of the fiber reinforcement within the matrix[72].

I.4.2.2 Classification of composites based on the nature of the fibers

Classification of composite materials can extend to the nature of the fibers employed as reinforcement, with the chosen fibers exerting a substantial impact on the mechanical, thermal, and various other properties of the composite. The subsequent list outlines some prevalent composite types categorized according to the nature of their fiber reinforcement (refer to **Figure I-10**):

I.4.2.2.1 Glass Fiber-Reinforced Composites (GFRP):

The composite materials reinforced with glass fibers, often referred to by the acronym GFRP (Glass Fiber-Reinforced Composites), are assemblies where glass strands play the primary role as the reinforcing material within a matrix[73] (refer to **Figure I-12**). These composites are valued for their high strength, light weight, and corrosion resistance, making them highly sought after in sectors such as shipbuilding, the automotive industry, the manufacturing of tanks and pipes, as well as the production of sports equipment and lightweight components[74, 75]. Glass fibers, often in the form of fabrics or mats, are integrated into a matrix typically composed of polymers, creating a hybrid material with enhanced properties. Despite the undeniable advantages of glass fiber-reinforced composites, they do have some drawbacks, such as their brittleness under high impact loads, which can lead to cracks or fractures[76]. Additionally, their initial cost may be relatively high compared to certain traditional materials. Recycling also presents challenges due to the difficulty of separating glass fibers from the polymer matrix[77]. Despite these drawbacks, the benefits of fiberglass composites continue to make them highly desirable in various industrial applications.

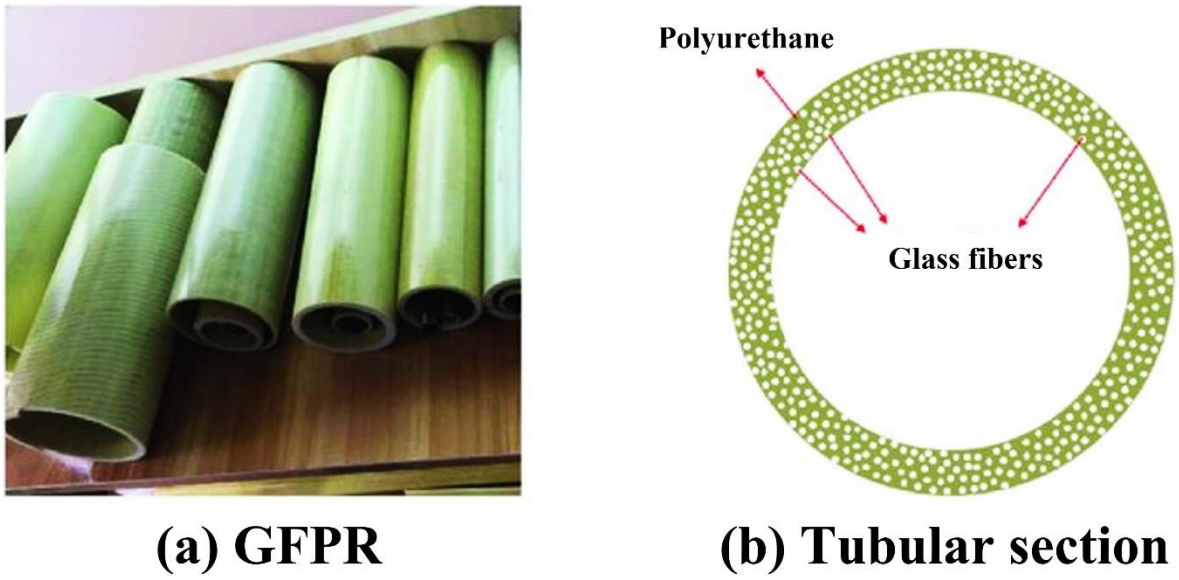

Figure I-12: Glass fiber reinforced polyurethane matrix composite (GFRP)[78].

I.4.2.2.2 Carbon Fiber-Reinforced Composites (CFRP)

CFRP constitute a category of composite materials in which carbon fibers play a predominant role as reinforcements within a matrix (refer to **Figure I-13**). These fibers are typically derived from carbonaceous precursors such as polyacrylonitrile (PAN) or rayon fibers, which often undergo a high-temperature carbonization process to become carbon fibers[79, 80]. The advantages of CFRP include exceptional tensile strength, rigidity, and lightness, along with resistance to corrosion, high electrical conductivity, and resilience to elevated temperatures[81]. These features make CFRP a preferred choice in fields such as aerospace, high-end automotive manufacturing, construction of lightweight and durable structures, as well as the production of premium sports equipment[82, 83]. However, these composites have some drawbacks, including high cost, susceptibility to impacts, and complexity in repairing damages. Despite these limitations, their demand continues to grow due to their unique combination of lightness and strength, making them ideal for various advanced applications[84, 85].

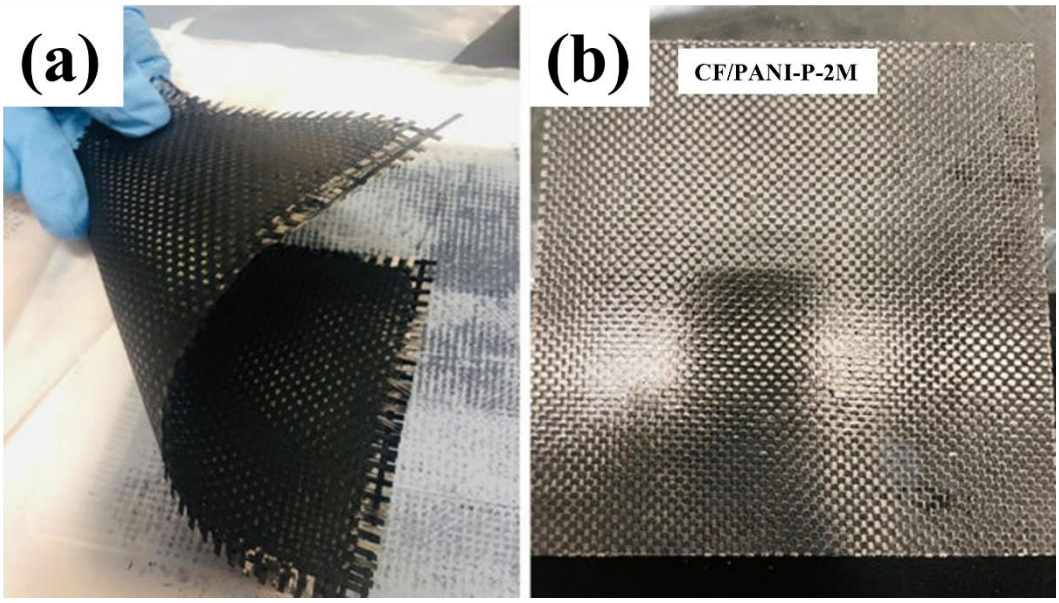

Figure I-13: (a) Prepreg of Carbon fiber impregnated with PANI/P-2 M resin, (b) Fabricated CFRP using the PANI/P-2 M resin[86].

I.4.2.2.3 Aramid Fiber-Reinforced Composites (AFRP):

Aramid fibers, such as Kevlar, play a central role as reinforcement material in AFRP (refer to **Figure I-14**). These aramid fibers, typically derived from aromatic polymers like poly-p-phenylene terephthalamide (PPTA), undergo a spinning process to form highly resilient and flexible fibers[87]. The advantages of composites reinforced with aramid fibers include exceptional tensile strength, the ability to absorb impact energy, resistance to corrosion, and flexibility[88]. These characteristics make them particularly suitable for applications such as manufacturing ballistic protection equipment and lightweight automotive components[89]. However, the disadvantages of aramid composites include their relatively high cost and susceptibility to abrasion. Nevertheless, their usage continues to grow, especially in industries where the specific combination of properties offered by aramid fibers is essential to meet the specific requirements of applications[90].

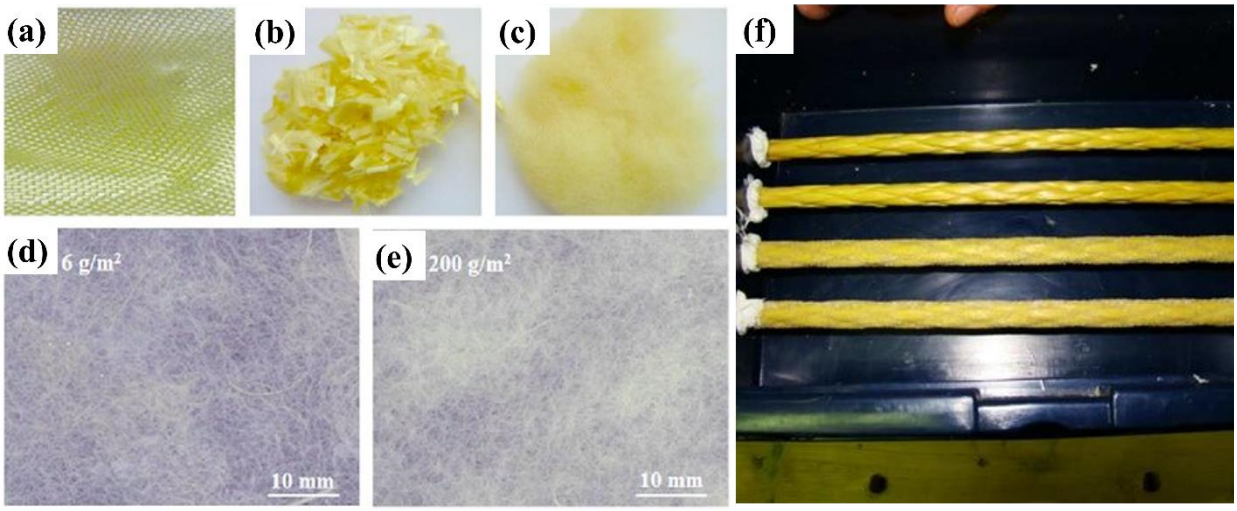

Figure I-14: (a) aramid-fiber fabric, (b) initially chopped aramid-fiber strands, (c) cotton-like aramid fibers, (d) 6 g/m^2 thin tissue of short aramid fibers, and (e) 200 g/m^2 thin tissue of short aramid fibers, (f) Braided AFRP bars[91, 92].

I.4.2.2.4 Metallic Fiber-Reinforced Composites:

Metal fiber-reinforced composites utilize metal fibers as reinforcement embedded within a matrix. These fibers, typically composed of steel, aluminum, or titanium, are integrated into the matrix to enhance the mechanical properties of the composite material[93, 94] (refer to **Figure I-15**). The manufacturing process involves blending the metal fibers with the matrix, followed by consolidation into sheets or layers. The benefits of these composites encompass high tensile strength, notable thermal and electrical conductivity, and effective corrosion resistance. They are extensively applied across various industries such as aerospace, automotive, construction, and electronics, where a combination of mechanical strength and conductivity is crucial. These composites are utilized to manufacture lightweight yet sturdy components, including aircraft body parts, structural elements, and electronic devices. Nevertheless, potential drawbacks may include their relatively high cost, greater weight compared to certain non-metallic fiber-reinforced composites, and challenges associated with corrosion in specific applications[95].

Figure I-15: NexGen porous titanium fiber-mesh (Ti) tibial metal-backing with 4 short pegs for screw fixation in the proximal tibia[96].

I.4.2.2.5 Natural Fiber-Reinforced Composites:

Composite materials enhanced with natural fibers represent an innovative class wherein fibers sourced from natural origins like flax, hemp, jute, or coconut are combined with a matrix to create a durable and adaptable structure. These composites present an eco-friendly substitute for traditional materials owing to the renewable, biodegradable, and often lighter characteristics of natural fibers[97]. Their manufacturing process entails a meticulous blending of these fibers with the matrix, followed by consolidation into sheets or molded components. Although natural fibers might demonstrate slightly lower mechanical strength compared to synthetic counterparts, they still exhibit compelling mechanical properties, particularly in lightweight and non-structural applications[98]. These composites serve various industries including automotive, construction, packaging, and furniture manufacturing, benefiting from their minimal environmental impact, biodegradability, and versatility, which address contemporary concerns regarding material sustainability[99, 100] (refer to **Figure I-16**). Nevertheless, it's crucial to acknowledge that certain natural fibers may be prone to moisture sensitivity, necessitating appropriate management to uphold optimal performance. In essence, natural fiber-reinforced composites offer a promising solution for eco-conscious applications, presenting a diverse range of options to cater to the specific requirements of diverse industries[101].

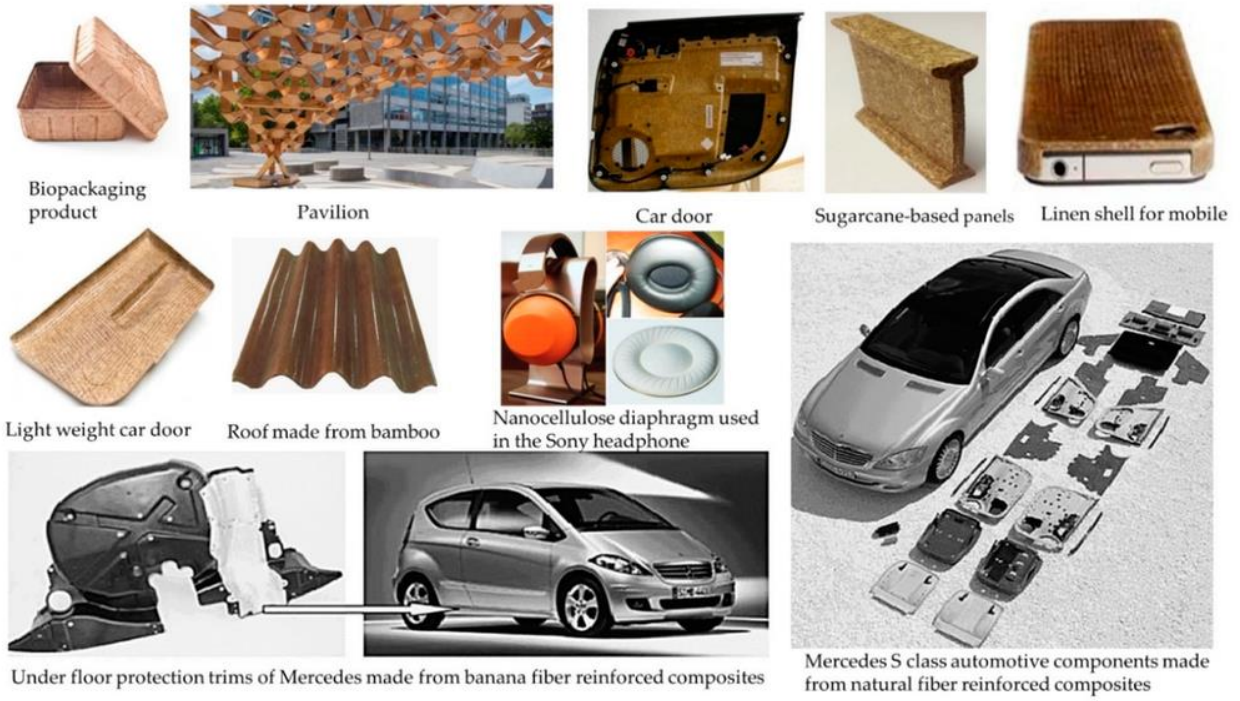

Figure I-16: The use of Natural Fiber-Reinforced Composites in many different sectors[102].

I.5 Presentation of some plant fibers and their distinctive characteristics

I.5.1 Hemp fiber

Hemp fiber, derived from the hemp plant (Cannabis sativa) (see **Figure I-17**), possesses outstanding qualities that solidify its standing as both an environmentally friendly and high-performing material[103]. Demonstrating impressive mechanical strength, this fiber showcases a tensile strength of approximately 550 MPa, comparable to that of glass[104]. Its environmental credentials are equally notable, requiring 50% less water for cultivation compared to cotton, while its rapid growth minimizes the need for pesticides. With its lightweight composition, boasting a density of roughly 1.48 g/cm³, hemp fiber is a favored option for lightweight composite materials. Additionally, it offers efficient thermal insulation and exceptional moisture absorption capabilities, capable of absorbing up to 20% of its weight in water, thus enhancing its versatility across a range of applications. These attributes position hemp fiber as highly esteemed in various sectors including the textile industry, construction, and the burgeoning field of sustainable composites[105, 106].

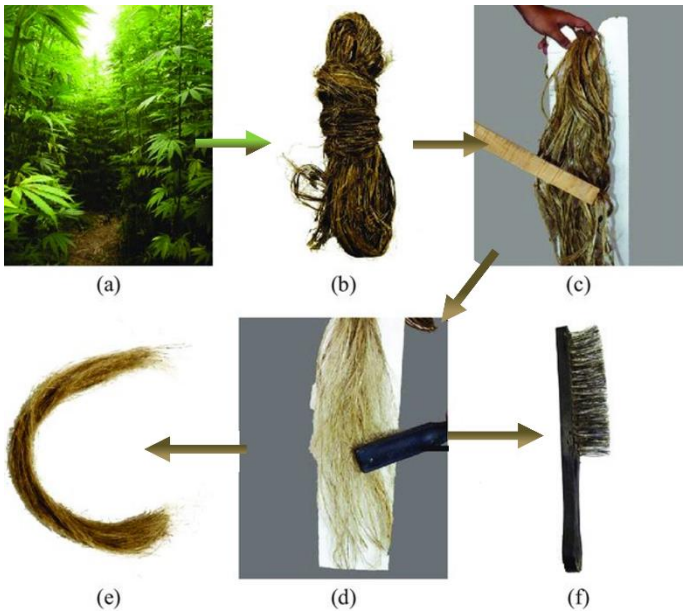

Figure I-17: Extraction of hemp fibers [107]

I.5.2 Jute fiber

Jute fiber, derived from the Corchorus plant, is characterized by an impressive tensile strength, typically ranging between 400 and 650 MPa, contributing to its robustness[108]. With a moderate density of approximately 1.3 g/cm³, it is considered lightweight and easy to handle[109]. Regarding moisture absorption, jute fiber can absorb up to 15% of its weight in water, making it suitable for applications requiring effective moisture management. Cultivated primarily in tropical regions, the jute plant is renowned for its rapid growth and ability to thrive with minimal resources. These characteristics make it an environmentally friendly choice for various applications, including the production of bags, carpets, and other textile products[110]. (Refer to **Figure I-18**)

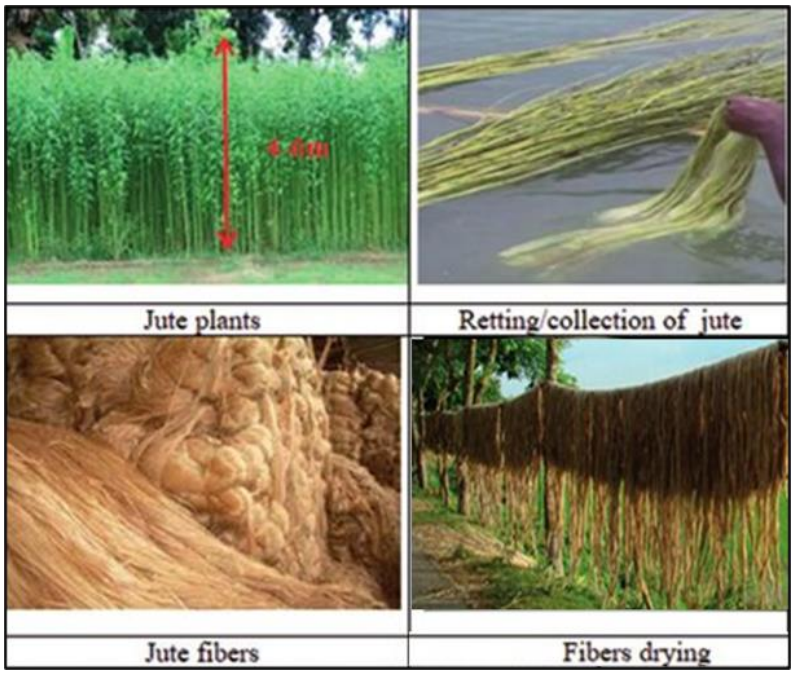

Figure I-18: Extraction of jute fibers [111]

I.5.3 Kenaf fiber

kenaf fiber, extracted from the Hibiscus cannabinus plant (see **Figure I-19**), is distinguished by its outstanding mechanical properties, rendering it an appealing material for various applications. Its tensile strength typically falls within the range of 420 to 920 MPa, indicating notable robustness. With an elasticity modulus fluctuating between 10 and 20 GPa, it demonstrates the capability to retain its shape and resist deformation under stress[112]. The elongation at break, estimated between 1.8% and 3.5%, underscores a degree of ductility prior to rupture. Concerning compressive strength, kenaf fiber exhibits values ranging from 150 to 300 MPa. Alongside these mechanical attributes, it is characterized as lightweight, biocompatible, renewable, and biodegradable. Its ability to offer thermal insulation, sound absorption, coupled with its competitive cost, renders it a versatile material. These specific figures elucidate the superior mechanical performance of kenaf fibers compared to other natural counterparts like jute and hemp[113-115].

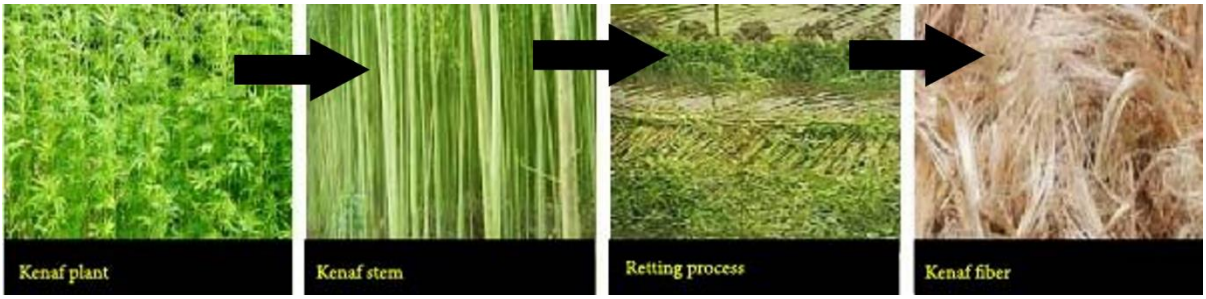

Figure I-19: Extraction of kenaf fibers [116]

Developing composite materials with non-traditional (plant) reinforcements demands a profound comprehension of the physical and chemical properties inherent in these materials. Hence, the present study is dedicated to examining these properties specifically in the utilized fibers (date palm fibers).

I.5.4 Palm fiber

I.5.4.1 Chemical composition and structure

The intricate arrangement of plant fiber is depicted in **Figure 1-20**. Within the cell wall of plant fibers, several layers are discernible: the secondary wall, the primary wall, and the middle lamella. The secondary wall comprises three sub-layers arranged from innermost to outermost: S3, S2, and S1. Of these, the S2 layer is the most substantial and significantly influences the overall fiber performance. Additionally, the hollow space, referred to as the lumen, facilitates the transport of water and nutrients during the plant's growth and photosynthesis[117, 118].

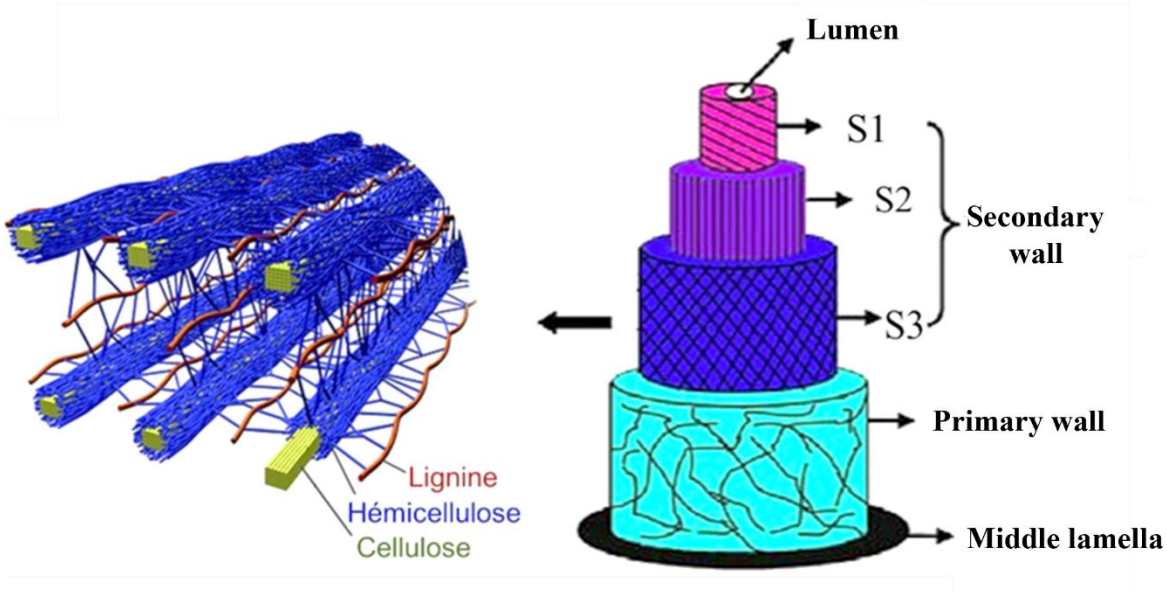

Figure I-20: Visual representation detailing the anatomy of plant fibers[119].

The chemical composition of palm fiber can vary depending on the specific source of the fiber, whether it is from oil palm, date palm, or other types of palms. Palm fiber is mainly composed of cellulose, hemicellulose, and lignin, which are the predominant components of plant fibers[120].

I.5.4.2 Cellulose

Cellulose is a complex macromolecule composed of multiple glucose units linked together by β-1,4 glycosidic bonds. It serves as the primary structural component of the cell walls in plants and certain algae. Its general chemical formula is $(C_6H_{10}O_5)_n$, where "n" represents the number of repetitions of the glucose unit in the molecule (refer to **Figure I-21**). In summary, cellulose is an

essential polysaccharide composed of glucose, playing a crucial role in the structure of plant cells. Although the cellulose content of palm fiber may vary, it is generally between 40% and 50%, and even higher in certain varieties of palm fibers[121, 122].

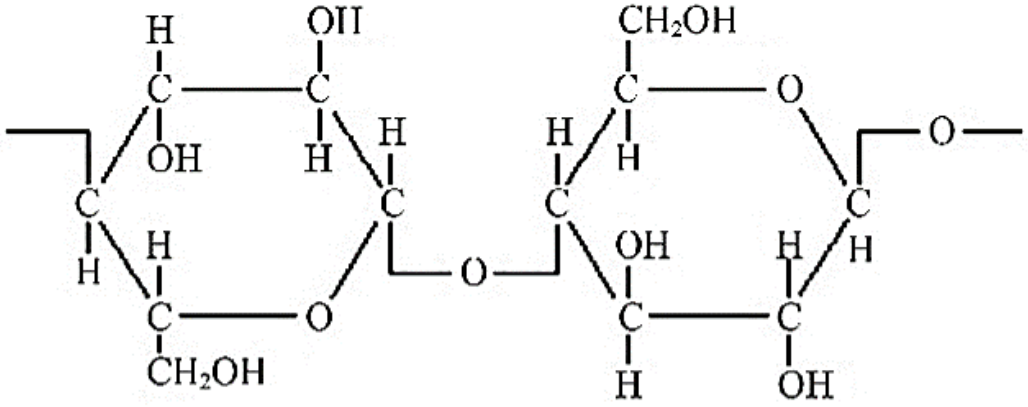

Figure I-21: Structure of cellulose[123].

I.5.4.3 Hemicellulose

Hemicellulose, a class of complex polysaccharides present in plant cell walls, coexists with cellulose within this structure. Unlike cellulose, hemicellulose is characterized by a more diverse composition, typically encompassing monosaccharides such as glucose, xylose, mannose, galactose, and others. The glycosidic bonds within hemicellulose exhibit diversity, potentially taking various forms, such as β-1,4, β-1,3, and others (refer to **Figure I-22**). This structural diversity imparts flexibility and solubility in water to hemicellulose, a distinguishing feature from cellulose, which remains insoluble[124]. The proportion of hemicellulose in palm fiber is estimated to be between 20% and 30%[125].

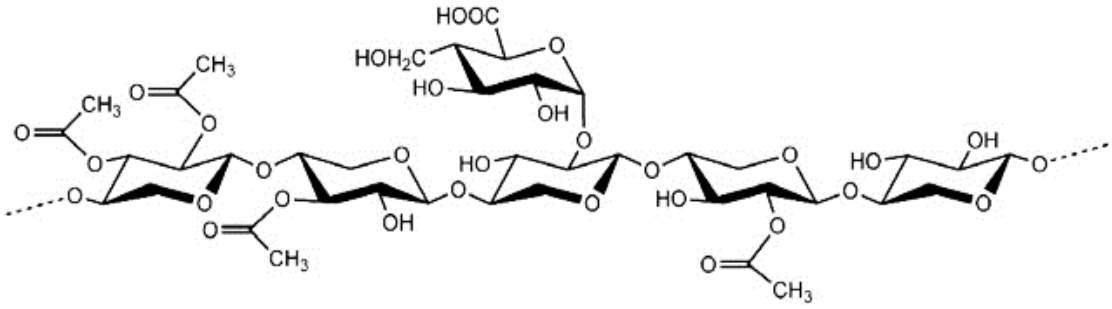

Figure I-22: Structure of Hemicellulose[126].

I.5.4.4 Lignin

Lignin, a complex amorphous polymeric compound comprised of diverse phenolic monomers like coniferyl, sinapyl, and p-coumaryl, serves as a crucial component in the cell walls of vascular plants, playing a key role in their mechanical strength and tissue rigidity. Its formation

occurs through the radical polymerization of phenolic monomers, resulting in an intricate three-dimensional structure (refer to **Figure I-23**). The precise composition of lignin can vary depending on the plant species[127]. For instance, the lignin content of palm fiber typically ranges from 20 to 30%[128].

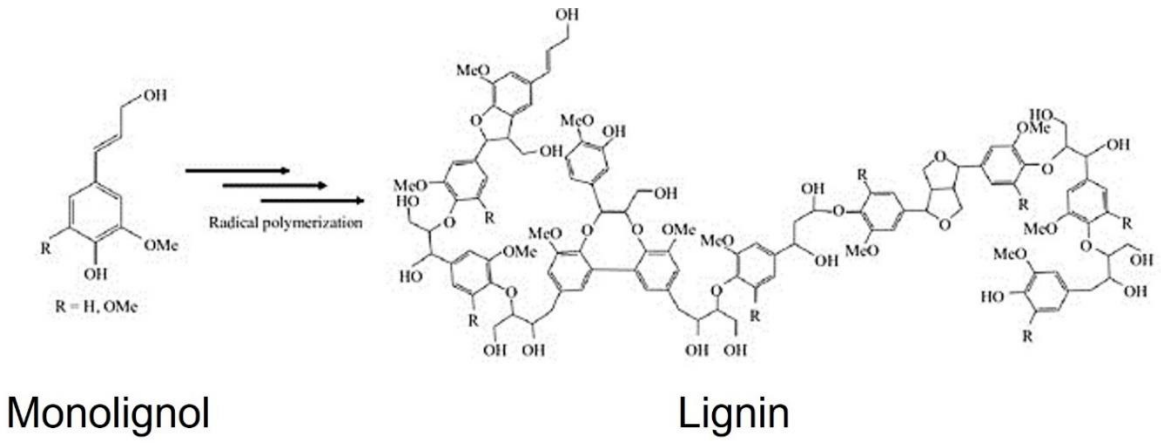

Figure I-23: Structure of Lignin[129].

The chemical composition varies across different plant species. **Table I-1** illustrates a broad spectrum of average chemical constituents observed in various plants.

Table I-1: Chemical composition of selected natural fibers[130-132].

Fibers	**Chemical Composition (%)**		
	Cellulose	Hemicellulose	Lignin
Bambo	26-43	30	21-31
Coir	32-43	10-20	43-49
Ramie	68.6-76.2	13.1-16	0.6-0.7
Cotton	95	2	1
Cuara	73.6	9.9	7.5
Abaca	56-63	20-25	7-9
Hemp	70-75	18-23	3.5-6
Jute	61-71	14-20	12-13
Kenaf	72	20.3	9
Flax	71	18.6-20.6	2.2
Palm	32-35.8	24.4-28.1	26.7-28.1

I.5.4.5 Physical and mechanical properties

Palm fiber, extracted from palm tree leaves such as oil palm or date palm, exhibits unique characteristics that make it an exceptional material. Its tensile strength, typically ranging between 300 and 1000 MPa, attests to its mechanical robustness. The elasticity modulus, varying from 12 to 30 GPa, indicates its ability to maintain shape and resist deformation under stress. The elongation at break, ranging from 2% to 4%, demonstrates a certain ductility before failure. With a relatively low density of approximately 1.2 g/cm³, palm fiber is lightweight and easy to handle[133-135]. It also displays excellent compression resistance, typically between 200 and 500 MPa. These mechanical properties make palm fiber an attractive material for various applications, from construction to furniture manufacturing[136]. In terms of sustainability, this fiber is renewable, being extracted from regenerative natural resources, and it is biodegradable, contributing to environmentally friendly choices. Its versatility, availability, and mechanical properties make it a crucial element for the development of sustainable solutions in the materials industry.

Natural fibers exhibit a distinct array of physical and mechanical attributes, rendering them highly valuable in a variety of industrial applications. Physical properties encompass features like density, moisture absorption, and thermal conductivity, all of which play a vital role in comprehending how fibers interact with their environment. On the flip side, mechanical properties involve factors such as tensile strength, modulus of elasticity, and elongation at break, offering insights into the strength and flexibility of fibers across diverse conditions[137]. The physical and mechanical properties of different fibers are detailed in **Table I-2** and **Table I-3** respectively. This examination of the physical and mechanical characteristics of natural fibers plays a pivotal role in unlocking their full potential across industries such as textiles, composites, construction, and more. A profound understanding of these properties empowers researchers, engineers, and manufacturers to optimize the utilization of natural fibers, thereby contributing to the advancement of sustainable materials and environmentally conscious practices[138].

Table I-2: Physical properties of different fibers natural[139].

Fibers	**Physical properties**			
	Density (g/cm^3)	Moisture Absorption (%)	Length (mm)	Diameter (µm)
Cotton	1.54	25	10-60	11-22
Wool	1.31	30	15-150	20-200
Silk	1.34	20	300-1600	10-13
Hemp	1.5	20	1-4 m	16-50
Coconut Coir	0.1-0.3	10	4-12 inches	100-500
Palm	1.2	5.36-8.7	200-300	80-120

Table I-3: Mechanical properties of different fibers natural.

Fibers	Mechanical properties			Ref
	Tensile strenght (MPa)	Young's modulus (GPa)	Elongation at break (%)	
Abaca	400	12	3-10	[140]
Kenaf	930	53	1.6	[141]
Coir	105-593	2-8	15-51	[142]
Cotton	287-597	2.2-12.6	7.0-8.0	[143]
Flax	1339±486	58±15	3.27±0.4	[144]
Palm	68	3.774	20-25	[145]

I.6 Absorption behavior of bio composites

Moisture absorption in natural fiber-reinforced composite materials is a significant aspect that greatly impacts their performance and durability. This is attributed to the fact that natural fibers possess hygroscopic properties. The presence of moisture in composite materials can have profound effects on their mechanical, thermal, and dimensional stability properties[146]. Understanding and managing moisture absorption are of paramount importance to ensure the long-term reliability and structural integrity of these bio-based composites. The present work presents some previous studies that focused on studying the adsorption behavior of bio composites, including:

Arunkumar et al[147]. Investigated the impact of incorporating Samanea Saman Pod (SSP) pulp on the water absorption behavior of epoxy resin composites reinforced with sisal and hemp fibers. The researchers utilized a 40 wt% reinforcement ratio of sisal/hemp fibers to fabricate the hybrid composite. In contrast, varying proportions of SSP paste (0, 5, 10, 15 wt%) and epoxy resin (60, 55, 50, and 45 wt%) were blended for the matrix preparation. The findings revealed an increase in water absorption up to a certain threshold with the rise in SSP paste content. Furthermore, the results demonstrated that the absorption rate stabilized after 25 days.

Ghasemzadeh et al[148]. Have explored the water absorption characteristics of polypropylene (PP) composites reinforced with hybrid glass/flax fibers. The composite fabrication involved setting the combined volume of glass and flax fibers at 40 vol% relative to the PP content. Furthermore, a PP hybrid composite containing 10% glass fiber and 10% flax (G10F10) was formulated. Each composition was represented by five samples measuring 25 × 76 × 3 mm^3, which were fully immersed in distilled water maintained at 85°C in a container. To expedite the experiment, a high temperature was selected for their tests. The results indicated a rapid initial increase in water absorption rate, followed by a decrease towards saturation for all samples except

PP and G40. Moreover, all samples except PP reached equilibrium after approximately 1000 hours (42 days).

Kairytė et al[149]. Conducted an experimental investigation on thermally self-treated wood plastic composites (WPC) derived from wood bark and a binder based on rapeseed oil. Various proportions of wood bark particles ranging from 0.7 to 1.0 were selected for sample preparation. The specimens were initially oven-dried at 70°C and then conditioned for a minimum of 72 hours to reach equilibrium at 23 ± 5°C and 50 ± 5% relative humidity. Subsequently, specimens measuring 200×200×50 mm^3 were immersed in water at 20°C and drained for 10 minutes on a 45° inclined drainage surface at the end of each immersion period. The swelling test in thickness was conducted following the EN 317 standard, with measurements taken at intervals of 1, 7, 14, and 28 days. The results revealed that water absorption and thickness swelling increased over time. Notably, WPC-0.85 samples exhibited reduced water absorption (~65% after 7 days and 19% after 14 and 28 days of immersion) and thickness swelling (~14% after 7 days and 19% after 14 and 28 days of immersion) compared to WPC-0.70 samples.

Tezara et al[150]. Carried out an experimental inquiry to examine the influence of hybridizing the stacking sequence in jute-ramie composites on water absorption behavior. Epoxy resin (816A) with a density of 1.2 g/cm^3 and cured (651) was employed as the matrix to manufacture composite films. The absorption of distilled water was assessed over a 4-week period for various types of five-layer tensile samples with dimensions of 30 cm × 30 cm × 4 mm. The maximum percentage gain in weight was observed in the following descending order: Jute (8.10%) > RJJJR “Ramie-Jute-Jute-Jute-Ramie” (8.02%) > JRRRJ “Jute-Ramie-Ramie-Ramie-Jute” (8.01%) > JRJRJ “Jute-Ramie-Jute-Ramie-Jute” (7.93%) > RJRJR “Ramie-Jute-Ramie-Jute-Ramie” (7.90%) > RJRJ “Ramie-Jute-Ramie-Jute” (7.58%). The results indicated that the water absorption behavior of jute fibers was lower than that of ramie fibers. The stacking sequence and the choice of materials emerged as two primary factors influencing water absorption behavior.

Ferede et al[151]. assessed the water absorption characteristics of a polypropylene (PP) composite reinforced with alkaline-treated sawdust. Composite materials were fabricated through a melt-mixing process followed by die casting, incorporating sawdust quantities ranging from 10 to 50 wt%. The authors observed absorption rates of 70%, 79%, 90%, 155%, and 180%, respectively. These findings align with previous studies on PBS composites with kenaf fibers[152] and silk fibers [153], as well as poly lactic acid (PLA) composites with 15% and 70% kenaf [154] and Flax/PLA composites[155] . The authors noted a direct (linear) correlation between the water absorption rate and the fiber content, attributed to the hydrophilic nature of these fibers. This characteristic facilitated the formation of hydrogen bonds with water molecules [156].

I.7 The machinability of bio composites

Drilling holds significant importance as a machining process in the final stage of part assembly within the manufacturing industry[157]. Nevertheless, it presents a complex undertaking fraught with various challenges, such as delamination, fiber breakage, thermal degradation, deterioration of surface integrity, and fiber pull-out. Exploring the drilling process of biocomposites offers valuable insights into specific aspects of their mechanical characteristics. To comprehensively evaluate their mechanical behavior through drilling investigations, several factors are typically taken into account. Firstly, the analysis involves measuring the cutting forces and power consumption during drilling to understand the biocomposite's resistance to deformation and the energy required for material removal. Additionally, examining the chips generated during drilling provides insight into the material's brittleness, ductility, or shear behavior based on chip type, size, and morphology. Furthermore, assessing the surface finish of drilled holes offers information on the biocomposite's machinability and its response to cutting forces. Moreover, studying the impact of different drilling parameters, such as cutting speed, feed rate, and depth of cut, helps optimize machining conditions for enhanced mechanical performance. Integrating these considerations allows for a more thorough understanding of the mechanical behavior of biocomposites during the drilling process. While drilling studies provide valuable information, a comprehensive understanding of the mechanical behavior of biocomposites often involves additional tests. Tensile tests, compression tests, flexural tests, and impact tests are commonly employed to assess parameters such as modulus of elasticity, tensile strength, compressive strength, and impact resistance. Combining drilling studies with these tests can offer a more complete picture of the mechanical properties of biocomposites.

The current study is focused on analyzing the drilling behavior of bio composites. Below are some prior investigations that have explored this behavior in detail.

Yallew et al[158]. Examined the impact of various drilling process parameters (spindle speed (N), feed rate (f), and drill tip geometry) on the drilling performance of woven jute fiber-reinforced polypropylene (PP) composites. The study utilized PP pellets as the matrix and incorporated 30%, 40%, and 50% weight of reinforcement (jute fabrics) to form the composite. Twist drills, Jo drills, and parabolic carbide drills with an 8 mm diameter and an angle of 118° were employed for drilling the samples. The feed rate was varied at 0.05, 0.12, and 0.19 mm/rev, while spindle speeds were set at 900, 1800, and 2800 rpm. The test results revealed an increase in the delamination factor with higher feed rates for twist drill and Jo geometries, whereas the parabolic drill showed a decrease in this factor. Conversely, the delamination factor decreased with

increasing spindle speed for twist and Jo geometries, while it slightly increased with the parabolic drilling geometry.

Kumar et al[159]. Investigated delamination during the drilling process of sisal/banana fiber reinforced composites, which were manufactured with a volume ratio of (20:80) for fiber to matrix using the hand stratification method. The drilling operations on these bio composites involved three carbide tools with diameters of 6, 8, and 10 mm, along with three varying feed rates (50, 100, and 150 mm/min) and three different spindle speeds (500, 1000, and 1500 rpm). Their findings revealed a consistent reduction in the delamination factor as spindle speed increased across all machining scenarios. Optimal drilling conditions were achieved at 1500 rpm, 50 mm/min feed rate, and a 6 mm drill diameter.

Sridharan et al[160]. Conducted an experimental investigation on the impact of matrix type, fiber treatment, and graphene addition on delamination during the drilling of a nano-hybrid jute/epoxy composite. Woven jute fabric and two different resins, polyester and epoxy, were utilized for specimen preparation. The jute fibers underwent a surface treatment with 5% NaOH for 2 hours. Graphene was incorporated into the resin at three concentrations: 0.3 wt% (denoted as lowest-L), 1 wt% (middle-M), and 3 wt% (highest-H). High-speed steel (HSS) twist drills were employed for drilling, with spindle speeds ranging from 500 to 1400 rpm and feed rates from 0.03 to 0.12 mm/rev. The findings revealed that epoxy outperformed polyester, and the alkali treatment of fibers significantly enhanced the drilled hole quality, showing maximum improvements of 3.3% and 12.5% at the entrance and exit, respectively, in T-JFRP. Moreover, increasing graphene content in the resin resulted in reduced delamination at higher spindle speed and feed rate levels, with the maximum reductions observed at 5.4% and 13.8%, 6.4% and 10.9%, and 7.1% and 17.5% in L, M, and H-JFRP, respectively. Similar to prior research, the delamination factor was observed to increase with both spindle speed and feed rate.

Pramod et al[161]. Concurred with the findings of the aforementioned research in their investigation, focusing on the assessment of drilling-induced delamination in nanoparticle-reinforced polymer matrix composites. The study involved drilling all samples using Brad and Spur type carbide tools with diameters of 5, 6, 8, and 10mm. Various feed rates (0.5, 1.0, 1.5, and 2 mm/rev) and spindle speeds (1000, 1500, 2000, and 2500 rpm) were applied under dry conditions. The results indicated that minimizing delamination damage and achieving a better circularity ratio were associated with higher spindle speeds, smaller drill diameters, and lower forward speeds.

Chaudhary et al[162].Explored the impact of varying feed rates (0.05, 0.15, 0.25 mm/rev), spindle speeds (1500, 3000, 4500 rpm), and drill point angles (90º, 104º, 118º) on the machining characteristics of bi-directional cotton polyester composites during the drilling process. The study

utilized Taguchi's analysis, ANOVA, and regression analysis for data analysis. The research findings suggest that, within the tested range of variables, achieving superior hole quality (Thrust force (TF) = 9.85 N, delamination factor (DF) = 1.1446, and torque = 0.0083 Nm) was associated with lower feed rates (0.05 mm/rev), reduced point angles (90°), and higher cutting speeds (4500 rpm). Furthermore, the study revealed that the mathematical models proposed exhibited a strong correlation between the predicted values and the experimental outcomes for process and machinability parameters (The adjusted R2 value was 94.79% for TF, 83.26% for torque, and 90.93% for DF).

Vinayagamoorthy et al [163]. Conducted a study focused on investigating the drilling parameters (feed rates: 0.2, 0.4, 0.6 mm/rev; spindle speeds: 1000, 2000, 3000 rpm; and point angles: 60°, 90°, 120°) for a natural fiber-reinforced composite. In this study, chemically treated vetiver was employed as a reinforcing element, constituting a reinforcement/matrix composition of 25%/75% w.t. The researchers utilized a central composite design-based fuzzy logic methodology to optimize machining parameters and simultaneously evaluated the resulting defects and cutting forces during the drilling process on these composite materials. The study revealed that the primary factors influencing the entry defect were the feed rate and point angle, with the drilling speed showing negligible impact on the entry defect. In contrast, the exit defect was primarily influenced by the drilling speed, feed rate, and point angle. The optimal drilling conditions were identified as 1450 rpm, 0.2 mm/rev, and a 60° angle for spindle speed, feed rate, and point angle, respectively.

Diaz Alvarez et al[164]. Conducted a research study focusing on the experimental analysis of drilling-induced damage in aramid composites. These composites were manufactured with a density of 8.86 kg/m^2 and were in the form of rectangular sheets measuring 200 × 28 × 3.5 mm^3, consisting of 12 layers of aramid fabric impregnated in a phenolic matrix. Their findings indicated that using a 110° drill resulted in reduced delamination at both entry and exit sides. Conversely, employing a 118° drill demonstrated improved delamination performance at both sides of entry and exit when higher feed rates and cutting speeds were applied.

I.8 Conclusion

The preliminary chapter presents a comprehensive overview of the properties, applications, and experimental analyses related to composite materials. Through a detailed exploration of various composite types, including natural fiber-reinforced composites. One of the key results discussed in the chapter is the enhanced mechanical properties of composites reinforced with natural fibers such as palm fiber. The unique characteristics of palm fiber, including its strength

and durability, make it a promising reinforcement material for composite applications. Experimental studies on water absorption behavior and machinability parameters of composite materials provide valuable insights into optimizing fabrication processes and enhancing performance. Moreover, the chapter emphasizes the importance of understanding drilling parameters and machinability characteristics for natural fiber-reinforced composites, as demonstrated in studies focusing on drilling-induced damage and optimization of machining parameters. The findings underscore the significance of selecting appropriate drilling conditions to minimize defects and improve the overall quality of machined composite components. Overall, the chapter serves as a valuable resource for researchers, engineers, and industry professionals interested in composite materials, offering insights into material properties, fabrication techniques, and performance optimization strategies. The results presented in the chapter contribute to the ongoing efforts to develop sustainable and high-performance composite materials for a wide range of industrial applications.

Chapter II

Materials and Methods

II Chapter II: Materials and Methods

II.1 Introduction

The second chapter of the thesis focuses on the Materials and Methods employed in the investigation of bio composites reinforced with date palm fibers. This section is crucial for understanding the experimental protocols, data collection techniques, and analytical approaches utilized in the study. It outlines the systematic procedure followed for extracting date palm fibers, preparing bio composites, and examining their physical attributes and machinability. The chapter explores various methodologies such as artificial neural networks (ANN), response surface methodology (RSM), and the Taguchi method, underscoring their significance in the analysis and optimization of bio composite materials. Detailed explanations, equations, and diagrams are provided to elucidate the modeling processes and flowcharts associated with these methodologies.

Moreover, the chapter delves into the absorption behavior of date palm fiber/Iso-polyester composites, shedding light on the diffusion coefficient and water uptake characteristics of the materials. It also presents the physical and chemical properties of the liquids used in the research, providing valuable insights into the environmental conditions during the testing of bio composites. Additionally, it investigates the drilling behavior of date palm fiber/Iso-polyester composites with a 40% fiber rate (DPFP40) and Palm fiber powder/epoxy composites (PFPEs), explaining the delamination factor, circularity, and cylindricity errors of drilled holes.

II.2 Fiber extraction

The fibers were obtained from the cluster arms of date palm trees cultivated in Biskra, Algeria. Initially, the cluster arms were immersed in distilled water for around 30 days to ease the fiber extraction process [165]. Subsequently, the stems underwent peeling to remove the outer layer. The fibers were then delicately separated from the lignin by gently rubbing the surfaces of the cluster arms with a hammer and a wire brush, ensuring minimal damage to the fibers. (Refer to **Figure II-1**)

Figure II-1: The different steps for fiber extraction.

II.3 Preparation of developed bio composites

In this study, three types of bio composites were developed to investigate their physical, mechanical properties, and machinability, comprising:

II.3.1 The first type of developed bio composites: Date Palm Fibers/ Iso-polyester (DPFPs)

The bio composites were fabricated in three different configurations: unidirectional (UD) and crossed (C), with ply numbers ranging from 2 to 4. DPFPs were formulated with Iso-polyester matrix mass fractions of 85%, 80%, and 73%, along with date palm fiber reinforcements of 15%, 20%, and 27%, respectively. Iso-polyester resin was chosen for its cost-effectiveness and ease of handling, commonly preferred in marine applications due to its high wax content and low water absorption rate. Vacuum molding, employing the 'bag' technique, was utilized for the fabrication of all bio composites (27 samples). Following fabrication, the specimens were subjected to a 70°C oven treatment for 24 hours to ensure complete polymerization and moisture removal. All specimens were then cut into rectangular pieces measuring $50\times15\times5mm^3$, adhering to the AFNOR 57-101 standard. The specific sample configurations used in this study are detailed in **Table II-1**.

Table II-1: Formulation and composition of DPFPs composites.

Sample	Fiber content	Some samples used
DPFP 1 (UD-2 plies)	15%	
DPFP 2 (C-3 plies)	20%	
DPFP 3 (UD-4 plies)	27%	

II.3.2 The second type of developed bio composites: Date Palm Fibers/ Iso-polyester (DPFP40)

A bio composite of date palm fiber /Iso-polyester was created with a reinforcement volume fraction of 40% by weight. Fabrication involved utilizing a vacuum molding technique to create two equally crossed plies of fibers, each ply measuring 5mm thick. The resulting sample was shaped into a rectangular piece measuring 240×55×8 mm^3, as illustrated in **Figure II-2**. Subsequently, the sample underwent 20 hours curing process in an oven set at 75°C to ensure thorough polymerization. Following curing, the sample was cut into three equal pieces for dedicated use in the drilling process.

Figure II-2: DPFP40 composite: (a) top view, and (b) side view.

II.3.3 The third type of developed bio composites: Palm Fibers Powder / Epoxy (PFPEs)

Following the fiber extraction process, the fibers underwent crushing using a PULVERISETTE 6 planetary mono-mill with a maximum speed of 650 rpm. Fibers measuring 630 µm in length were specifically chosen through sieving analysis.

Epoxy was selected as the matrix for this type of bio composite, being a thermosetting polymer widely utilized in industries requiring both lightweight and high-strength materials, such as aeronautics, automotive, shipbuilding, and others. This matrix type was preferred due to its distinct characteristics, including high mechanical strength, rigidity, dimensional stability, chemical resistance, thermal resistance, and ease of processing.[166-168]

The palm fiber powder epoxy (PFPE) composite comprised 18% by weight of palm fiber powder reinforcement. A total of 27 specimens were manufactured using a molding technique, with fibers randomly dispersed within the matrix. These specimens were shaped into rectangular pieces measuring 50 × 25 × 10 mm^3 (length × width × thickness). Afterward, they were left to cure at room temperature (25°C) for 72 hours to allow the structure to solidify, facilitating easy removal from the mold. Subsequently, the specimens were placed in an oven set at 50°C for 12 hours to ensure complete polymerization [169, 170].(Refer to **Figure II-3**)

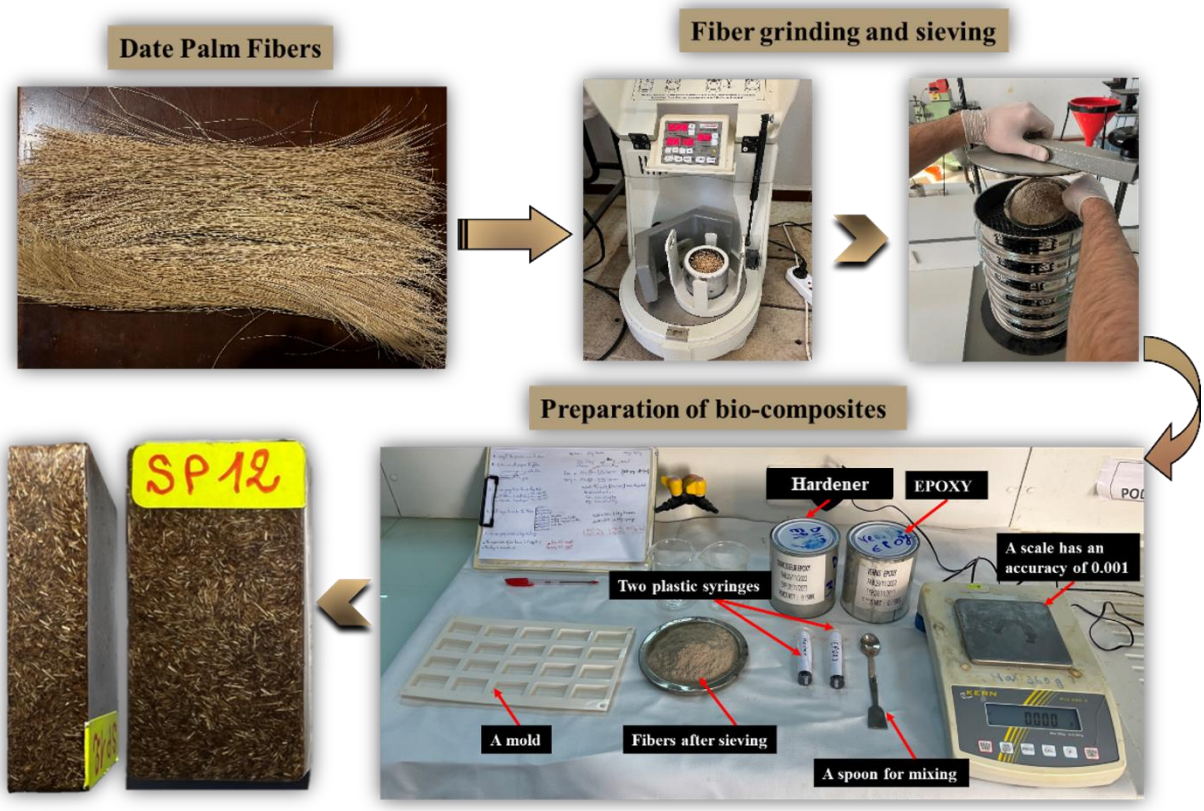

Figure II-3: PFPEs manufacturing steps.

II.4 Experimental tests

II.4.1 Absorption test

II.4.1.1 Evaluation of water absorption property of DPF and DPFPs

The water absorption characteristics of DPFPs were assessed following the ISO 62:1999 standard protocol[171]. Initially, specimens were oven-dried at 70°C for 24 hours and subsequently cooled to room temperature (25°C). After precise weighing using a PLS360-3 type balance with a 0.001 g precision, the dried samples were immersed in 50 mL containers filled with three distinct types of water (distilled water, seawater, and rainwater) each with experimentally determined properties (refer to **Table II-2**), all maintained at room temperature (25°C). At 24-hour intervals, the specimens were removed, gently blotted to eliminate excess surface moisture, and then reweighed. This procedure was repeated over a span of six days, with subsequent weight measurements taken every 48 hours for a total duration of 24 days, completing a 30-day evaluation period. (Refer to **Figure II-4**)

Concurrently, the water absorption properties of date palm fibers (DPF) were investigated using three identical masses (5 g each), each immersed in separate graduated test tubes filled with the fluids specified for this study (80 mL per liquid), as depicted in **Figure II-5**. The amount of water absorbed was monitored at two-hour intervals over a 20-hour period. The relative water absorption (*Mt*) was calculated using Equation **II-1**:

$$Mt = \frac{Wt - W0}{W0} \qquad \textbf{(II-1)}$$

Here, W_t denotes the current weight of the sample at time *t*, and W_o represents the initial weight of the sample.

The mechanism of water absorption in bio composites can be elucidated by Fick's second law of diffusion, expressed as:

$$\frac{\mathrm{Mt}}{\mathrm{Ms}} = 1 - \frac{8}{\pi^2}\sum_{\mathrm{n}=0}^{\infty}\frac{1}{(2\mathrm{n}+1)^2}\exp\left[-\frac{(2\mathrm{n}+1)^2\pi^2\mathrm{Dt}}{\mathrm{h}^2}\right] \qquad \textbf{(II-2)}$$

Here, M_t represents the water uptake at time *t*, M_s denotes the water uptake when the sample is fully saturated, *n* is the summation index, and *D* signifies the diffusion coefficient[172-174].

Table II-2: Physical and chemical properties of the liquids used.

Type of liquid	Density (g/cm^3)	pH	Conductivity (mS/m) $\times 10^{-3}$	TAC (mol/L) $\times 10^{-3}$	Chloride content (mg /L)	Hardness (°f)
Distilled water	0.966 ± 0.014	6.635 ± 0.191	6.000 ± 0.003	1.4	3.2	14
Seawater	1.025 ± 0.015	6.565 ± 0.346	4965 ± 0.064	5.4	19000	28
Rainwater	0.907± 0.066	7.750 ± 0.212	9.000 ± 0.001	3.2	3	13

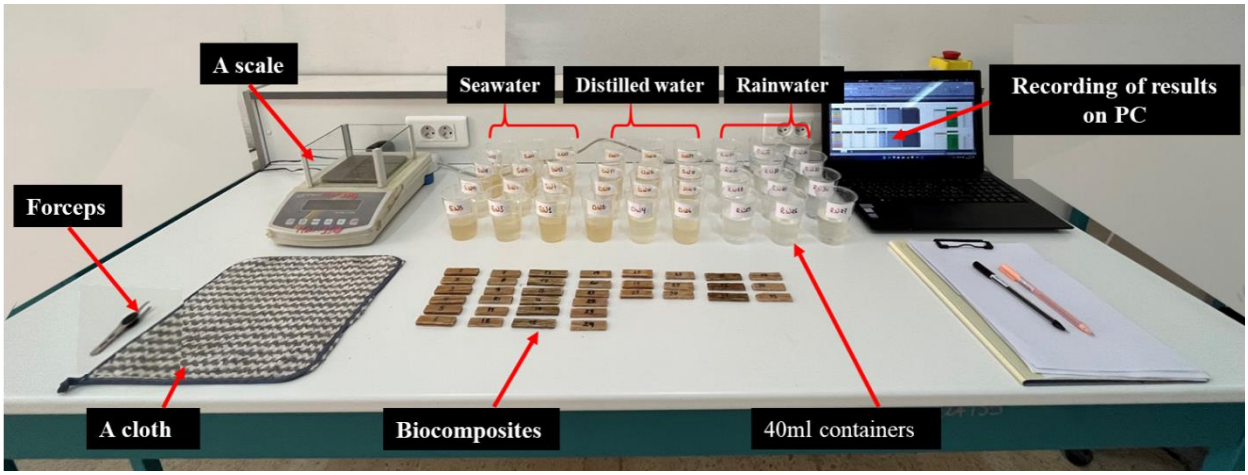

Figure II-4: Assessment of the water absorption characteristics of DPFPs.

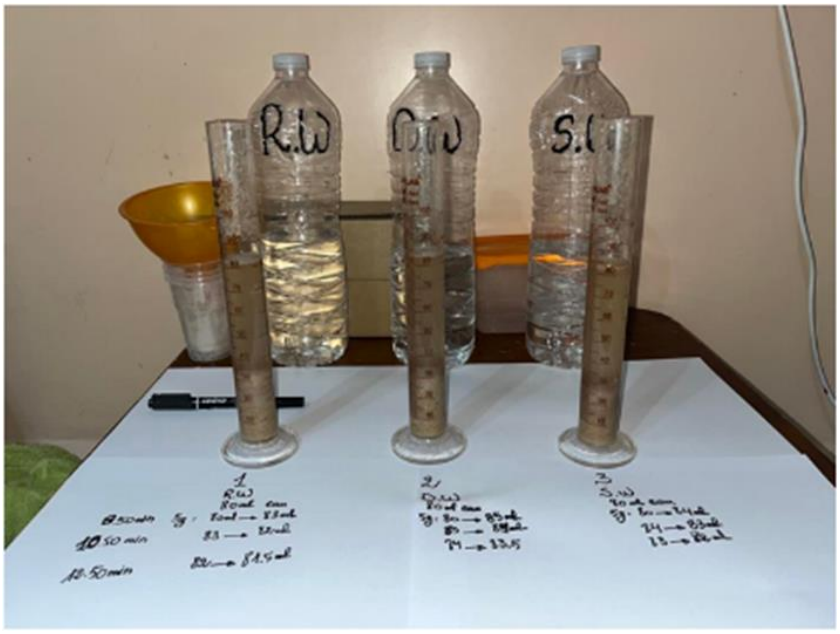

Figure II-5: Water absorption evaluation of date palm fiber (DPF).

II.4.1.2 Diffusion coefficient of DPFPs

The primary function of the diffusion coefficient (*D*) lies in characterizing the capacity of water molecules to permeate and traverse the structure of bio composites. Consequently, the diffusion coefficient assumes a pivotal role in comprehending the absorption behavior exhibited

by bio composites[175, 176]. It is influenced by diverse factors, including the material's porosity, the characteristics of the matrix, and the type and alignment of reinforcing fibers. The determination of the diffusion coefficient contributes significantly to enhancing the design and performance of bio composite materials tailored for specific applications. This is particularly crucial in scenarios where water absorption can exert substantial impacts on both the structural integrity and overall functionality of the material, The diffusion coefficient is an important factor in Fick's law. By solving the diffusion equation, we get the following relation (Equation **II-3**)[177]:

$$\frac{Mt}{Ms} = \frac{4}{h}\sqrt{\frac{Dt}{\pi}} \qquad \textbf{(II-3)}$$

The diffusion coefficient can be determined using Equation (**II-4**):

$$D = \pi\left(\frac{kh}{4M_s}\right)^2 \qquad \textbf{(II-4)}$$

Here, k represents the initial slope observed in a plot of M_t against $\sqrt{t}$, M_s denotes the maximum weight gain, and h stands for the thickness of the sample.

II.4.1.3 The porosity of natural fibers

The porosity of natural fibers refers to the presence of voids or pores within their structure, with these spaces varying in size and being inherent to the porous nature of materials such as wood, bamboo, or plant fibers[178-180]. The role of the porosity of natural fibers is crucial in the water absorption behavior of bio composites, as these fibers can act as pathways for water, allowing moisture to penetrate into the structure of the bio composite[181]. A high porosity of natural fibers increases the water absorption capacity of the bio composite, which can be beneficial in certain applications where water absorption is desired, such as to improve fire resistance or in thermal insulation applications[182]. However, excessive porosity can lead to excessive water absorption, which may alter the mechanical properties of the bio composite and result in premature degradation[183](refer to **Figure II-6**). The current investigation seeks to analyze and determine the porosity of palm fibers, intending to evaluate the extent to which these fibers influence the water absorption behavior of bio composites.

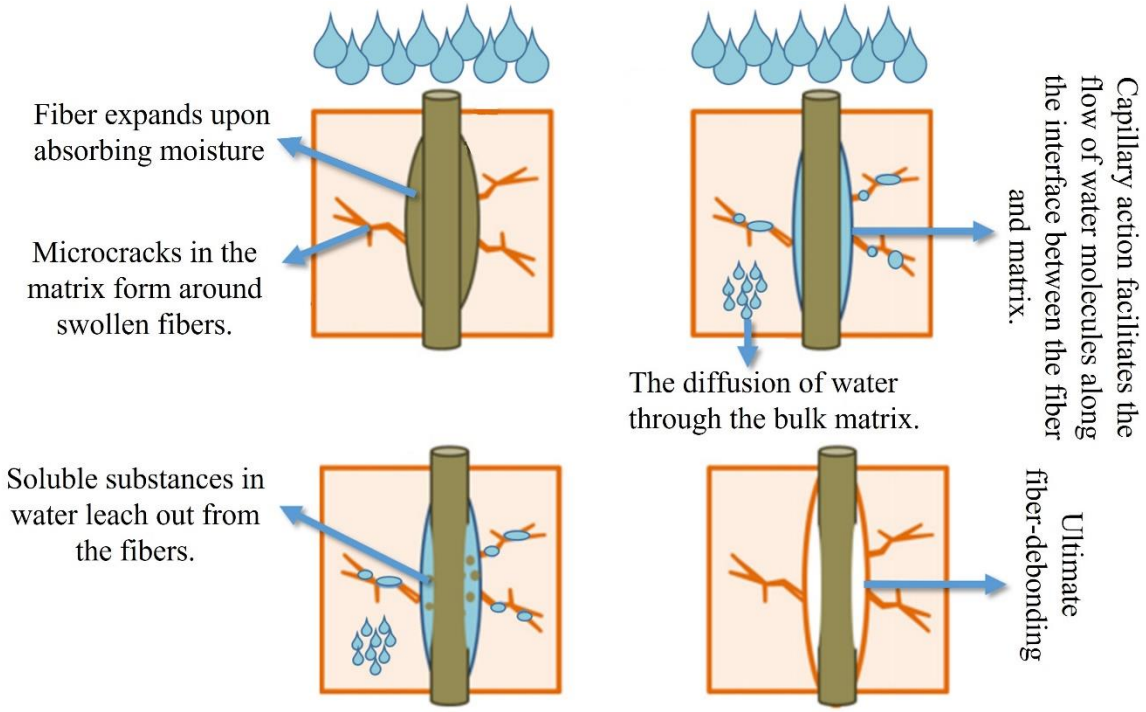

Figure II-6: Impact of water on the interface between fiber and matrix[131].

II.4.2 Drilling test

II.4.2.1 Drilling procedure for DPFP40

The drilling experiments were conducted utilizing a DOOSAN DNM 6700 universal CNC milling machine equipped with a spindle rotating at 8000 rpm and a feed speed ranging from 3.6 to 1200 mm/rev (refer to **Figure II-7**). The sample developed was divided into three specimens measuring 80×55×8 mm³ each. Three distinct types of drill bits were employed: a high-speed steel drill bit with a TiN protective layer (HSS-TITAN), a carbide drill bit (HSS-CARBIDE), and a super high-speed steel drill bit (HSS-SUPER), all having a uniform diameter of 10 mm.

Additionally, three spindle speeds (560, 1120, and 2240 rpm) and three feed speeds (40, 80, and 200 mm/min) were utilized, with cutting conditions summarized in **Table II-3**. The selection of these cutting parameters was informed by a comprehensive literature review, as outlined in **Table II-4**. Each drill was used to create nine holes per plate, resulting in a total of 27 holes drilled. The drilling took place under dry-cutting conditions, and the hole depth could reach up to 8 mm, corresponding to the sample thickness.

The drilling process was programmed on a CNC machine using MasterCam software. Initially, two-dimensional parts (2D) were designed, which were then converted into three-dimensional parts (3D), considering precise geometric dimensions. The center of the sample served as the reference point for drilling (hole center 2:2). The drill moved along the x-axis at a distance of 25 mm and along the y-axis at a distance of 15 mm in both positive and negative directions for

each drilling center (refer to **Figure II-8a**) ranging from order 1:1 to 3:3 (9 holes) for the first plate, order 4:4 to 6:6 for the second plate, and order 7:7 to 9:9 for the third plate. Subsequently, separate operating conditions for spindle speed and feed were established for each hole, and the same process was iterated for all three drill bits (27 drilling operations). The entire procedure was executed in multiple stages, beginning with the selection of the machine type (default milling), followed by the choice of the path (drilling), and subsequent adjustments to working conditions for each drilling operation. Ultimately, G-code programs were automatically generated by the G-code generation module in MasterCam based on fundamental information about machining features, including basic dimensions and cutting specifications[184]. (**Figure II-8c**). The latter translates the part's geometry and cutting parameters into preparatory functions G and auxiliary functions M (such as G90 for absolute programming, G80 for cancelation of drilling cycles, G83 for Peck drilling cycle, M3 for spindle rotation clockwise, etc.), facilitating the implementation of manufacturing conditions by the CNC machine[185].

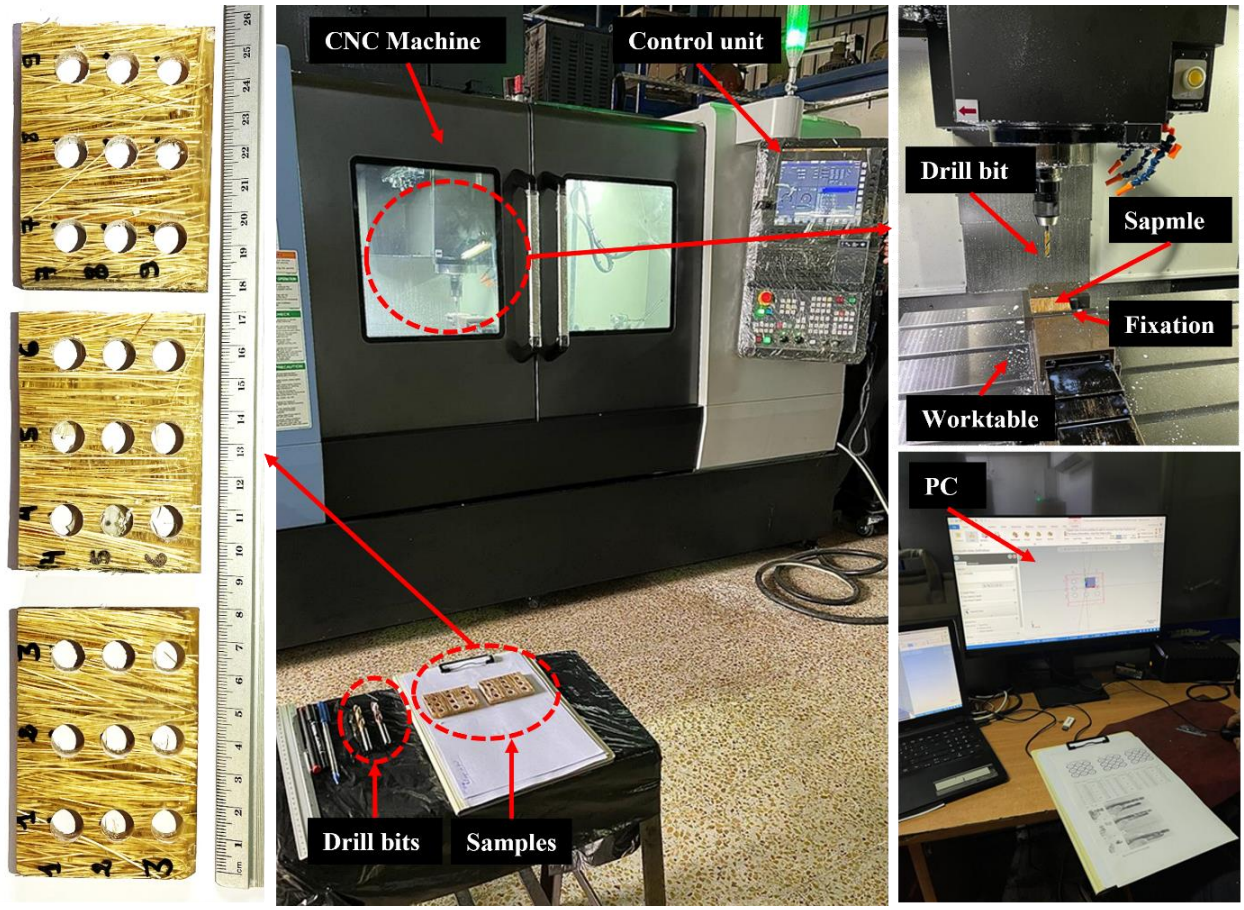

Figure II-7: Configuration for drilling of DPFP40 using the DOOSAN DNM 6700 CNC machine.

Table II-3: Machining conditions during drilling DPFP40.

N°	Factor	Notation	Unit	Level		
				-1	0	+1
A	Spindle speed	N	tr/min	560	1120	2240
B	Feed rate	*f*	mm/min	40	80	200
C	Drill material	~	~	T1: HSS TITAN	T2: HSS CARBIDE	T3: HSS SUPER

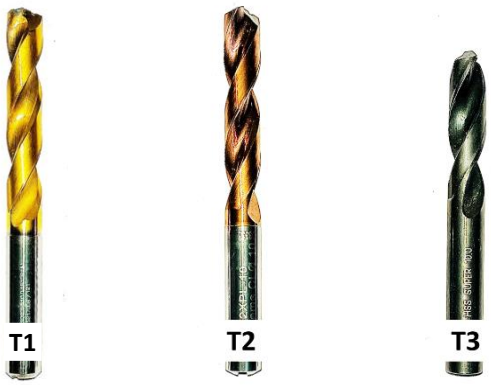

Table II-4: Machining parameters available in the literature for drilling bio composites.

Fiber	%	Matrix	Cutting parameters				Ref
			f (mm/min)	N (mm/min)	Drill material	d (mm)	
Hemp	52	Polyester	100,200, 300	1000, 1500,2000	Carbide drill	5	[186]
Bamboo and basalt	~	Epoxy	0.08, 0.125, 0.20	450,710, 1120	Standard twist drill-carbide	6	[187]
Rice husk	10	Polyester	0.1, 0.15, 0.2	1500, 2000,2500	twist 118° drill, brad drill, endmill	6	[188]
flax and Jute fabric	~	Epoxy	0.01, 0.015, 0.020	2500, 5000, 7500	HSS, HSS-TiN, WC	4	[189]
Unidirectional jute	30	Polypropylene	0.1, 0.2, 0.3	600, 1260 2700	HSS, Co-HSS	2,3, 4	[190]
Glass-sisal-jute	~	Polyester	0.04, 0.06, 0.08	1000, 2000, 3000	Brad and spur, coated carbide	6, 9, 12	[191]
Palm	**40**	**iso-polyester**	**40, 80,200**	**560, 1120,2240**	**HSS-TITAN, HSS-CARBIDE, HSS-SUPER**	**10**	**Our work**

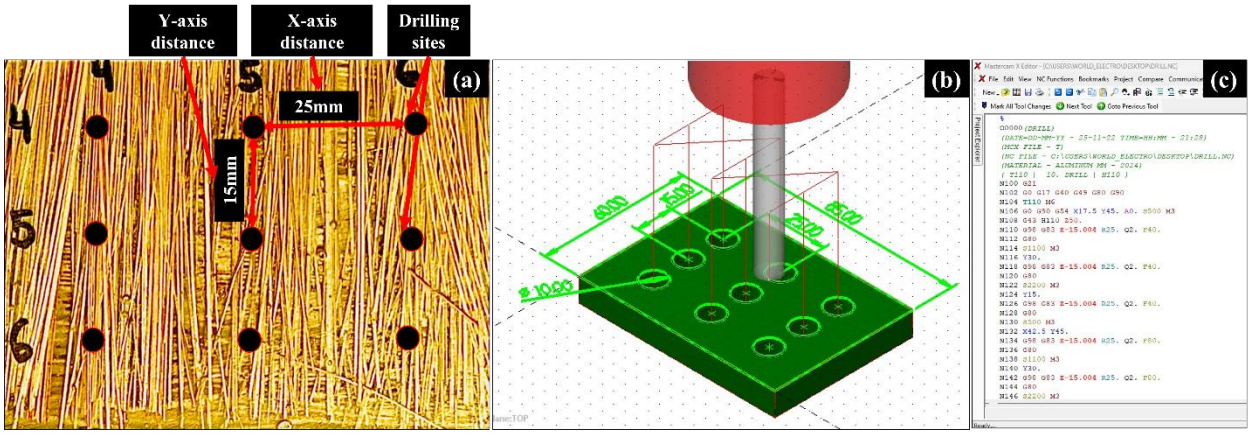

Figure II-8: (a) A depiction revealing the locations of the holes, (b) the drilling simulation in MasterCam, and (c) the G-code program.

II.4.2.2 Drilling procedure for PFPEs

The PFPEs drilling procedure was executed utilizing a LEADWELL V-40 CNC machine, where the spindle operated at speeds ranging from 10 to 10,000 rpm, and a feed rate of 3.0 to 2000 mm/min was maintained, employing 10 mm diameter drilling tools (HSS-SUPER). Various point angles (85°, 115°, and 135°), spindle speeds (500, 1000, and 1500 rpm), and feed rates (50, 100, and 150 mm/min) were employed. To ensure the production of high-quality holes, a specific approach was adopted.

Initially, meticulous preparation of the CNC apparatus was carried out to ensure accurate installation and calibration. Following this, the drilling process was programmed utilizing MasterCam 2021 software. This involved defining the drilling trajectory, including the initiation and cessation points, drilling depths, as well as determining the spindle speed and feed rates required for each hole. The central reference point for drilling was established at the center of the sample. The drill bit was guided along the x-axis for 25 mm and along the y-axis for 25/2 mm in both positive and negative directions from the drilling center. Upon completion of the programming, a G-Code was generated. In the subsequent phase, the drill bits were securely affixed within the machine's tool holder, and the samples were firmly clamped onto the machine table using the screw clamping technique to minimize undesirable vibrations during the drilling process[192]. The executed G-Code initiated the drilling process, prompting the CNC machine to autonomously perform the designated drilling procedure according to the specified cutting parameters [184, 193, 194]. The drilling process underwent careful examination to identify any potential issues, such as excessive vibrations, chipping, or positional discrepancies. Finally, after completing the drilling process, the specimens were removed from the CNC machine, and a

comprehensive inspection of the drilled holes was conducted to verify their compliance with the prescribed specifications in terms of depth and diameter (refer to **Figure II-9** and **Table II-5**).

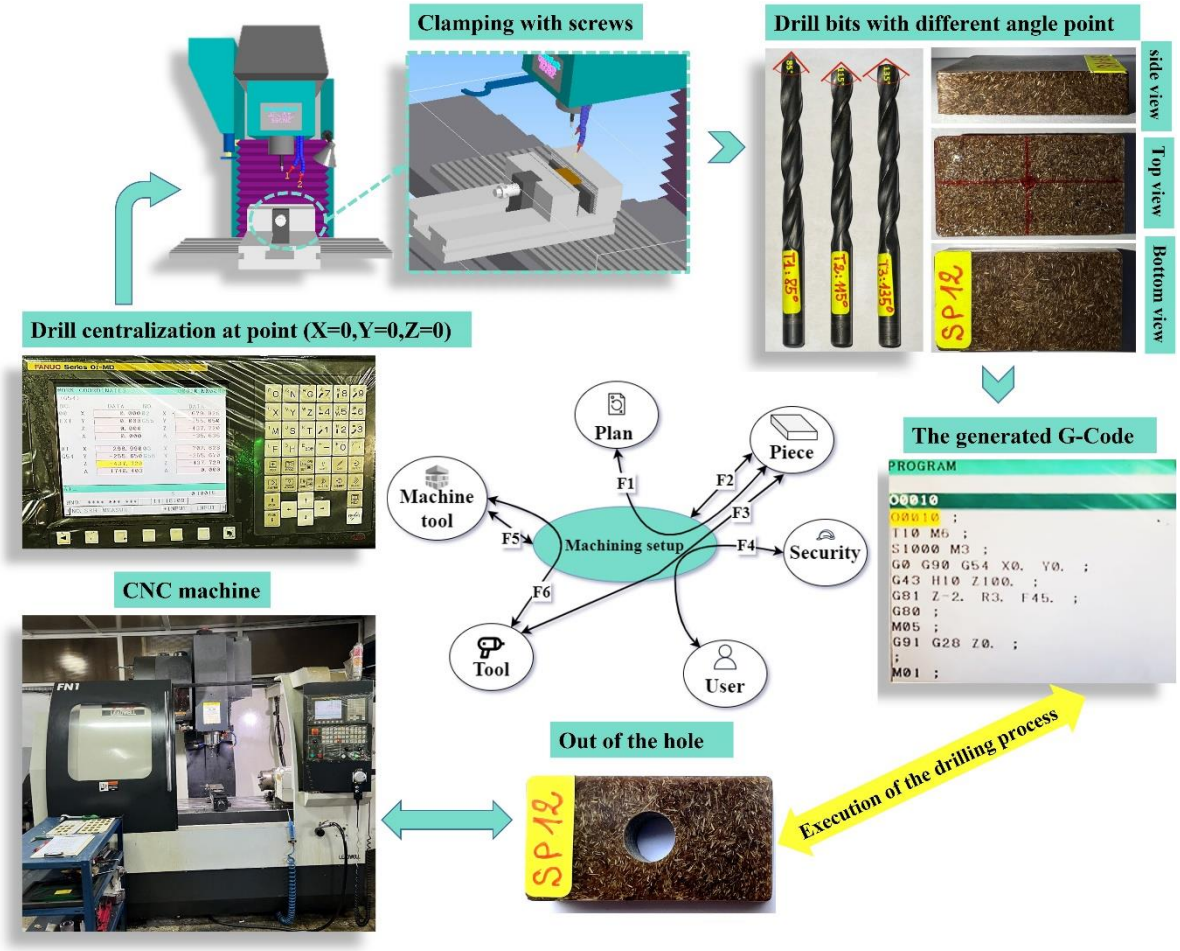

Figure II-9: Configuration of the drilling process using the LEADWELL V-40 CNC machine.

Table II-5: The functions of the machining fixture.

N°	The functions of the machining fixture
F1	The machining setup must allow compliance with the plan.
F2	The machining setup must allow the part to be placed in an isostatic position.
F3	The machining setup must allow the part to be maintained in isostatic position during machining.
F4	The machining setup must allow the operator (user) to machine the part in complete safety.
F5	The machining setup must be adapted to the machine tool used.
F6	The machining fixture must resist the forces of the tool during cutting.

Table II-6: Representative specimens at the exit of holes (push out) after the drilling process.

		50 mm/min	100 mm/min	150 mm/min
HSS-SUPER 85°	500 rpm			
	1000 rpm			
	1500 rpm			
HSS-SUPER 115°	500 rpm			
	1000 rpm			
	1500 rpm			
HSS-SUPER 135°	500 rpm	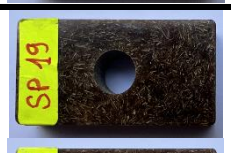		
	1000 rpm			
	1500 rpm			

II.4.2.3 Assessment of hole geometry

II.4.2.3.1 Evaluation of delamination for drilled holes of DPFP40

Delamination poses a significant challenge in achieving high-quality drilled holes in composite CRFNs. To assess the varying degrees of these defects resulting from hole manufacturing, post-drilling, the samples were subjected to microscopic examination to observe the damage incurred during the drilling process. The delamination factor at the exit of the drilled holes was determined using the free software *Image J*, as depicted in **Figure II-10**. This delamination factor is calculated as the ratio of diameters between the maximum delamination diameter (D_{max}) and the drill diameter, expressed by the following equation **II-5**:

$$F_d = \frac{D_{max}}{D_{drill}} \qquad \textbf{(II-5)}$$

In this context, D_{max} denotes the maximum damage diameter, while D_{drill} refers to the drill diameter[195] .

The delamination factor in this investigation is computed using the subsequent equation **II-6**:

$$F_d = \frac{A_{max}}{A_{nom}} \qquad \text{(II-6)}$$

Here, A_{max} denotes the maximum damage area surrounding the periphery of the hole, while A_{nom} represents the area associated with the actual hole[196].

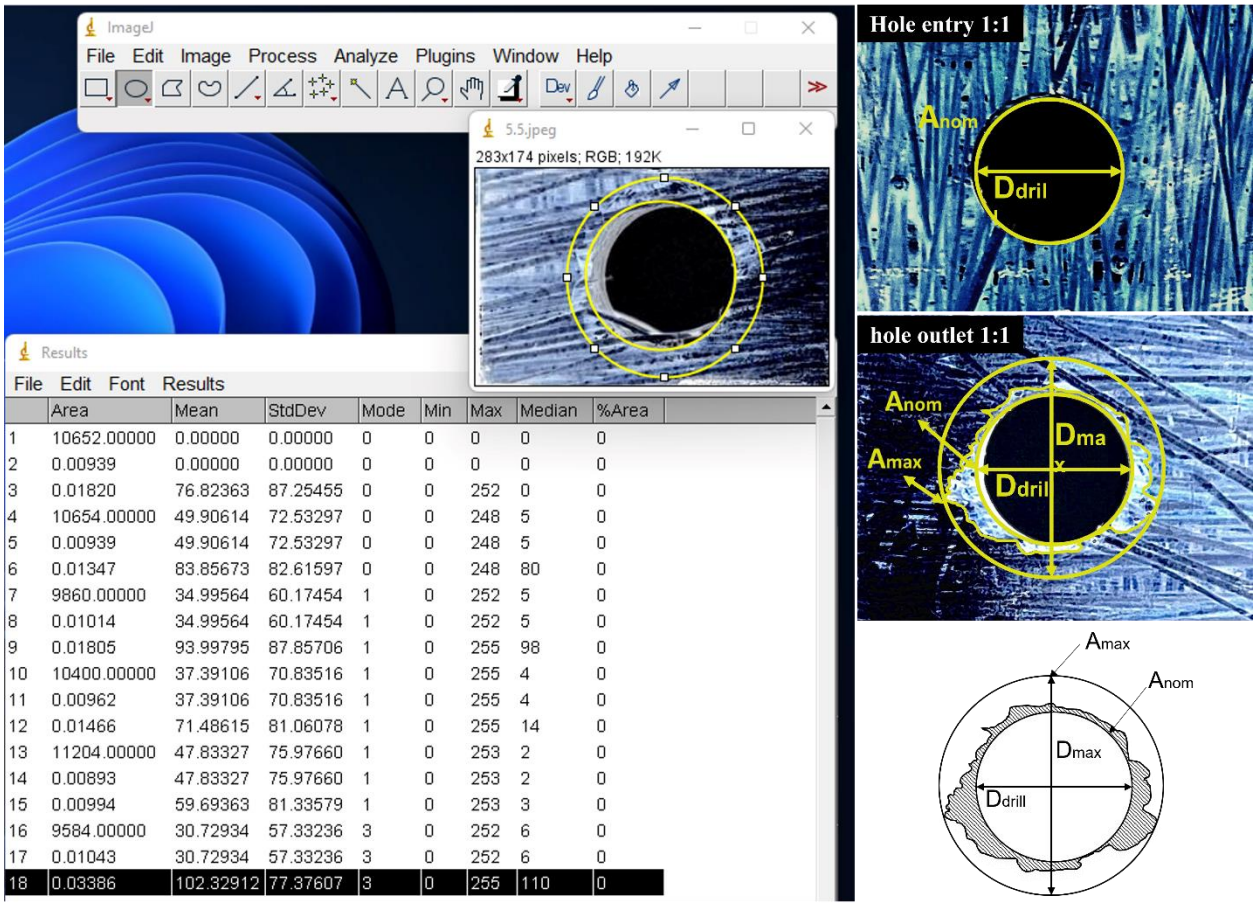

	Area	Mean	StdDev	Mode	Min	Max	Median	%Area
1	10652.00000	0.00000	0.00000	0	0	0	0	0
2	0.00939	0.00000	0.00000	0	0	0	0	0
3	0.01820	76.82363	87.25455	0	0	252	0	0
4	10654.00000	49.90614	72.53297	0	0	248	5	0
5	0.00939	49.90614	72.53297	0	0	248	5	0
6	0.01347	83.85673	82.61597	0	0	248	80	0
7	9860.00000	34.99564	60.17454	1	0	252	5	0
8	0.01014	34.99564	60.17454	1	0	252	5	0
9	0.01805	93.99795	87.85706	1	0	255	98	0
10	10400.00000	37.39106	70.83516	1	0	255	4	0
11	0.00962	37.39106	70.83516	1	0	255	4	0
12	0.01466	71.48615	81.06078	1	0	255	14	0
13	11204.00000	47.83327	75.97660	1	0	253	2	0
14	0.00893	47.83327	75.97660	1	0	253	2	0
15	0.00994	59.69363	81.33579	1	0	253	3	0
16	9584.00000	30.72934	57.33236	3	0	252	6	0
17	0.01043	30.72934	57.33236	3	0	252	6	0
18	0.03386	102.32912	77.37607	3	0	255	110	0

Figure II-10: Quantification of the delamination factor utilizing *Image J* software.

II.4.2.3.2 Evaluation of circularity and cylindricity for drilled holes of DPFP40

Circularity and cylindricity are crucial geometric properties for perforations in bio composites, playing a significant role in the suitability, functionality, and overall effectiveness of bio composite components [197]. Consequently, this study emphasizes investigating these two parameters across the design, manufacturing, and quality assessment phases. A Coordinate Measuring Machine (CMM) employing a contact scanning technique was utilized to ascertain the values of these two parameters.

Circularity holds paramount importance due to its potential impact on fit, functionality, and the structural integrity of components. Opting for circular apertures is generally preferred for

several compelling reasons. Firstly, circular perforations facilitate a more uniform distribution of stresses compared to irregularly shaped openings, thereby reducing the risk of stress concentration-induced failures. Additionally, circular holes are often favored for their ease of manufacturing and ability to provide predictable performance characteristics, particularly in terms of fatigue resistance[198, 199]. The circularity values for the holes were obtained within a plane located 4 mm away from the drill exit point (**Figure II-11c**).

Similarly, maintaining cylindricity within holes is deemed essential due to its direct influence on achieving interference fits. Ensuring that apertures maintain a consistent diameter along their entire length is crucial to ensuring a precise match with mating components, thereby preventing undesirable outcomes such as loose connections and excessive friction. Furthermore, in fields where bio composites are utilized for fluid containment, meticulous adherence to cylindricality assumes critical importance as it acts as a barrier against leakage and inadvertent fluid seepage [200-202]. The cylindricity measurements were derived by averaging values obtained from scans conducted at three distinct plane levels, with a 2 mm separation between each level (**Figure II-11d**).

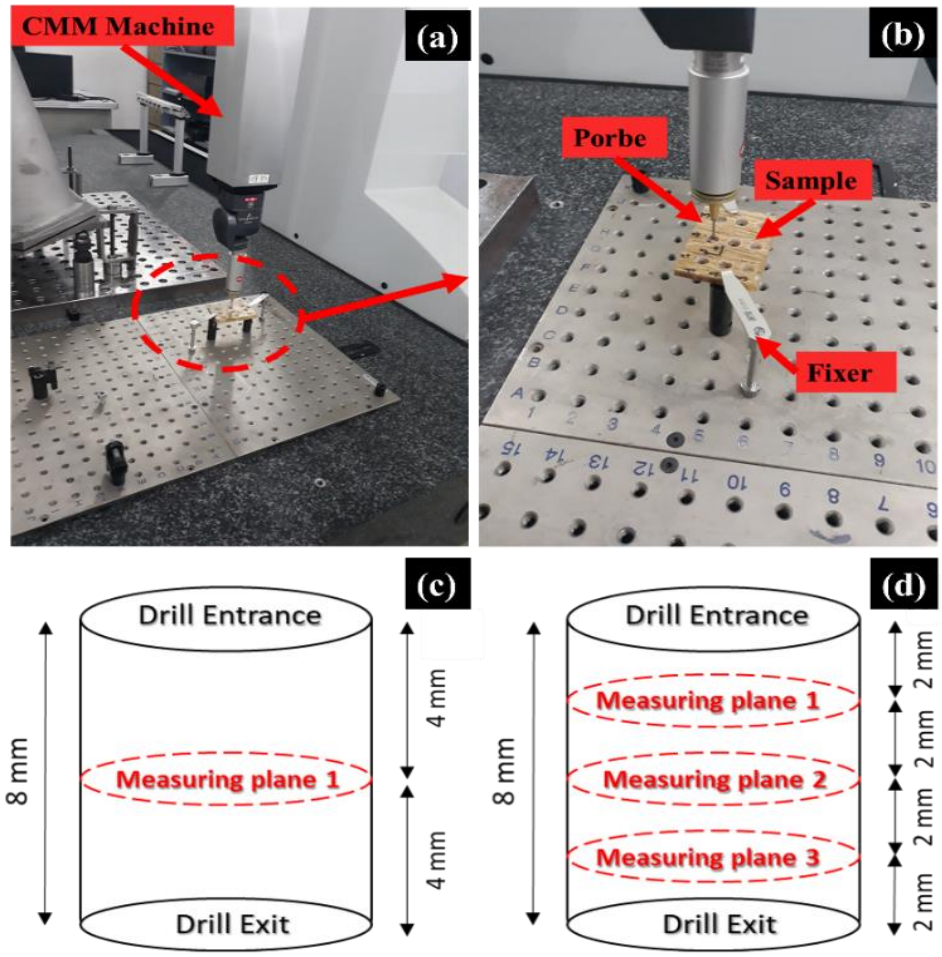

Figure II-11: (a, b) CMM Machine, (c, d) plans for measuring circularity and cylindricity errors in holes drilled into DPFPs.

II.4.2.3.3 Evaluation of circularity and cylindricity for drilled holes of PFPEs

The method used to assess circularity and cylindricity errors in holes drilled in PFPEs closely mirrored the procedure employed for DPFPs. These measurements were conducted at a comparable precision level. Specifically, circularity errors for PFPEs were evaluated within a plane positioned 5 mm from the drill entrance, while the average cylindrical errors were determined through scanning at three distinct levels, each separated by 2 mm. (Refer to **Figure II-12**)

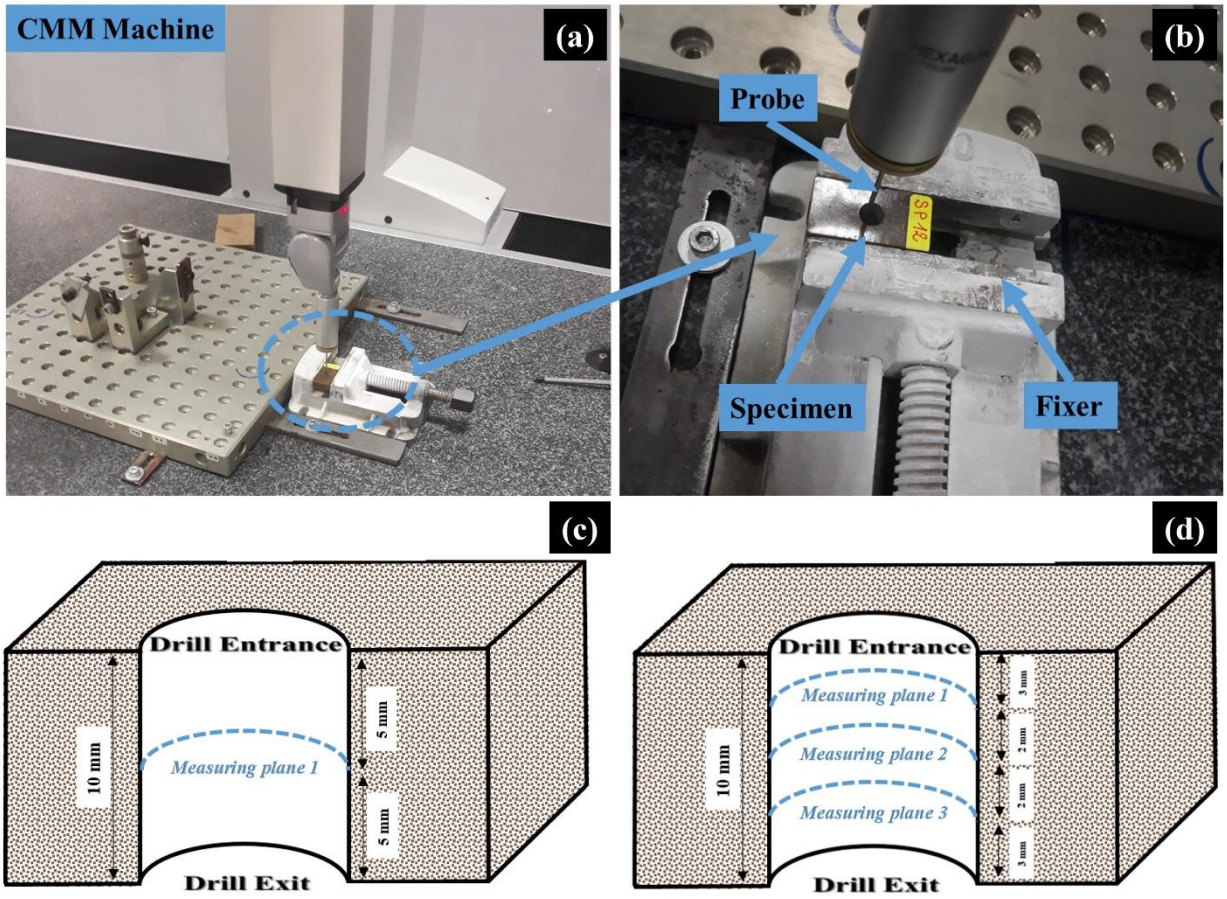

Figure II-12: (a, b) CMM Machine, (c, d) plans for measuring circularity and cylindricity errors in holes drilled into PFPEs.

II.5 Methods

Lately, the use of various methods of analysis and optimization has become essential in a wide range of studies. These methods are crucial for optimization as they enable the search for parameters or conditions that maximize or minimize a specific cost function or criterion, thereby improving the performance of the system or process. They are also pivotal in the field of modeling, where they are employed to develop mathematical or statistical models to represent and understand the relationships between variables in complex systems. Additionally, these methods are utilized to reduce data dimensionality, enhance performance, and make predictions using models to

anticipate future outcomes based on available data. Among the numerous methods commonly used in this field, such as linear regression, principal component analysis (PCA), finite element method (FEM), particle swarm optimization (PSO), genetic algorithm, sensitivity analysis, etc., the current focus is on three of the most significant methods in analysis and optimization: artificial neural networks (ANN), response surface methodology (RSM), and the Taguchi method.

II.5.1 Artificial Neural Networks (ANN)

The diagram depicted in **Figure II-13** illustrates the modeling methodology and flowchart of an artificial neural network (ANN). This network comprises interconnected units referred to as artificial neurons, which consist of the input layer (referred to as X_i), the hidden layer (referred to as H_j, according to Equation II-7), and the output layer (referred to as O_k, according to Equation II-8), with each unit being assigned a distinct weight (w_i). These units are connected through either mono-directional or bi-directional connectivity ($w_{ij}X_i$, H_jw_{jk})[203, 204].

Input parameters encompass a time range (from 24 to 672 hours), types of liquids (Sea, Distilled, and Rainwater), and fiber rates (15%, 20%, and 27%), while output parameters involve the water uptake rate by DPFPs (Mass of DPFPs). Additionally, input parameters include feed rates (40, 80, and 200 mm/min), spindle speeds (560, 1120, and 2240 rpm), and drill bit materials (HSS-TITAN, HSS-CARBIDE, and HSS-SUPER), with output parameters focusing on the delamination factor of drilled holes in DPFP40. Further input parameters consist of feed rates (50, 100, and 1500 mm/min), spindle speeds (500, 1000, and 1500 rpm), and various drill bit angles (85°, 115°, and 135°), while output parameters encompass circularity errors and cylindricity errors of drilled holes in PFPEs.

The training dataset encompasses 70% of the entire data, with 107, 19, and 19 samples allocated for testing DPFPs, DPFP40, and PFPEs, respectively. In the data validation phase, 20% comprises 31 samples for DPFPs, and 15% includes 4 samples each for both DPFP40 and PFPEs. For the data test phase, 10% comprises 15 samples for DPFPs, while 15% includes 4 samples each for both DPFP40 and PFPEs.

The Levenberg–Marquardt algorithm was employed to train the network, with 29 epochs utilized for the water uptake rate by DPFPs, 19 epochs for the delamination factor of DPFP40, and 5 and 6 epochs for circularity errors and cylindricity errors of PFPEs, respectively, using separate training sets. The implementation of the ANN structure was carried out using MATLAB software.

$$H_j = f(\sum w_{ij} X_i + \theta_j) \quad \text{(II-7)}$$

$$O_k = \sum H_j \, w_{jk} + b_k \quad \text{(II-8)}$$

In the context of the network, X_i represents input layer, H_j represents hidden layer, O_k denotes the output layer, f is the chosen activation function, w_{ij} signifies the weight between the i^{th} input and the jt^h neuron in the hidden layer, w_{jk} indicates the weight between the j^{th} neuron in the hidden layer and the k^{th} neuron in the output layer, and both θ and b stand for the bias parameters[205]

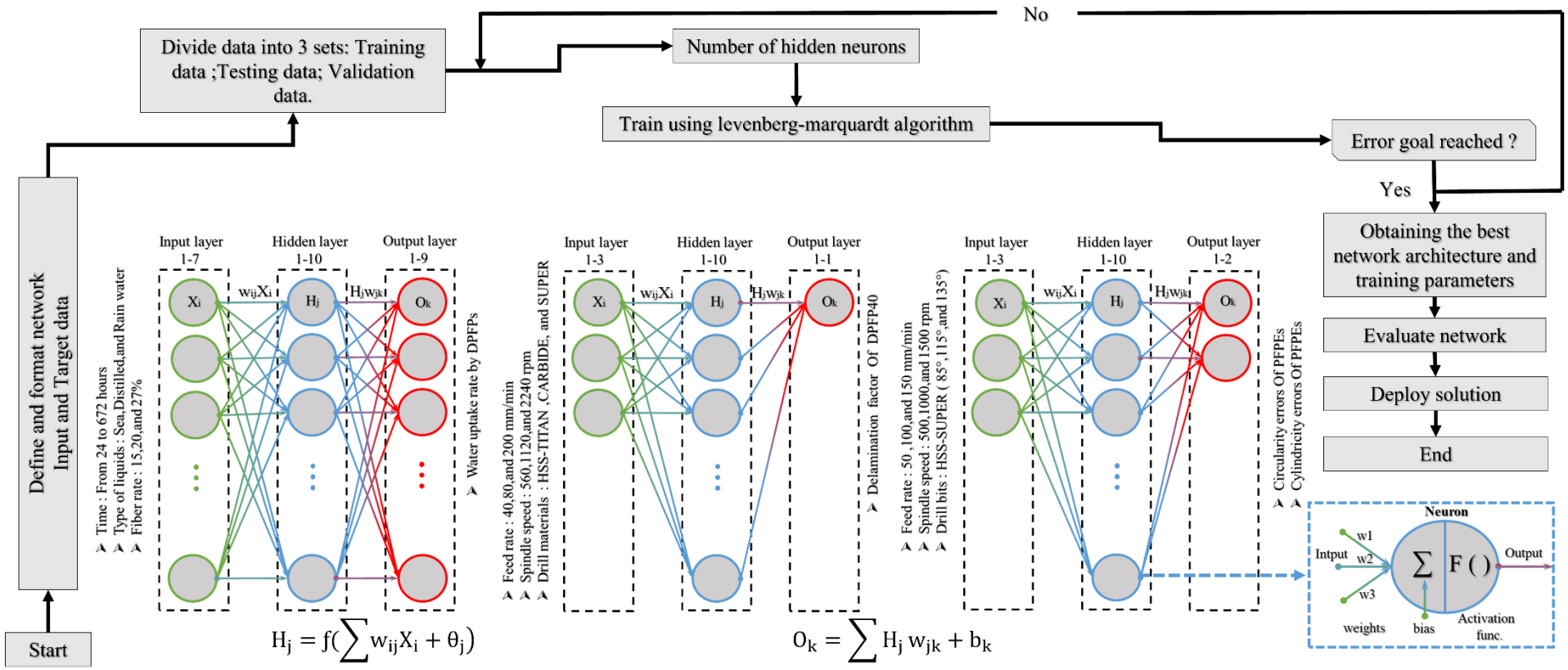

Figure II-13: Diagram and flowchart of developed artificial neural network model.

II.5.2 Response Surface Methodology (RSM)

Response surface methodology (RSM) stands as a robust statistical technique utilized for enhancing system response by constructing refined approximations of structural responses through result analysis, thereby exploring the correlation between input parameters and output responses [206, 207]. This method proves advantageous in scenarios where the relationship is intricate or nonlinear [208]. Its applications span various industries including chemical engineering, manufacturing, biotechnology, and pharmaceuticals. RSM finds utility in optimizing the production of intricate chemical compounds, enhancing efficiency in manufacturing processes, and refining the performance of medical devices [209].

In this investigation, a model with 10 specified points and 143 points indicating lack-of-fit (resulting in a total of 153 outcomes) was employed to examine the impact of three variables: time (ranging from 24 to 672 hours), liquid type (including distilled water, seawater, and rainwater), and fiber loading (at 15%, 20%, and 27%) on the response, which is the water uptake rate by DPFPs (Mass of DPFPs). For the study of three factors (spindle speed, feed rate, and drill materials) each having three levels as previously outlined in **Table II-3**, a model with 10 specified points and 17 lack-of-fit points (resulting in 27 experimental runs) was used to analyze their influence on the response, specifically the delamination factor (F_d) of drilled holes of DPFP40. The data underwent Analysis of Variance (ANOVA), which dissects the overall observed variability in the response, isolating contributions from each factor along with their interactions[210].

RSM entails conducting a series of experiments guided by the principles of Design of Experiments (DOE) to methodically assess the impact of variables on the response variable. Additionally, RSM enables the estimation of optimal values for independent variables and the determination of their primary effects[211]. The data underwent Analysis of Variance (ANOVA), which dissects the overall observed variability in the response, isolating contributions from each factor along with their interactions.

Equation **II-9** illustrates the correlation between the input parameters and the corresponding responses.

$$Y = f(x_1, x_2, \dots x_n) + \varepsilon \qquad \textbf{(II-9)}$$

The controllable variables are represented by (x_1, x_2 ... x_n), while ε denotes the error detected in the response (Y)[212].

The relationship between the predictor variables and the response parameters is uncertain; it is approximately represented by a second-degree polynomial (Eq. **II-10**).

$$Y = \beta_0 + \sum_{i=1}^{k} \beta_i X_i + \sum_{i=1}^{k} \beta_{ii} X_i^2 + \sum_{i=1}^{k-1} \sum_{j=2}^{k} \beta_{ij} X_i X_j \quad \text{(II-10)}$$

where i=1,2,3…, (k–1), and j=1,2,3…, k and $i<j$ [213, 214].

II.5.3 Taguchi method

Lately, the Taguchi method has gained widespread acceptance in various sectors, including automotive, aerospace, chemical industries, and environmental engineering[215-217]. Its significant effectiveness in promoting robust designs and improving both product and process performance has been instrumental in its extensive adoption. The method is acclaimed for its ability to enhance quality, reduce variability, and mitigate the impact of external factors on system dynamics[218, 219] .

The Design of Experiments (DOE) was utilized to systematically investigate the effects of multiple factors, including feed rate, spindle speed, and drill bit point angles, as well as their interactions, on output variables such as circularity and cylindricity errors of PFPEs. This analysis was conducted using Minitab software version 21.2. An experimental design based on an L27 (3^13) orthogonal matrix was chosen to address the study's requirements. This matrix enabled the examination of primary effects and lower-order interactions, necessitating a total of 27 experimental runs [220].

The Taguchi method introduces the concept of utilizing the signal-to-noise ratio (*S/N*) as an indicator of system performance. This ratio evaluates the quality of a product or process by considering both the mean performance (signal) and the variance or noise associated with the performance [221, 222]. Within the Taguchi method framework, maximizing the *S/N* ratio is crucial for achieving an optimal and robust design that enhances desirable outcomes (signal) while minimizing undesirable outcomes (noise). Various forms of *S/N* ratios exist, each tailored to specific objectives, and the selection of the appropriate ratio depends on the characteristics of the response variable being analyzed [223-225]. The three primary types of *S/N* ratios are as follows:

Larger is Better:

$$S/N = -10 \cdot \log_{10}\left(\frac{1}{n}\sum_{i=1}^{n}\left(\frac{1}{y_i^2}\right)\right) \quad \text{(II-11)}$$

Nominal is Best:

$$S/N = -10 \cdot \log_{10}\left(\frac{1}{n}\sum_{i=1}^{n}\left(\frac{1}{(y_i-T)^2}\right)\right) \quad \text{(II-12)}$$

Smaller is Better:

$$S/N = -10 \cdot \log_{10}\left(\frac{1}{n}\sum_{i=1}^{n}\left(y_i^2\right)\right) \quad \text{(II-13)}$$

In this context, y_i signifies the performance observed in the i^{th} experimental run, n denotes the total number of experiments, and T represents the target or desired value.

Considering the current experimental focus on minimizing circularity and cylindricity errors of PFPEs, the *S/N* ratio computation was conducted according to **Equation II-13**.

II.6 Conclusion

The second chapter encapsulates a wealth of critical information essential for understanding the development and evaluation of bio composites incorporating date palm fibers and Iso-polyester-Epoxy resins. Key highlights from this chapter include:

- Fiber Extraction: Detailed procedures for extracting fibers from date palm trees, emphasizing the importance of gentle handling to preserve fiber integrity.
- Bio Composite Preparation: The fabrication of bio composites in various configurations, highlighting the matrix mass fractions and fiber reinforcements used in the study.
- Absorption Behavior: Discussion on the porosity of natural fibers and its impact on water absorption in bio composites, emphasizing the role of porosity in influencing water absorption capacity and mechanical properties.
- Drilling Behavior: the chapter includes methodologies for evaluating the drilling behavior of the bio composites, assessing factors such as delamination factor, circularityt and cylindricity errors of drilled holes of DPFP40 and PFPEs
- Analytical Techniques: Mention of analytical tools such as ANN,RSM,Taguchi methods for modeling and optimizing the properties of bio composites.

In conclusion, the second chapter provides a comprehensive overview of the processes involved in creating and testing bio composites with date palm fibers and Iso-polyester resin. The chapter's emphasis on fiber extraction, composite preparation, absorption behavior, and analytical techniques underscores the meticulous approach taken to study the performance of these innovative materials. By integrating experimental methodologies with theoretical frameworks, this chapter lays a solid foundation for further exploration into the absorption and drilling behavior of bio composites, offering valuable insights for researchers and practitioners in the field of composite materials.

Chapter III

Absorption behavior of (Date Palm Fiber /Iso-Polyester) composites

III Chapter III: Absorption behavior of (Date Palm Fiber /Iso-Polyester) composites

III.1 Introduction

In the realm of bio-polymeric materials, a prevalent trait among many is their inherent hydrophilic nature. As such, a meticulous examination of the water absorption characteristics of bio-composites is imperative. This study delves into the comprehensive analysis of these properties, aiming to shed light on the intricate dynamics at play within these materials. Central to this investigation is the utilization of the water absorption test, a widely recognized methodology employed to gauge the extent of water uptake by a substance within a defined timeframe[226]. Through this exploration, we aim to unravel the nuances of water absorption behavior exhibited by the bio-composites under scrutiny, providing valuable insights into their suitability and performance across various applications.

III.2 Assessment of the average mass gain

The examination of average mass gain stands as a pivotal element offering invaluable insights into the water absorption tendencies of DPFPs. This scrutiny not only fosters a thorough comprehension of how these composites absorb water but also serves as a guiding instrument for devising tailored approaches to enhance their efficacy and utility. Through the optimization of water absorption properties, these composites hold promise for diverse applications across industries where meticulous control over water absorption behavior is paramount.

Figure III-1 illustrates the progression of average mass gain over various immersion durations, regardless of fiber contents and water types. As depicted in the figure, the trend in average mass gain reveals a steady increase with prolonged immersion times, signifying the substantial influence of exposure duration on the water absorption behavior of DPFPs. Nevertheless, with continued extension of immersion times, the rate of mass gain begins to decelerate, eventually reaching a plateau. The saturation behavior, depicted in **Figure I-1**, implies that there exists a limit to the water absorption capacity of DPFPs.

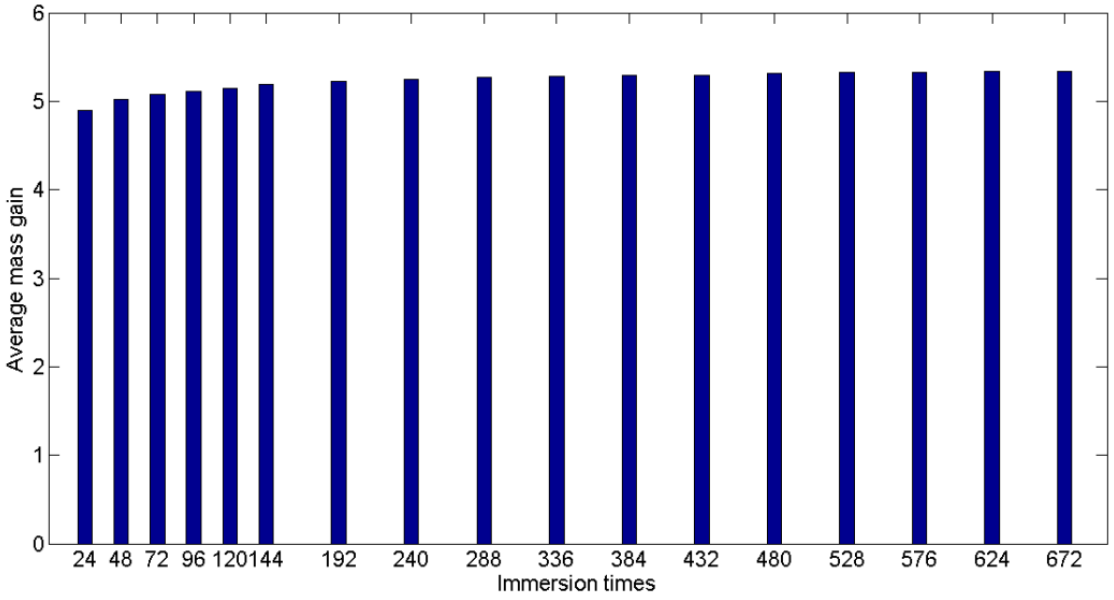

Figure III-1: The progression of average mass gain of DPFPs over immersion durations.

Moreover, the examination of the variance in mass gain between successive immersion durations, depicted in **Figure III-2**, unveils a diminishing pattern with the augmentation of immersion time. This implies that the composites are nearing saturation, where the incremental mass gain between consecutive immersions diminishes progressively. The saturation trend, illustrated in **Figure III-2**, signifies that the composites have attained their peak water absorption capacity.

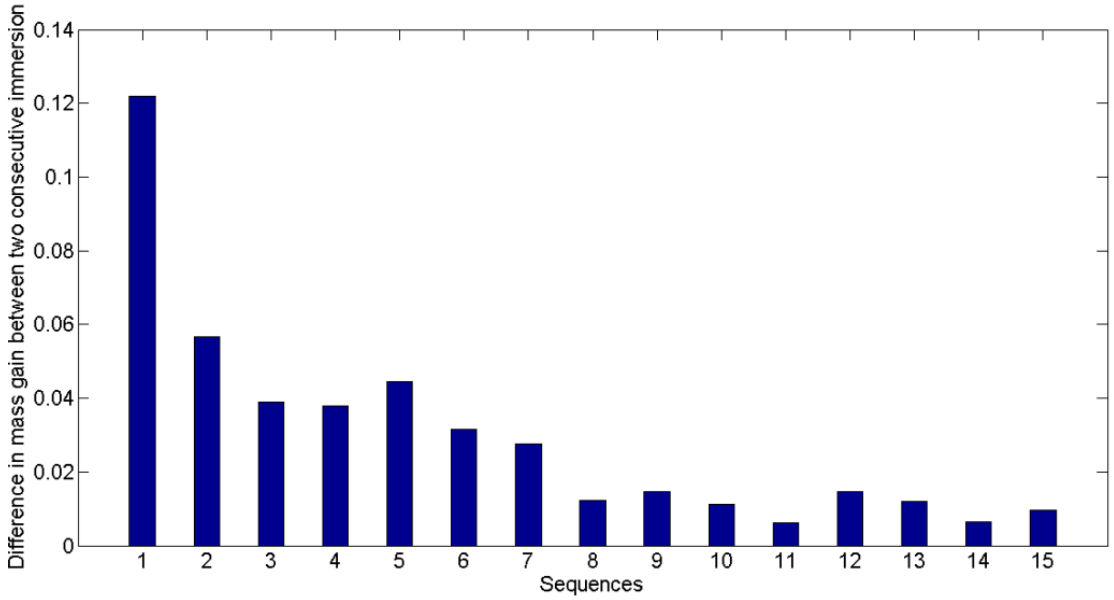

Figure III-2: Disparities in mass gain of DPFPs between every two successive immersion intervals.

The evolution of average mass gain with fiber content whatever the immersion times and the type of water, as illustrated in **Figure III-3**, shows that higher fiber contents result in greater mass gains. This indicates that the amount of fiber incorporated into the composites directly affects their water absorption behavior. Previous research has also identified a parallel trend, linking higher fiber content to a heightened water absorption rate[192]. This phenomenon is attributed to reduced adhesion between the fiber and matrix, as elucidated in[193], elucidating the underlying cause for this elevated water absorption rate.

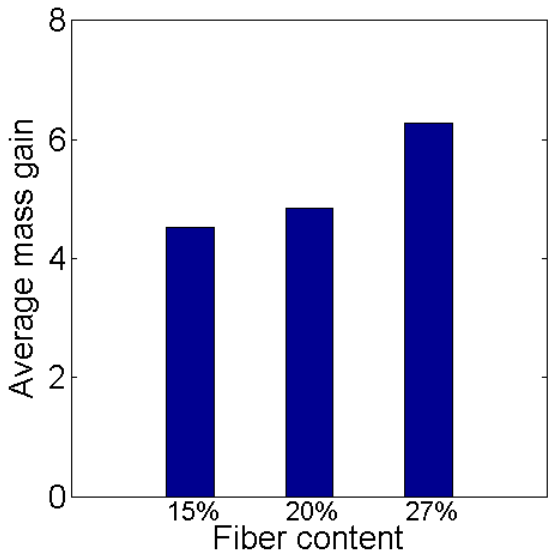

Figure III-3: The progression of average mass gain with varying fiber content.

The fluctuation in average mass gain across different water types, irrespective of immersion durations and fiber contents, as portrayed in **Figure III-4**, implies that the choice of water source employed during the water absorption process influences the water absorption behavior of the composites. Distinct water sources such as distilled water, rainwater, and seawater exhibit diverse water absorption characteristics, resulting in varying levels of mass gain in the composites. A noteworthy observation highlights those fibers demonstrate the highest water absorption capacity in Rainwater, attributed to its elevated *pH* level, as indicated in **Table II-2.** In contrast, Seawater, characterized by its comparatively lower *pH* level, exhibited the lowest water absorption among the three types.

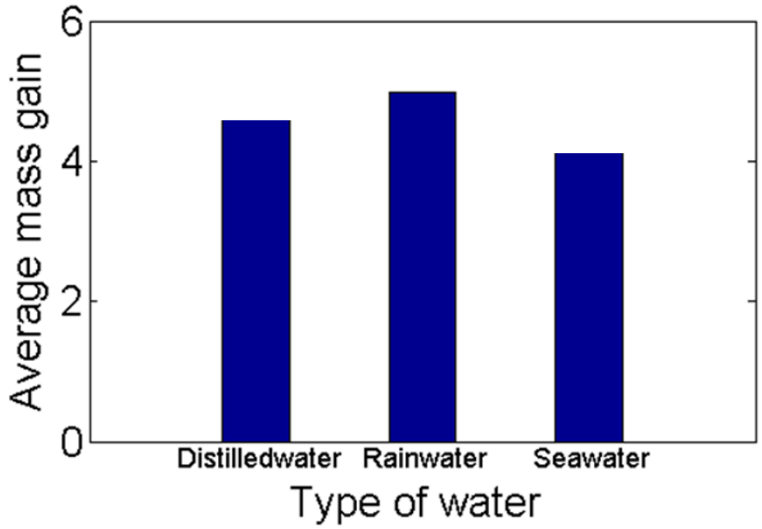

Figure III-4: The progression of average mass gain with varying water types.

III.3 Assessment of Percentage Contribution

The assessment of percentage contributions is pivotal for comprehending the significance of diverse factors in the water absorption process of DPFPs. Through the precise quantification of the individual and interactive impacts of fiber content, immersion time, and water type, researchers and engineers acquire valuable insights into the influence of these factors on mass gain. The percentage contribution serves as a definitive measure of the relative sway of each factor, facilitating well-informed decision-making during the design and fabrication phases of composites. This information aids in the selection of optimal fiber content, regulation of immersion time, and consideration of specific water types to attain desired water absorption characteristics. Furthermore, percentage contribution assists in discerning interactions between these factors, shedding light on combined effects that may contribute to determining water absorption behavior. In essence, a comprehensive understanding of percentage contribution enhances our capacity to optimize the properties and performance of DPFPs across various applications where water absorption behavior holds critical significance.

Figure III-5 depicts the individual contributions of each factor to the mass gain observed in the water absorption process. Examination of the water absorption dynamics of DPFPs reveals the predominant role of fiber content (*Fc*), contributing approximately 96.61% to the overall mass gain. This underscores the critical importance of selecting an appropriate fiber content to achieve the desired water absorption properties. These findings align with previous studies emphasizing the significant influence of fiber content on water absorption properties[194, 227, 228]. An increase in the quantity of fiber corresponds to an elevated rate of water absorption[192, 229-231]. This

heightened water absorption rate is primarily attributed to reduced adhesion between the fiber and matrix[193]. The quantity of fiber employed significantly influences the mass gain during water absorption, rendering it a pivotal factor to consider in composite fabrication.

On the other hand, the impacts of immersion time (*T*) and water type (*W*) are comparatively minimal, constituting approximately 2.11% and 1.28% respectively. Despite appearing less significant in comparison to the effect of fiber content, these contributions still provide meaningful insights into the water absorption characteristics of the composites[232]. The modest contribution of immersion time underscores its role in mass gain. Extended immersion periods lead to relatively lower mass gains, indicating that the duration of exposure has a diminishing influence on water retention properties compared to fiber content.

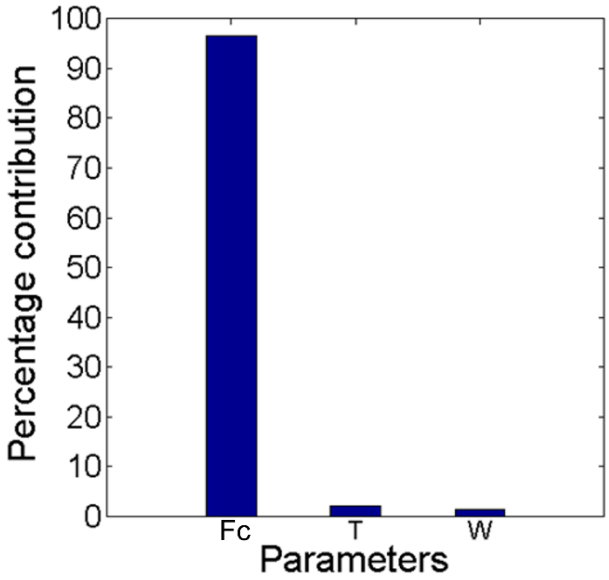

Figure III-5: Separate contributions of factors to the mass gain in the water absorption process of DPFPs.

Fine-tuning the immersion time continues to be crucial for customizing the composites for specific applications that demand precise water absorption properties. To ascertain the importance of immersion time in mass gain, additional statistical analysis is required, and this aspect will be thoroughly explored in the subsequent sections of this thesis. Further comprehensive statistical analysis will be undertaken in the upcoming sections of this thesis to determine the true significance of immersion time in relation to mass gain.

Similarly, the influence of water type suggests that the selection of a water source has a relatively marginal impact on the water absorption behavior of DPFPs. While varying water sources may result in slight differences in water absorption, the overall effect of water type is comparably smaller when contrasted with the influence of fiber content. Nevertheless, understanding these nuances can be pertinent for applications requiring precise control over water absorption properties. To discern the significance of water type in mass gain, additional statistical analysis is imperative, and this aspect will be thoroughly addressed in the subsequent sections of this thesis.

When considering the interplay between these factors, the analysis of the water absorption process in DPFPs reveals notable distinctions. **Figure III-6** illustrates the collaborative contributions of these factors to the mass gain in the water absorption process.

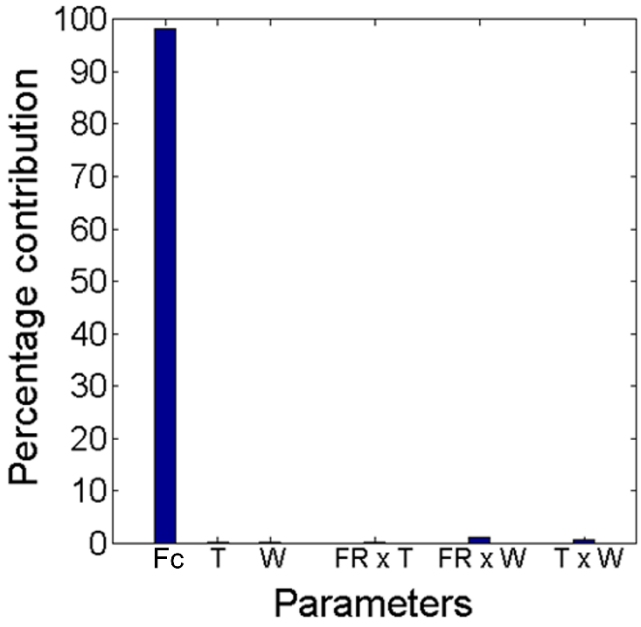

Figure III-6: Collaborative impacts of factors on mass gain in the water absorption process of DPFPs.

The interplay among factors, including the interactions between fiber content and immersion time (*Fc*×*T*), fiber content and water type (*Fc*×*W*), and immersion time and water type (*T*×*W*), collectively shapes the overall behavior of the composites. While their individual impacts may be modest, examining these interactions provides a comprehensive understanding of how multiple factors interact and influence the water absorption process. The percentage contribution of the interaction between fiber content and water type (*Fc*×*W*) exhibited a significant effect on the absorbed water percentage, followed by the interaction between immersion time and water type (*T*×*W*), and finally, the interaction between fiber content and immersion time (*Fc*×*T*). (Refer to **Figure III-6**)

III.4 Fickian Behavior

Many bio-polymeric materials exhibit hydrophilic properties. Therefore, it is crucial to investigate the water absorption characteristics of the bio-composites prepared in this study. The water absorption test is a common method used to assess the amount of water absorbed by a substance over a specified period[226]. **Figures III-7, III-8, and III-9** illustrates the weight gain evolution resulting from water absorption at room temperature (25°C) plotted against the square root of time for palm fiber composites with varying fiber loadings, ply stacking sequences, and densities. The density of 27 samples was measured, and the average density of three pieces for each composite type is presented in **Table III-1**.

The water absorption characteristics of DPFPs are depicted in **Figures III-7, III-8, and III-9**, where these Figures represent the ratio (*Mt/Ms*) plotted against the square root of time (√h). These graphs exhibit two distinct phases. The initial phase shows rapid linear absorption, resulting in ratios (*Mt/Ms*) exceeding 0.39, 0.50, 0.82 for seawater, and 0.40, 0.56, 0.73 for distilled water, and 0.37, 0.51, 0.63 for rainwater, with respective fiber contents of 15% (UD), 20% (C), and 27% (UD) during the initial 25 hours. In the subsequent phase, the rate (*Mt/Ms*) irregularly increases with time at a considerably slower pace compared to the first phase, eventually reaching a plateau indicative of water uptake equilibrium. These results suggest Fickian behavior.

These findings indicate that composites with a higher proportion of natural fibers absorb more water as anticipated, compared to those with lower fiber content. Additionally, it was observed that composites featuring fibers arranged in unidirectional stacking sequences absorb more water than those with crisscross layers. This phenomenon is attributed to the presence of polar hydroxyl groups in the structure of cellulose fibers, hemicellulose, and lignin, which can form hydrogen bonds with water[233-236].

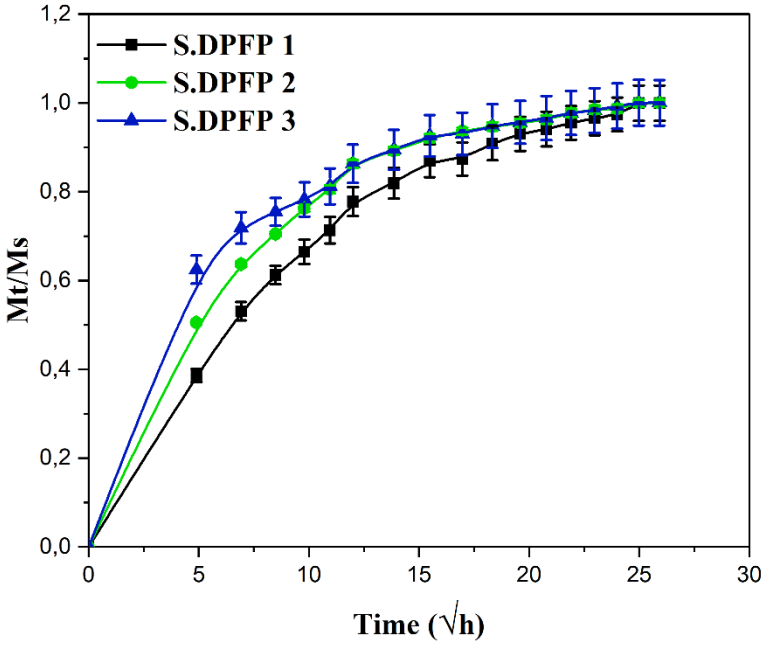

Figure III-7: The Absorption behavior of Seawater by DPFPs as a function of the square root of time (√h).

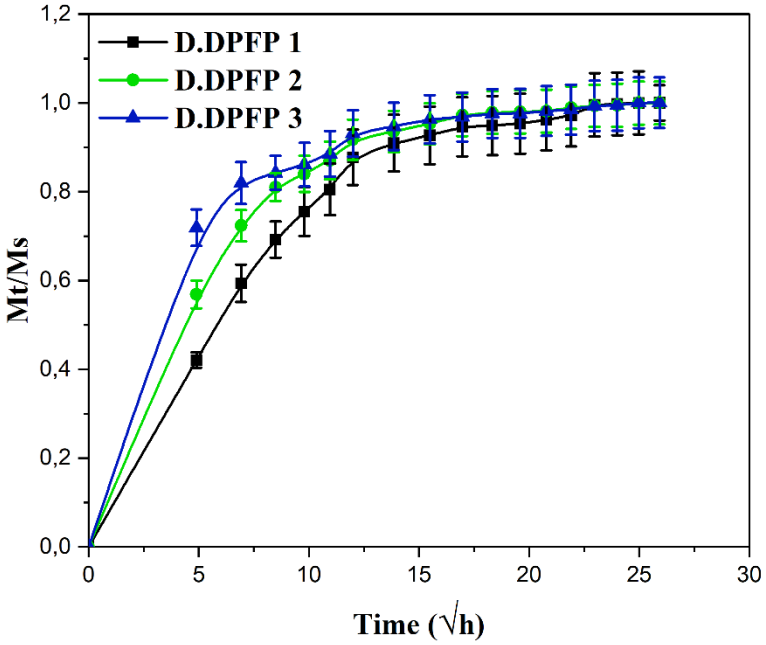

Figure III-8: The Absorption behavior of Distilled water by DPFPs as a function of the square root of time (√h).

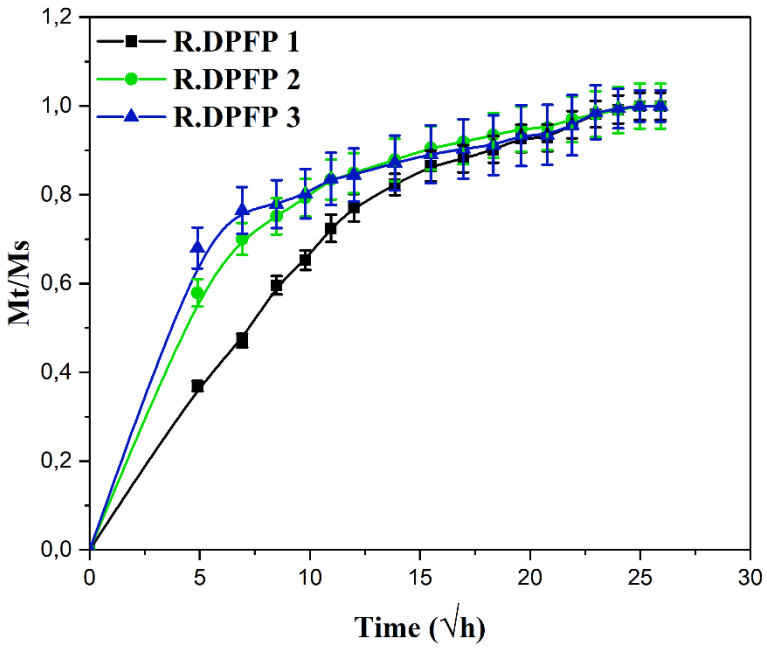

Figure III-9: The Absorption behavior of Rainwater by DPFPs as a function of the square root of time (√h).

Table III-1: Density of DPFPs.

Material	Sample N°	Density (g/cm³)			Average density (g/cm³)	Standard deviation (SD)	Coefficient of variance (CV)
		Trial 1	Trial 2	Trial 3			
DPFP 1	SP1	1.216	1.207	1.040	1.154	0.099	0.086
	SP2	1.166	1.131	1.073	1.123	0.047	0.042
	SP3	1.137	1.041	0.998	1.059	0.071	0.067
DPFP 2	SP4	1.150	1.120	1.112	1.127	0.020	0.018
	SP5	1.142	1.126	1.018	1.096	0.067	0.061
	SP6	1.131	1.207	0.957	1.098	0.128	0.117
DPFP 3	SP7	1.013	0.941	0.965	0.973	0.037	0.038
	SP8	1.075	1.111	0.865	1.017	0.133	0.130
	SP9	1.123	1.065	0.851	1.013	0.143	0.141

The absorption capacity of the date palm fiber (DPF) for the liquids under investigation is depicted in curves in **Figure III-10a**. Water absorption increases rapidly within the initial five hours, with the ratio (*Mt/Ms*) surpassing 0.70. Subsequently, the weight gain gradually rises until the fibers enter a relatively stable phase, typically after about 9 hours. Meanwhile, **Figure III-10b** illustrates the water absorption rate of the fibers alone, reaching 52.63% for seawater, 53.25% for distilled water, and 86.55% for rainwater after reaching saturation. These relatively high percentage

values are primarily attributed to the physical composition of DPF, which aids in facilitating water diffusion compared to bio-composites. The water absorption rate of the "fiber alone" varies with the type of water. The lowest absorption rate was observed for fibers immersed in seawater, possibly due to salt particles hindering the free movement of water molecules, resulting in lower absorption compared to distilled water. Moreover, the presence of inert salt particles on the fiber contributes to reduced water absorption. Rainwater comprises various gases that can alter the water's *pH* level. Specifically, carbon dioxide induces mild acidity upon dissolution in rainwater. This slight acidity may create pathways within the fiber, thereby facilitating water absorption[237, 238].

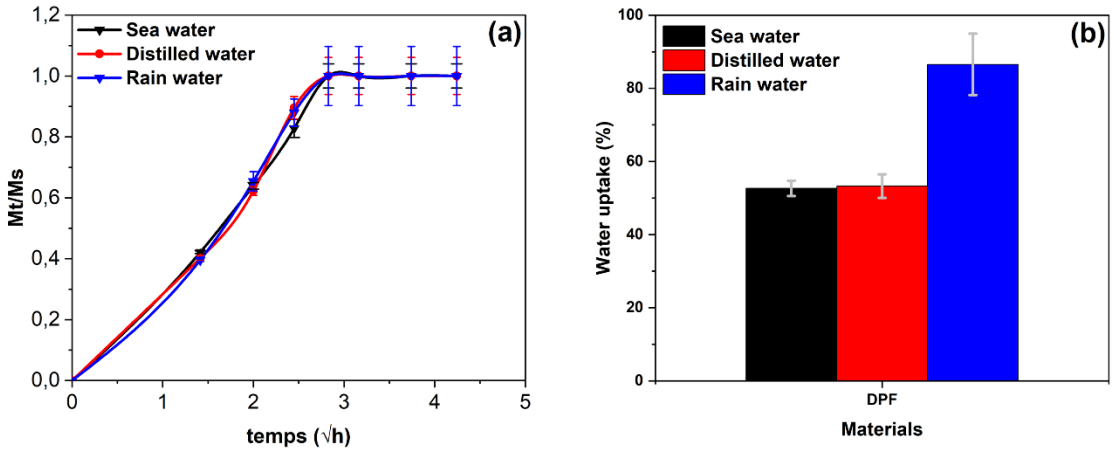

Figure III-10: Water absorption by various types of water by date palm fiber (DPF).

III.5 Diffusion coefficient of DPFPs

The diffusion coefficient values are presented in **Table III-2** . **Table III-2** represents the average of three measurements for each type of composite. The results indicate a significant variation in water diffusion parameters, primarily influenced by two factors: fiber content and the stacking sequence of plies in the bio composites. Concerning the first factor, a higher percentage of fibers resulted in a higher diffusion coefficient value, with *D* (DPFP 3_27%) being greater than *D* (DPFP 1_15%). Regarding the second factor, unidirectional stacking sequences allowed for greater water penetration compared to cross-stacking sequences, with *D* (UD_ DPFP 3) being greater than *D* (C_ DPFP 2). Additionally, it is important to note that the water diffusion coefficient values showed insignificant differences based on the type of liquid used. This phenomenon was attributed to the distinct physical and chemical compositions of each liquid.

Table III-2: Diffusion parameters for the DPFPs.

Type of liquid	Material	$K \times 10^{-3}$	$D \times 10^{-6}$ (mm^2/s)	Mm (%)
Seawater	DPFP 1	1.8	2.20573	67
	DPFP 2	3.6	2.31613	120
	DPFP 3	4.0	3.99549	158
Distilled water	DPFP 1	1.7	2.1155	66
	DPFP 2	2.9	2.25995	110
	DPFP 3	3.2	3.74372	144
Rainwater	DPFP 1	1.6	2.11015	55
	DPFP 2	2.5	2.33936	100
	DPFP 3	2.9	3.53131	125

III.6 Scanning electron microscopy analysis of date palm fibers (DPF) for the assessment of their porosity

The images depicted in **Figure III-11** were captured using the ESEM QUANTA 200 environmental scanning electron microscope (SEM), offering a resolution of up to 3584 x 3094 pixels. **Figures III-11a**, **III-3b**, and **III-11c** showcase cross-sections of an FPD composite with varying zoom levels. Conversely, **Figures III-11d** and **III-11e** display the cross-section of date palm fibers, highlighting details of their cells with distinct zoom levels. These images are invaluable for analyzing fiber morphology and measuring porosity. In this phase, ImageJ software was introduced and utilized to quantify the porosity of palm fibers, as illustrated in **Figure III-11f**.

The micrograph of the FPD cross-section reveals the composition of numerous porous cells with a round and undulating shape. Notably, some centrally located cells exhibit significantly larger sizes compared to their surroundings, contributing to the overall porous nature of the fibers. Similar observations have been reported in other studies on date palm fibers by Kaddami et al[239]. and Amroune et al[240]. It's worth noting that the shape, volume, and location of these larger cells can vary even among fibers of the same origin and within the same species.

The identification of pores using *Image J* indicates that palm fibers exhibit significant porosity, with the measured porosity exceeding 51,130%. This validates the hypothesis proposed earlier in this study, suggesting that an increase in the volume fraction of fibers correlates with a higher porosity capacity. Consequently, this leads to an elevated absorption rate of the composite.

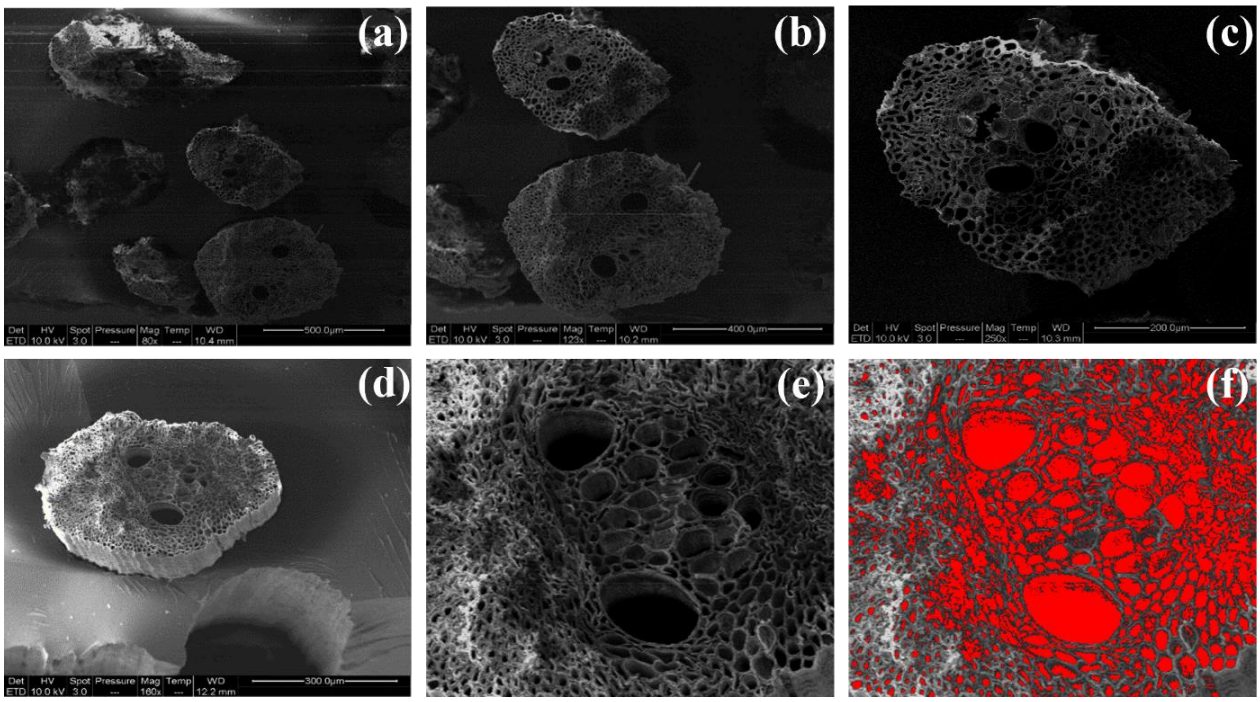

Figure III-11: (a), (b), and (c): Cross-sectional SEM images of DPFPs with varying zooms. (d) and (e): Cross-sectional SEM images of a palm fiber with different zooms. (f): *Image J* detection of pores in palm fiber.

The findings of this investigation align with previous research, as demonstrated by Chen et al[241]. In their study, it was observed that longer soaking times and higher fiber loadings of rice husk resulted in increased water absorption and diffusion coefficients. Moreover, they determined the absorption rates for bio composites with fiber loadings of 40%, 60%, and 80% to be 6.331%, 13.729%, and 18.974% for distilled water, and 5.772%, 11.028%, and 22.936% for seawater, respectively. Additionally, the diffusion coefficient values were found to be 1.668, 3.467, and 42.540 $\times 10^{-13}$ m^2/s for distilled water, and 1.683, 2.221, and 23.692×10^{-13} m^2/s for seawater. Similarly, in a related study by Sair et al[242], which focused on the mechanical and thermal conductivity properties of hemp fiber-reinforced polyurethane composites, they found that the absorption rates were 28.98% for 5% PU and 64.3% for PU30%. The diffusion coefficient values were determined to be 1.47×10^{-5} mm^2/s and 7.45×10^{-5} mm^2/s, respectively. Their results indicated that the water absorption rate of polyurethane composites increased with higher hemp fiber content, leading to the conclusion that the water uptake rate of polyurethane composites escalates with increasing hemp fiber content. Furthermore, Sodoke et al [243] conducted a study estimating the diffusion coefficient to be $3.98 \pm 0.120 \times 10^{-6}$ mm^2/s and the upper limit of humidity to be 25.68 ± 1.36%. The rapid increase in water uptake was primarily attributed to the substantial fiber proportion (68.07%) and inherent gaps in the material.

III.7 conclusion

In conclusion, the chapter on the absorption behavior of (Date palm fiber /Iso-polyester) composites provides valuable insights into the intricate dynamics of water absorption in bio-composites. The study highlights the Fickian behavior of bio-polymeric materials and emphasizes the significance of understanding water absorption characteristics for composite design and application. Key findings include the critical role of fiber content in mass gain, the impact of immersion time on water absorption properties, and the influence of water type on composite behavior. Optimization of fiber content is crucial for enhancing water absorption properties, while considering the interplay between fiber content, immersion time, and water type is essential for tailoring composite performance. By providing a comprehensive analysis of the absorption behavior of (Date palm fiber /Iso-polyester) composites, the chapter offers valuable insights for optimizing the performance and application of these materials in various industries.

Chapter IV

Drilling behavior of DPFP40, PFPEs

IV Chapter IV: Drilling behavior of DPFP40, PFPEs

IV.1 Introduction

The fourth chapter delves into the intricacies of drilling of DPFP40,PFPEs composites . This chapter serves as an in-depth exploration of machining performance, parameter optimization, and the critical factors influencing the quality of machined features in natural fiber-reinforced materials. Through a detailed analysis of key parameters affecting drilling performance and the importance of selecting optimal parameters, this chapter illuminates the challenges associated with achieving high-quality machined features. Additionally, the discussion on the impact of feed rate, spindle speed, drill bit materials, and drill bit point angles on hole quality, alongside the utilization of advanced tools and methodologies for parameter optimization, provides valuable insights into enhancing drilling processes. Visual aids such as Ishikawa diagrams are utilized to visually represent the multifaceted variables affecting machining quality, offering a comprehensive understanding of the complexities and considerations involved in drilling DPFP40 and PFPEs. In summary, Chapter IV presents a thorough examination of drilling behavior in biocomposites, offering a pathway toward improved drilling processes and superior quality of machined features in natural fiber-reinforced materials.

IV.2 Machining performance of bio composites

The machining performance of composites reinforced with natural fibers involves a nuanced interplay between fiber characteristics, matrix properties, and machining processes. The heterogeneous nature of natural fibers, including variations in length, diameter, and alignment, introduces challenges during machining. Fiber orientation significantly impacts the cutting forces and tool wear, with machining across the fibers being particularly sensitive to potential issues like fiber pullout and delamination. The type of natural fiber used, such as flax or hemp, introduces variability in mechanical properties, affecting the overall machinability of the composite[244].

The choice of matrix material is critical. Thermosetting resins, like epoxy, may require different machining strategies compared to thermoplastics such as polypropylene. The curing behavior of thermosetting matrices adds complexity, influencing cutting speeds and tool selection. Natural fiber composites can be abrasive, necessitating the use of robust tools, possibly with diamond or carbide coatings, to withstand wear[245].

Optimizing cutting parameters becomes crucial for achieving a balance between material removal rates and minimizing heat generation. Excessive heat can impact the resin matrix and

compromise the integrity of the fibers. Cooling and lubrication strategies play a vital role in dissipating heat and reducing thermal damage.

Tool wear, an inherent challenge in machining composites, requires continuous monitoring. Wear patterns can vary based on the abrasive nature of natural fibers and the matrix material. The consideration of tool life is essential for maintaining machining efficiency and achieving desired surface finishes[246].

Post-machining processes contribute to the final quality of the product. Sanding and coating may be necessary to address surface irregularities and enhance the aesthetic and functional aspects of the machined components. Achieving a balance between machining efficiency and product quality requires a comprehensive understanding of the composite's composition, coupled with meticulous planning and optimization of machining parameters. Successful machining of natural fiber composites demands a holistic approach that considers the intricacies of the material system, the chosen machining method, and the desired properties of the final product.

Holes can be generated through machining methods like drilling[247, 248] or non-machining methods like punching[249]. In their review, Ramnath et al[250] identified key parameters affecting machining performance, including cutting speed, feed rate, and depth of cut. Nassar et al[251] outlined numerous factors influencing machined features' quality, offering a guideline for parameter selection, especially in drilling, using the fishbone diagram method. Another approach involves enhancing machining performance to minimize waste during production. For instance, when drilling holes in composite panels, it is crucial to use optimal parameters to reduce rejection, typically referring to significant damage around the machined holes, known as delamination. Delaminated holes can compromise the structure during application. To mitigate this, Madhavan et al[252] and Turki et al[253] proposed optimal machining parameters. Similarly, Zain et al[254] investigated the impact of die clearance and puncher profile on delamination in the punching process. Babu et al[255] recommended optimal milling parameters to enhance surface quality. Ismail et al[256] explored the effects of drilling parameters, such as feed rate, thrust force, and cutting speed, on the types of chips formed in hole drilling, demonstrating that higher feed rates and cutting speeds produce wider, longer, lighter, and more ribbon-like hybrid fiber-reinforced polymer (HFRP) chips. Powdery or dusty, smaller, and darker chips are observed with converse conditions in carbon fiber-reinforced polymer (CFRP). These chip characteristics result in lower surface roughness for CFRP and reduced delamination and drill wear for HFRP[257].

The presence of moisture from coolants or lubricants used during machining composite panels may impact material integrity[258]. For this reason, Josyula et al[259] enhanced the machinability of metal-based composites (MMCs) by introducing pressurized liquid nitrogen (LN_2) as a substitute for conventional coolant. LN_2 was found to reduce surface roughness, tool wear, cutting temperatures, and built-up edge formation, while being harmless and environmentally friendly.

Numerous studies emphasize optimizing machining parameters, such as feed rate, cutting speed, and thrust force, by observing factors like hole diameter, chip formation, delamination, and surface roughness. Research suggests that minimal surface roughness and delamination are associated with a low feed rate, moderate-to-high cutting speed, and a small drill diameter[260, 261].

In the context of energy optimization for machining, minimizing torque and thrust force is essential. Therefore, Ramesh et al[191] and Debnath et al[262] recommend a combination of low feed, high spindle speed, and a parabolic drill. Ghalme et al [263] discovered that for milling glass fiber-reinforced polymer (GFRP), speed is the most influential parameter on surface roughness, aligning with similar findings in Meena and Kumar[264] and Panduranguda et al[265]. Various tools and methods, such as the Taguchi Method[266], grey-fuzzy algorithm[267], and neural network[268, 269] , have been developed and employed for determining optimal parameters.

Figure IV-1 visually presents the variables influencing the quality of machined features in Natural Fiber Reinforced Composites (NFRCs). Meanwhile, **Figure IV-2** (thesis focus) visually represents the phenomenon of delamination, circularity, and cylindricity errors.

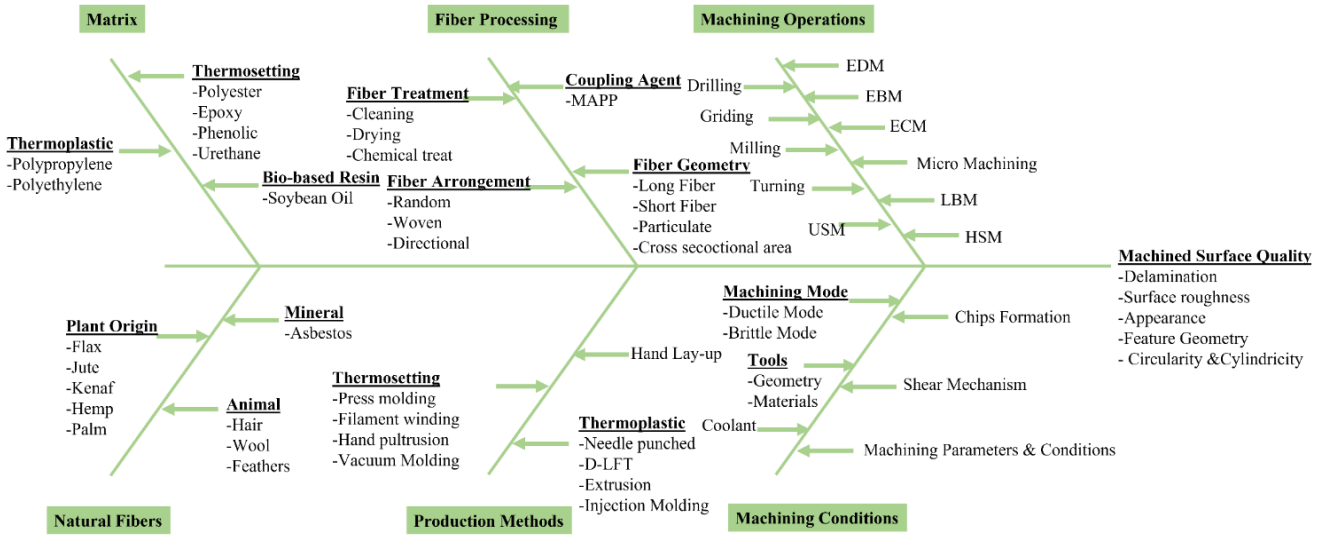

Figure IV-1: Ishikawa diagram of variables that impact the quality of machined features in Natural Fiber Reinforced Composites (NFRCs).

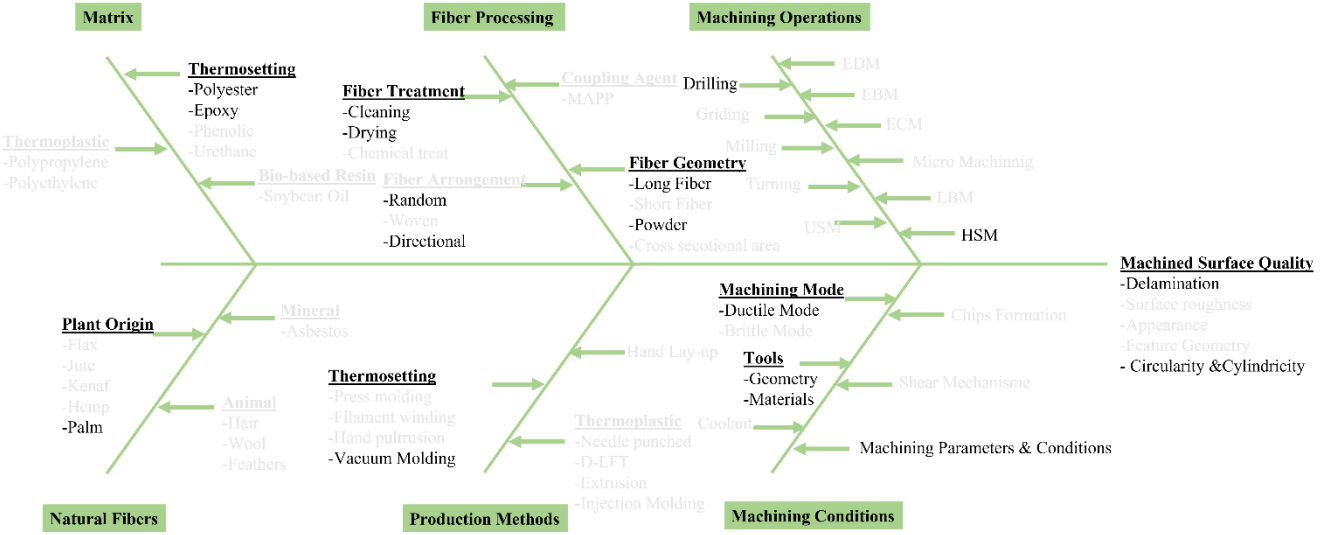

Figure IV-2: Ishikawa diagram of variables that impact the delamination and the circularity and cylindricity errors of DPFP40, PFPEs.

IV.3 Drilling of DPFP40

IV.3.1 Delamination

The samples were drilled using the specified cutting conditions. Delamination factors were compared for all the drilled holes. **Table IV -1** compiles the averages of three distinct delamination factor values for each hole in the DPFP40, considering various spindle speeds, feed rates, and drill materials.

Table IV -1 validates that cutting parameters significantly influence delamination factor values. It was observed that the feed rate has a more pronounced effect compared to the spindle speed. Increasing the feed rate resulted in higher delamination factor values, whereas increasing the cutting speed reduced this factor. For the DPFP40 drilled with the HSS-TITAN drill, the delamination factor value at a feed rate of 40 mm/min was reduced by approximately 29% compared to a 200 mm/min feed rate. Similarly, at a spindle speed of 2240 rpm, the delamination factor value decreased by approximately 22% compared to a spindle speed of 560 rpm.

Additionally, it was observed that the drill materials also play a significant role in determining the delamination factor value. The study revealed that the uncoated drill (HSS-SUPER) caused less delamination compared to the TITAN and CARBIDE-coated HSS drills. For the DPFP40 drilled with the HSS-SUPER drill, the delamination factor value at a feed rate of 40 mm/min and a spindle speed of 560 rpm was reduced by approximately 19% compared to the DPFP40 drilled with the HSS-TITAN drill, and approximately 38% compared to the DPFP40 drilled with the HSS-CARBIDE drill. These findings suggest that the optimal cutting parameters are as follows: spindle speed = 2240 rpm, feed rate = 40 mm/min, and drill materials = HSS-SUPER. While the most unfavorable hole quality was obtained with the HSS-CARBIDE drill, with a spindle speed of 560 rpm and a feed rate of 200 mm/min (refer to **Figure IV -3**).

The findings from this study align closely with earlier research, such as the results reported by Zohir et al[270], where they discovered that the lowest delamination occurred at the lowest and highest values of cutting feed rate and speed (f=51.162 mm/min, N=1397.54 rpm, respectively) for HSS-TiN. Similarly, Lotfi et al[271] observed that increasing the spindle speed reduced the size of delamination in drilled holes, while higher feed rates resulted in a significant increase in the delamination factor. They found that optimal hole quality was achieved with samples drilled at a spindle speed and feed rate of 3000 rpm and 0.11 mm/rev, respectively. In another investigation by Senol Bayraktar[272], the same observations regarding cutting conditions were noted. Additionally, the results indicated that uncoated drills caused less delamination compared to TiN and TiAlN-coated HSS drills under the same cutting conditions.

Table IV-1: Entrance (Peel-up) and exit (Push-down) of the drilled holes under various drilling conditions for "HSS TITAN / 10mm."

No.	Code	Drill entrance (Peel-up)	Drill exit (Push-down)	Drilling condition		Delamination factor, F_d
				N (rpm)	f (mm/min)	
1	1:1			560	40	1.37
2	2:1		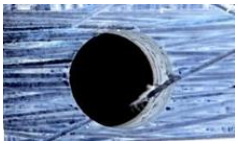	1120	40	1.31
3	3:1	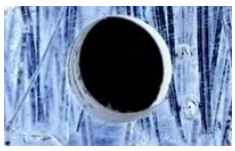	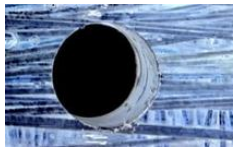	2240	40	1.07
4	1:2		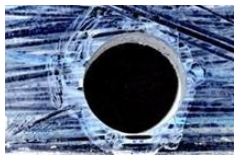	560	80	1.87
5	2:2	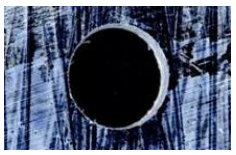	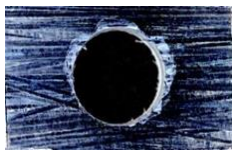	1120	80	1.57
6	3:2		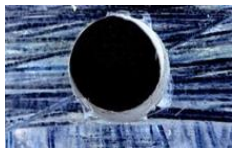	2240	80	1.21
7	1:3		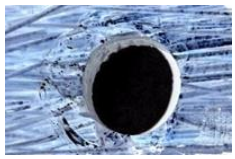	560	200	1.91
8	2:3	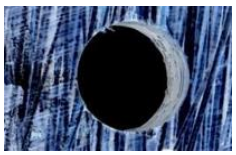	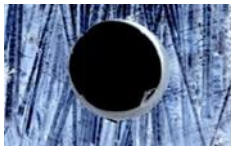	1120	200	1.64
9	3:3			2240	200	1.43

Table IV-1: (Continued). "HSS CARBIDE / 10 mm".

No.	Code	Drill entrance (Peel-up)	Drill exit (Push-down)	Drilling Condition		Delamination factor, F_d
				N (rpm)	f(mm/min)	
10	4:4		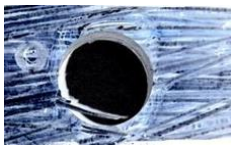	560	40	1.78
11	5:4	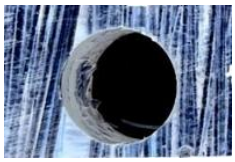	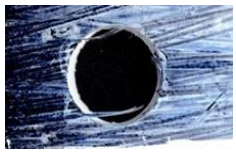	1120	40	1.52
12	6:4			2240	40	1.11
13	4:5		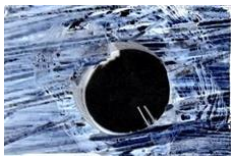	560	80	1.90
14	5:5	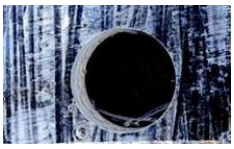		1120	80	1.68
15	6:5			2240	80	1.24
16	4:6		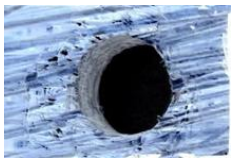	560	200	1.98
17	5:6	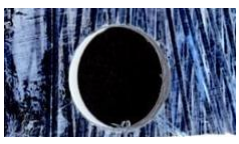		1120	200	1.84
18	6:6			2240	200	1.54

Table IV-1: (Continued). "HSS SUPER / 10 mm".

No.	Code	Drill entrance (Peel-up)	Drill exit (Push-down)	Drilling condition		Delamination factor, F_d
				N (rpm)	f(mm/min)	
19	7:7		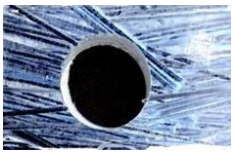	560	40	1.11
20	8:7		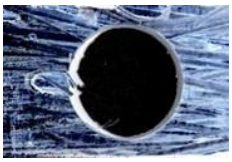	1120	40	1.09
21	9:7	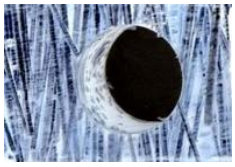	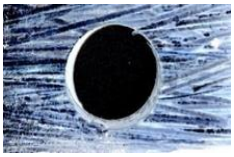	2240	40	1.02
22	7:8		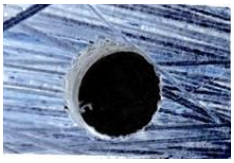	560	80	1.26
23	8:8	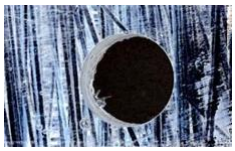	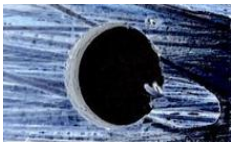	1120	80	1.14
24	9:8		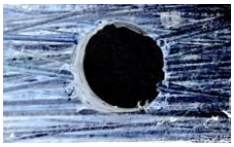	2240	80	1.09
25	7:9	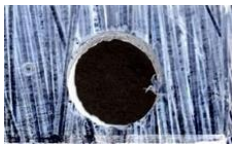		560	200	1.33
26	8:9	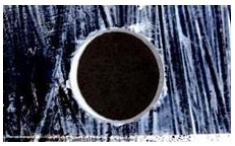		1120	200	1.17
27	9:9	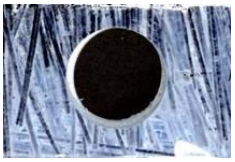	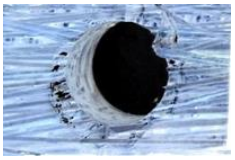	2240	200	1.14

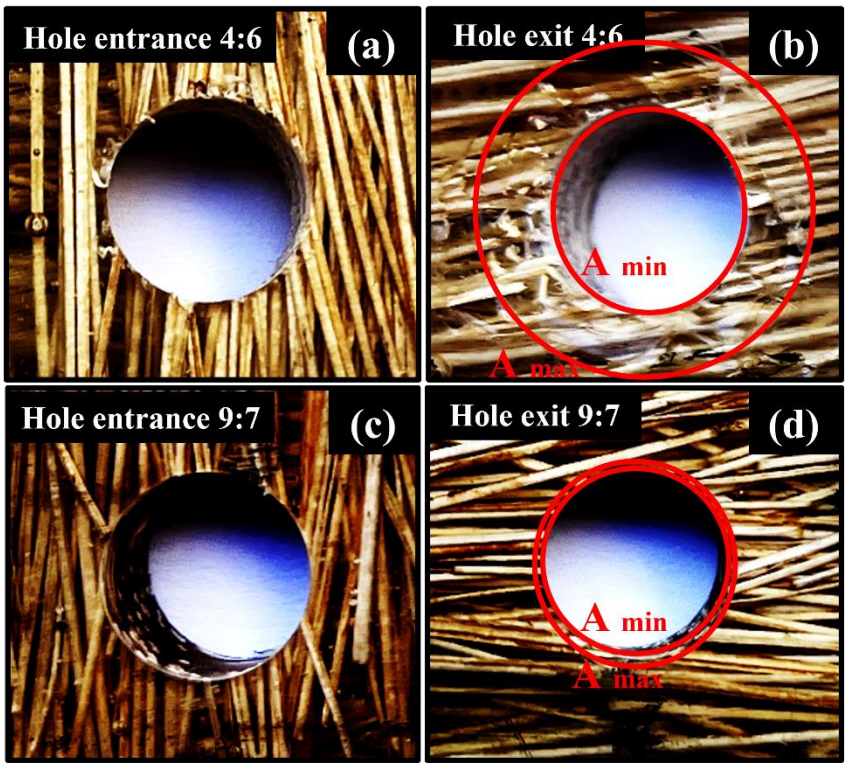

Figure IV-3: (a), (b) the lowest hole quality, and (c), (d) the highest hole quality.

IV.3.2 Circularity and cylindricity measurements for DPFP40 holes

Figure IV-4 illustrates the circularity and cylindricity errors of the drilled holes using the tools involved in this study, considering various feed rates and spindle speeds (refer to **Table IV-2**) The findings indicate that variations in the feed rate had a more significant impact compared to changes in spindle speed, a trend consistent with previous research by Koklu et al[273]. Their study demonstrated that hole circularity at the top was notably affected by the feed rate, which increased as the feed rate increased, leading to a degradation of circularity and cylindricity.

The increase in feed rate necessitates a greater pushing force, contributing to elevated temperatures in the cutting zone, and leading to chip adhesion to the drill bit[274, 275]. Moreover, holes drilled using coated tools (T1 and T2) exhibited fewer deviations and errors compared to the uncoated tool (T3). **Figure IV-5** visually depicts the condition of the drills after completing the drilling process, indicating that chips tend to adhere to the drill body due to heat generated from various sources, such as tool/chip and tool/part interaction and heat-induced by fracture zones[276]. Lower adhesion observed with tools T1 and T2 suggests that accurate holes are generated compared to T3, where chip adherence to the drill body affects hole accuracy.

These findings underscore that the tools coated with thinner layers result in holes drilled with higher accuracy[277, 278]. The optimal cutting parameters for achieving better circularity are a spindle speed of 1120 rpm, a feed rate of 80 mm/min, and drill material of HSS-TITAN. For

improved cylindricity, the recommended parameters are a spindle speed of 560 rpm, a feed rate of 80 mm/min, and a drill material of HSS-CARBIDE.

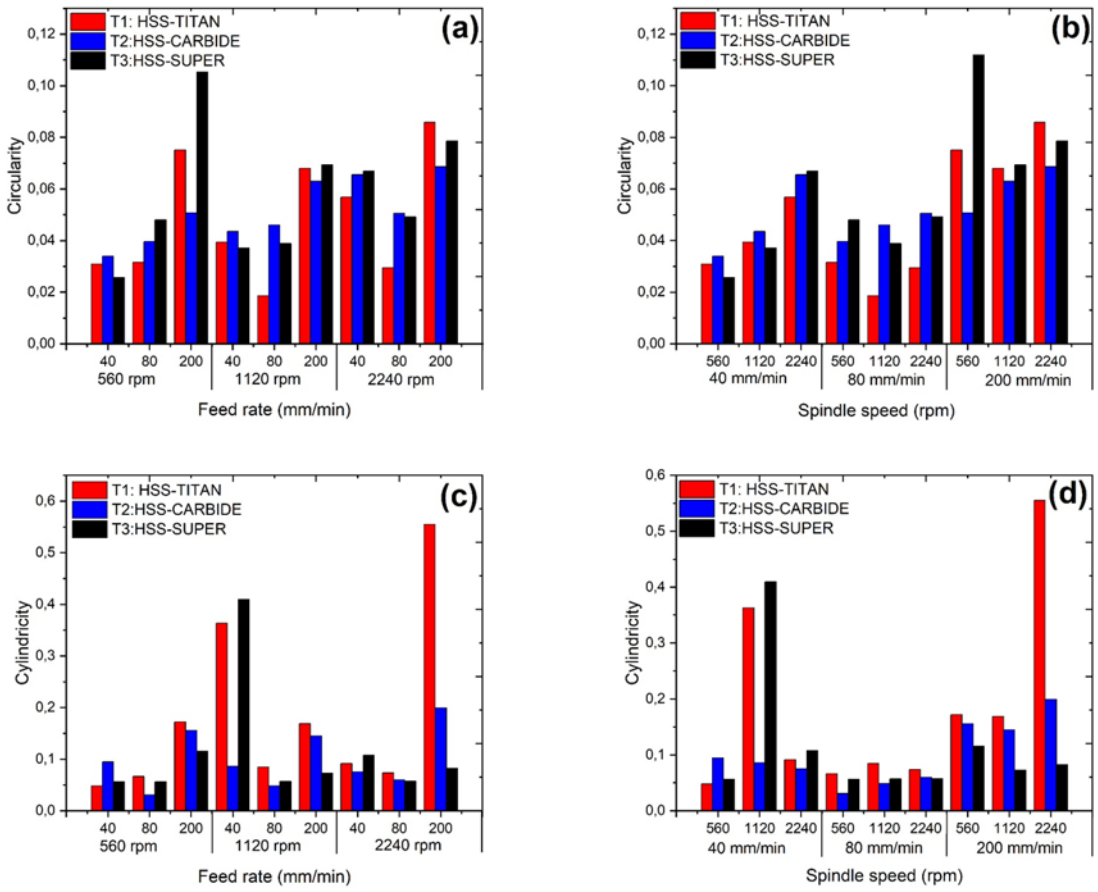

Figure IV-4: Circularity and cylindrical errors for tools T1, T2, and T3 as a function of (a) and (c): feed rate, (b) and (d): spindle speed.

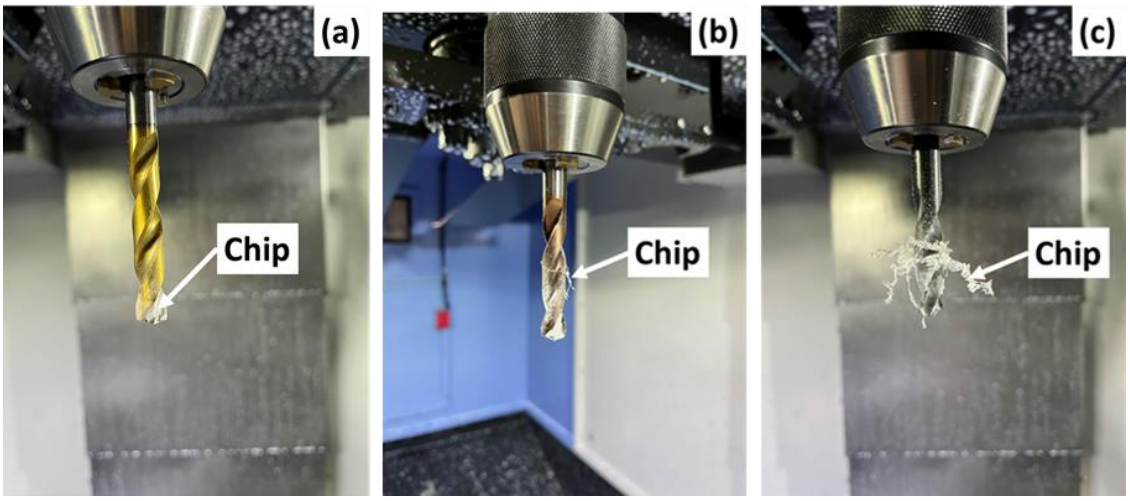

Figure IV-5: Chip adhesion on the drill bits. a) T1: HSS-TITAN, b) T2: HSS-CARBIDE and c) HSS-SUPER.

Table IV-2: Circularity and cylindricity error data for DPFP40 holes drilled using "HSS TITAN / 10 mm" tools.

No.	Code	Drilling Condition		Circularity	pat-downs	Cylindricity	pat-downs
		N (rpm)	*f* (mm/min)				
1	1:1	560	40	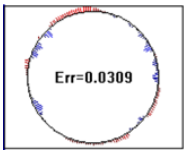	134	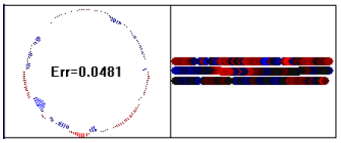	384
2	2:1	1120	40	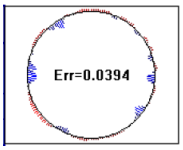	162	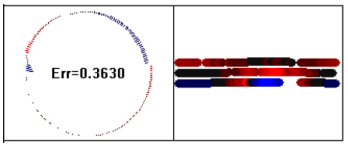	361
3	3:1	2240	40	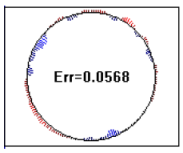	134	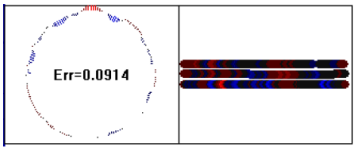	399
4	1:2	560	80	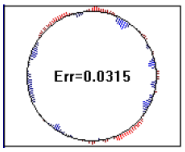	120	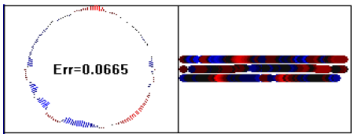	377
5	2:2	1120	80	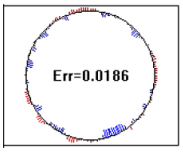	124	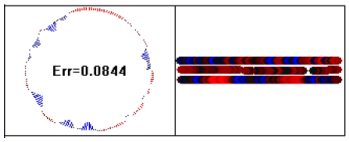	391
6	3:2	2240	80	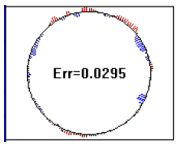	129	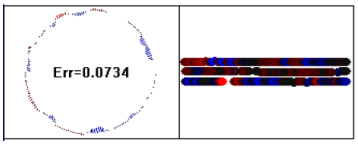	387
7	1:3	560	200	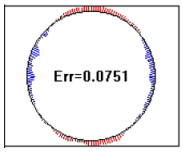	135	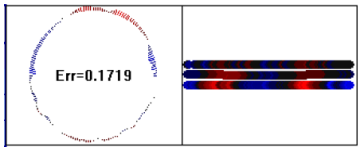	403
8	2:3	1120	200	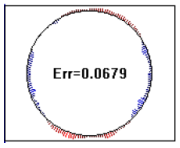	134	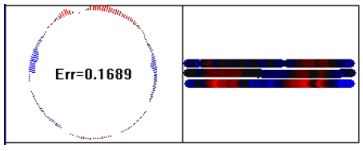	398
9	3:3	2240	200	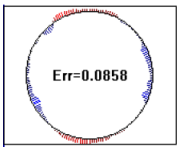	114	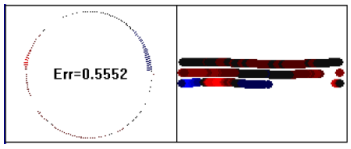	331

Table IV-2: (Continued). "HSS CARBIDE / 10 mm".

No.	Code	Drilling Condition		Circularity	pat-downs	Cylindricity		pat-downs
		N (rpm)	*f* (mm/min)					
10	4:4	560	40	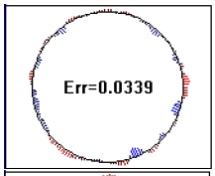	127	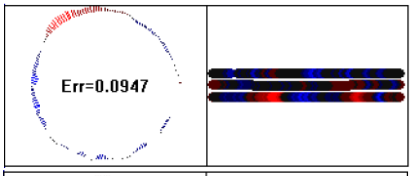		387
11	5:4	1120	40	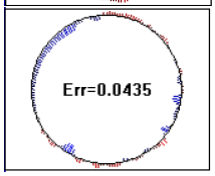	133	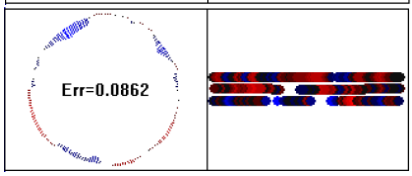		348
12	6:4	2240	40	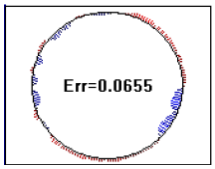	124	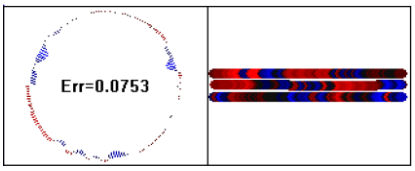		402
13	4:5	560	80	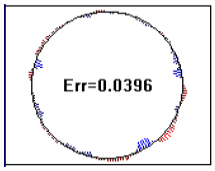	132	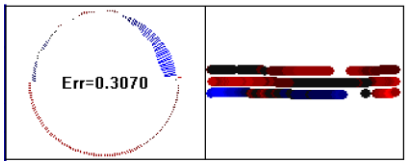		390
14	5:5	1120	80	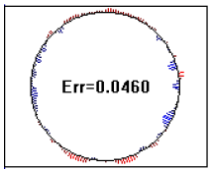	129	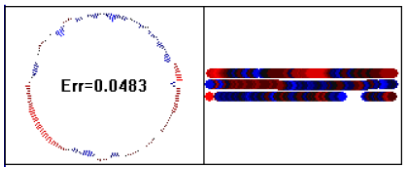		364
15	6:5	2240	80	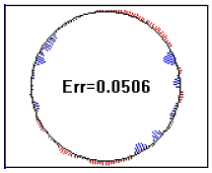	128	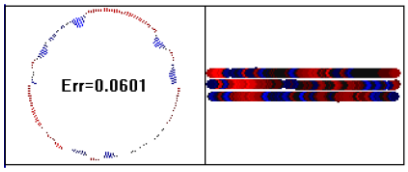		392
16	4:6	560	200	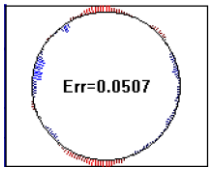	134	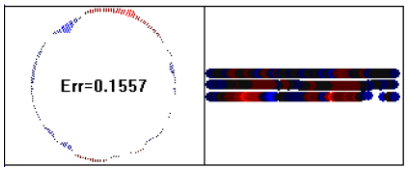		403
17	5:6	1120	200	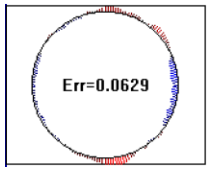	134	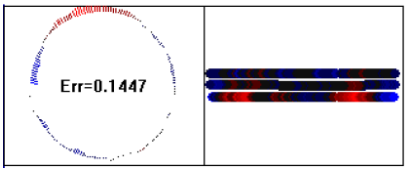		397
18	6:6	2240	200	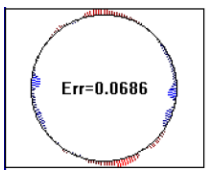	134	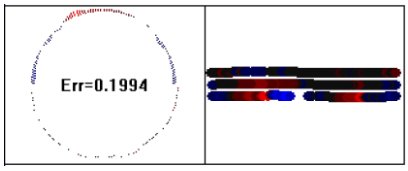		392

Table IV-2: (Continued). "HSS SUPER / 10 mm".

No.	Code	Drilling Condition		Circularity	pat-downs	Cylindricity	pat-downs
		N (rpm)	*f* (mm/min)				
19	7:7	560	40	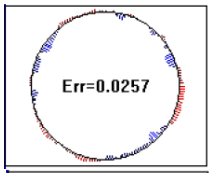	127	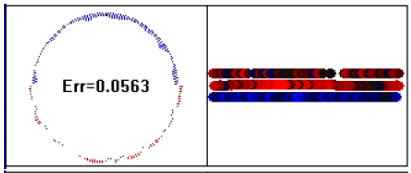	387
20	8:7	1120	40	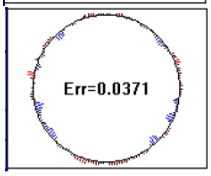	133	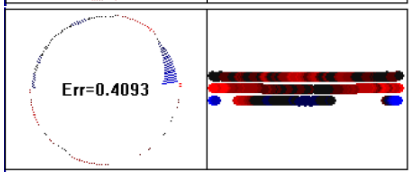	348
21	9:7	2240	40	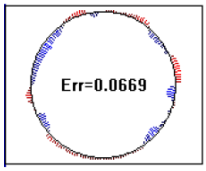	124	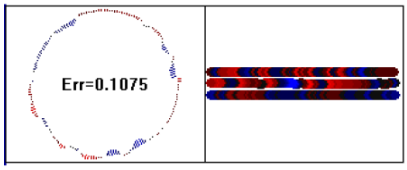	402
22	7:8	560	80	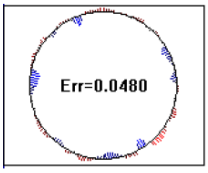	132	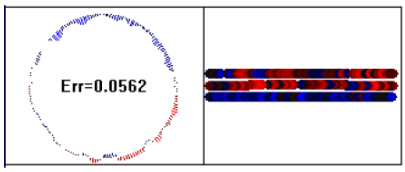	390
23	8:8	1120	80	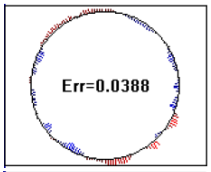	129	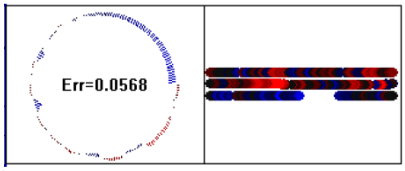	364
24	9:8	2240	80	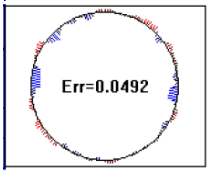	128	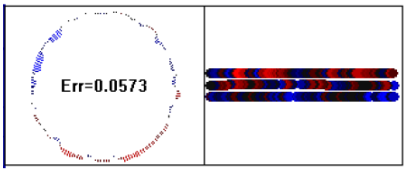	392
25	7:9	560	200	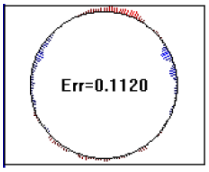	134	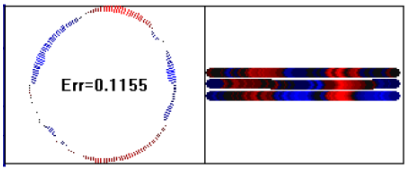	403
26	8:9	1120	200	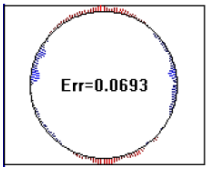	134	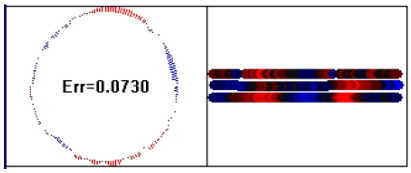	397
27	9:9	2240	200	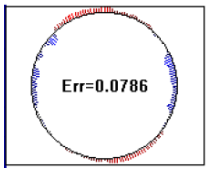	134	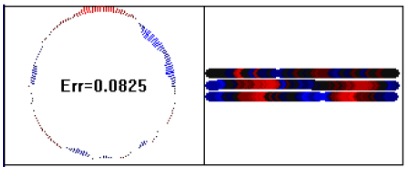	392

IV.4 Drilling of PFPEs

IV.4.1 Circularity and cylindricity measurements for PFPEs holes

Table IV-3 illustrates the variations in circularity and cylindricity errors observed during the drilling operation of PFPEs, contingent upon the feed rate and different spindle speeds utilized in this research. The results demonstrate that at a spindle speed of 500 rpm, the circularity error reaches 0.1807, which experiences a notable decrease of 58.32% at 1000 rpm, reaching 0.0753. This reduction can be attributed to the increased spindle speed leading to a decrease in drilling force, consequently minimizing the formation of burrs and contributing to an improvement in the circularity of the drilled holes[279, 280]. Conversely, circularity responds inversely to the feed rate variable: at 50 mm/min, the circularity error is 0.1105, but it increases by 80.18% at 100 mm/min, reaching 0.1991. The drill bit point angle also significantly influences circularity, with the 115° HSS-SUPER drill bit outperforming the 85° and 135° counterparts, yielding values of 0.1108, 0.1554, and 0.2204, respectively.

In terms of cylindricity errors, it demonstrates a linear response to both spindle speed and feed rate. This indicates that an increase in cylindricity values corresponds directly to increases in both spindle speed and feed rate. At a spindle speed of 1000 rpm, cylindricity errors are recorded at 0.1861, which rise by 51.07% at 1500 rpm, reaching 0.2811. This phenomenon can be attributed to the misalignment of holes and indentations resulting from the uneven distribution of palm fiber powder. This imbalance becomes more pronounced at higher spindle speeds, leading to an increase in cylindrical error[281]. Similarly, at a feed rate of 100 mm/min, cylindricity errors measure 0.1323, but they experience an 23.28% increase at 150 mm/min, reaching 0.1631. The drill point angle also influences cylindricity, with the 85° drill showing inferior performance compared to the 115° and 135° drills. For instance, at 1500 rpm and a feed rate of 50 mm/min, cylindricity errors are 0.2082 for the 85° drill, while they decrease to 0.1895 and 0.1323 for the 135° and 115° drills, respectively.

Table IV-3: Experimental outcomes for the circularity and cylindricity errors of the holes drilled in PFPEs under diverse cutting conditions.

N°	Drilling Condition			circularity errors	cylindricity errors
	Feed rate	Spindle speed	Point angles of the drill bits		
1		500		0.1105	0.1247
2	50	1000		0.1992	0.1861
3		1500		0.2367	0.2811
4		500		0.1991	0.1699
5	100	1000	HSS-SUPER 85°	0.2204	0.2082
6		1500		0.2091	0.2040
7		500		0.1779	0.2106
8	150	1000		0.2087	0.2055
9		1500		0.1328	0.1840
10		500		0.1807	0.2028
11	50	1000		0.0753	0.0928
12		1500		0.1288	0.2315
13		500		0.0346	0.0356
14	100	1000	HSS-SUPER 155°	0.1108	0.1323
15		1500		0.1147	0.1723
16		500		0.1239	0.1607
17	150	1000		0.1198	0.1631
18		1500		0.1280	0.1503
19		500		0.2095	0.2662
20	50	1000		0.1682	0.1872
21		1500		0.1940	0.2085
22		500		0.0900	0.1021
23	100	1000	HSS-SUPER 135°	0.1554	0.1895
24		1500		0.1447	0.1768
25		500		0.1803	0.2051
26	150	1000		0.0986	0.1299
27		1500		0.1037	0.1404

The optimal quality of the drilled holes in PFPEs was attained using an HSS-SUPER drill with a 115°-point angle, operating at a spindle speed of 500 rpm and a feed rate of 100 mm/min (shown in **Figures IV-6a** and **IV-6b**). Conversely, the least desirable hole quality was observed when employing an HSS-SUPER drill with an 85°-point angle, at a spindle speed of 1500 rpm and a feed rate of 50 mm/min (depicted in **Figures IV-6c** and **IV-6d**).

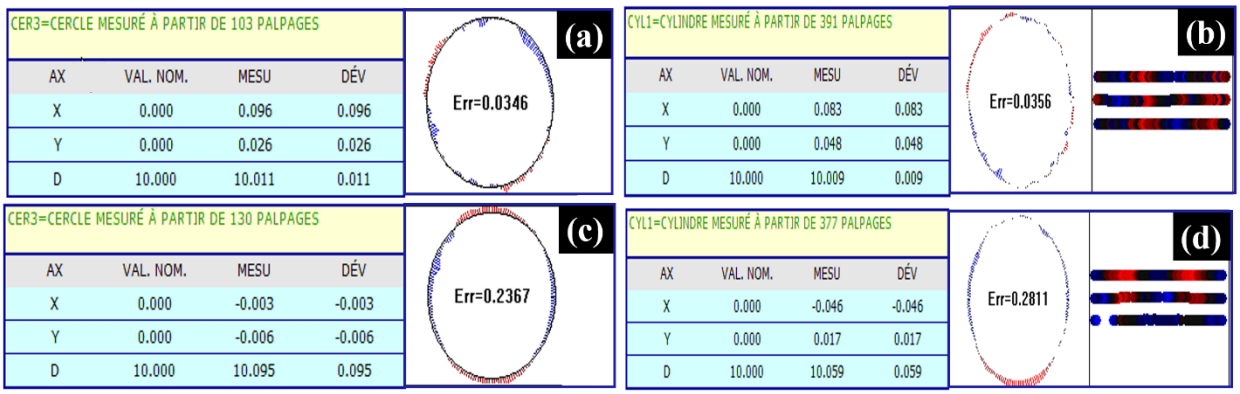

Figure IV-6: (a), (b) Best value Circularity and Cylindricity errors of PFPEs (hole of specimen 13), and (c), (d) Worst value Circularity and Cylindricity errors of PFPEs (hole of specimen 03).

The findings of this study are consistent with previous research, exemplified by the work of Farzad et al[282]. They extensively investigated the effect of drilling parameters on hole geometry and circularity in a composite material consisting of walnut shell powder and polyethylene. Their findings revealed a direct relationship between increasing spindle speed and a decrease in circularity error, accompanied by an increase in cylindricity error for the drilled holes. Specifically, at a spindle speed of 1100 rpm, the circularity error was 0.014, while the cylindricity error was 0.007. Conversely, at 1400 rpm, the circularity error decreased to 0.009, while the cylindricity error increased to 0.012. Moreover, an increase in feed rate led to a simultaneous increase in both circularity and cylindricity errors. For example, at a feed rate of 20 mm/min, the circularity error was 0.014, and the cylindricity error was 0.007. At 100 mm/min, the circularity error decreased to 0.0018, while the cylindricity error increased to 0.0019. In another study, Krishnamurthy et al[283]. Aimed to optimize machining parameters for drilling CFRP composites. Their results indicated that lower feed rates, higher spindle speeds, and shallower drill point angles contribute to improved surface quality. Additionally, Rubio et al[284]. Examined the influence of feed rate, spindle speed, and drill point angle on thrust force and circularity error during the drilling of unreinforced and reinforced polyamide. Their findings suggested a significant effect of drill point angle on both thrust force and circularity error, with these parameters reaching their minimum values at the highest drill point angle of 130° and the lowest drill point angle of 85°, respectively.

IV.5 Conclusion

In summary, the fourth chapter of the thesis investigating the drilling behavior of DPFP40 and PFPEs in biocomposites has yielded noteworthy insights and key discoveries. The study revealed that the optimal quality of drilled holes in DPFP40, as determined by the delamination factor, was achieved using an HSS-SUPER drill bit operated at a spindle speed of 2240 rpm and a feed rate of 40 mm/min. Conversely, the least favorable hole quality was observed when employing an HSS-CARBIDE drill bit at a spindle speed of 560 rpm and a feed rate of 200 mm/min. Moreover, for enhanced circularity of the drilled holes of DPFP40, the recommended cutting parameters include a spindle speed of 1120 rpm, a feed rate of 80 mm/min, and an HSS-TITAN drill material, while for improved cylindricity, the suggested parameters are a spindle speed of 560 rpm, a feed rate of 80 mm/min, and an HSS-CARBIDE drill material. Similarly, in PFPEs, the optimal quality of drilled holes was achieved using an HSS-SUPER drill with a 115° point angle, operating at a spindle speed of 500 rpm and a feed rate of 100 mm/min. Conversely, the least desirable hole quality was observed with an HSS-SUPER drill featuring an 85° point angle, at a spindle speed of 1500 rpm and a feed rate of 50 mm/min.

These findings highlight the critical importance of selecting appropriate drilling parameters to enhance the quality of machined features in natural fiber-reinforced materials. Overall, Chapter IV underscores the significance of parameter optimization and the selection of suitable drilling tools in achieving superior quality machined features in biocomposites. By understanding and implementing the optimal parameters identified in this study, manufacturers and researchers can improve drilling processes, minimize waste production, and enhance the overall quality of machined features in biocomposites.

Chapter V

Analysis, optimization and modeling of outcomes

V Chapter V: Analysis, optimization and modeling of outcomes

V.1 Introduction

The concluding chapter of the thesis extensively examines the detailed analysis, optimization, and modeling of the absorption behavior of DPFPs, as well as the drilling behavior of DPFO40 and PFPEs. This section employs sophisticated methodologies such as Artificial Neural Networks (ANN) and Response Surface Methodology (RSM) to forecast and refine the absorption properties of DPFPs and the drilling behavior of DPFP40. Furthermore, it utilizes ANN and the Taguchi method to predict and enhance the drilling behavior of PFPEs. Through regression analysis, error histograms, and a comparative assessment of experimental and predicted values, this chapter offers valuable insights into the accuracy and reliability of the developed models. Moreover, it discusses the research findings in relation to prior studies, underscoring the consistency and significance of the outcomes. In essence, this chapter provides a comprehensive exploration of modeling and optimizing the absorption behavior of DPFPs, along with DPFP40 and PFPEs drilling behavior, showcasing the potential of advanced techniques in predicting and improving material properties.

V.2 Optimization and modelization of absorption behavior of DPFPs using ANN and RSM

V.2.1 ANN

Mean Squared Error (*MSE*) and regression analysis were employed to evaluate the precision of the fit. An *MSE* value below 0.001 is considered acceptable, thus, a lower *MSE* value indicates higher accuracy in the predictions[285]. **Figures V-1** and **V-2**, along with **Table V-1**, demonstrate that *MSE* values are notably low, approximately 1.20×10^{-4} for training, 1.38×10^{-4} for validation, and 7.04×10^{-4} for tests. Furthermore, the correlation coefficient "*R*" values for the training, validation, and test datasets all exceed 0.99 across all studied samples. **Figure V-3b** and **Table V-2** provide a comparison between the actual experimental data for the average mass of DPFPs and the expected values generated by the ANN model, as well as the residual between them. The maximum mass values after the saturation phase are summarized in **Table V-2**. In **Figure V-3a**, all 153 average mass values from the initial to the final measurement are depicted, illustrating the proximity between the experimental and expected data with minimal error deviation, estimated at an average value of 3×10^{-5}. Consequently, based on these findings, it can be inferred that the optimized ANN model exhibits favorable and high accuracy.

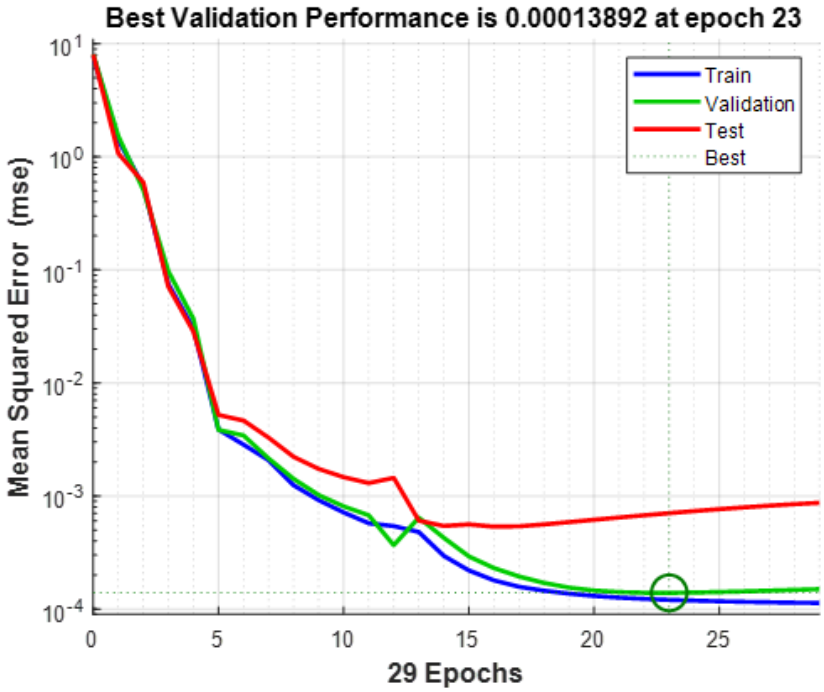

Figure V-1: *MSE* of network data with increasing epoch.

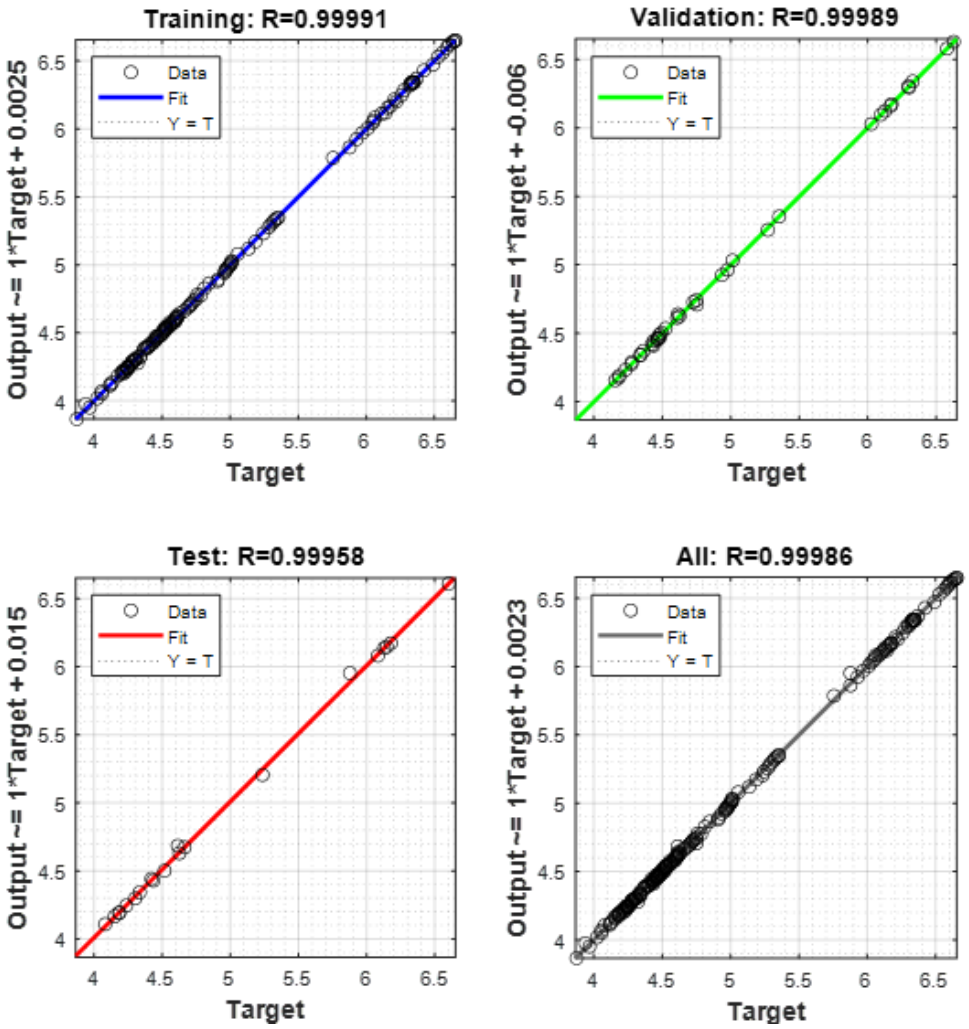

Figure V-2: Regression analysis of the ANN model.

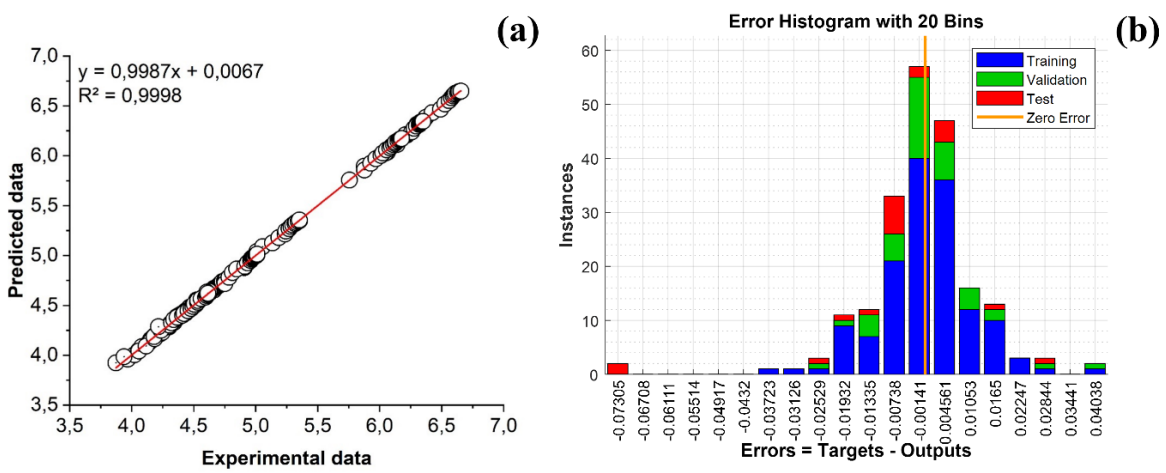

Figure V-3: a) Experimental and predicted values from the ANN model, b) Graphical representation of errors from the ANN model using a histogram.

Table V-1: Performance evaluation of the ANN architecture.

Materials	**Data used**	**Sample (weight)**	***MSE*×10^{-4}**	***R²***
DPFPs	Training	107	1.20369	0. 999908
	Validation	31	1.38922	0. 999889
	Testing	15	7.04631	0.999582

Table V-2: Analysis of process parameter effects on the absorption responses of DPFPs.

N° Experience	**Input**		**Output**					
	Type of liquid	Fiber content	Exp	ANN	Error E-P	*RMSE*	*R²*	% Error E−P/ E× 100
1	Seawater	15%	4.7483	4.7456	0.0028	0.0063	0.9998	0.0585
2	Seawater	20%	6.6553	6.6487	0.0066	0.0123	0.9945	0.0989
3	Seawater	27%	5.3537	5.3559	-0.0023	0.0143	0.9931	-0.0425
4	Distilled water	15%	4.6262	4.6416	-0.0154	0.0075	0.9950	-0.3330
5	Distilled water	20%	6.3490	6.3438	0.0052	0.0109	0.9924	0.0825
6	Distilled water	27%	5.0121	5.0125	-0.0005	0.0137	0.9847	-0.0090
7	Rainwater	15%	4.5233	4.5540	-0.0307	0.0109	0.9883	-0.6789
8	Rainwater	20%	6.1770	6.1728	0.0042	0.0059	0.9973	0.0678
9	Rainwater	27%	4.6140	4.6210	-0.0070	0.0192	0.9706	-0.1522

$$MSE = \frac{1}{n}\sum_{i=1}^{n}\left|(Y_{p,i} - Y_{e,i})^2\right| \quad \text{(V-1)}$$

$$RMSE = \sqrt{\frac{\sum_{i=1}^{n}(Y_{p,i}-Y_{e,i})^2}{n}} \quad \text{(V-2)}$$

$$R^2 = 1 - \frac{\sum_{i=1}^{n}(Y_{p,i}-Y_{e,i})^2}{\sum_{i=1}^{n}(Y_{p,i}-Y_e)^2} \quad \text{(V-3)}$$

MSE represents the mean square error, *RMSE* is the square root of the *MSE*, and R^2 stands for the coefficient of determination. The variables $Y_{e,i}$ and $Y_{p,i}$ denote the experimental and predicted corresponding data, respectively. Y_e represents the mean value of the experimental data, and *n* represents the number of experimental runs[286-289].

V.2.2 RSM

In this experiment, the RSM design was employed to construct a quadratic model consisting of 153 trials. The "optimal design" approach was applied to assess the influence of three variables "Levels $^{\text{Factors}}$ =3^3" (Time: 24 to 672h, Fiber rate: 15,20, and 27%, and type of liquids: Sea, Distilled, and Rain water) with varied tiers on the DPFPs mass responses by manipulating the input factors during the absorption process of the bio composites. The algebraic expression for the quadratic regression, which correlates the DPFPs mass with the three aforementioned factors, is presented in **Table V-3**. This equation was derived using Design Expert software, which recommends the use of quadratic models.

The outcomes of the ANOVA model are detailed in **Table V-4**. The R^2 and adjusted R^2 coefficients for the Mass of DPFPs are 99.63% and 99.61%, respectively, indicating an excellent alignment between responses and factors. The regression model is statistically significant, with a P-value less than 0.0001. The linear coefficients A, B, and C, along with the quadratic term coefficients B×C, A×A, and B×B, exhibit significant impacts on the Mass of DPFPs, as evidenced by their substantial *F-value* and small *P-value*. The *F-value* is utilized to identify and assess the relative impact of different factors; a higher *F-value* and lower *P-value* signify a greater influence on the response of the process[290].

From the data in **Table V-4**, it can be deduced that the most influential variable affecting the Mass of DPFPs in the engineered bio composites is the Type of liquids, with an *F-value* of 2195.14, followed by fiber rate with a value of 1116.01, and time with a value of 617.40. Another crucial coefficient is the predicted R^2, which has a high value of 99.57%, signifying a robust association between the anticipated and actual values, as demonstrated in **Figure V-5**.

All 153 average mass values of DPFPs are depicted in **Figure V -5**. The data indicates that the measured and anticipated values are very similar, with a slim differential of error and a high R^2

coefficient of 99.63%, 99.52%, and 99.80% for seawater, distilled water, and rainwater, respectively. Therefore, based on these results, it can be inferred that the optimized RSM model is accurate and reliable.

Figure V-4a illustrates the relationship between predicted and experimental results for the DPFPs mass. The results demonstrate substantial agreement with the regression model, as the anticipated and experimental values align statistically with a confidence level of 99.63%. In **Figure V-4b,** the normal probability curve of the residuals for DPFPs mass is presented. The residuals predominantly follow a linear pattern, indicating a favorable distribution of errors. These observations imply that the quadratic model is statistically significant in analyzing DPFPs mass, and there is no evidence of any violation in the assumptions of independence or constant variance[291, 292].

Table V-3: Algebraic model representing the DPFPs mass obtained through the RSM approach.

RSM output	Algebraic Model
Mass of DPFPs	-15.23627 + 0.001480×Time + 1.99773×Fiber rate + 0.301623×Type of liquids + 8.57385×10^{-6}× Time×Fiber rate - 0.000081× Time×Type of liquids - 0.020600×Fiber rate×Type of liquids - 1.45041×10^{-06}×$Time^2$ - 0.045988× Fiber rate ² - 0.019289× Type of liquids²

Table V-4: ANOVA for the Quadratic Model of DPFPs Mass.

Source	Sum Of Squares	Df	Mean Square	*F-Value*	*P-Value*	
Model	96.41	9	10.71	4295.75	< 0.0001	**significant**
A-Time	1.54	1	1.54	617.40	< 0.0001	
B-Fiber Rate	2.78	1	2.78	1116.01	< 0.0001	
C-Type of Liquids	5.47	1	5.47	2195.14	< 0.0001	
AB	0.0118	1	0.0118	4.71	0.0316	
AC	0.0286	1	0.0286	11.49	0.0009	
BC	1.05	1	1.05	420.41	< 0.0001	
A^2	0.3915	1	0.3915	157.00	< 0.0001	
B^2	87.28	1	87.28	34998.22	< 0.0001	
C^2	0.0127	1	0.0127	5.07	0.0258	
Residual	0.3566	143	0.0025			
Cor Total	96.77	152				
d. Dev.	0.0499		***R²***			99.63%
Mean	5.22		**Adjusted *R²***			99.61%
C.V. %	0.9572		**Predicted *R²***			99.57%

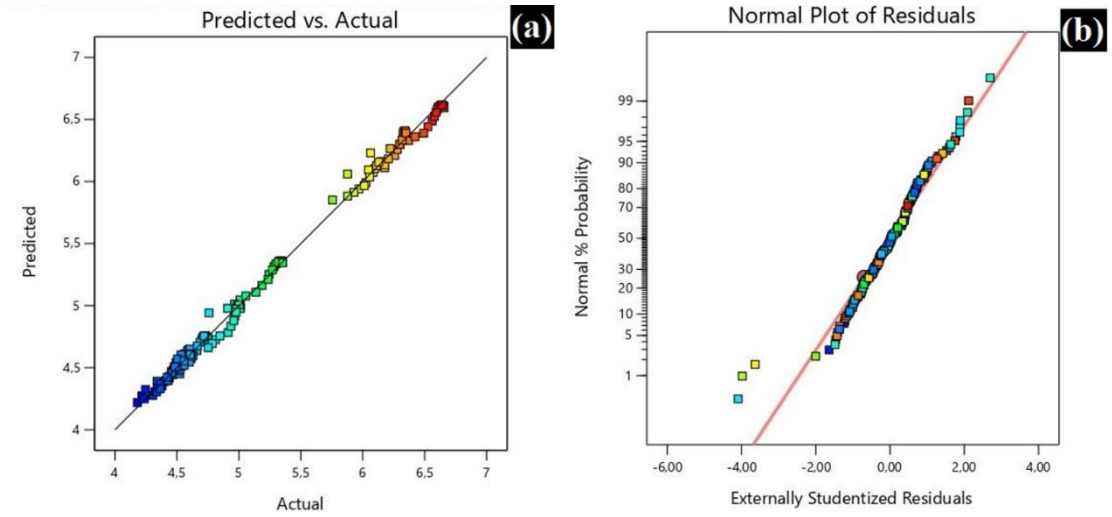

Figure V-4: a) A comparison between anticipated and actual values for DPFPs mass. b) The normal probability distribution of deviations in DPFPs mass.

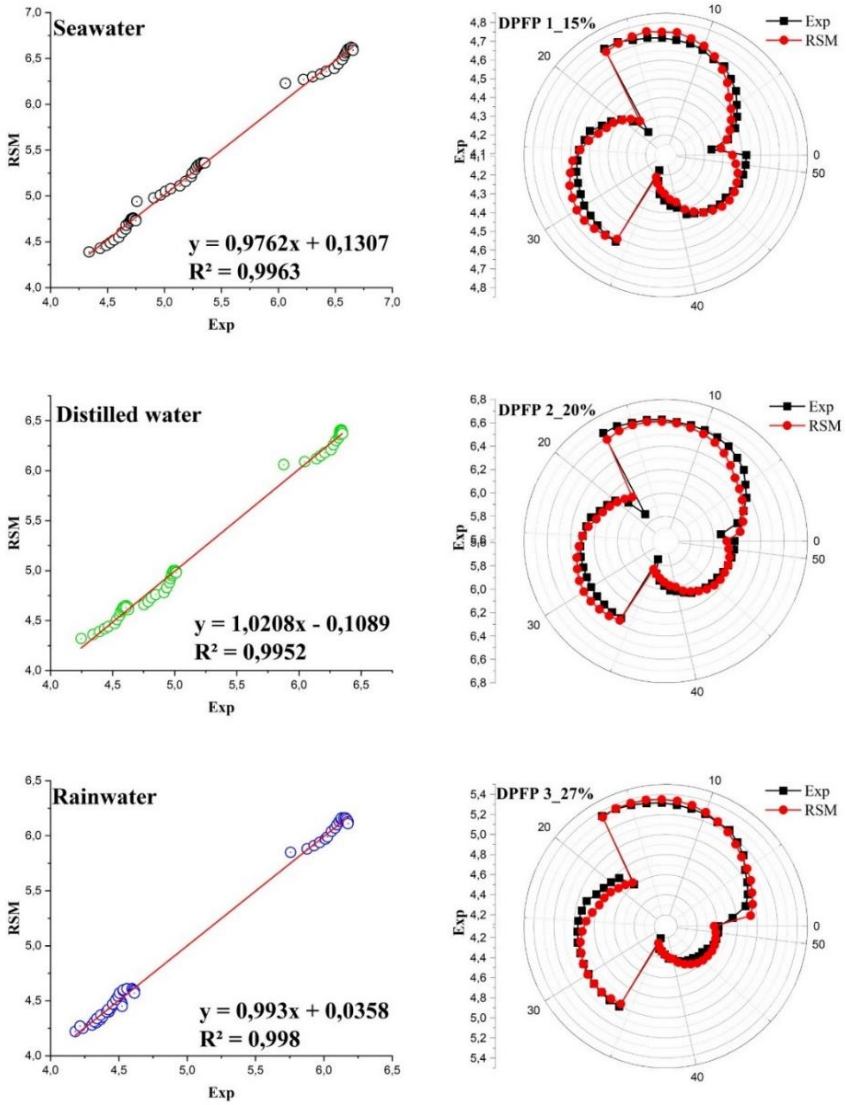

Figure V-5: Comparison between observed experimental values and predicted values from the RSM model.

Figure V-6 illustrates 3D surface plots depicting the Mass of DPFPs concerning different types of liquids, varied Fiber rates, and diverse times. These surface plots can aid in forecasting the absorption rate analysis at any point within the experimental zone. **Figures V-6a**, **V-6b**, and **V-6c** demonstrate the variation in the Mass of DPFPs concerning Time. The absorption rate rises with an increase in the immersion time of the bio composites in liquids. For instance, the Mass of DPFPs, with 15% fiber reinforcement and immersed in seawater for 24 hours, is estimated at 4.439g. Contrastingly, it reaches a higher estimated value of 4.804 g after 670 hours under the same conditions of liquid type and fiber rate. Meanwhile, **Figures V-6d**, **V-6e**, and **V-6f** reveal that the fiber content and the arrangement of fiber layers significantly impact the absorption rate. For instance, the absorption rate peaks at 12.30% for the bio composite immersed in seawater for 24 hours with a 15% fiber content, compared to the bio composite with a 27% fiber content. This percentage reaches a maximum of approximately 41.30% for the bio composite with a 20% fiber content under the same immersion conditions. On the other hand, **Figures V-6g**, **V-6h**, and **V-6i** highlight the substantial effect of different types of liquids on the absorption rate. For instance, the absorption rate for bio composites with 15% fiber reinforcement, immersed in seawater for 24 hours, is estimated at 38.60%. This percentage increases to an estimated rate of 42.10% when the same bio composite is immersed in distilled water.

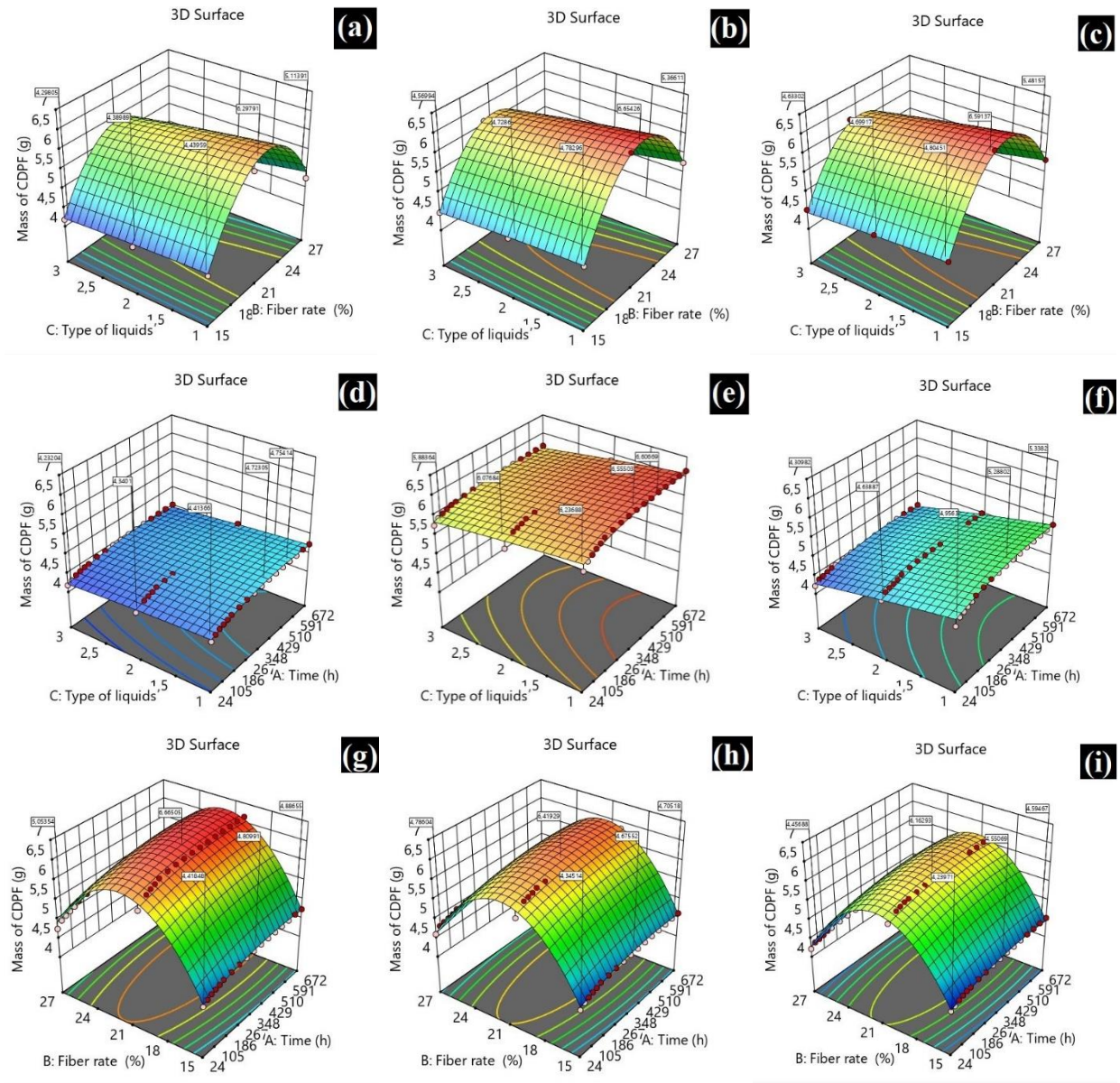

Figure V-6: 3D surface plots illustrating the Mass of DPFPs as a function of Time, Fiber rate, and Type of liquids (water): (a) 24h, (b) 336h, and (c) 672h, (d) 15%, (e) 20%, and (f) 27%, (g) Seawater, (h) Distilled water, and (i) Rainwater.

These findings are in accordance with the observations reported by Makhlouf et al[293]. In their study on the water sorption behavior of bio composites (*HDPE/%JF*), absorption experiments were conducted by immersing the bio composite samples in distilled water at 24°C for several days until the water uptake rate stabilized. The researchers noted a direct correlation between the amount of jute filler in the samples, the duration of immersion, and the amount of water absorbed. They observed that the absorption rate was initially rapid, reaching saturation after approximately 120 hours of immersion. Similar observations were reported by Lekrine et al[294]. In their investigation of water absorption behavior and bio-composite kinetics. They immersed HDPE matrices reinforced with varying contents of Washingtonia filifera (*WF*) fibers (10%, 20%, and 30%) in

distilled water at 25°C. The study, which analyzed the RSM model to assess the impact of *WF* fiber content and immersion time on water absorption in *HDPE/WF* bio composites, found that the water absorption process followed the Fickian diffusion mode, and the addition of *WF* fibers to the *HDPE* matrix reduced diffusivity. The results indicated that the most favorable conditions for achieving the highest absorption were a fiber rate of 29.88% and a submersion period of 751 hours.

V.3 Optimization and modelization of drilling behavior of DPFP40 using ANN and RSM

V.3.1 ANN

Figures **Figure V-7a** and **Figure V-8**, along with **Table V-6**, highlight the exceptional values of *MSE*, approximately 1.04×10^{-7} for training, 1.09×10^{-4} for validation, and 2.51×10^{-4} for testing, alongside correlation coefficient "*R*" values exceeding 0.98 for training, validation, and testing datasets. Furthermore, **Table V-5** and **Figure V-7b** present the comparison between experimental and expected values for ANN regarding the delamination factor, revealing closely aligned values with minimal deviation error, averaging at 4.3×10^{-4}. These findings are consistent with the outcomes of Tabet et al[270], who investigated the impact of drilling parameters on delamination damage in a bio sandwich structure, highlighting the effectiveness of ANN models developed for HSS drills TiN and BSD as predictive tools for the delamination factor.

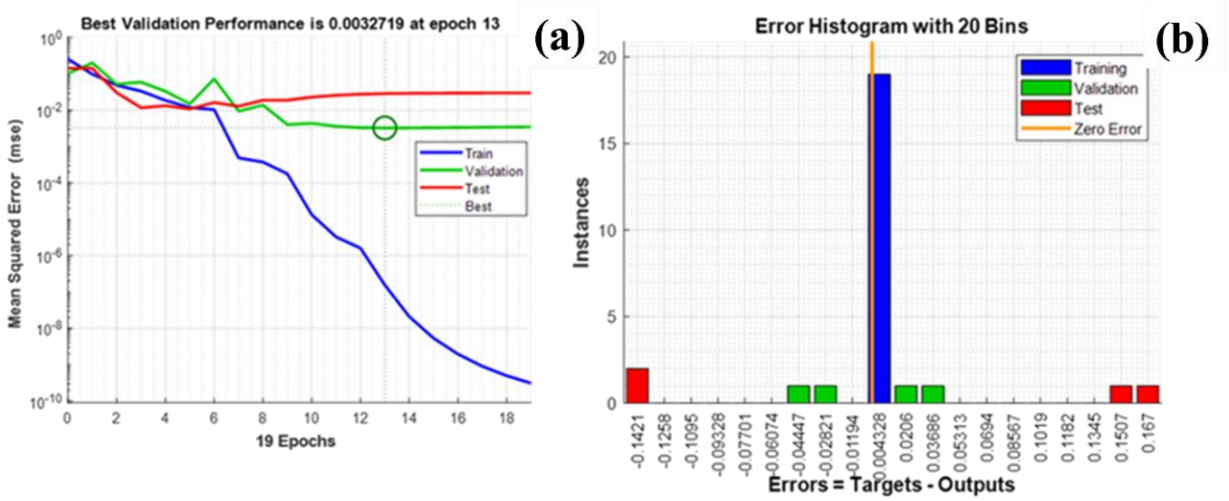

Figure V-7: a) *MSE* of network data, b) Error histogram of ANN model.

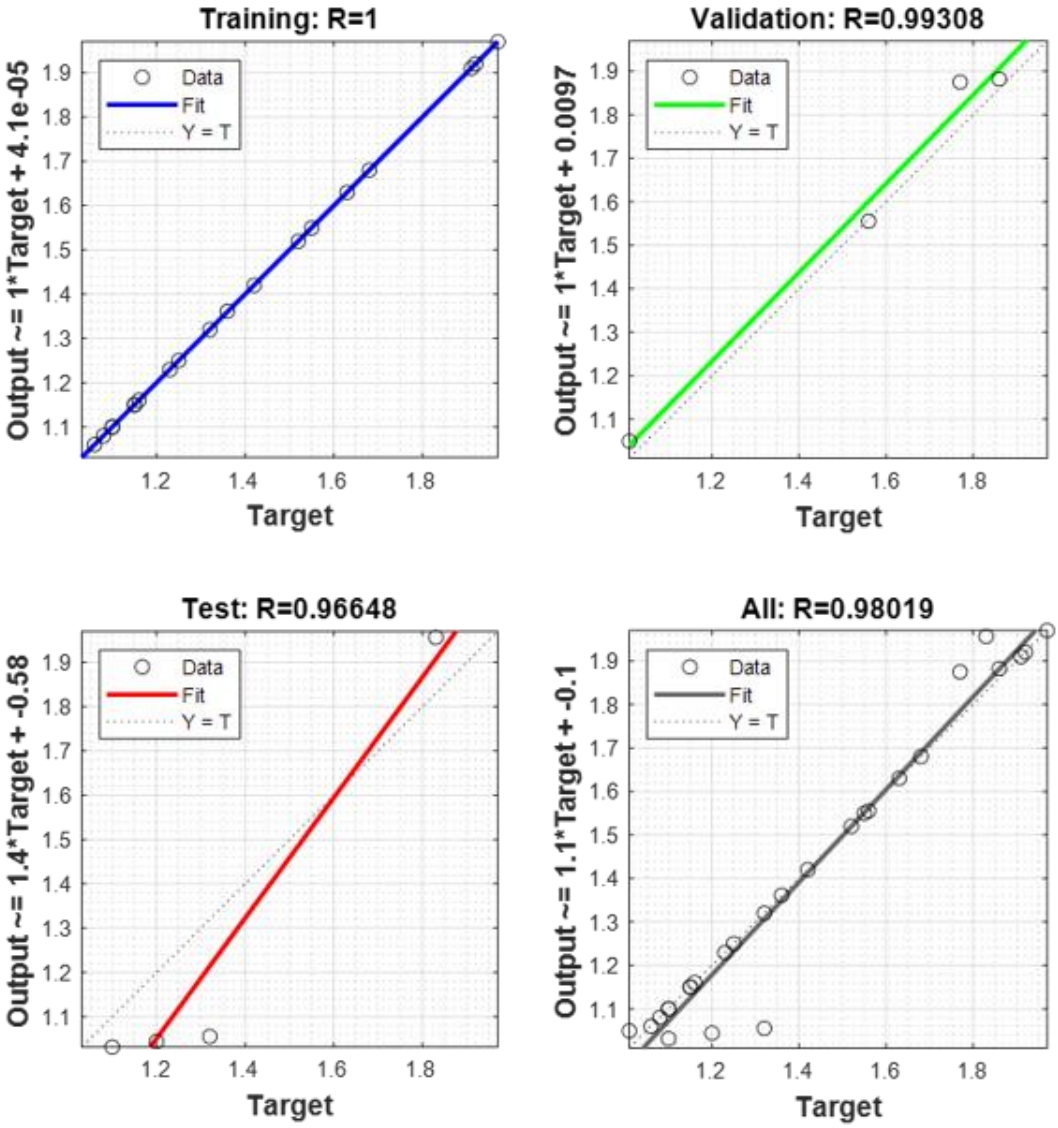

Figure V-8: ANN model regression analysis.

Table V-5: Experimental and predicted outcomes using ANN for the delamination factor of DPFP40.

N°	Input variables			Output variables		
	f **(mm/min)**	**N (rpm)**	**Drill materials**	F_d		
				EXP	**ANN**	**Error**
1	560	40	HSS-TITAN	1.37	1.36	-0.006
2	1120	40		1.31	1.31	0.001
3	2240	40		1.07	1.05	-0.019
4	560	80		1.87	1.87	0.002
5	1120	80		1.57	1.61	0.047
6	2240	80		1.21	1.21	0.004
7	560	200		1.91	1.88	-0.022
8	1120	200		1.64	1.62	-0.014
9	2240	200		1.43	1.42	-0.005
10	560	40	HSS –CARBIDE	1.78	1.79	0.011
11	1120	40		1.52	1.52	0.001
12	2240	40		1.11	1.10	-0.003
13	560	80		1.90	1.88	-0.013
14	1120	80		1.68	1.67	-0.008
15	2240	80		1.24	1.24	0.008
16	560	200		1.98	2.03	0.051
17	1120	200		1.84	1.9	0.140
18	2240	200		1.54	1.54	0.006
19	560	40	HSS-SUPER	1.11	1.08	-0.027
20	1120	40		1.09	1.09	0.005
21	2240	40		1.02	1.00	-0.012
22	560	80		1.26	1.30	0.040
23	1120	80		1.14	1.16	0.020
24	2240	80		1.09	1.10	0.016
25	560	200		1.33	1.31	-0.015
26	1120	200		1.17	1.17	0.001
27	2240	200		1.14	1.09	-0.042

Table V-6: Performance of ANN Architecture.

Materials	Data used	Sample	*MSE*	R^2
DPFP40	Training	19	1.04731×10^{-7}	0.999999
	Validation	41	1.09879×10^{-4}	0.996943
	Testing	20	2.51005×10^{-4}	0.987593

V.3.2 RSM

Table V-7 displays the output parameters, specifically the delamination factor (F_d), for the drills utilized in this study (HSS-TITAN, HSS-CARBIDE, and HSS-SUPER) across various machining conditions. The experimental setup employed the RSM design to construct a quadratic model, comprising 27 trials. These outcomes were derived from an optimal design aimed at

investigating the impact of three factors (feed rate, spindle speed, and drill material) with three levels on the delamination factor (F_d) responses. The mathematical equation representing the second-order regression for the delamination factor concerning these factors is outlined in **Table V-8**. This equation was generated using the Design Expert software, which advocates quadratic models for such analyses.

Table V-7: Experimental and predicted outcomes using RSM for the delamination factor of DPFP40.

N° Test	Input variables			Output variables		
	***f* (mm/min)**	**N (rpm)**	**Drill materials**	***F_d***		
				EXP	**RSM**	**Error**
1	560	40	HSS-TITAN	1.37	1.56	-0.19
2	1120	40		1.31	1.33	-0.01
3	2240	40		1.07	0.97	0.10
4	560	80		1.87	1.76	0.11
5	1120	80		1.57	1.53	0.04
6	2240	80		1.21	1.18	0.03
7	560	200		1.91	1.94	-0.03
8	1120	200		1.64	1.72	-0.09
9	2240	200		1.43	1.4	0.04
10	560	40	HSS-CARBIDE	1.78	1.67	0.11
11	1120	40		1.52	1.49	0.03
12	2240	40		1.11	1.24	-0.13
13	560	80		1.90	1.84	0.06
14	1120	80		1.68	1.66	0.02
15	2240	80		1.24	1.42	-0.18
16	560	200		1.98	1.94	0.04
17	1120	200		1.84	1.77	0.06
18	2240	200		1.54	1.56	-0.01
19	560	40	HSS-SUPER	1.11	1.17	-0.06
20	1120	40		1.09	1.05	0.04
21	2240	40		1.02	0.91	0.11
22	560	80		1.26	1.31	-0.05
23	1120	80		1.14	1.19	-0.05
24	2240	80		1.09	1.06	0.02
25	560	200		1.33	1.33	0.01
26	1120	200		1.17	1.22	-0.05
27	2240	200		1.14	1.11	0.03

Table V-8: A mathematical model for the delamination factor of DPFP40 using the RSM method.

RSM response	Mathematical model
F_d	$0.8687 - 0.0006 \times A + 0.0082 \times B + 0.9935 \times C + 1.5894\times10^{-7} \times AB + 9.7861\times10^{-5} \times AC - 0.0007 \times BC + 5.640910^{-8} \times A^2 - 2.1566\times10^{-5} \times B^2 - 0.3035 \times C^2$

Table V-9 presents the outcomes of the quadratic ANOVA model for delamination. The R^2 coefficient and adjusted R^2 coefficient associated with delamination are 93.09% and 89.43%, respectively. This indicates a strong alignment between the regression model and the factors influencing delamination. The model is statistically significant, as the *P-value* for the model is below 0.0001. Moreover, the linear coefficients A, B, and C, along with the quadratic term coefficient C×C, exhibit significant effects on delamination, evident from their substantial *F-values* and small *P-values*. *The F-value* provides qualitative insights into the relative effects of factors, with larger values and smaller *P-values* indicating greater significance in influencing the process response[295]. From the data presented in Table V-9, it can be inferred that spindle speed is the most crucial variable affecting the delamination factor in the engineered bio composites, accounting for 69.13%. Following this, drill material contributes by 47.95%, and feed rate by 37.25%. Another noteworthy coefficient is the predicted R^2, known as the coefficient of determination in the ANOVA tables, with a high value of 82.44%, indicating a robust correlation between experimental and predicted values.

Table V-9: ANOVA for the Quadratic Model of DPFP40 delamination.

Source	Sum of squares	Df	Mean square	*F*-value	*P*-value	Remarks
Model	2.32	9	0.2581	25.43	<.0001	**significant**
A-Spindle speed	0.7017	1	0.7017	69.13	<.0001	
B-Feed rate	0.3781	1	0.3781	37.25	<.0001	
C-Drill materials	0.4866	1	0.4866	47.95	<.0001	
AB	0.0015	1	0.0015	0.1515	0.7019	
AC	0.0841	1	0.0841	8.29	0.0104	
BC	0.0420	1	0.0420	4.14	0.0579	
A^2	0.0072	1	0.0072	0.7136	0.4100	
B^2	0.0593	1	0.0593	5.85	0.0271	
C^2	0.5530	1	0.5530	54.48	<.0001	
Residual	0.1725	17	0.0101			
Cor Total	2.50	26				
Std. Dev.	0.1007				R^2	93.09%
Mean	1.42				Adjusted R^2	89.43%
C.V. %	7.10				Predicted R^2	82.44%

Figure V-9a illustrates the correlation between predicted and experimental outcomes for the delamination of the DPFP40 produced in this study using the T1, T2, and T3 drills. The obtained results demonstrate a satisfactory agreement with the regression model, as the predicted values align statistically with the experimental values at a confidence level of 82.44%. In **Figure V-9b**, the normal probability curve of delamination residuals (F_d) is presented. The residuals exhibit a generally linear distribution, indicating a favorable error distribution. These findings affirm that the quadratic model is statistically significant for delamination analysis, and there is no indication of a violation of the assumptions of independence or constant variance[292, 296, 297].

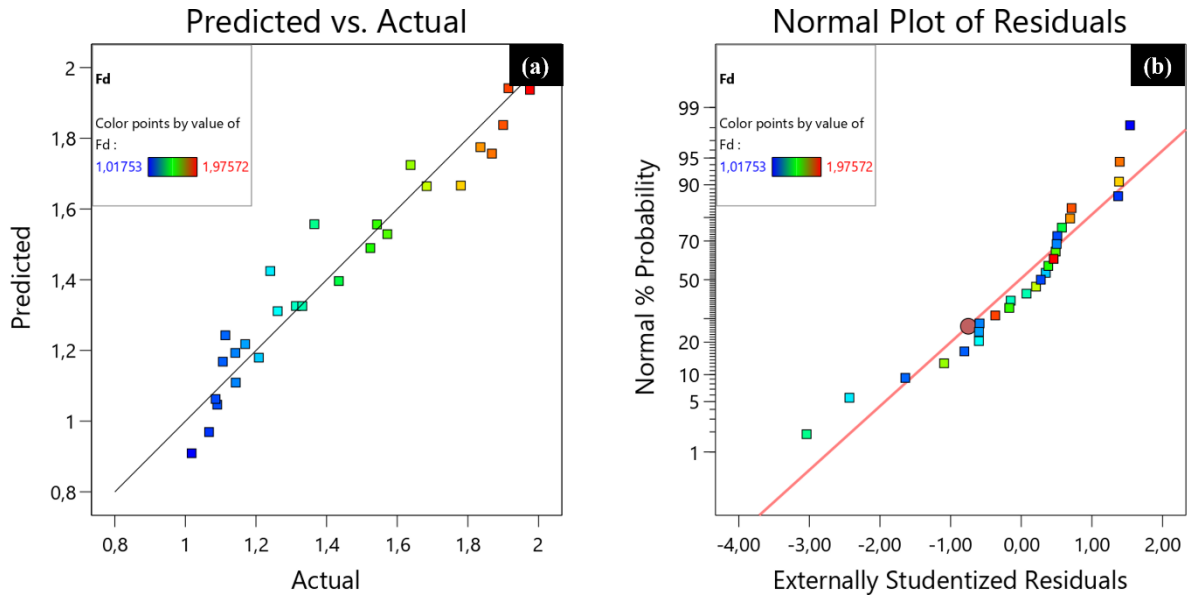

Figure V-9: a) Predicted vs. actual values and b) Normal probability distribution of the F_d residuals of DPFP40.

Figures V-10 and **V-11** depict 3D contour and surface plots illustrating delamination (F_d) in the DPFP40, showcasing its relationship with the feed rate across various spindle speeds for different drill materials. These plots serve as valuable tools for predicting delamination analysis across the experimental spectrum. The results indicate that when utilizing the HSS-TITAN tool, delamination remains below 1.0 within a feed rate range of 40 to 50 mm/min and spindle speeds of 2000 to 2240 rpm. However, delamination exceeds 1.8 at feed rates between 120 and 160 mm/min, along with spindle speeds ranging from 560 to 980 rpm (**Figure V-10a**). Similarly, for the HSS-CARBIDE tool, delamination surpasses 1.8 within a feed rate range of 120 to 160 mm/min and spindle speeds between 560 and 1050 rpm, while it remains below 1.4 at feed rates of 40 to 60 mm/min and spindle speeds ranging from 560 to 980 rpm (**Figure V-10b**). Regarding the HSS-SUPER tool, delamination stays below 1.0 for feed rates between 40 and 50 mm/min, coupled with

spindle speeds of 1400 to 1820 rpm. However, it exceeds 1.3 within a feed rate range of 120 to 160 mm/min and spindle speeds between 560 and 1000 rpm (**Figure V-10c**).

The delamination factor exhibits a notable increase with escalating feed rate, as evidenced in **Figures V-11a**, **V-11b**, and **V-11c**. This cutting condition exerts a significant influence on the delamination factor. Conversely, **Figures V-11d**, **V-11e**, and **V-11f** distinctly demonstrate a decrease in the delamination factor with rising spindle speed. Additionally, **Figures V-11g**, **V-11h**, and **V-11i** elucidate the impact of drill material and feed rate on F_d across three constant spindle speed values. It was observed that when drilling with the HSS-CARBIDE drill under the same cutting conditions (feed rate of 40 mm/min and spindle speed of 560 rpm), the delamination factor exhibited a higher value compared to the utilization of the other two drills (F_d (HSS-CARBIDE) = 1.78, exceeding F_d (HSS-TITAN) = 1.37 and F_d (HSS-SUPER) = 1.11). These findings align closely with those reported in the studies conducted by Kant et al[298], which assessed the mechanical properties and delamination factor of polymer composites reinforced with cellulose fibers (nettle), and Belaadi et al[299], who investigated the mechanical and drilling performance of bio composite polymers reinforced with short jute fibers.

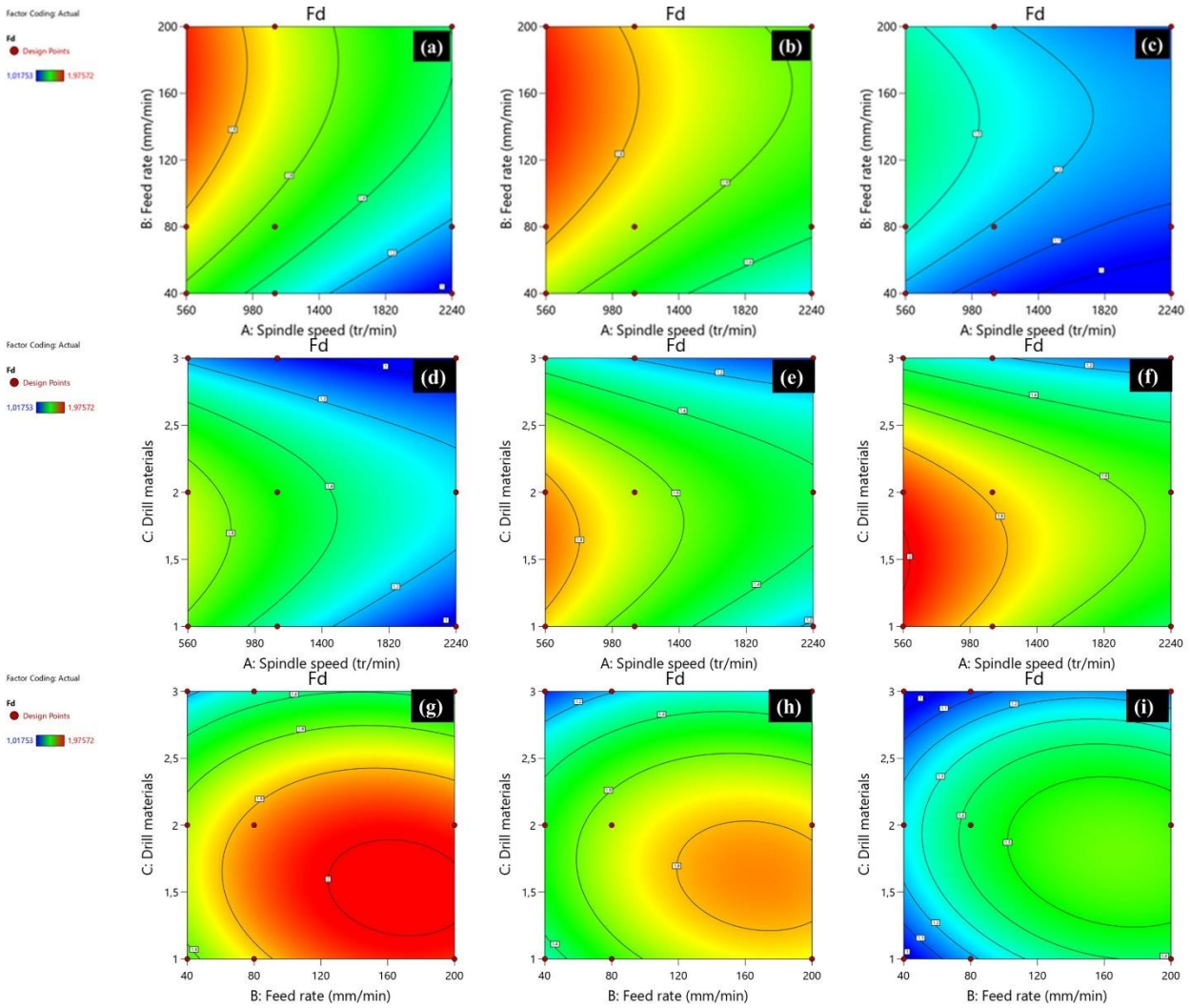

Figure V-10: Representation of response surfaces of F_d data of DPFP40 versus f, N, and drill materials: a) HSS TITAN, b) HSS CARBIDE, and c) HSS SUPER, d) 40mm/min, e) 80mm/min, f) 200 mm/min, g) 560 rpm, h) 1120 rpm, i) 2240 rpm.

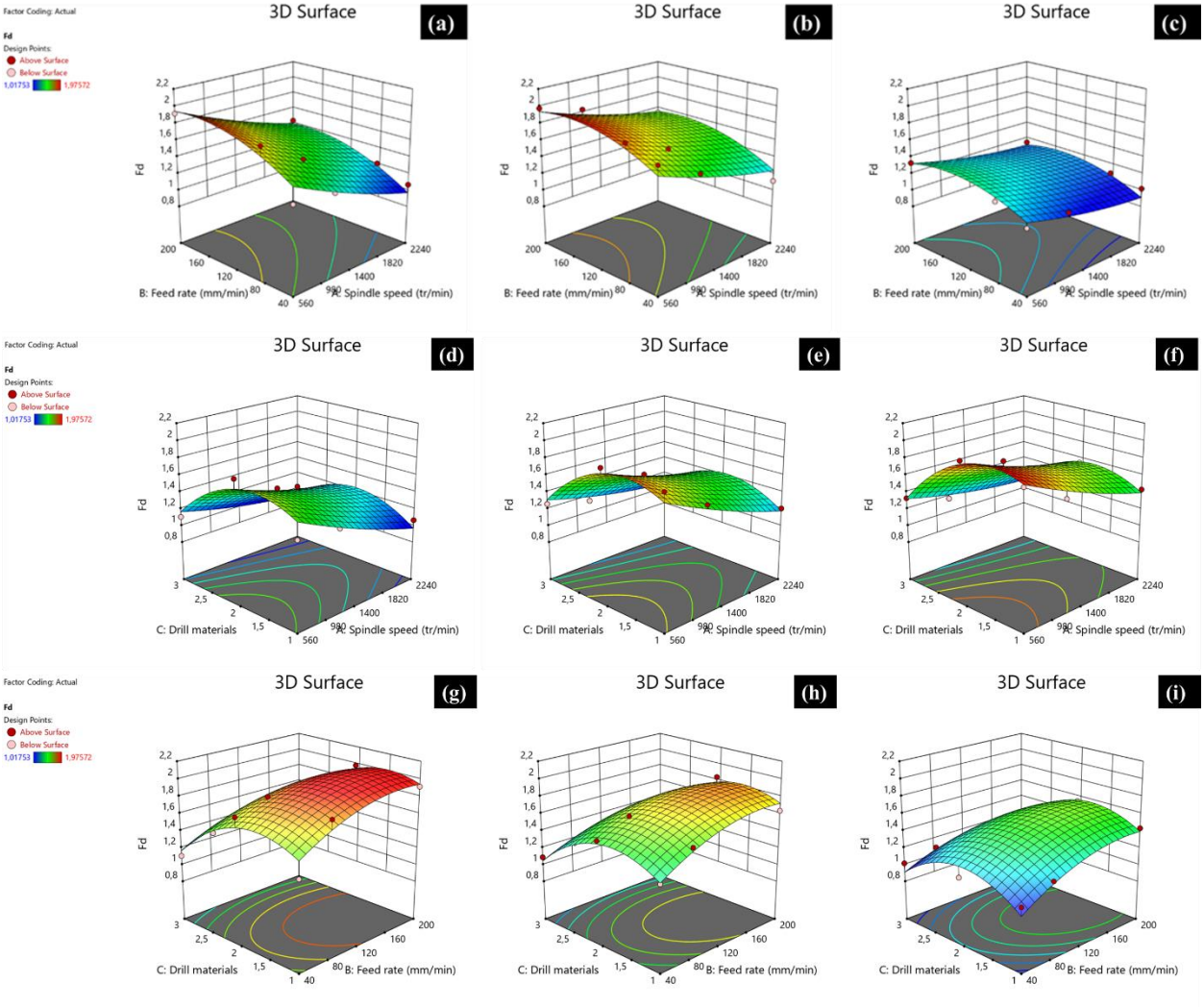

Figure V-11: 3D surface plots of F_d data of DPFP40 versus f, N, and drill materials: a) HSS-TITAN, b) HSS-CARBIDE, and c) HSS-SUPER, d) 40mm/min, e) 80mm/min, f) 200 mm/min, g) 560 rpm, h) 1120 rpm, i) 2240 rpm.

V.4 Optimization and modelization of drilling behavior of PFPEs using ANN and Taguchi

V.4.1 ANN

In this study, a neural network was constructed with three input layers consisting of spindle speed, feed rate, and various drill bit point angles, along with ten hidden layers and two output layers. The primary objective of the network is to predict the circularity and cylindricity errors of the drilled holes in PFPEs. The determination of the number of neurons in the hidden layers relies on minimizing the error with an increasing number of hidden nodes[300, 301]. The training of the artificial neural network (ANN) model utilized the Levenberg–Marquardt algorithm, which combines the principles of the quasi-Newton algorithm and steepest descent backpropagation. This algorithm was specifically tailored for solving nonlinear least squares problems and curve fitting. Neural network modeling provides a powerful methodology, allowing for the emulation of the behavior of various nonlinear processes[302]. The accuracy of the ANN model's predictions is evaluated using mean squared error (*MSE*) and regression analysis. A lower *MSE* value indicates higher prediction accuracy, typically set at < 0.001 for acceptance. Analysis of **Figure V-12** and **Table V-10** indicates that the *MSE* values are very low, approximately 1.70×10^{-4} and 1.85×10^{-4} for training, 2.38×10^{-4} and 2.27×10^{-4} for validation, and 6.03×10^{-4} and 9.08×10^{-4} for tests related to circularity and cylindricity errors, respectively. The correlation coefficient "*R*" for the training, validation, and test datasets ranges between 0.89 and 0.99 for all studied samples, except for the cylindricity test dataset, where *R*= 0.47446. Consequently, the developed ANN models demonstrate a robust ability to effectively interpret data, serving as efficient tools for predicting the circularity and cylindricity errors of holes.

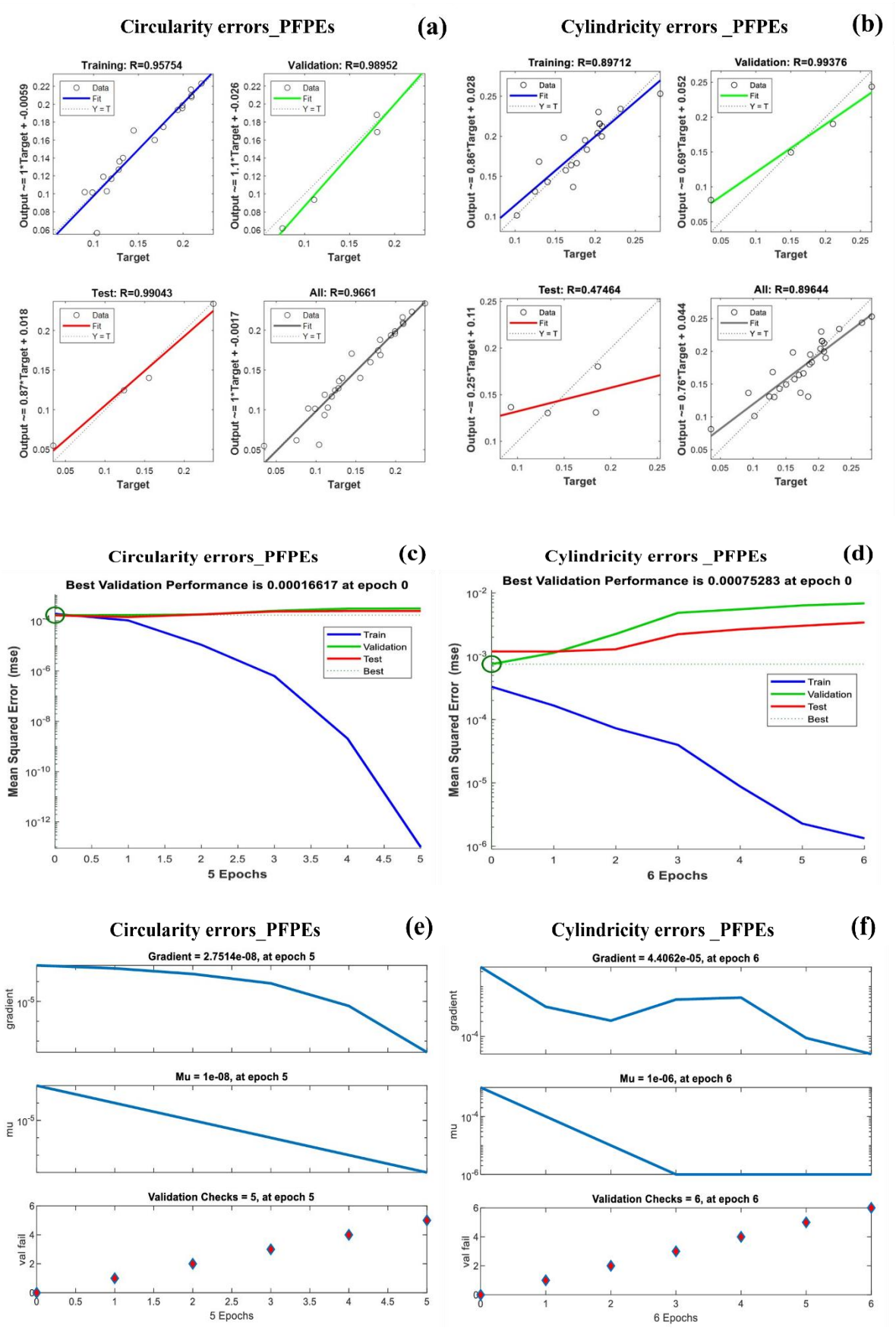

Figure V-12: ANN outcomes.

Table V-10: ANN structure performance.

Material	Data used	samples	*MSE*	*R*
PFPEs	**Circularity errors**			
	Training	19	1.70359×10^{-4}	0. 95754
	Validation	04	2.38122×10^{-4}	0. 98952
	Testing	04	6.02630×10^{-4}	0.99043
	Cylindricity errors			
	Training	19	1.85369×10^{-4}	0. 89712
	Validation	04	2.26902×10^{-4}	0. 99376
	Testing	04	9.07521×10^{-4}	0.47446

Table V-11: Experimental and predictive outcomes for the circularity and cylindricity errors of the holes drilled in PFPEs under diverse cutting conditions.

N°	Input variables			Output variables											
				Circularity errors						Cylindricity errors					
	Feed rate (mm/min)	Spindle speed (rpm)	Drill bit	EXP	ANN	Err_ANN	Taguchi	Err_Taguchi	*S/N* ratios	EXP	ANN	Err	Taguchi	Err_Taguchi	*S/N* ratios
1		500		0.1105	0.0936	0.0169	0.1613	-0.0508	19.133	0.1247	0.131	-0.006	0.1793	-0.0546	18.083
2	50	1000		0.1992	0.1987	0.0005	0.1834	0.0158	14.014	0.1861	0.180	0.006	0.1664	0.0197	14.605
3		1500		0.2367	0.2338	0.0029	0.2017	0.0350	12.516	0.2811	0.253	0.028	0.2462	0.0349	11.023
4		500		0.1991	0.1959	0.0032	0.1546	0.0445	14.019	0.1699	0.164	0.006	0.1240	0.0459	15.396
5	100	1000	HSS-SUPER 85°	0.2204	0.2232	-0.0028	0.2503	-0.0299	13.136	0.2082	0.200	0.008	0.2278	-0.0196	13.630
6		1500		0.2091	0.2095	-0.0004	0.2237	-0.0146	13.593	0.2040	0.230	-0.026	0.2303	-0.0263	13.807
7		500		0.1779	0.1747	0.0032	0.1716	0.0063	14.997	0.2106	0.190	0.020	0.2019	0.0087	13.531
8	150	1000		0.2087	0.2163	-0.0076	0.1946	0.0141	13.610	0.2055	0.215	-0.010	0.2056	-0.0001	13.744
9		1500		0.1328	0.1401	-0.0073	0.1532	-0.0204	17.536	0.1840	0.131	0.053	0.1925	-0.0085	14.704
10		500		0.1807	0.1689	0.0118	0.1333	0.0474	14.861	0.2028	0.204	-0.001	0.1704	0.0324	13.859
11	50	1000		0.0753	0.0618	0.0135	0.0973	-0.0220	22.464	0.0928	0.137	-0.044	0.1223	-0.0295	20.649
12		1500		0.1288	0.1361	-0.0073	0.1541	-0.0253	17.802	0.2315	0.234	-0.003	0.2344	-0.0029	12.709
13		500		0.0346	0.0548	-0.0202	0.0577	-0.0231	29.219	0.0356	0.081	-0.046	0.0561	-0.0205	28.971
14	100	1000	HSS-SUPER 115°	0.1108	0.1191	-0.0083	0.0953	0.0155	19.109	0.1323	0.130	0.002	0.1247	0.0076	17.569
15		1500		0.1147	0.1029	0.0118	0.1071	0.0076	18.809	0.1723	0.137	0.036	0.1594	0.0129	15.274
16		500		0.1239	0.1246	-0.0007	0.1482	-0.0243	18.139	0.1607	0.198	-0.038	0.1726	-0.0119	15.880
17	150	1000		0.1198	0.1169	0.0029	0.1132	0.0066	18.431	0.1631	0.158	0.005	0.1412	0.0219	15.751
18		1500		0.1280	0.1271	0.0009	0.1102	0.0178	17.856	0.1503	0.149	0.001	0.1603	-0.0100	16.461
19		500		0.2095	0.2081	0.0014	0.2061	0.0034	13.576	0.2662	0.244	0.023	0.2440	0.0222	11.496
20	50	1000		0.1682	0.1600	0.0082	0.1620	0.0062	15.484	0.1872	0.195	-0.008	0.1774	0.0098	14.554
21		1500		0.1940	0.1936	0.0004	0.2036	-0.0096	14.244	0.2085	0.213	-0.004	0.2405	-0.0320	13.618
22		500		0.0900	0.1018	-0.0118	0.1114	-0.0214	20.915	0.1021	0.101	0.001	0.1275	-0.0254	19.820
23	100	1000	HSS-SUPER 135°	0.1554	0.1402	0.0152	0.1410	0.0144	16.171	0.1895	0.183	0.006	0.1775	0.0120	14.448
24		1500		0.1447	0.1707	-0.0260	0.1377	0.0070	16.791	0.1768	0.166	0.010	0.1633	0.0135	15.050
25		500		0.1803	0.1880	-0.0077	0.1623	0.0180	14.880	0.2051	0.216	-0.011	0.2018	0.0033	13.761
26	150	1000		0.0986	0.1015	-0.0029	0.1192	-0.0206	20.123	0.1299	0.168	-0.038	0.1517	-0.0218	17.728
27		1500		0.1037	0.0563	0.0474	0.1011	0.0026	19.684	0.1404	0.143	-0.003	0.1219	0.0185	17.053

V.4.2 Taguchi

Figure V-13 illustrates the primary influence of means and *S/N* ratios on circularity and cylindricity errors concerning feed rate, spindle speed, and drill bit point angles. Analysis of **Figure V-13** and **Table V-11** indicates that the factors of feed rate and drill bit point angles have a more significant impact compared to the spindle speed factor. The slope below the levels of each factor signifies the effects on the machining process response[303, 304]. As discussed previously in the context of the Taguchi method. Highlighting the importance of maximizing the signal-to-noise ratio (*S/N*) for an optimal and robust design, it is notable that circularity and cylindricity errors peak at a feed rate of 50 mm/min, spindle speed of 1500 rpm, and drill bit angle of 85°. The corresponding minimum *S/N* ratios are estimated at 12.516 and 11.0228 for circularity and cylindricity errors, respectively. Conversely, the lowest values for circularity and cylindricity errors are observed at a feed rate of 100 mm/min, spindle speed of 500 rpm, and drill bit angle of 115°, with maximum *S/N* ratios estimated at 29.2185 and 28.971, respectively.

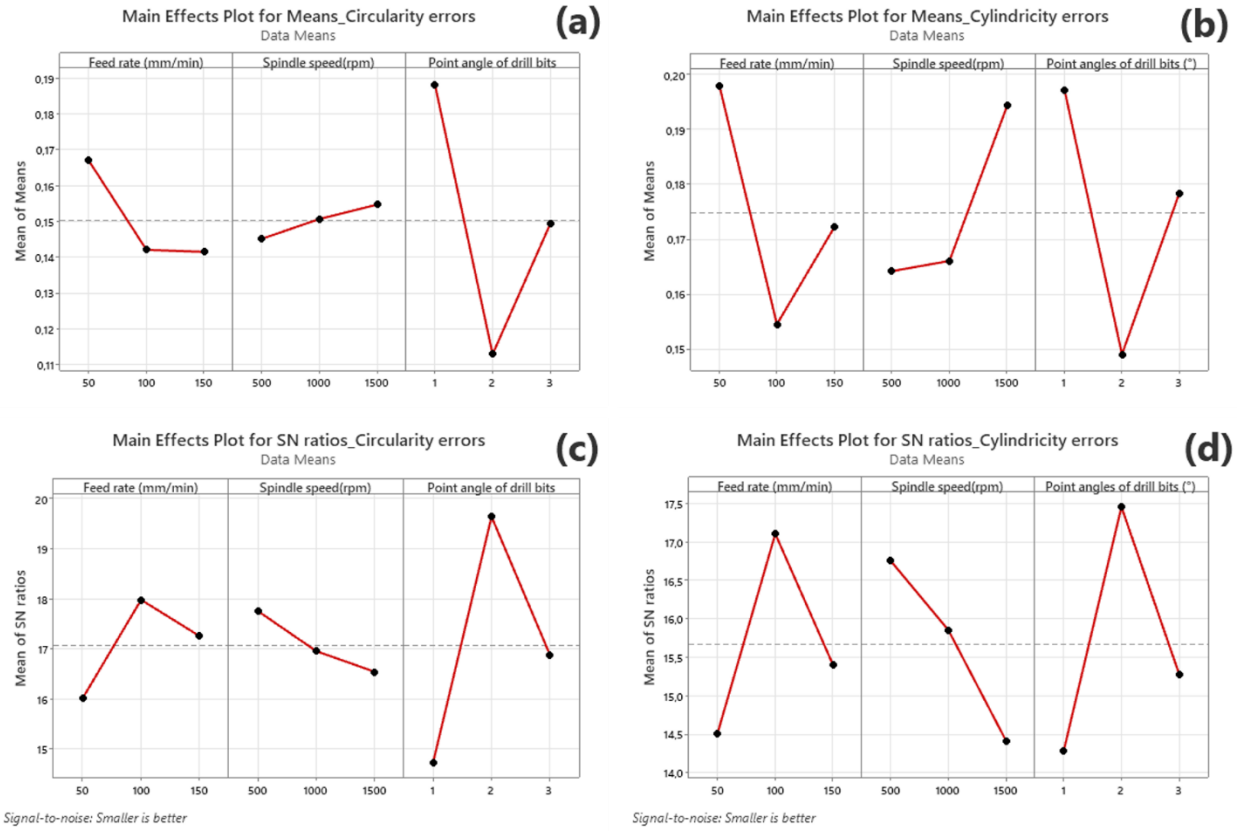

Figure V-13: The main effect for means and *S/N* ratios for circularity and cylindricity error of PFPEs.

Figure V-14 presents residual plots for means and *S/N* ratios in relation to circularity and cylindricity errors as functions of input parameters. The alignment of points along a straight line in these plots validates the normal distribution of residuals for all output parameters, consistent with the indications from Normal Probability Plots. Analyzing the histogram of residuals provides insights into the overall characteristics of the data, encompassing typical values and spread[305]. It was noted that circularity errors show a milder deviation compared to cylindricity errors. The presence of long tails in the plot suggests notable skewness in the data.

Versus Fits Plots revealed that the percent deviation ranged between -0.025% and +0.025% for both circularity and cylindricity errors. Some outliers reached a percentage deviation of ±0.05%. In an ideally constructed experimental design, residual plots would display a random distribution of points around zero[306, 307]. Circularity and cylindricity errors exhibit a positive correlation, as most residues share the same sign. Analysis of residuals against control order plots during 27 runs, a method that serves as a tool for discerning the characteristics of errors (random or non-random), unveils subtle and closely grouped fluctuations in the signs of successive residuals, suggesting a positive relationship. In the context of circularity and cylindricity errors, there was a dispersion of positive residuals prevailing over negative residuals, signifying the non-random nature of the errors.

Figure V-15 presents the Interaction plot depicting means and *S/N* ratios for circularity and cylindricity errors. It provides insights into the relationships among different input parameters and their impact on the output response. Nonparallel lines on the plot suggest a significant interaction between the factors[308, 309]. Specifically, for circularity errors, the interaction effect is notable for the feed rate and point angles of drill bits, as evidenced by nonparallel lines. Conversely, for the spindle speed factor, the interaction effect is relatively lower, as indicated by the lines appearing near parallel (refer to **Figure V-16a**). In terms of cylindricity errors, the spindle speed factor exerts the most significant influence on the response values, followed by the feed rate factor and subsequently the point angles of the drill bits, respectively (refer to **Figure V-16b**).

A predictive regression model is developed by integrating statistically significant main effects and interactions, with the aim of forecasting circularity and cylindricity errors within the specified factor ranges. The estimated coefficients derived from factorial analysis are utilized in constructing the regression model for output parameters in coded variables, as depicted in **Table V-12**.

The ANOVA model results are presented in **Table V-13**, revealing R^2 coefficients of 78.33% and 79.22% for circularity and cylindricity errors of PFPEs, respectively. These

coefficients suggest a strong alignment between responses and factors, affirming the statistical significance of the regression model. Notably, the linear coefficients A and C, along with the coefficients A×B and C×A, demonstrate significant effects on circularity errors. Similarly, the linear coefficients A and C, in conjunction with the coefficients A×B and B×A, exhibit significant effects on cylindricity errors, as evidenced by their substantial *F-values* and small *P-values*[310]. In conclusion, the point angle of drill bits emerges as the variable exerting the most significant influence on the circularity and cylindricity errors of PFPEs, with *F-values* of 7.01 and 2.89, respectively. This is followed by the feed rate with values of 1.05 and 2.34, and spindle speed with values of 0.11 and 1.40 for circularity and cylindricity errors, respectively.

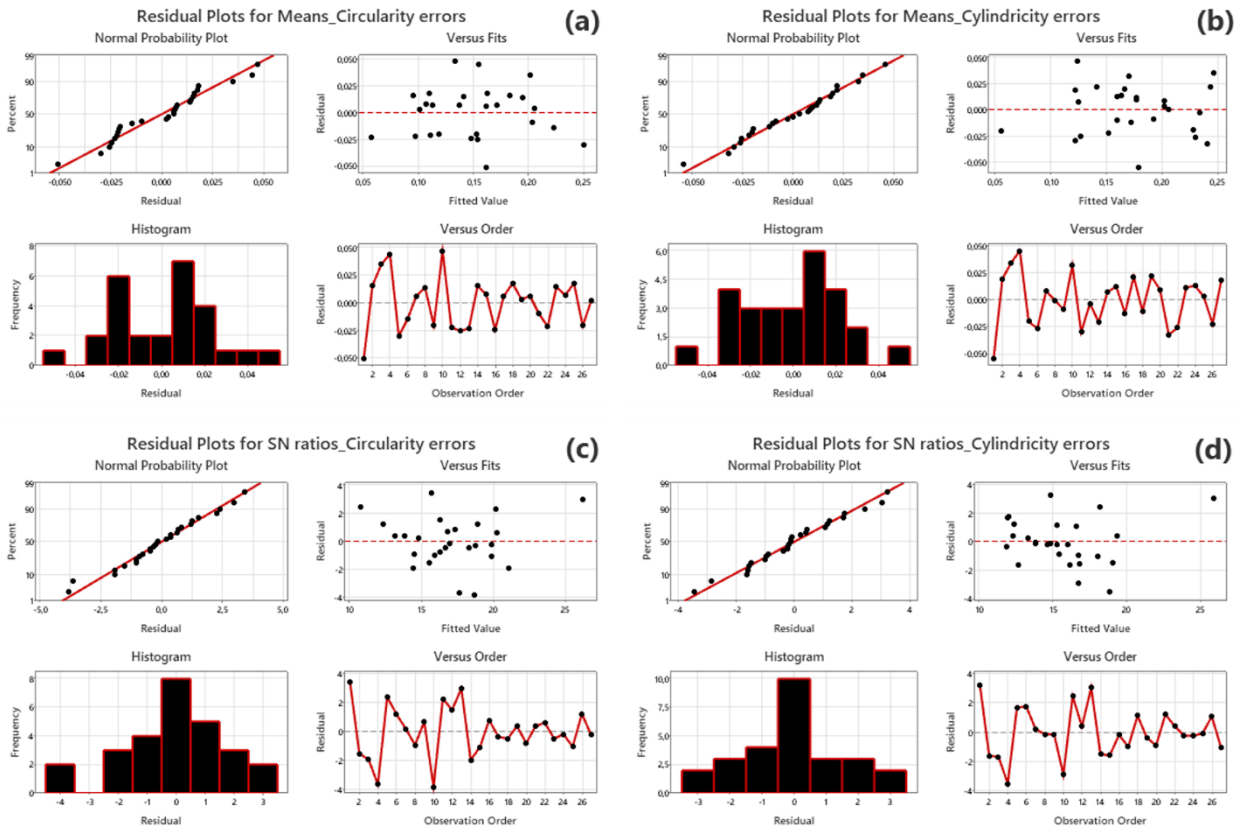

Figure V-14: Residual plots for means and *S/N* ratios for circularity and cylindricity errors of PFPEs.

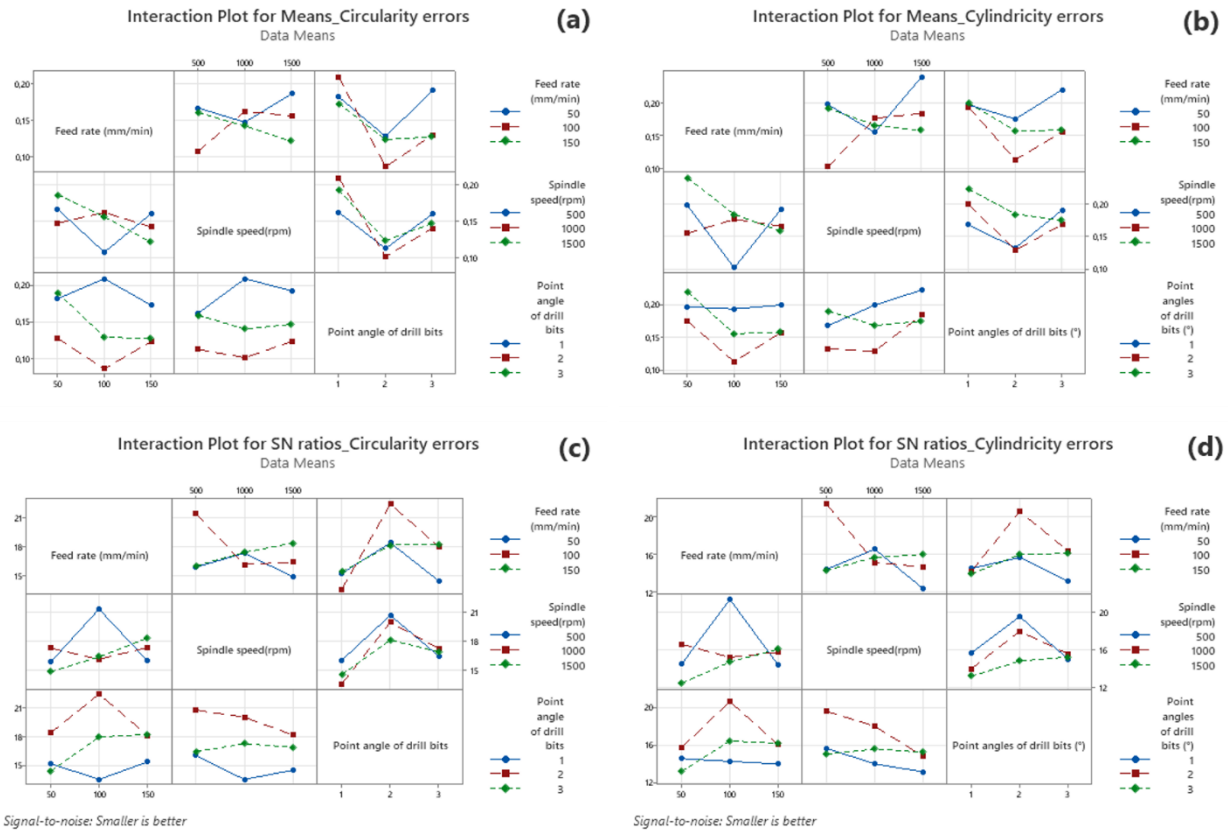

Figure V-15: Interaction plot for means and *S/N* ratios for circularity and cylindricity errors of PFPEs.

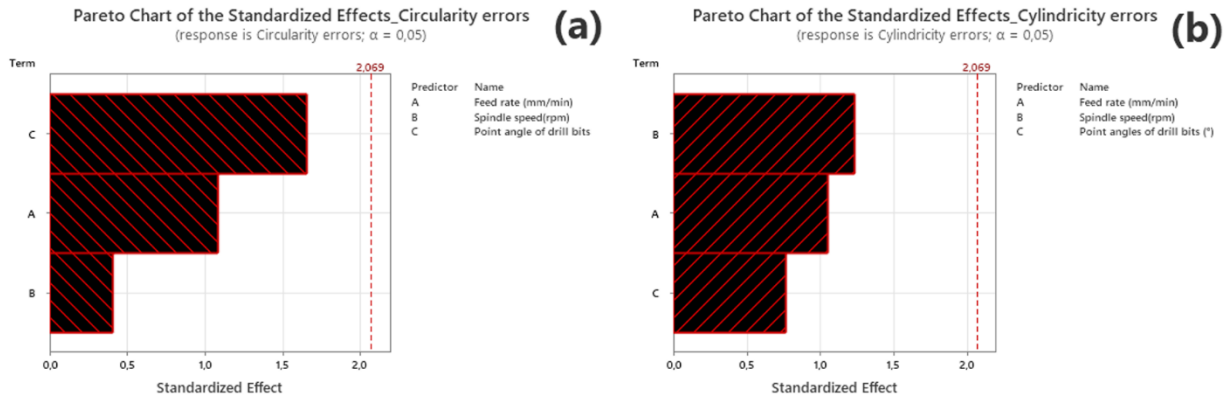

Figure V-16: Pareto chart of the standardized effects for circularity and cylindricity errors of PFPEs.

Table V-12: The regression equation for circularity and cylindricity errors of PFPEs.

Reponses	**Regression equation**
Circularity errors_PFPEs	0,2050 - 0,000255 Feed rate + 0,000010 Spindle speed - 0,0194 Point angle of drill bits
Cylindricity errors_PFPEs	0,1891 - 0,000257 Feed rate + 0,000030 Spindle speed- 0,0094 Point angles of drill bits

Table V-13: Analysis of variance for means for circularity and cylindricity errors of PFPEs.

Source	DF	Seq SS	Adj SS	Adj MS	*F*	*P*
~ Circularity errors ~						
A: Feed rate (mm/min)	2	0.003807	0.003807	0.001903	1.05	0.395
B: Spindle speed (rpm)	2	0.000414	0.000414	0.000207	0.11	0.894
C: Point angle of drill bits	2	0.025532	0.025532	0.012766	7.01	0.017
Feed rate * Spindle speed	4	0.009482	0.009482	0.002371	1.30	0.347
Feed rate * Point angle of drill bits	4	0.009125	0.009125	0.002281	1.25	0.363
Spindle speed * Point angle of drill bits	4	0.004272	0.004272	0.001068	0.59	0.682
Residual Error	8	0.014563	0.014563	0.001820		
Total	26	0.067194				
					R^2	78.33%
~ Cylindricity errors ~						
A: Feed rate (mm/min)	2	0.008556	0.008556	0.004278	2.34	0.158
B: Spindle speed (rpm)	2	0.005130	0.005130	0.002565	1.40	0.300
C: Point angle of drill bits	2	0.010572	0.010572	0.005286	2.89	0.113
Feed rate * Spindle speed	4	0.019846	0.019846	0.004961	2.71	0.107
Feed rate * Point angle of drill bits	4	0.005714	0.005714	0.001429	0.78	0.568
Spindle speed * Point angle of drill bits	4	0.005913	0.005913	0.001478	0.81	0.553
Residual Error	8	0.014622	0.014622	0.001828		
Total	26	0.070353				
					R^2	79.22%

V.4.3 Comparison of Experimental, ANN, and Taguchi Results

Figure V-17 presents a comparison between the results predicted by the ANN and Taguchi models and those obtained experimentally. It is evident that both models effectively describe the experimentally obtained results. The correlation coefficients for predicting circularity and cylindricity errors of PFPEs by the ANN model are 96.61% and 89.64%, respectively. In contrast, the Taguchi model yields percentages of 78.33% for circularity errors and 79.22% for cylindricity errors. The high correlation coefficients signify the appropriateness of the optimization process. Consequently, the ANN model demonstrates a more precise prediction compared to the Taguchi model.

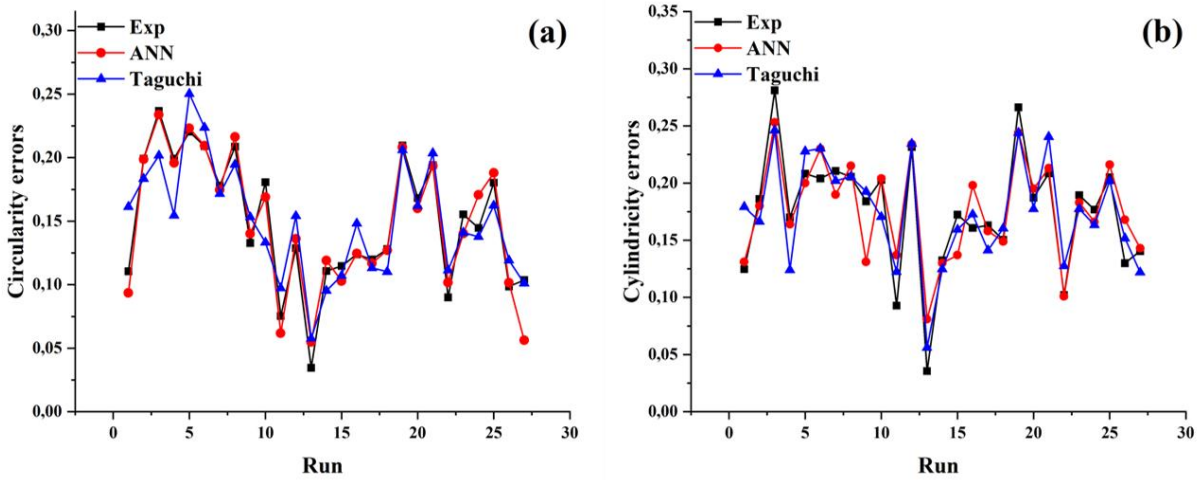

Figure V-17: Comparison of Experimental, ANN, and Taguchi Results.

V.5 Conclusion

In summary, Chapter V of the thesis offers significant insights into the absorption behavior of DPFPs, as well as the drilling behavior of DPFP40 and PFPEs. By employing advanced methodologies including Artificial Neural Networks (ANN), Response Surface Methodology (RSM), and the Taguchi method, the chapter provides a thorough analysis, optimization, and modeling of outcomes for these materials. Key outcomes from this chapter can be summarized as follows:

1. Regarding the absorption behavior of DPFPs:
   - Algebraic models were developed using Artificial Neural Networks (ANN) and Response Surface Methodology (RSM), establishing correlations between the mass of DPFPs and input factors such as time, fiber rate, and liquid type.
   - Utilizing ANN, correlation coefficient "*R*" values for training, validation, and test datasets consistently exceeded 0.99 across all studied samples.
   - RSM analysis demonstrated statistical significance with a low *P-value* (<0.0001), underscoring the reliability of the regression model.
   - High R^2 and adjusted R^2 coefficients (99.63% and 99.61%, respectively) indicated a robust alignment between responses and factors in the regression model.
   - 2D and 3D surface plots illustrated the impact of input parameters on the mass of DPFPs, offering insights into absorption rate analysis.
2. Concerning the drilling behavior of DPFP40 and PFPEs:
   - Algebraic models were developed using ANN, RSM, and the Taguchi method, correlating delamination factor, circularity, and cylindricity errors with input factors such as feed rate, spindle speed, and drill bit materials (for DPFP40) or feed rate, spindle speed, and drill bit point angles (for PFPEs).
   - ANN models accurately predicted cutting parameters in DPFP40 drilling processes, exhibiting strong correlation with experimental data and an average error value of 4.3×10^{-4}.
   - The preponderant importance of drill material and spindle speed in relation to feed rate on delamination factor of DPFP40 was highlighted, with contributions as follows: spindle speed 69.13%, drill material 47.95%, and feed rate 37.25%.
   - ANN models accurately predicted circularity and cylindricity errors in drilled holes of PFPEs, demonstrating strong correlation coefficients ranging from 0.89 to 0.99 with experimental data.

- Circularity and cylindricity errors of PFPEs peaked at a feed rate of 50 mm/min, spindle speed of 1500 rpm, and drill bit angle of 85°, with corresponding minimum *S/N* ratios estimated at 12.516 and 11.0228, respectively.
- The lowest values for circularity and cylindricity errors of PFPEs were observed at a feed rate of 100 mm/min, spindle speed of 500 rpm, and drill bit angle of 115°, with maximum *S/N* ratios estimated at 29.2185 and 28.971, respectively.

These collective results underscore the efficacy of advanced modeling techniques in predicting and optimizing the absorption and drilling behavior of DPFPs, DPFP40, and PFPEs. The findings significantly contribute to a deeper understanding of the absorption and drilling dynamics of these materials, paving the way for further research and advancements in the field of composite materials and machining processes.

Conclusion and Perspectives

V.6 Conclusion and Perspectives

The thesis conducted a comprehensive examination of the physical properties of newly manufactured Date Palm Fiber/ Iso polyester composites (DPFPs) in three different configurations: unidirectional (UD) and cross-linked (C), with layer numbers ranging from 2 to 4. Moreover, it explored the mechanical behavior and the machinability of two recently developed biocomposites: DPFP40 (Date Palm Fiber/ Iso polyester), characterized by a 40% by-weight fiber reinforcement, and PFPEs (palm fiber powder/epoxy) featuring an 18% by-weight fiber reinforcement.

The absorption behavior of the DPFPs was scrutinized across three water types - seawater, distilled water, and rainwater. This examination encompassed parameters such as the percentage of water absorbed, diffusion coefficient, and fiber porosity. Subsequently, the drilling behavior of DPFP40 was investigated using both coated and uncoated tools (HSS-TITATN, HSS-CARBIDE, and uncoated HSS-SUPER tool) under varying cutting conditions. The impact of machining parameters, specifically spindle speed and feed rate, along with the drill bit materials, was assessed in terms of delamination factor, circularity, and cylindricity errors of holes. Following this, the study extended to the drilling behavior of PFPEs utilizing tools with different point angles (85°, 115°, and 135°). This exploration also considered diverse cutting conditions, evaluating the influence of machining parameters on the drilling process concerning circularity and cylindricity errors of holes.

To enhance performance and facilitate predictive capabilities based on existing data, three optimization, analysis, and modelization methods were developed. These methods comprised Artificial Neural Networks (ANN), Response Surface Methodology (RSM), and the Taguchi approach.

The water absorption study reveals a clear relationship between absorption rates and increased fiber content in the bio composite. Notably, the lowest absorption rates were achieved at 39.20%, 40.41%, and 37.00% with 15% reinforcement, while the highest rates reached 82.99%, 73.08%, and 63.94% with 27% reinforcement for seawater, distilled water, and rainwater, respectively. The examination of diffusion coefficients unveiled minimum and maximum values of approximately 2.11×10^{-6}mm²/s and 3.99×10^{-6}mm²/s with 15% reinforcement in rainwater and 27% reinforcement in seawater, respectively. SEM images, analyzed using *Image J*, highlighted the notably high porosity of palm fibers, exceeding 51%. The application of ANN modeling, subjected to rigorous statistical evaluation, demonstrated an exemplary trend with an average error value of 3×10^{-5}. The Mean Squared Error (*MSE*) values were commendable, standing at about 1.2×10^{-4} for training, 1.4×10^{-4} for validation, and 7.0×10^{-4} for testing, indicating the robustness of the model. Correlation coefficient (*R*) values across datasets surpassed 0.99. Furthermore, the

results of RSM showcased an exceptional alignment between experimental and predicted data, with correlation coefficients (R^2 and adjusted R^2) reaching approximately 99.63% and 99.61%, respectively.

Examination of the drilling properties of DPFP40 indicated that an increase in the feed rate led to a rise in the delamination factor, while elevating the spindle speed mitigated this factor. Notably, the uncoated HSS-SUPER drills exhibited less delamination compared to TITAN and CARBIDE-coated HSS drills. Optimal hole quality in terms of delamination was achieved using the HSS SUPER drill at a spindle speed of 2240 rpm and a feed rate of 40 mm/min. For optimal circularity, the recommended cutting parameters include a spindle speed of 1120 rpm, a feed rate of 80 mm/min, and HSS-TITAN drill material. Similarly, for optimal cylindricity, the suggested parameters are a spindle speed of 560 rpm, a feed rate of 80 mm/min, and HSS-CARBIDE drill material.

The Artificial Neural Network (ANN) models demonstrated a high correlation with experimental data, with an average error value of 4.3×10^{-4}. The correlation coefficient "R" values across datasets exceeded 0.98, indicating strong agreement. According to ANOVA analysis, the R^2 coefficient and adjusted R^2 coefficient for delamination were determined to be 93.09% and 89.43%, respectively, indicating excellent agreement between the predictive model and experimental measurements. Furthermore, the contribution of various elements to the optimal drilling conditions was assessed. Spindle speed accounted for 69.13% of the contribution, followed by drill material at 47.95%, and feed rate at 37.25%.

The analysis of PFPEs drilling characteristics revealed that increasing the feed rate led to heightened circularity errors in drilled holes, whereas raising the spindle speed improved hole circularity. Simultaneous increases in both feed rate and spindle speed resulted in elevated cylindricity errors. The drill point angle exerted a significant influence on circularity and cylindricity errors, with the 115° drill exhibiting superior performance compared to the 85° and 135° drills. Peak circularity and cylindricity errors were observed at a feed rate of 50 mm/min, spindle speed of 1500 rpm, and a drill bit angle of 85°. Correspondingly, the minimum signal-to-noise (*S/N*) ratios were estimated at 12.516 and 11.0228 for circularity and cylindricity errors, respectively. Conversely, the lowest values for circularity and cylindricity errors were identified at a feed rate of 100 mm/min, spindle speed of 500 rpm, and a drill bit angle of 115°, with maximum *S/N* ratios estimated at 29.2185 and 28.971, respectively. The ANN and Taguchi models provided accurate predictions of the experimentally obtained results. Notably, the correlation coefficients for predicting circularity and cylindricity errors of PFPEs using the ANN model reached impressive

values of 96.61% and 89.64%, respectively. Conversely, the Taguchi model yielded slightly lower percentages, with 78.33% for circularity errors and 79.22% for cylindricity errors. These robust correlation coefficients affirm the effectiveness of the optimization process. Consequently, the ANN model stands out for its precision in prediction when compared to the Taguchi model.

Certainly, manufacturers are actively seeking improved machinability for their products. The outcomes from this study offer valuable insights into selecting optimal machining conditions. These findings can guide the enhancement of machinability for newly developed Natural Fiber Reinforced Composites (NFRCs), particularly those utilized in lightweight structural applications across various industries, such as shipbuilding, aeronautics, and automotive. This becomes particularly crucial as the substitution of synthetic fibers with natural fibers becomes essential, driven by both environmental concerns and economic considerations.

Through the assessment of biocomposite absorption behavior, this thesis neglects the consideration of evaluating the absorption rate under diverse conditions. For instance, the utilization of various types of oils (such as vegetable or mineral oil) could be explored to understand absorption characteristics in scenarios involving oil contact, such as in applications like food packaging or lubrication. Additionally, investigating the absorption behavior in biological fluids like blood, urine, or saliva can simulate real-world conditions relevant to medical or bioengineering applications. Recognizing the importance of these alternative conditions, which are equally crucial as those employed in the current absorption rate assessment, future research endeavors should encompass tests conducted under such conditions.

Shifting the focus to the machinability of biocomposites, this thesis disregards the consideration of the trimming of these composites, which aims to assess or enhance the quality of contours or cut surfaces in manufactured parts. It also overlooks the measurement of thrust force and torque concerning the drilling behavior, despite their significance comparable to the evaluation of delamination, circularity, and cylindricity errors that impact the quality of drilled holes. Consequently, the validity of this assertion should be examined in subsequent studies.

References

V.7 References

1. Rajiv Kumar, Mir Irfan Ul Haq, Ankush Raina, and Ankush Anand, *Industrial applications of natural fibre-reinforced polymer composites – challenges and opportunities.* International Journal of Sustainable Engineering, **2019**. 12(3): p. **212-220**.DOI: 10.1080/19397038.2018.1538267.
2. Mouad Chakkour, Mohamed Ould Moussa, Ismail Khay, Mohamed Balli, and Tarak Ben Zineb, *Towards widespread properties of cellulosic fibers composites: A comprehensive review.* Journal of Reinforced Plastics and Composites, **2022**. 42(5-6): p. **222-263**.DOI: 10.1177/07316844221112974.
3. Salah AMROUNE, *Caractérisations mécaniques et étude de l'endommagement des matériaux composites renforcés par des fibres de palmier*, 2016.
4. Elwaleed Awad Khidir, *A review on the potential of using date palm fibers as sound absorption material.* AIP Conference Proceedings, **2023**. 2689(1): p. **030005**.DOI: 10.1063/5.0117003.
5. Rolf E Hummel, *Understanding materials science: history, properties, applications*. 1998: Springer.
6. Narendra Kumar and Ambesh Dixit, *Historical Perspective of Materials and Contemporary Warfare Technologies*, in *Nanotechnology for Defence Applications*, Narendra Kumar and Ambesh Dixit, Editors. 2019, Springer International Publishing: Cham. p. 1-33.
7. Samuel Abalansa, Badr El Mahrad, John Icely, and Alice Newton *Electronic Waste, an Environmental Problem Exported to Developing Countries: The GOOD, the BAD and the UGLY*. Sustainability, 2021. 13, DOI: 10.3390/su13095302.
8. Murray Grant Norton, *A Modern History of Materials: From Stability to Sustainability*. 2023: Springer International Publishing.
9. AN Emin, *How Composite Materials Influence Sustainable Development.* Euro Economica, **2021**. 40(2): p. **202-210**.
10. Ashwani Kumar Singh, Raman Bedi, and Balbir Singh Kaith, *Mechanical properties of composite materials based on waste plastic – A review.* Materials Today: Proceedings, **2020**. 26: p. **1293-1301**.DOI: https://doi.org/10.1016/j.matpr.2020.02.258.
11. ES Gevorkyan and VP Nerubatskyi, *Technological and scientific aspects of consolidation of refractory composites*, 2022, LLC "Voskhod-Print".
12. Mahesh Bhong, Tasneem K. H. Khan, Kiran Devade, B. Vijay Krishna, Sreekanth Sura, H. K. Eftikhaar, H. Pal Thethi, and Nakul Gupta, *Review of composite materials and applications.* Materials Today: Proceedings, **2023**.DOI: https://doi.org/10.1016/j.matpr.2023.10.026.
13. Shoaib Iqbal, Tariq Jamil, and Syed Murtuza Mehdi, *Numerical simulation and validation of MWCNT-CFRP hybrid composite structure in lightweight satellite design.* Composite Structures, **2023**. 303: p. **116323**.DOI: https://doi.org/10.1016/j.compstruct.2022.116323.
14. Yadav Khagendra Kumar and Dalbir Lohchab, *Influence of Aviation Fuel on Mechanical properties of Glass Fiber-Reinforced Plastic Composite*, 2016.
15. M. S. Ayar, P. M. George, and R. R. Patel, *Advanced research progresses in aluminium metal matrix composites: An overview.* AIP Conference Proceedings, **2021**. 2317(1): p. **020026**.DOI: 10.1063/5.0036141.
16. G. Abouelmagd, *Hot deformation and wear resistance of P/M aluminium metal matrix composites.* Journal of Materials Processing Technology, **2004**. 155-156: p. **1395-1401**.DOI: https://doi.org/10.1016/j.jmatprotec.2004.04.223.
17. Vladimir V. Popov, Alla Pismenny, Natalya Larianovsky, Anna Lapteva, and Daniel Safranchik *Corrosion Resistance of Al–CNT Metal Matrix Composites*. Materials, 2021. 14, DOI: 10.3390/ma14133530.

18. J. Amirtharaj and M. Mariappan, *Exploring the potential uses of Aluminium Metal Matrix Composites (AMMCs) as alternatives to steel bar in Reinforced Concrete (RC) structures-A state of art review*. Journal of Building Engineering, **2023**. 80: p. **108085**.DOI: https://doi.org/10.1016/j.jobe.2023.108085.
19. Jun Li, Fucheng Wang, Chunsheng Shi, Enzuo Liu, Chunnian He, and Naiqin Zhao, *High strength-ductility synergy of MgAlB4 whisker reinforced aluminum matrix composites achieved by in situ synthesis.* Materials Science and Engineering: A, **2021**. 799: p. **140127**.DOI: https://doi.org/10.1016/j.msea.2020.140127.
20. J. A. Hooker and P. J. Doorbar, *Metal matrix composites for aeroengines.* Materials Science and Technology, **2000**. 16(7-8): p. **725-731**.DOI: 10.1179/026708300101508414.
21. Xiulei Wang, Xiaodong Gao, Zhenghe Zhang, Lisheng Cheng, Haopeng Ma, and Weimin Yang, *Advances in modifications and high-temperature applications of silicon carbide ceramic matrix composites in aerospace: A focused review*. Journal of the European Ceramic Society, **2021**. 41(9): p. **4671-4688**.DOI: https://doi.org/10.1016/j.jeurceramsoc.2021.03.051.
22. Krishan K. Chawla, *Ceramic Matrix Composites*, in *Composite Materials: Science and Engineering*, Krishan K. Chawla, Editor. 2019, Springer International Publishing: Cham. p. 251-296.
23. Friedrich Raether, *CERAMIC MATRIX COMPOSITES- AN ALTERNATIVE FOR CHALLENGING CONSTRUCTION TASKS.* Ceramic Applications, **2013**. 1(1): p. **45-49**.
24. Arun Kumar Sharma, Rakesh Bhandari, Chaitanya Sharma, Shri Krishna Dhakad, and Camelia Pinca-Bretotean, *Polymer matrix composites: A state of art review*. Materials Today: Proceedings, **2022**. 57: p. **2330-2333**.DOI: https://doi.org/10.1016/j.matpr.2021.12.592.
25. Satish Bhalerao, Nitin Ambhore, and Munjadas Kadam, *Polymer matrix composite in high voltage applications: a review*. Biointerface Res. Appl. Chem, **2022**. 12(6): p. **8343-8352**.
26. J. P. Davim and Pedro Reis, *Study of delamination in drilling carbon fiber reinforced plastics (CFRP) using design experiments.* Composite Structures, **2003**. 59(4): p. **481-487**.DOI: https://doi.org/10.1016/S0263-8223(02)00257-X.
27. Malik Abdul Karim, Mohamad Zaki Abdullah, Ahmed Farouk Deifalla, Marc Azab, and Ahsan Waqar, *An assessment of the processing parameters and application of fibre-reinforced polymers (FRPs) in the petroleum and natural gas industries: A review*. Results in Engineering, **2023**. 18: p. **101091**.DOI: https://doi.org/10.1016/j.rineng.2023.101091.
28. Mateus Hofmann, Abu T. Shahid, Marina Machado, Mário Garrido, João C. Bordado, and João R. Correia, *GFRP biocomposites produced with a novel high-performance bio-based unsaturated polyester resin.* Composites Part A: Applied Science and Manufacturing, **2022**. 161: p. **107098**.DOI: https://doi.org/10.1016/j.compositesa.2022.107098.
29. Md Shahin Akanda, Md Shariful Islam, Md Ali Akbar, A. M. Sarwaruddin Chowdhury, M. A. Gafur, and Md Sahab Uddin, *Thermal and Morphological Assessment of the Penta-Layered, Hybrid U-Polyester Composite Reinforced with Glass Fibers and Polypropylene.* Advances in Materials Science and Engineering, **2024**. 2024: p. **3911466**.DOI: 10.1155/2024/3911466.
30. Swapnil Chandgude and Sachin Salunkhe, *In state of art: Mechanical behavior of natural fiber-based hybrid polymeric composites for application of automobile components.* Polymer Composites, **2021**. 42(6): p. **2678-2703**.DOI: https://doi.org/10.1002/pc.26045.
31. Amos A Wambura, *Investigating the mechanical properties of glass reinforced polymer as material for solar hot water tanks in coastal areas*, 2015, University of Nairobi.
32. Burcu Ertuğ, *Advanced Fiber-Reinforced Composite Materials for Marine Applications.* Advanced Materials Research, **2013**. 772: p. **173-177**.DOI: 10.4028/www.scientific.net/AMR.772.173.

33. A Mohan Kumar, R Parameshwaran, and R Rajasekar, *Effect of abaca reinforced polymer composite on dynamic mechanical analysis.* Colloid & Polymer Science, **2021**. 299(11): p. **1657-1667**.DOI: 10.1007/s00396-021-04881-y.
34. Ismet Baran, Remko Akkerman, and Jesper H. Hattel, *Material characterization of a polyester resin system for the pultrusion process.* Composites Part B: Engineering, **2014**. 64: p. **194-201**.DOI: https://doi.org/10.1016/j.compositesb.2014.04.030.
35. Mei-Xian Li, Hui-Lin Mo, Sung-Kwon Lee, Yu Ren, Wei Zhang, and Sung-Woong Choi *Rapid Impregnating Resins for Fiber-Reinforced Composites Used in the Automobile Industry*. Polymers, 2023. 15, DOI: 10.3390/polym15204192.
36. Somanath Ojha, Himanshu Bisaria, Smita Mohanty, and Krishnan Kanny, *Mechanical performance of e-glass reinforced polyester resins (isophthalic and orthophthalic) laminate composites used in marine applications.* Proceedings of the Institution of Mechanical Engineers, Part L: Journal of Materials: Design and Applications, **2023**: p. **14644207231194437**.DOI: 10.1177/14644207231194437.
37. Abeer Farouk Al-Attar, Hussein Alaa Jaber, and Ammar Mousa Hasan, *Enhancement of Mechanical Properties in Glass-Fiber Woven Reinforced Hybrid Composites for Aerospace Applications: An Empirical Investigation.* Journal of Composite & Advanced Materials/Revue des Composites et des Matériaux Avancés, **2023**. 33(6).
38. Changpei Qin, Qikai Jin, Junxian Zhao, Yixuan Wang, and Chaohua Jiang *Study on the Mechanical Characteristics, Heat Resistance, and Corrosion Resistance of Unsaturated Polyester Resin Composite*. Buildings, 2023. 13, DOI: 10.3390/buildings13071700.
39. Murat Ramazan İLtar, Engin Barut, Özkan Ayan, and Emine Can, *Risk Analysis in Polyester Resin Production Facility with Functional Resonance Analysis Method(FRAM).* OHS ACADEMY, **2024**. 6(3): p. **173-183**.DOI: 10.38213/ohsacademy.1415230.
40. AD Omah, HU Eze, EC Omah, SN Ude, O Nwoke, PO Offor, RE Njoku, and E Oji, *The Effect of Filler Variation and Interfacial Behaviour on the Dielectric Performance of Snail Shell Particulate Polyester Composites.* J. Mater. Environ. Sci., 14 (7), 750, **2023**. 761.
41. P. B. Bamane, K. K. Wadgaonkar, S. U. Chambhare, L. B. Mehta, and R. N. Jagtap, *Replacement of traditional unsaturated acid by bio-based itaconic acid in the preparation of isophthalic acid-based unsaturated polyester resin.* Progress in Organic Coatings, **2020**. 147: p. **105743**.DOI: https://doi.org/10.1016/j.porgcoat.2020.105743.
42. Nasmi Herlina Sari, Suteja, R. A. Ilyas, Edi Syafri, and S. Indran, *Characterization of the density and mechanical properties of corn husk fiber reinforced polyester composites after exposure to ultraviolet light.* Functional Composites and Structures, **2021**. 3(3): p. **034001**.DOI: 10.1088/2631-6331/ac0ed3.
43. Hien Tran Thi Thu, Chuc Nguyen Van, Hung Khong Manh, Thuy Ly Bich, and Thang Le Minh, *Determination of potential odor causing compounds in the condensate water from the manufacturing process of unsaturated polyester resin.* Vietnam Journal of Catalysis and Adsorption, **2021**. 10(4): p. **137-143**.DOI: https://doi.org/10.51316/jca.2021.080.
44. Chandrabhan Verma, Lukman O. Olasunkanmi, Ekemini D. Akpan, M. A. Quraishi, O. Dagdag, M. El Gouri, El-Sayed M. Sherif, and Eno E. Ebenso, *Epoxy resins as anticorrosive polymeric materials: A review.* Reactive and Functional Polymers, **2020**. 156: p. **104741**.DOI: https://doi.org/10.1016/j.reactfunctpolym.2020.104741.
45. Jaworski C. Capricho, Bronwyn Fox, and Nishar Hameed, *Multifunctionality in Epoxy Resins.* Polymer Reviews, **2020**. 60(1): p. **1-41**.DOI: 10.1080/15583724.2019.1650063.
46. Yuta Tsuji, Yasuhiro Kitamura, Masao Someya, Toshihiko Takano, Michio Yaginuma, Kohei Nakanishi, and Kazunari Yoshizawa, *Adhesion of Epoxy Resin with Hexagonal Boron Nitride and Graphite.* ACS Omega, **2019**. 4: p. **4491-4504**.DOI: 10.1021/acsomega.9b00129.

47. N. Nithin Kumar, SiddeshChincholi, Preran R. Hegde, S. Y. Shivagiri, and M. Revanasiddappa, *Synthesis and characterization of Fly ash /Wooden fiber reinforced Epoxy resin polymer composite.* Materials Today: Proceedings, **2018**. 5(1, Part 1): p. **501-507**.DOI: https://doi.org/10.1016/j.matpr.2017.11.111.
48. Mariya Kyulavska, Natalia Toncheva-Moncheva, and Joanna Rydz, *Biobased Polyamide Ecomaterials and Their Susceptibility to Biodegradation*, in *Handbook of Ecomaterials*, Leticia Myriam Torres Martínez, Oxana Vasilievna Kharissova, and Boris Ildusovich Kharisov, Editors. 2019, Springer International Publishing: Cham. p. 2901-2934.
49. Patrycja Bazan, Przemysław Nosal, Anna Wierzbicka-Miernik, and Stanisław Kuciel, *A novel hybrid composites based on biopolyamide 10.10 with basalt/aramid fibers: Mechanical and thermal investigation.* Composites Part B: Engineering, **2021**. 223: p. **109125**.DOI: https://doi.org/10.1016/j.compositesb.2021.109125.
50. Fang-Liang Guo, Di Tan, Tao Wu, Pei Huang, Yuan-Qing Li, Ning Hu, and Shao-Yun Fu, *Experimental characterization and molecular dynamics simulation of thermal stability, mechanical properties and liquid oxygen compatibility of multiple epoxy systems for cryotank applications.* Extreme Mechanics Letters, **2021**. 44: p. **101227**.DOI: https://doi.org/10.1016/j.eml.2021.101227.
51. T. Ramakrishnan, K. Raja Karthikeyan, V. Tamilselvan, S. Sivakumar, Durgaprasad Gangodkar, H. R. Radha, Anoop Narain Singh, and Yosef Asrat Waji, *Study of Various Epoxy-Based Surface Coating Techniques for Anticorrosion Properties.* Advances in Materials Science and Engineering, **2022**. 2022: p. **5285919**.DOI: 10.1155/2022/5285919.
52. Rashid Dallaev, Tatiana Pisarenko, Nikola Papež, Petr Sadovský, and Vladimír Holcman *A Brief Overview on Epoxies in Electronics: Properties, Applications, and Modifications*. Polymers, 2023. 15, DOI: 10.3390/polym15193964.
53. Alok K. Srivastava, Umang Desai, and Aparna Singh, *Effect of graphene coating on modified and pristine carbon fibers on the tribological response of carbon fiber epoxy composites.* Composites Part B: Engineering, **2023**. 250: p. **110412**.DOI: https://doi.org/10.1016/j.compositesb.2022.110412.
54. Yuxin Cai, Wulong Zhang, Linwen Yu, Mengzhu Chen, Changhui Yang, Raoul François, and Kai Yang, *Characteristics of the steel-concrete interface and their effect on the corrosion of steel bars in concrete.* Construction and Building Materials, **2020**. 253: p. **119162**.DOI: https://doi.org/10.1016/j.conbuildmat.2020.119162.
55. Anila Paul, Athira Ajayan, and Abraham Joseph, *Protection of mild steel in acidic and saline media using a novel surface coat developed with Pueraria phaseoloides seed extract and epoxy resin.* Next Materials, **2024**. 2: p. **100130**.DOI: https://doi.org/10.1016/j.nxmate.2024.100130.
56. Ummu R. Hashim, Aidah Jumahat, Mohammad Jawaid, Rudi Dungani, and Salman Alamery *Effects of Accelerated Weathering on Degradation Behavior of Basalt Fiber Reinforced Polymer Nanocomposites*. Polymers, 2020. 12, DOI: 10.3390/polym12112621.
57. Zhanghao Hou, Xiaoyong Tian, Junkang Zhang, Lu Zhe, Ziqi Zheng, Dichen Li, Andrei V. Malakhov, and Alexander N. Polilov, *Design and 3D printing of continuous fiber reinforced heterogeneous composites.* Composite Structures, **2020**. 237: p. **111945**.DOI: https://doi.org/10.1016/j.compstruct.2020.111945.
58. Narasimha Boddeti, Yunlong Tang, Kurt Maute, David W. Rosen, and Martin L. Dunn, *Optimal design and manufacture of variable stiffness laminated continuous fiber reinforced composites.* Scientific Reports, **2020**. 10(1): p. **16507**.DOI: 10.1038/s41598-020-73333-4.
59. Chao Hu, Zeyu Sun, Yi Xiao, and Qinghua Qin, *Recent Patents in Additive Manufacturing of Continuous Fiber Reinforced Composites.* Recent Patents on Mechanical Engineering, **2019**. 12(1): p. **25-36**.DOI: 10.2174/2212797612666190117131659.

60. Ludwig Schöttl, Dominik Dörr, Pascal Pinter, Kay André Weidenmann, Peter Elsner, and Luise Kärger, *A novel approach for segmenting and mapping of local fiber orientation of continuous fiber-reinforced composite laminates based on volumetric images.* NDT & E International, **2020**. 110: p. **102194**.DOI: https://doi.org/10.1016/j.ndteint.2019.102194.
61. Li Li, Xueting Liu, Xiaoou Zhou, Jie Hong, Xingmin Zhuang, and Xiong Yan, *Mechanical properties of unidirectional continuous fiber self-reinforced polyethylene graded laminates.* Polymer Composites, **2015**. 36(1): p. **128-137**.DOI: https://doi.org/10.1002/pc.22921.
62. Jeffery W. Baur, Andrew C. Abbott, Philip R. Barnett, Gyaneshwar P. Tandon, Jevan Furmanski, Nathan A. Stranberg, and Tyler B. Alvarado, *Mechanical properties of additively printed, UV cured, continuous fiber unidirectional composites for multifunctional applications.* Journal of Composite Materials, **2022**. 57(4): p. **865-882**.DOI: 10.1177/00219983221146264.
63. Kok-Heng Chong and John Chai, *Strength and mode of failure of unidirectional and bidirectional glass fiber-reinforced composite materials.* International Journal of Prosthodontics, **2003**. 16(2).
64. Moyed A Al-Nueimi and Edrees E Al-Obeidi, *The effect of (E-glass) fibers and glass powder addition on the alternating fatigue behavior of unsaturated polyester resin.* Rafidain Journal of Science, **2013**. 24(11): p. **96-115**.
65. Talita G. Targino, Sérgio R. L. Tinô, and Eve M. F. de Aquino, *Anisotropy, hole, and hybridization influences in polyester polymer composites reinforced by glass and glass/Kevlar.* Polymer Composites, **2019**. 40(12): p. **4669-4681**.DOI: https://doi.org/10.1002/pc.25335.
66. Komlan Akoussan, Mohamed Hamdaoui, and El Mostafa Daya, *Improved layer-wise optimization algorithm for the design of viscoelastic composite structures.* Composite Structures, **2017**. 176: p. **342-358**.DOI: https://doi.org/10.1016/j.compstruct.2017.05.047.
67. Sebastian Goris, Teresa Back, Angel Yanev, Dave Brands, Dietmar Drummer, and Tim A. Osswald, *A novel fiber length measurement technique for discontinuous fiber-reinforced composites: A comparative study with existing methods.* Polymer Composites, **2018**. 39(11): p. **4058-4070**.DOI: https://doi.org/10.1002/pc.24466.
68. Shashi Bahl, *Fiber reinforced metal matrix composites - a review.* Materials Today: Proceedings, **2021**. 39: p. **317-323**.DOI: https://doi.org/10.1016/j.matpr.2020.07.423.
69. Ilyas Rushdan Ahmad, Sapuan Salit Mohd, Ishak Mohamad Ridzwan, and Zainudin Edi Syams, *Water Transport Properties of Bio-Nanocomposites Reinforced by Sugar Palm (Arenga Pinnata) Nanofibrillated Cellulose.* Journal of Advanced Research in Fluid Mechanics and Thermal Sciences, **2018**. 51(2): p. **234-246**.
70. Meng Zhang and Jukka Pekka Matinlinna, *E-Glass Fiber Reinforced Composites in Dental Applications.* Silicon, **2012**. 4(1): p. **73-78**.DOI: 10.1007/s12633-011-9075-x.
71. Hairul Abral, Jeri Ariksa, Melbi Mahardika, Dian Handayani, Ibtisamatul Aminah, Neny Sandrawati, Angga Bahri Pratama, Nural Fajri, S. M. Sapuan, and R. A. Ilyas, *Transparent and antimicrobial cellulose film from ginger nanofiber.* Food Hydrocolloids, **2020**. 98: p. **105266**.DOI: https://doi.org/10.1016/j.foodhyd.2019.105266.
72. Przemyslaw Daniel Pastuszak and Aleksander Muc, *Application of Composite Materials in Modern Constructions.* Key Engineering Materials, **2013**. 542: p. **119-129**.DOI: 10.4028/www.scientific.net/KEM.542.119.
73. Junho Jang, Hyeon-Gyun Im, DaeSeop Lim, and Byeong-Soo Bae, *Preparation of high-performance transparent glass-fiber reinforced composites based on refractive index-tunable epoxy-functionalized siloxane hybrid matrix.* Composites Science and Technology, **2021**. 201: p. **108527**.DOI: https://doi.org/10.1016/j.compscitech.2020.108527.

74. Syafiqah Nur Azrie Bt Safri, M. T. H. Sultan, and Mohammad Jawaid, *7 - Damage analysis of glass fiber reinforced composites*, in *Durability and Life Prediction in Biocomposites, Fibre-Reinforced Composites and Hybrid Composites*, Mohammad Jawaid, Mohamed Thariq, and Naheed Saba, Editors. 2019, Woodhead Publishing. p. 133-147.
75. F. Fatih Melemez, Talha Boz, Pandian Chelliah, Gokhan Bektas, Mehmet Yildiz, Cem Ozturk, and Yusuf Z. Menceloglu, *Study of Local and Transient Buckling in Glass Fiber Reinforced Composite Using Fiber Bragg Grating.* Key Engineering Materials, **2013**. 543: p. **346-351**.DOI: 10.4028/www.scientific.net/KEM.543.346.
76. Priyadarsini Morampudi, Kiran Kumar Namala, Yeshwanth Kumar Gajjela, Majjiga Barath, and Ganaparthy Prudhvi, *Review on glass fiber reinforced polymer composites.* Materials Today: Proceedings, **2021**. 43: p. **314-319**.DOI: https://doi.org/10.1016/j.matpr.2020.11.669.
77. Essam Shehab, Arshyn Meiirbekov, Akniyet Amantayeva, and Serik Tokbolat *Cost Modelling for Recycling Fiber-Reinforced Composites: State-of-the-Art and Future Research*. Polymers, 2023. 15, DOI: 10.3390/polym15010150.
78. Hongshuai Gao, Yue Sun, Jiashuo Jian, Dong Yaqiao, and Hongbo Liu, *Study on mechanical properties and application in communication pole line engineering of glass fiber reinforced polyurethane composites (GFRP).* Case Studies in Construction Materials, **2023**. 18: p. **e01942**.DOI: 10.1016/j.cscm.2023.e01942.
79. T. Takahagi, I. Shimada, M. Fukuhara, K. Morita, and A. Ishitani, *XPS studies on the chemical structure of the stabilized polyacrylonitrile fiber in the carbon fiber production process.* Journal of Polymer Science Part A: Polymer Chemistry, **1986**. 24(11): p. **3101-3107**.DOI: https://doi.org/10.1002/pola.1986.080241134.
80. Huichao Liu, Shuo Zhang, Jinglong Yang, Muwei Ji, Jiali Yu, Mingliang Wang, Xiaoyan Chai, Bo Yang, Caizhen Zhu, and Jian Xu *Preparation, Stabilization and Carbonization of a Novel Polyacrylonitrile-Based Carbon Fiber Precursor*. Polymers, 2019. 11, DOI: 10.3390/polym11071150.
81. Dipen Kumar Rajak, Pratiksha H. Wagh, Hassan Moustabchir, and Catalin I. Pruncu, *Improving the tensile and flexural properties of reinforced epoxy composites by using cobalt filled and carbon/glass fiber.* Forces in Mechanics, **2021**. 4: p. **100029**.DOI: https://doi.org/10.1016/j.finmec.2021.100029.
82. Jiang Zhi Zhang, *Study on Carbon Fiber Composite Materials in Sports Equipment.* Applied Mechanics and Materials, **2013**. 329: p. **105-108**.DOI: 10.4028/www.scientific.net/AMM.329.105.
83. Anders Carolin, *Strengthening of concrete structures with CFRP: shear strengthening and full scale applications*, 2001, Luleå tekniska universitet.
84. Dipen K. Rajak, Pratiksha H. Wagh, and Emanoil Linul *Manufacturing Technologies of Carbon/Glass Fiber-Reinforced Polymer Composites and Their Properties: A Review*. Polymers, 2021. 13, DOI: 10.3390/polym13213721.
85. Andreas Wilken, Michael Albrecht, Jens Kosmann, and Erik Klaas. *Concept development of a visual assistance system for manual scarf repairs of composite structures made of fibre reinforced plastics*. in *Proceedings of the 7th International Workshop on Aircraft System Technologies*. 2019. Shaker verlag.
86. Santwana Pati, Siwat Manomaisantiphap, T. Goto, Tatsuhiro Takahashi, and Tomohiro Yokozeki, *Development of CFRP with Polyaniline-based Resin using Curable Dopants Employing Storage Stable Prepregs.* Applied Composite Materials, **2021**. 28: p. **1-14**.DOI: 10.1007/s10443-020-09856-w.
87. Ren-Qin Cai, Tao Peng, Feng-De Wang, Guang-Dou Ye, and Jian-Jun Xu, *Improvement of surface wettability and interfacial adhesion of poly-(p-phenylene terephthalamide) by*

incorporation of the polyamide benzimidazole segment. Applied Surface Science, **2011**. 257(22): p. **9562-9567**.DOI: https://doi.org/10.1016/j.apsusc.2011.06.064.

88. Jalal Nasser, Jiajun Lin, and Henry Sodano, *High strength fiber reinforced composites with surface fibrilized aramid fibers.* Journal of Applied Physics, **2018**. 124(4): p. **045305**.DOI: 10.1063/1.5026987.
89. Prakash M. Gore and Balasubramanian Kandasubramanian, *Functionalized Aramid Fibers and Composites for Protective Applications: A Review.* Industrial & Engineering Chemistry Research, **2018**. 57(49): p. **16537-16563**.DOI: 10.1021/acs.iecr.8b04903.
90. Kadir Bilisik, *18 - Aramid fiber reinforced composites*, in *Fiber Reinforced Composites*, Kuruvilla Joseph, Kristiina Oksman, Gejo George, Runcy Wilson, and Saritha Appukuttan, Editors. 2021, Woodhead Publishing. p. 515-559.
91. Zhi Sun, Mathavaraja Jeyaraman, Shanshan Shi, Shiyong Sun, and Ha Ran Chen, *Processing and property of carbon-fiber aluminum-foam sandwich with aramid-fiber composite adhesive joints.* Journal of Adhesion Science and Technology, **2014**. 28: p. **1835-1845**.DOI: 10.1080/01694243.2014.925385.
92. Arnaud Rolland, Karim Benzarti, M. Quiertant, Sylvain Chataigner, and Pierre Argoul, *Characterization of Aramid FRP rebars and study of their bond behaviour with concrete*. 2014.
93. Alireza Dashti, Clément Keller, Benoit Vieille, Alain Guillet, and Christophe Bouvet *Experimental and Finite Element Analysis of the Tensile Behavior of Architectured Cu-Al Composite Wires*. Materials, 2021. 14, DOI: 10.3390/ma14216305.
94. Yunhai Ma, Qian Wu, Lingjian Duanmu, Siyang Wu, Qingping Liu, Bingqian Li, and Xueli Zhou, *Bioinspired composites reinforced with ordered steel fibers produced via a magnetically assisted 3D printing process.* Journal of Materials Science, **2020**. 55(32): p. **15510-15522**.DOI: 10.1007/s10853-020-05092-6.
95. R. K. Misra and S. Kumar, *Static and dynamic mechanical analysis of chemically modified randomly distributed short banana fiber reinforced high-density Polyethylene/Poly (E-caprolactonc) Composites.* **2009**. 29(4): p. **213-248**.DOI: doi:10.1515/POLYENG.2009.29.4.213.
96. Maiken Stilling, Frank Madsen, Anders Odgaard, Lone Rømer, Niels Andersen, Ole Rahbek, and Kjeld Søballe, *Superior fixation of pegged trabecular metal over screw-fixed pegged porous titanium fiber mesh: A randomized clinical RSA study on cementless tibial components.* Acta orthopaedica, **2011**. 82: p. **177-86**.DOI: 10.3109/17453674.2011.566139.
97. Sandeep Kumar, Alakesh Manna, and Rakesh Dang, *A review on applications of natural Fiber-Reinforced composites (NFRCs).* Materials Today: Proceedings, **2022**. 50: p. **1632-1636**.DOI: https://doi.org/10.1016/j.matpr.2021.09.131.
98. P. Venkateshwar Reddy, R. V. Saikumar Reddy, J. Lakshmana Rao, D. Mohana Krishnudu, and P. Rajendra Prasad, *An overview on natural fiber reinforced composites for structural and non-structural applications.* Materials Today: Proceedings, **2021**. 45: p. **6210-6215**.DOI: https://doi.org/10.1016/j.matpr.2020.10.523.
99. Ayyappa Atmakuri, Arvydas Palevicius, Madhusudan Siddabathula, Andrius Vilkauskas, and Giedrius Janusas *Analysis of Mechanical and Wettability Properties of Natural Fiber-Reinforced Epoxy Hybrid Composites*. Polymers, 2020. 12, DOI: 10.3390/polym12122827.
100. Isaac Mugarura and Mehmet Çevik, *Natural Fibers in Uganda Suitable for Sustainable Natural Fiber Reinforced Composites.* **2023**.
101. Jorge Neto, Henrique Queiroz, Ricardo Aguiar, Rosemere Lima, Daniel Cavalcanti, and Mariana Doina Banea, *A review of recent advances in hybrid natural fiber reinforced polymer composites.* Journal of Renewable Materials, **2022**. 10(3): p. **561**.

102. Maria Carolina Teles, Gabriel Glória, Giulio Altoe, Pedro Netto, Frederico Margem, Fábio de Oliveira Braga, and Sergio Monteiro, *Evaluation of the Diameter Influence on the Tensile Strength of Pineapple Leaf Fibers (PALF) by Weibull Method.* Materials Research, **2015**. 18.DOI: 10.1590/1516-1439.362514.
103. Kaitlyn Jo Engle, *Environmentally friendly industrial hemp processing for high quality fibers*, Hang Liu, Editor 2018, Washington State University: [Pullman, Washington] :.
104. T. Sathish, Kumaran Palani, L. Natrayan, Anjibabu Merneedi, Melvin Victor De Poures, and Dinesh Kumar Singaravelu, *Synthesis and Characterization of Polypropylene/Ramie Fiber with Hemp Fiber and Coir Fiber Natural Biopolymer Composite for Biomedical Application.* International Journal of Polymer Science, **2021**. 2021: p. **2462873**.DOI: 10.1155/2021/2462873.
105. T Sathish, Kumaran Palani, L Natrayan, Anjibabu Merneedi, Melvin Victor De Poures, and Dinesh Kumar Singaravelu, *Research Article Synthesis and Characterization of Polypropylene/Ramie Fiber with Hemp Fiber and Coir Fiber Natural Biopolymer Composite for Biomedical Application.* **2021**.
106. Helong Song, Tao Liu, and Florent Gauvin, *Enhancing mechanical performance of green fiber cement composites: Role of eco-friendly alkyl ketene dimer on surfaces of hemp fibers.* Journal of Materials Research and Technology, **2024**. 28: p. **3121-3132**.DOI: https://doi.org/10.1016/j.jmrt.2023.12.255.
107. Jasti Anurag and Sandhyarani Biswas, *Characterization of Elementary Industrial Hemp (Cannabis Sativa L.) Fiber and Its Fabric.* Journal of Natural Fibers, **2023**. 20.DOI: 10.1080/15440478.2022.2158982.
108. Yaseen A Salih, Nadia N Sabeeh, Muhammed F Yass, Ahmed S Ahmed, and Ektiffa Saleh Khudhurr, *Concrete beams strengthened with jute fibers.* Civil Engineering Journal, **2019**. 5(4): p. **767-776**.
109. N Dayananda, BS Keerthi Gowda, and GL Easwara Prasad. *A study on compressive strength attributes of jute fiber reinforced cement concrete composites*. in *IOP Conference Series: Materials Science and Engineering*. 2018. IOP Publishing.
110. Sumit Kumar, Sohan Lal, Geetanjali Jagdeva, Sanjiv Arora, Parvin Kumar, R. K. Soni, Harish Kumar, Sunil Kumar, and Suresh Panchal, *Performance-based natural rubber composites reinforced with jute fibers and nano-silica: thermal, morphological, and mechanical studies with statistical optimization.* Iranian Polymer Journal, **2023**. 32(5): p. **609-619**.DOI: 10.1007/s13726-023-01148-x.
111. Youssef Bensmail, Ahmed el moumen, A. Imad, Fatima Lmai, and M. ezahri, *Effect of heat treatment on the mechanical properties of jute yarns.* Journal of Composite Materials, **2021**: p. **1-16**.DOI: 10.1177/0021998321999103.
112. Ayou Hao, Haifeng Zhao, and Jonathan Y. Chen, *Kenaf/polypropylene nonwoven composites: The influence of manufacturing conditions on mechanical, thermal, and acoustical performance.* Composites Part B: Engineering, **2013**. 54: p. **44-51**.DOI: https://doi.org/10.1016/j.compositesb.2013.04.065.
113. Vishwas Mahesh and Vinyas Mahesh, *Development and Mechanical Characterization of Light Weight Fiber Metal Laminate using Jute, Kenaf and Aluminium.* Mechanics of Advanced Composite Structures, **2024**. 11(2): p. **259-270**.DOI: 10.22075/macs.2023.30686.1506.
114. Qiushi Wang, Joydan Jones, Na Lu, Ralph Johnson, Haibin Ning, and Selvum Pillay, *Development and characterization of high-performance kenaf fiber–HDPE composites.* Journal of Reinforced Plastics and Composites, **2017**. 37(3): p. **191-200**.DOI: 10.1177/0731684417739127.
115. Ida Norfaslia Nasidi, Lokman Hakim Ismail, Emedya Samsudin, and Muhammad Ismail Jaffar, *Effects of Kenaf Fiber Strand Treatment by Sodium Hydroxide On Sound*

Absorption. Journal of Natural Fibers, **2022**. 19(13): p. **6727-6736**.DOI: 10.1080/15440478.2021.1932670.

116. Natrayan L, Kaliappan Seeniappan, Gururaj Hatti, Pravin Patil, Piyush Gaur, T. Manikandan, and P. Murugan, *Journal of Nanomaterials.* Journal of Nanomaterials, **2022**. 2022.DOI: 10.1155/2022/3554026.
117. H. P. S. Abdul Khalil, A. H. Bhat, and A. F. Ireana Yusra, *Green composites from sustainable cellulose nanofibrils: A review.* Carbohydrate Polymers, **2012**. 87(2): p. **963-979**.DOI: https://doi.org/10.1016/j.carbpol.2011.08.078.
118. Alexis Pietak, Sandra Korte, Emelyn Tan, Alison Downard, and Mark P. Staiger, *Atomic force microscopy characterization of the surface wettability of natural fibres.* Applied Surface Science, **2007**. 253(7): p. **3627-3635**.DOI: https://doi.org/10.1016/j.apsusc.2006.07.082.
119. Ning Zhang, Shi Li, Liming Xiong, Yu Hong, and Youping Chen, *Cellulose-hemicellulose interaction in wood secondary cell-wall.* Modelling and Simulation in Materials Science and Engineering, **2015**. 23: p. **085010**.DOI: 10.1088/0965-0393/23/8/085010.
120. Lili Lin, Rong Yan, Wenju Jiang, Fei Shen, Xiaohong Zhang, Yanzong Zhang, Shihuan Deng, and Zhuang Li, *Enhanced Enzymatic Hydrolysis of Palm Pressed Fiber Based on the Three Main Components: Cellulose, Hemicellulose, and Lignin.* Applied Biochemistry and Biotechnology, **2014**. 173(2): p. **409-420**.DOI: 10.1007/s12010-014-0848-8.
121. Thomas Heinze, *Cellulose: Structure and Properties*, in *Cellulose Chemistry and Properties: Fibers, Nanocelluloses and Advanced Materials*, Orlando J. Rojas, Editor. 2016, Springer International Publishing: Cham. p. 1-52.
122. Paladugula Pradeep and J. Dhas, *Characterization of Chemical and Physical Properties of Palm Fibers.* Advances in Materials Science and Engineering: An International Journal (MSEJ), **2015**. 2: p. **01-06**.DOI: 10.5121/msej.2015.2401.
123. Heidi Richards, Priscilla Baker, and Emmanuel Iwuoha, *Metal Nanoparticle Modified Polysulfone Membranes for Use in Wastewater Treatment: A Critical Review.* Journal of Surface Engineered Materials and Advanced Technology, **2012**. 2: p. **183**.DOI: 10.4236/jsemat.2012.223029.
124. Henrik Vibe Scheller and Peter Ulvskov, *Hemicelluloses.* Annual review of plant biology, **2010**. 61: p. **263-289**.
125. Chung Loong Yiin, Syhui Ho, Suzana Yusup, Armando T. Quitain, Yi Herng Chan, Adrian Chun Minh Loy, and Yong Ling Gwee, *Recovery of cellulose fibers from oil palm empty fruit bunch for pulp and paper using green delignification approach.* Bioresource Technology, **2019**. 290: p. **121797**.DOI: https://doi.org/10.1016/j.biortech.2019.121797.
126. Lisong hu, Xuezhi Fang, Menghao Du, Fan Luo, and Shaohai Guo, *Hemicellulose-Based Polymers Processing and Application.* American Journal of Plant Sciences, **2020**. 11: p. **2066-2079**.DOI: 10.4236/ajps.2020.1112146.
127. Brianna M. Upton and Andrea M. Kasko, *Strategies for the Conversion of Lignin to High-Value Polymeric Materials: Review and Perspective.* Chemical Reviews, **2016**. 116(4): p. **2275-2306**.DOI: 10.1021/acs.chemrev.5b00345.
128. G. Rajeshkumar, V. Hariharan, G. L. Devnani, J. Prakash Maran, M. R. Sanjay, Suchart Siengchin, Naif Abdullah Al-Dhabi, and K. Ponmurugan, *Cellulose fiber from date palm petioles as potential reinforcement for polymer composites: Physicochemical and structural properties.* Polymer Composites, **2021**. 42(8): p. **3943-3953**.DOI: https://doi.org/10.1002/pc.26106.
129. Takashiro Akitsu and Daisuke Nakane, *Recent Topics of Laccase Focused on Chemical Reactions and Applications.* Universal Journal of Green Chemistry, **2022**. 1: p. **2-17**.DOI: 10.37256/ujgc.1120231901.

130. L Mwaikambo, *Review of the history, properties and application of plant fibres.* African Journal of Science and Technology, **2006**. 7(2): p. **121**.
131. Xiaohui Zhang, *Manufacturing of hemp/PP composites and study of its residual stress and aging behavior*, 2016, Université de Technologie de Troyes.
132. Gökhan Kaplan and Oğuzhan Yavuz Bayraktar, *The effect of hemp fiber usage on the mechanical and physical properties of cement based mortars.* Res. Eng. Struct. Mater, **2021**. 7: p. **245-258**.
133. Abolfazl Eslami, Hosein Mohammadi, and Hosein Mirabi Banadaki, *Palm fiber as a natural reinforcement for improving the properties of traditional adobe bricks.* Construction and Building Materials, **2022**. 325: p. **126808**.DOI: https://doi.org/10.1016/j.conbuildmat.2022.126808.
134. Musa Adamu, Fayez Alanazi, Yasser E. Ibrahim, Hani Alanazi, and Veerendrakumar C. Khed *A Comprehensive Review on Sustainable Natural Fiber in Cementitious Composites: The Date Palm Fiber Case*. Sustainability, 2022. 14, DOI: 10.3390/su14116691.
135. Govardhana Rao Chilukoti, B. Venkatesh, M. Siva Jagadish Kumar, S. Kubera Sampath Kumar, C. Prakash, and Aravin Prince Periyasamy, *Study of Alkali Treatment and Its Influence on Characteristics of Borassus Palm Fiber.* Journal of Natural Fibers, **2022**. 19(16): p. **14951-14962**.DOI: 10.1080/15440478.2022.2069197.
136. Dong Xiaoyuan, *Theoretical and Empirical Research on the Industrial Restructuring in Shenzhen*, in *Studies on China's Special Economic Zones 3*, Yiming Yuan, Editor. 2020, Springer Singapore: Singapore. p. 21-35.
137. Sakil Mahmud, K. M. Faridul Hasan, Md Anwar Jahid, Kazi Mohiuddin, Ruoyu Zhang, and Jin Zhu, *Comprehensive review on plant fiber-reinforced polymeric biocomposites.* Journal of Materials Science, **2021**. 56(12): p. **7231-7264**.DOI: 10.1007/s10853-021-05774-9.
138. Mohammed Mohammed, Jawad K. Oleiwi, Aeshah M. Mohammed, Anwar Ja'afar Mohamad Jawad, Azlin F. Osman, Tijjani Adam, Bashir O. Betar, Subash C. B. Gopinath, Omar S. Dahham, and Mustafa Jaafar, *Comprehensive insights on mechanical attributes of natural-synthetic fibres in polymer composites.* Journal of Materials Research and Technology, **2023**. 25: p. **4960-4988**.DOI: https://doi.org/10.1016/j.jmrt.2023.06.148.
139. K. N. Bharath, P. Madhu, T. G. Yashas Gowda, Akarsh Verma, M. R. Sanjay, and Suchart Siengchin, *Mechanical and Chemical Properties Evaluation of Sheep Wool Fiber–Reinforced Vinylester and Polyester Composites.* Materials Performance and Characterization, **2021**. 10(1): p. **99-109**.DOI: 10.1520/mpc20200036.
140. Omar Faruk, Andrzej K. Bledzki, Hans-Peter Fink, and Mohini Sain, *Biocomposites reinforced with natural fibers: 2000–2010.* Progress in Polymer Science, **2012**. 37(11): p. **1552-1596**.DOI: https://doi.org/10.1016/j.progpolymsci.2012.04.003.
141. Toshihiko Hojo, Zhilan Xu, Yuqiu Yang, and Hiroyuki Hamada, *Tensile Properties of Bamboo, Jute and Kenaf Mat-reinforced Composite.* Energy Procedia, **2014**. 56: p. **72-79**.DOI: https://doi.org/10.1016/j.egypro.2014.07.133.
142. Adewale George Adeniyi, Damilola Victoria Onifade, Joshua O. Ighalo, and Akorede Samson Adeoye, *A review of coir fiber reinforced polymer composites.* Composites Part B: Engineering, **2019**. 176: p. **107305**.DOI: https://doi.org/10.1016/j.compositesb.2019.107305.
143. Elsadig Mahdi and Aamir Dean *The Effect of Filler Content on the Tensile Behavior of Polypropylene/Cotton Fiber and poly(vinyl chloride)/Cotton Fiber Composites*. Materials, 2020. 13, DOI: 10.3390/ma13030753.
144. C. Baley, *Analysis of the flax fibres tensile behaviour and analysis of the tensile stiffness increase.* Composites Part A: Applied Science and Manufacturing, **2002**. 33(7): p. **939-948**.DOI: https://doi.org/10.1016/S1359-835X(02)00040-4.

145. Changjie Chen, Jing Tan, and Xinhou Wang, *Mechanical properties of toughened windmill palm fibre with different chemical compositions.* Carbohydrate Polymers, **2022**. 297: p. **119996**.DOI: https://doi.org/10.1016/j.carbpol.2022.119996.
146. Amandine Célino, Sylvain Freour, Frederic Jacquemin, and Pascal Casari, *The hygroscopic behavior of plant fibers: a review.* Frontiers in Chemistry, **2014**. 1.DOI: 10.3389/fchem.2013.00043.
147. Akash, D. S. Arunkumar, N. S. Venkatesha Gupta, and K. V. Sreenivas Rao, *Effect of Samanea Saman Pod Pulp on Mechanical and Water Absorption Properties of Bio-Composites.* Materials Today: Proceedings, **2017**. 4(9): p. **9592-9596**.DOI: https://doi.org/10.1016/j.matpr.2017.06.230.
148. Massoud Ghasemzadeh-Barvarz, Carl Duchesne, and Denis Rodrigue, *Mechanical, water absorption, and aging properties of polypropylene/flax/glass fiber hybrid composites.* Journal of Composite Materials, **2015**. 49(30): p. **3781-3798**.DOI: 10.1177/0021998314568576.
149. Agnė Kairytė, Arūnas Kremensas, Giedrius Balčiūnas, Ieva Matulaitienė, Sylwia Członka, and Natalia Sienkiewicz, *Evaluation of self-thermally treated wood plastic composites from wood bark and rapeseed oil-based binder.* Construction and Building Materials, **2020**. 250: p. **118842**.DOI: https://doi.org/10.1016/j.conbuildmat.2020.118842.
150. Cionita Tezara, Agung E. Hadi, Januar P. Siregar, Zalinawati Muhamad, Mohammad H. Hamdan, Ahmed N. Oumer, Jamiluddin Jaafar, Agustinus P. Irawan, Teuku Rihayat, and Deni F. Fitriyana *The Effect of Hybridisation on Mechanical Properties and Water Absorption Behaviour of Woven Jute/Ramie Reinforced Epoxy Composites*. Polymers, 2021. 13, DOI: 10.3390/polym13172964.
151. Eyasu Ferede, *Evaluation of Mechanical and Water Absorption Properties of Alkaline-Treated Sawdust-Reinforced Polypropylene Composite.* Journal of Engineering, **2020**. 2020: p. **3706176**.DOI: 10.1155/2020/3706176.
152. J. M. Lee, Z. A. Mohd Ishak, R. Mat Taib, T. T. Law, and M. Z. Ahmad Thirmizir, *Mechanical, Thermal and Water Absorption Properties of Kenaf-Fiber-Based Polypropylene and Poly(Butylene Succinate) Composites.* Journal of Polymers and the Environment, **2013**. 21(1): p. **293-302**.DOI: 10.1007/s10924-012-0516-4.
153. Byung Kuk Kim, Oh Hyeong Kwon, Won Ho Park, and Donghwan Cho, *Thermal, mechanical, impact, and water absorption properties of novel silk fibroin fiber reinforced poly(butylene succinate) biocomposites.* Macromolecular Research, **2016**. 24(8): p. **734-740**.DOI: 10.1007/s13233-016-4102-9.
154. Nazila Dehbari, Nima Moazeni, and W. A. Wan Abdul Rahman, *Effects of Kenaf core on properties of poly(lactic acid) bio-composite.* Polymer Composites, **2014**. 35(6): p. **1220-1227**.DOI: https://doi.org/10.1002/pc.22771.
155. Shah Alimuzzaman, R. H. Gong, and Mahmudul Akonda, *Biodegradability of nonwoven flax fiber reinforced polylactic acid biocomposites.* Polymer Composites, **2014**. 35(11): p. **2094-2102**.DOI: https://doi.org/10.1002/pc.22871.
156. M. Z. Ahmad Thirmizir, Z. A. Mohd Ishak, R. Mat Taib, R. Sudin, and Y. W. Leong, *Mechanical, Water Absorption and Dimensional Stability Studies of Kenaf Bast Fibre-Filled Poly(butylene succinate) Composites.* Polymer-Plastics Technology and Engineering, **2011**. 50(4): p. **339-348**.DOI: 10.1080/03602559.2010.531871.
157. K. Ganesan, C. Kailasanathan, N. Rajini, Sikiru O. Ismail, Nadir Ayrilmis, Faruq Mohammad, Hamad A. Al-Lohedan, Ahmed M. Tawfeek, Zuheir A. Issa, and Daifallah M. Aldhayan, *Assessment on hybrid jute/coir fibers reinforced polyester composite with hybrid fillers under different environmental conditions.* Construction and Building Materials, **2021**. 301: p. **124117**.DOI: https://doi.org/10.1016/j.conbuildmat.2021.124117.

158. Temesgen Berhanu Yallew, Pradeep Kumar, and Inderdeep Singh, *A study about hole making in woven jute fabric-reinforced polymer composites.* Proceedings of the Institution of Mechanical Engineers, Part L: Journal of Materials: Design and Applications, **2015**. 230(4): p. **888-898**.DOI: 10.1177/1464420715587750.
159. A. Saravana Kumar, P. Maivizhi Selvi, and L. Rajeshkumar, *Delamination in Drilling of Sisal/Banana Reinforced Composites Produced by Hand Lay-Up Process.* Applied Mechanics and Materials, **2017**. 867: p. **29-33**.DOI: 10.4028/www.scientific.net/AMM.867.29.
160. V. Sridharan, T. Raja, and N. Muthukrishnan, *Study of the Effect of Matrix, Fibre Treatment and Graphene on Delamination by Drilling Jute/Epoxy Nanohybrid Composite.* Arabian Journal for Science and Engineering, **2016**. 41(5): p. **1883-1894**.DOI: 10.1007/s13369-015-2005-2.
161. R. Pramod, S. Basavarajappa, G. B. Veeresh Kumar, and Murthy Chavali, *Drilling induced delamination assessment of nanoparticles reinforced polymer matrix composites.* Proceedings of the Institution of Mechanical Engineers, Part C: Journal of Mechanical Engineering Science, **2021**. 236(6): p. **2931-2948**.DOI: 10.1177/09544062211030967.
162. Vijaykumar Chaudhary and Piyush P. Gohil, *Investigations on Drilling of Bidirectional Cotton Polyester Composite.* Materials and Manufacturing Processes, **2016**. 31(7): p. **960-968**.DOI: 10.1080/10426914.2015.1059444.
163. R. Vinayagamoorthy, I. V. Manoj, G. Narendra Kumar, I. Sai Chand, G. V. Sai Charan Kumar, and K. Suneel Kumar, *A central composite design based fuzzy logic for optimization of drilling parameters on natural fiber reinforced composite.* Journal of Mechanical Science and Technology, **2018**. 32(5): p. **2011-2020**.DOI: 10.1007/s12206-018-0409-0.
164. A. Díaz-Álvarez, M. Rodríguez-Millán, J. Díaz-Álvarez, and M. H. Miguélez, *Experimental analysis of drilling induced damage in aramid composites.* Composite Structures, **2018**. 202: p. **1136-1144**.DOI: https://doi.org/10.1016/j.compstruct.2018.05.068.
165. Landis W. Doner and Kevin B. Hicks, *Isolation of Hemicellulose from Corn Fiber by Alkaline Hydrogen Peroxide Extraction.* Cereal Chemistry, **1997**. 74(2): p. **176-181**.DOI: https://doi.org/10.1094/CCHEM.1997.74.2.176.
166. Andressa Cecília Milanese, Kelly Cristina Coelho de Carvalho Benini, Maria Odila Hilário Cioffi, and Herman Jacobus Cornelis Voorwald, *Thermal Analysis of Sisal/Epoxy Composite Processed by RTM.* Applied Mechanics and Materials, **2015**. 719-720: p. **50-54**.DOI: 10.4028/www.scientific.net/AMM.719-720.50.
167. Thiagamani Senthil Muthu Kumar, Krishnasamy Senthilkumar, Muthukumar Chandrasekar, Saravanasankar Subramaniam, Sanjay Mavinkere Rangappa, Suchart Siengchin, and Nagarajan Rajini, *Influence of Fillers on the Thermal and Mechanical Properties of Biocomposites: An Overview*, in *Biofibers and Biopolymers for Biocomposites: Synthesis, Characterization and Properties*, Anish Khan, Sanjay Mavinkere Rangappa, Suchart Siengchin, and Abdullah M. Asiri, Editors. 2020, Springer International Publishing: Cham. p. 111-133.
168. Indra Mawardi, Sri Aprilia, Muhammad Faisal, and Samsul Rizal *Characterization of Thermal Bio-Insulation Materials Based on Oil Palm Wood: The Effect of Hybridization and Particle Size*. Polymers, 2021. 13, DOI: 10.3390/polym13193287.
169. T. Suzuki, Y. Oki, M. Numajiri, T. Miura, K. Kondo, N. Oshima, T. Hayashi, H. Nakamura, and Y. Ito, *Free volume of cyanate resins studied by positron annihilation.* Journal of Radioanalytical and Nuclear Chemistry, **1996**. 210(2): p. **555-562**.DOI: https://doi.org/10.1007/bf02056395.

170. William Buschle, *Effect of Polymerization Variables on the Properties of Poly(N-Ethyl aniline)*, 2009, University of Cincinnati.
171. British Standard and B ISO, *Plastics-determination of water absorption.* PN-EN ISO, **1999**. 62.
172. Y. Z. Wan, Honglin Luo, F. He, H. Liang, Y. Huang, and X. L. Li, *Mechanical, moisture absorption, and biodegradation behaviours of bacterial cellulose fibre-reinforced starch biocomposites.* Composites Science and Technology, **2009**. 69(7): p. **1212-1217**.DOI: https://doi.org/10.1016/j.compscitech.2009.02.024.
173. Y. Ratna Kumari, K. Ramanaiah, A. V. Ratna Prasad, K. Hemachandra Reddy, Srinivas Prasad Sanaka, and A. Kalyan Prudhvi, *Experimental investigation of water absorption behaviour of sisal fiber reinforced polyester and sisal fiber reinforced poly lactic acid composites.* Materials Today: Proceedings, **2021**. 44: p. **935-940**.DOI: https://doi.org/10.1016/j.matpr.2020.11.002.
174. Ali S Hammood, *Effect of erosion on water absorption and morphology for treated date palm fiber-reinforced polyester composites.* Int J Mech Mechatron Eng, **2015**. 15(6): p. **108**.
175. Amandine Célino, Sylvain Fréour, Frédéric Jacquemin, and Pascal Casari, *Characterization and modeling of the moisture diffusion behavior of natural fibers.* Journal of Applied Polymer Science, **2013**. 130(1): p. **297-306**.DOI: https://doi.org/10.1002/app.39148.
176. Mia Kurek, Sabina Galus, and Frédéric Debeaufort, *Surface, mechanical and barrier properties of bio-based composite films based on chitosan and whey protein.* Food Packaging and Shelf Life, **2014**. 1(1): p. **56-67**.DOI: https://doi.org/10.1016/j.fpsl.2014.01.001.
177. Patrick Ehi Imoisili and Tien-Chien Jen, *Mechanical and water absorption behaviour of potassium permanganate (KMnO4) treated plantain (Musa Paradisiacal) fibre/epoxy bio-composites.* Journal of Materials Research and Technology, **2020**. 9(4): p. **8705-8713**.DOI: https://doi.org/10.1016/j.jmrt.2020.05.121.
178. Mario Zauer, Alexander Pfriem, and André Wagenführ, *Toward improved understanding of the cell-wall density and porosity of wood determined by gas pycnometry*. Wood Science and Technology, **2013**. 47(6): p. **1197-1211**.DOI: 10.1007/s00226-013-0568-1.
179. Puxi Huang, Wen-Shao Chang, Martin P. Ansell, Chew Y. M. John, and Andy Shea, *Porosity estimation of Phyllostachys edulis (Moso bamboo) by computed tomography and backscattered electron imaging.* Wood Science and Technology, **2017**. 51(1): p. **11-27**.DOI: 10.1007/s00226-016-0865-6.
180. Chongqian Huang, Xueke Zhang, and Zhengqi Liu, *Effects of Porosity on the Static Compression of Foam Buffer Materials of Plant Fiber and Their Numerical Model.* Shock and Vibration, **2021**. 2021: p. **5568653**.DOI: 10.1155/2021/5568653.
181. Behnaz Baghaei, Mikael Skrifvars, Masoud Salehi, Tariq Bashir, Marja Rissanen, and Pertti Nousiainen, *Novel aligned hemp fibre reinforcement for structural biocomposites: Porosity, water absorption, mechanical performances and viscoelastic behaviour.* Composites Part A: Applied Science and Manufacturing, **2014**. 61: p. **1-12**.DOI: https://doi.org/10.1016/j.compositesa.2014.01.017.
182. Magdaléna Doleželová, Lenka Scheinherrová, Jitka Krejsová, Martin Keppert, Robert Černý, and Alena Vimmrová, *Investigation of gypsum composites with different lightweight fillers.* Construction and Building Materials, **2021**. 297: p. **123791**.DOI: https://doi.org/10.1016/j.conbuildmat.2021.123791.
183. Yu Hong, Wu-jie Wang, Jia-qin Liu, Wen-ming Tang, and Yu-cheng Wu, *Effect of porosity and interface structures on thermal and mechanical properties of SiCp/6061Al composites*

with high volume fraction of SiC. Transactions of Nonferrous Metals Society of China, **2019**. 29(5): p. **941-949**.DOI: https://doi.org/10.1016/S1003-6326(19)65003-X.

184. Trung Kien Nguyen, Lan Xuan Phung, and Ngoc-Tam Bui, *Novel integration of capp in a g-code generation module using macro programming for CNC application.* Machines, **2020**. 8(4): p. **61**.
185. C. Liu, J. Liu, and W. Gao. *Principle and application of mirror function in CNC system based on PMAC*. in *2017 IEEE 2nd Advanced Information Technology, Electronic and Automation Control Conference (IAEAC)*. 2017.
186. B Gowd, *Effects of Drilling Parameters on Delamination of Hemp Fiber Reinforced Composites.* **2012**.
187. Pulakesh Chetia, Sutanu Samanta, and Thingujam J. Singh, *Parametric optimization in drilling of Bamboo/Basalt hybrid composite.* Materials Today: Proceedings, **2018**. 5(2, Part 1): p. **5544-5552**.DOI: https://doi.org/10.1016/j.matpr.2017.12.145.
188. SA Azuan, JM Juraidi, and Wan Mansor Wan Muhamad. *Evaluation of delamination in drilling rice husk reinforced polyester composites*. in *Applied Mechanics and Materials*. 2012. Trans Tech Publ.
189. Yahya Hışman Çelik and Mehmet Suat Alp, *Determination of Milling Performance of Jute and Flax Fiber Reinforced Composites.* Journal of Natural Fibers, **2022**. 19(2): p. **782-796**.DOI: 10.1080/15440478.2020.1764435.
190. Sandhyarani Pailoor, H. N. Narasimha Murthy, and T. N. Sreenivasa, *Drilling of In-Line Compression Molded Jute / Polypropylene Composites.* Journal of Natural Fibers, **2021**. 18(1): p. **91-104**.DOI: 10.1080/15440478.2019.1612309.
191. M Ramesh, K Palanikumar, and K Hemachandra Reddy. *Experimental investigation and analysis of machining characteristics in drilling hybrid glass-sisal-jute fiber reinforced polymer composites*. in *5th international & 26th all india manufacturing technology, design and research conference AIMTDR*. 2014.
192. A. S. Singha and Vijay Kumar Thakur, *Mechanical properties of natural fibre reinforced polymer composites.* Bulletin of Materials Science, **2008**. 31(5): p. **791-799**.DOI: 10.1007/s12034-008-0126-x.
193. S. Jothibasu, S. Mohanamurugan, R. Vijay, D. Lenin Singaravelu, A. Vinod, and M. R. Sanjay, *Investigation on the mechanical behavior of areca sheath fibers/jute fibers/glass fabrics reinforced hybrid composite for light weight applications.* Journal of Industrial Textiles, **2018**. 49(8): p. **1036-1060**.DOI: 10.1177/1528083718804207.
194. Reza Masoodi and Krishna M. Pillai, *A study on moisture absorption and swelling in bio-based jute-epoxy composites.* Journal of Reinforced Plastics and Composites, **2012**. 31(5): p. **285-294**.DOI: 10.1177/0731684411434654.
195. Bachir Adda, Ahmed Belaadi, Messaouda Boumaaza, and Mostefa Bourchak, *Experimental investigation and optimization of delamination factors in the drilling of jute fiber–reinforced polymer biocomposites with multiple estimators.* The International Journal of Advanced Manufacturing Technology, **2021**. 116(9): p. **2885-2907**.DOI: 10.1007/s00170-021-07628-9.
196. Amirhossein Lotfi, Huaizhong Li, Dzung Viet Dao, and Gangadhara Prusty, *Natural fiber–reinforced composites: A review on material, manufacturing, and machinability.* Journal of Thermoplastic Composite Materials, **2019**. 34(2): p. **238-284**.DOI: 10.1177/0892705719844546.
197. Paulo Sérgio Martins, José Rubens Gonçalves Carneiro, Elhadji Cheikh Talibouya Ba, and Vitor Ferreira Vieira, *Study on roughness and form errors linked with tool wear in the drilling process of an Al-Si alloy under high cutting speed using coated diamond-like carbon high-speed steel drill bits.* Journal of Manufacturing Processes, **2021**. 62: p. **711-719**.DOI: https://doi.org/10.1016/j.jmapro.2021.01.006.

198. S. A. Kaloerov, E. S. Glushankov, and A. B. Mironenko, *Solution of Problems of Elasticity Theory for Multiply Connected Half-Planes and Strips.* Mechanics of Solids, **2023**. 58(4): p. **1063-1075**.DOI: 10.3103/s0025654422601100.
199. Jian Zhang, Valerian Hirschberg, and Denis Rodrigue, *Mechanical fatigue of recycled and virgin high-/low-density polyethylene.* Journal of Applied Polymer Science, **2023**. 140(2): p. **e53312**.DOI: https://doi.org/10.1002/app.53312.
200. Lili Wang, Xue Ge, Jingdong Duan, Longchao Li, and Yunlong Bao, *Study on the influence of journal form and position errors on the lubrication performance of four-recess capillary restrictor hybrid journal bearing.* Lubrication Science, **2023**. 35(5): p. **299-316**.DOI: https://doi.org/10.1002/ls.1641.
201. Andrew Rowe, Alokesh Pramanik, Animesh K. Basak, Chander Prakash, Shankar Subramaniam, Amit R. Dixit, and N. Radhika *Effects of Abrasive Waterjet Machining on the Quality of the Surface Generated on a Carbon Fibre Reinforced Polymer Composite*. Machines, 2023. 11, DOI: 10.3390/machines11070749.
202. LUBOSLAV STRAKA and TIBOR KRENICKY, *GEOMETRIC PRECISION OF THE CYLINDERS SURFACES MACHINED WITH WEDM TECHNOLOGY.* MM Science Journal, **2022**.DOI: DOI: 10.17973/MMSJ.2022_12_2022146.
203. Mohammad Hemmat Esfe, Davood Toghraie, and Fatemeh Amoozadkhalili, *Optimization and design of ANN with Levenberg-Marquardt algorithm to increase the accuracy in predicting the viscosity of SAE40 oil-based hybrid nano-lubricant.* Powder Technology, **2023**. 415: p. **118097**.DOI: https://doi.org/10.1016/j.powtec.2022.118097.
204. Nasibeh Talebi and Ali Motie Nasrabadi, *Investigating the discrimination of linear and nonlinear effective connectivity patterns of EEG signals in children with Attention-Deficit/Hyperactivity Disorder and Typically Developing children.* Computers in Biology and Medicine, **2022**. 148: p. **105791**.DOI: https://doi.org/10.1016/j.compbiomed.2022.105791.
205. Wooyeon Park, Jaejin Lee, Kyung-Chan Kim, JongKil Lee, Keunchan Park, Yukinaga Miyashita, Jongdae Sohn, Jaeheung Park, Young-Sil Kwak, and Junga Hwang, *Operational Dst index prediction model based on combination of artificial neural network and empirical model.* Journal of Space Weather and Space Climate, **2021**. 11: p. **38**.DOI: https://doi.org/10.1051/swsc/2021021.
206. Erol Kilickap, *Modeling and optimization of burr height in drilling of Al-7075 using Taguchi method and response surface methodology.* The International Journal of Advanced Manufacturing Technology, **2010**. 49(9): p. **911-923**.DOI: 10.1007/s00170-009-2469-x.
207. Ranjan Kumar Ghadai, Kanak Kalita, Subhas Chandra Mondal, and Bibhu Prasad Swain, *PECVD process parameter optimization: towards increased hardness of diamond-like carbon thin films.* Materials and Manufacturing Processes, **2018**. 33(16): p. **1905-1913**.DOI: 10.1080/10426914.2018.1512114.
208. Kanak Kalita, Partha Dey, and Salil Haldar, *Search for accurate RSM metamodels for structural engineering.* Journal of Reinforced Plastics and Composites, **2019**. 38(21-22): p. **995-1013**.DOI: 10.1177/0731684419862346.
209. Kalaivani Batumalaie, Elham Khalili, Naji Arafat Mahat, Fahrul Zaman Huyop, and Roswanira Abdul Wahab, *A statistical approach for optimizing the protocol for overexpressing lipase KV1 in Escherichia coli: purification and characterization.* Biotechnology & Biotechnological Equipment, **2018**. 32(1): p. **69-87**.DOI: 10.1080/13102818.2017.1407670.
210. Maria Manzoor, Usman R. Kamboh, Sumaira Gulshan, Sven Tomforde, Iram Gul, Alighazi Siddiqui, and Muhammad Arshad *Optimizing Sustainable Phytoextraction of Lead from Contaminated Soil Using Response Surface Methodology (RSM) and Artificial Neural Network (ANN)*. Sustainability, 2023. 15, DOI: 10.3390/su151411049.

211. Jing Li, Wei Zuo, Jiaqiang E, Yuntian Zhang, Qingqing Li, Ke Sun, Kun Zhou, and Guangde Zhang, *Multi-objective optimization of mini U-channel cold plate with SiO2 nanofluid by RSM and NSGA-II.* Energy, **2022**. 242: p. **123039**.DOI: https://doi.org/10.1016/j.energy.2021.123039.
212. Kanak Kalita, Partha Dey, Milan Joshi, and Salil Haldar, *A response surface modelling approach for multi-objective optimization of composite plates.* Steel and Composite Structures, An International Journal, **2019**. 32(4): p. **455-466**.
213. I. El Mrabet, B. Ihssane, H. Valdés, and H. Zaitan, *Optimization of Fenton process operating conditions for the treatment of the landfill leachate of Fez city (Morocco).* International Journal of Environmental Science and Technology, **2022**. 19(4): p. **3323-3336**.DOI: 10.1007/s13762-021-03393-0.
214. Anita Maslahati Roudi, Sultan Salem, Masoud Abedini, Amin Maslahati, and Muhammad Imran, *Response surface methodology (RSM)-based prediction and optimization of the fenton process in landfill leachate decolorization.* Processes, **2021**. 9(12): p. **2284**.
215. M. H. M. Haniff, A. R. Ismail, B. M. Deros, M. N. A. Rahman, and K. Kardigama, *The Taguchi Approach in Optimizing the Environmental Factors Towards Productivity at Automotive Industry.* International Journal of Automotive and Mechanical Engineering, **2022**. 3: p. **306-317**.
216. Anand Pandey, Ashish Goyal, and Rakesh Meghvanshi, *Experimental Investigation and Optimization of Machining Parameters of Aerospace Material Using Taguchi's DOE Approach.* Materials Today: Proceedings, **2017**. 4(8): p. **7246-7251**.DOI: https://doi.org/10.1016/j.matpr.2017.07.053.
217. Shadi Piramoon, Parviz Aberoomand Azar, Mohammad Saber Tehrani, and Sirwan Mohamadi Azar, *Optimization of solar-photocatalytic degradation of polychlorinated biphenyls using photocatalyst (Nd/Pd/TiO2) by taguchi technique and detection by solid phase nano extraction.* Iranian Journal of Chemistry and Chemical Engineering, **2021**. 40(5): p. **1541-1553**.
218. Mehmet Güldane, *Optimizing foam quality characteristics of model food using Taguchi-based fuzzy logic method.* Journal of Food Process Engineering, **2023**. 46(8): p. **e14384**.DOI: https://doi.org/10.1111/jfpe.14384.
219. Reddy Sreenivasulu, G Chaitanya, GV Kumar, and MR Devi, *Inverse Kinematic Solution for Five bar Parallel Linkage Planar Manipulator using PYTHON and Optimization by Taguchi Method.* International Journal of Engineering Trends and Technology, **2021**. 69(5): p. **94-100**.
220. N. Praveen, U. S. Mallik, A. G. Shivasiddaramaih, R. Suresh, C. Durga Prasad, and L. Shivaramu, *Synthesis and Wire EDM Characteristics of Cu–Al–Mn Ternary Shape Memory Alloys Using Taguchi Method.* Journal of The Institution of Engineers (India): Series D, **2023**.DOI: 10.1007/s40033-023-00501-x.
221. ERKAN TUR, *Optimization of Microresistor Beam Performance Using COMSOL Multiphysics and Taguchi Method.* INTERNATIONAL JOURNAL OF NEW HORIZONS IN THE SCIENCES, **2023**: p. **28-40**.DOI: https://orcid.org/0000-0002-3764-2184.
222. Negar Namjoo, Mohammad Delnavaz, and Seyed Sajad Mahdian, *Comparing removal of synthetic anthraquinone dye wastewater in an electrical discharge and UV-LED/WO3 reactors: using statistical Taguchi optimization approach.* Environmental Science and Pollution Research, **2023**. 30(51): p. **110539-110549**.DOI: 10.1007/s11356-023-30147-x.
223. H. K. Govindaraju, M. D. Kiran, and B. R. Lokesh Yadhav, *Wear behavior of aluminum metal matrix composites: A Taguchi approach.* AIP Conference Proceedings, **2020**. 2247(1): p. **040005**.DOI: 10.1063/5.0003802.
224. Sampath Suranjan Salins, Deepak Inder Kumar, and H. K. Sachidananda, *Optimization of welding parameters for improving welded joints used in rolling stock structures using*

experimental and Taguchi technique. International Journal on Interactive Design and Manufacturing (IJIDeM), **2024**. 18(1): p. **133-147**.DOI: 10.1007/s12008-023-01429-y.

225. Esra Uray, Serdar Carbas, Zong W. Geem, and Sanghun Kim *Parameters Optimization of Taguchi Method Integrated Hybrid Harmony Search Algorithm for Engineering Design Problems*. Mathematics, 2022. 10, DOI: 10.3390/math10030327.
226. Yuriy Tsapko, Oleksandra Horbachova, Serhii Mazurchuk, Aleksii Tsapko, Kostiantyn Sokolenko, and Andrii Matviichuk, *Establishing regularities of wood protection against water absorption using a polymer shell.* Eastern-European Journal of Enterprise Technologies, **2022**. 1(10): p. **115**.
227. K. Anbukarasi and S. Kalaiselvam, *Study of effect of fibre volume and dimension on mechanical, thermal, and water absorption behaviour of luffa reinforced epoxy composites.* Materials & Design (1980-2015), **2015**. 66: p. **321-330**.DOI: https://doi.org/10.1016/j.matdes.2014.10.078.
228. Govindaraju Rajkumar, Jagannathan Srinivasan, and Latchupathi Suvitha, *Natural protein fiber hybrid composites: Effects of fiber content and fiber orientation on mechanical, thermal conductivity and water absorption properties.* Journal of Industrial Textiles, **2013**. 44(5): p. **709-724**.DOI: 10.1177/1528083713512355.
229. Umit Huner, *Effect of water absorption on the mechanical properties of flax fiber reinforced epoxy composites.* Advances in Science and Technology Research Journal, **2015**. 9(26): p. **1--6**.
230. W. Z. W. Zahari, R. N. R. L. Badri, H. Ardyananta, D. Kurniawan, and F. M. Nor, *Mechanical Properties and Water Absorption Behavior of Polypropylene / Ijuk Fiber Composite by Using Silane Treatment.* Procedia Manufacturing, **2015**. 2: p. **573-578**.DOI: https://doi.org/10.1016/j.promfg.2015.07.099.
231. Ruey Shan Chen, Sahrim Ahmad, and Sinyee Gan, *Characterization of rice husk-incorporated recycled thermoplastic blend composites.* BioResources, **2016**. 11(4): p. **8470-8482**.
232. Aziz Saaidia, Ahmed Belaadi, Messaouda Boumaaza, Hassan Alshahrani, and Mostefa Bourchak, *Effect of Water Absorption on the Behavior of Jute and Sisal Fiber Biocomposites at Different Lengths: ANN and RSM Modeling.* Journal of Natural Fibers, **2023**. 20(1): p. **2140326**.DOI: 10.1080/15440478.2022.2140326.
233. Satya Panigrahi, *Characterization of palm fiber for development of biocomposites material for automotive industries.* SAE International Journal of Commercial Vehicles, **2010**. 3(2010-01-2029): p. **304-312**.DOI: https://doi.org/10.4271/2010-01-2029.
234. Sivarao Subramonian, Aidy Ali, Mohammad Amran, L. D. Sivakumar, Shukor Salleh, and A. Rajaizam, *Effect of fiber loading on the mechanical properties of bagasse fiber–reinforced polypropylene composites.* Advances in Mechanical Engineering, **2016**. 8(8): p. **1687814016664258**.DOI: 10.1177/1687814016664258.
235. Irina Turku, Anna Keskisaari, Timo Kärki, Ari Puurtinen, and Pasi Marttila, *Characterization of wood plastic composites manufactured from recycled plastic blends.* Composite Structures, **2017**. 161: p. **469-476**.DOI: https://doi.org/10.1016/j.compstruct.2016.11.073.
236. Sulawan Kaewkuk, Wimonlak Sutapun, and Kasama Jarukumjorn, *Effects of interfacial modification and fiber content on physical properties of sisal fiber/polypropylene composites.* Composites Part B: Engineering, **2013**. 45(1): p. **544-549**.DOI: https://doi.org/10.1016/j.compositesb.2012.07.036.
237. Zeynal Abidin Oğuz and Ahmet Erkliğ, *Evaluation of the hydrothermal aging effect on the buckling behavior of hybrid glass/aramid/epoxy composite plates: Comparison of distilled water and seawater*. Polymer Composites, **2022**. 43(7): p. **4463-4477**.DOI: https://doi.org/10.1002/pc.26705.

238. Anita Singh and Madhoolika Agrawal, *Acid rain and its ecological consequences.* Journal of Environmental Biology, **2007**. 29(1): p. **15**.
239. Hamid Kaddami, Alain Dufresne, Bertine Khelifi, Abdelkader Bendahou, Moha Taourirte, Mustapha Raihane, Nathalie Issartel, Henry Sautereau, Jean-François Gérard, and Noureddine Sami, *Short palm tree fibers – Thermoset matrices composites.* Composites Part A: Applied Science and Manufacturing, **2006**. 37(9): p. **1413-1422**.DOI: https://doi.org/10.1016/j.compositesa.2005.06.020.
240. Salah Amroune, Abderrezak Bezazi, Alain Dufresne, Fabrizio Scarpa, and Abdellatif Imad, *Investigation of the Date Palm Fiber for Green Composites Reinforcement: Thermo-physical and Mechanical Properties of the Fiber.* Journal of Natural Fibers, **2021**. 18(5): p. **717-734**.DOI: 10.1080/15440478.2019.1645791.
241. Ruey Shan Chen, Mohd Hafizuddin Ab Ghani, Mohd Nazry Salleh, Sahrim Ahmad, and Mou'ad A. Tarawneh, *Mechanical, water absorption, and morphology of recycled polymer blend rice husk flour biocomposites.* Journal of Applied Polymer Science, **2015**. 132(8).DOI: https://doi.org/10.1002/app.41494.
242. S. Sair, A. Oushabi, A. Kammouni, O. Tanane, Y. Abboud, and A. El Bouari, *Mechanical and thermal conductivity properties of hemp fiber reinforced polyurethane composites.* Case Studies in Construction Materials, **2018**. 8: p. **203-212**.DOI: https://doi.org/10.1016/j.cscm.2018.02.001.
243. Fabrice Kossi Sodoke, Lotfi Toubal, and Luc Laperrière, *Hygrothermal effects on fatigue behavior of quasi-isotropic flax/epoxy composites using principal component analysis.* Journal of Materials Science, **2016**. 51(24): p. **10793-10805**.DOI: 10.1007/s10853-016-0291-z.
244. Sonia S. Raj Raj, J. Edwin Raja Dhas, and C. P. Jesuthanam, *Challenges on machining characteristics of natural fiber-reinforced composites – A review.* Journal of Reinforced Plastics and Composites, **2020**. 40(1-2): p. **41-69**.DOI: 10.1177/0731684420940773.
245. Furkan Ahmad, Ankit Manral, and Pramendra Kumar Bajpai, *Machining of Thermoplastic Composites*, in *Processing of Green Composites*, Pawan Kumar Rakesh and Inderdeep Singh, Editors. 2019, Springer Singapore: Singapore. p. 107-123.
246. Vishwas Mahesh, Sharnappa Joladarashi, and Satyabodh M. Kulkarni, *Physio-mechanical and wear properties of novel jute reinforced natural rubber based flexible composite.* Materials Research Express, **2019**. 6(5): p. **055503**.DOI: 10.1088/2053-1591/ab0164.
247. K. Shunmugesh and K. Panneerselvam, *Machinability study of Carbon Fiber Reinforced Polymer in the longitudinal and transverse direction and optimization of process parameters using PSO–GSA.* Engineering Science and Technology, an International Journal, **2016**. 19(3): p. **1552-1563**.DOI: https://doi.org/10.1016/j.jestch.2016.04.012.
248. A. A. Abdul Nasir, A. I. Azmi, and A. N. M. Khalil, *Measurement and optimisation of residual tensile strength and delamination damage of drilled flax fibre reinforced composites.* Measurement, **2015**. 75: p. **298-307**.DOI: https://doi.org/10.1016/j.measurement.2015.07.046.
249. HY Chan, AB Abdullah, Z Samad, and MSM Zain, *Precision punching on laminates composite panel: effect of dual-stages puncher.* International Journal of Materials Engineering Innovation, **2015**. 6(4): p. **288-296**.
250. R. Arun Ramnath, P. R. Thyla, N. Mahendra Kumar, and S. Aravind, *Optimization of machining parameters of composites using multi-attribute decision-making techniques: A review.* Journal of Reinforced Plastics and Composites, **2017**. 37(2): p. **77-89**.DOI: 10.1177/0731684417732840.
251. Mahmoud M. A. Nassar, Ramanathan Arunachalam, and Khalid I. Alzebdeh, *Machinability of natural fiber reinforced composites: a review.* The International Journal of Advanced Manufacturing Technology, **2017**. 88(9): p. **2985-3004**.DOI: 10.1007/s00170-016-9010-9.

252. S Madhavan and S Balasivanandha Prabu, *An experimental study of influence of drill geometry on drilling of carbon fibre reinforced plastic composites.* Int J Eng Res Dev, **2012**. 3(1): p. **36-44**.
253. Yosra Turki, Malek Habak, Raphaël Velasco, Zoheir Aboura, Kamel Khellil, and Pascal Vantomme, *Experimental investigation of drilling damage and stitching effects on the mechanical behavior of carbon/epoxy composites.* International Journal of Machine Tools and Manufacture, **2014**. 87: p. **61-72**.DOI: https://doi.org/10.1016/j.ijmachtools.2014.06.004.
254. M. S. M. Zain, A. B. Abdullah, and Z. Samad, *Effect of puncher profile on the precision of punched holes on composite panels.* The International Journal of Advanced Manufacturing Technology, **2017**. 89(9): p. **3331-3336**.DOI: 10.1007/s00170-016-9339-0.
255. G Dilli Babu, K Sivaji Babu, and B Uma Maheswar Gowd, *Effect of machining parameters on milled natural fiber-reinforced plastic composites.* J. Adv. Mech. Eng, **2013**. 1: p. **1-12**.
256. Sikiru Oluwarotimi Ismail, Hom Nath Dhakal, Ivan Popov, and Johnny Beaugrand, *Comprehensive study on machinability of sustainable and conventional fibre reinforced polymer composites.* Engineering Science and Technology, an International Journal, **2016**. 19(4): p. **2043-2052**.DOI: https://doi.org/10.1016/j.jestch.2016.07.010.
257. A. B. Abdullah, S. M. Sapuan, and Z. Samad, *11 - Sustainability issues in hole-making technologies: Current practices and challenges*, in *Hole-Making and Drilling Technology for Composites*, A. B. Abdullah and S. M. Sapuan, Editors. 2019, Woodhead Publishing. p. 149-160.
258. J. Turner, R. J. Scaife, and H. M. El-Dessouky, *Effect of machining coolant on integrity of CFRP composites.* Advanced Manufacturing: Polymer & Composites Science, **2015**. 1(1): p. **54-60**.DOI: 10.1179/2055035914y.0000000008.
259. Sravan Kumar Josyula, Suresh Kumar Reddy Narala, E. Guru Charan, and H. A. Kishawy, *Sustainable Machining of Metal Matrix Composites Using Liquid Nitrogen.* Procedia CIRP, **2016**. 40: p. **568-573**.DOI: https://doi.org/10.1016/j.procir.2016.01.135.
260. DeFu Liu, YongJun Tang, and W. L. Cong, *A review of mechanical drilling for composite laminates.* Composite Structures, **2012**. 94(4): p. **1265-1279**.DOI: https://doi.org/10.1016/j.compstruct.2011.11.024.
261. G Dilli Babu, K Sivaji Babu, and B Gowd, *Optimization of machining parameters in drilling hemp fiber reinforced composites to maximize the tensile strength using design experiments.* **2013**.
262. Kishore Debnath, Inderdeep Singh, and Akshay Dvivedi, *Drilling Characteristics of Sisal Fiber-Reinforced Epoxy and Polypropylene Composites.* Materials and Manufacturing Processes, **2014**. 29(11-12): p. **1401-1409**.DOI: 10.1080/10426914.2014.941870.
263. Sachin Ghalme, Ankush Mankar, and Y. J. Bhalerao, *Parameter optimization in milling of glass fiber reinforced plastic (GFRP) using DOE-Taguchi method.* SpringerPlus, **2016**. 5(1): p. **1376**.DOI: 10.1186/s40064-016-3055-y.
264. Meenu Gupta and Surinder Kumar, *Investigation of surface roughness and MRR for turning of UD-GFRP using PCA and Taguchi method.* Engineering Science and Technology, an International Journal, **2015**. 18(1): p. **70-81**.DOI: https://doi.org/10.1016/j.jestch.2014.09.006.
265. Syed Altaf Hussain, V Pandurangadu, and K Palanikumar, *Surface roughness analysis in machining of GFRP composite by carbide tool (K20).* European journal of scientific research, **2010**. 41(1): p. **84-98**.
266. Vinod Kumar Vankanti and Venkateswarlu Ganta, *Optimization of process parameters in drilling of GFRP composite using Taguchi method.* Journal of Materials Research and Technology, **2014**. 3(1): p. **35-41**.DOI: https://doi.org/10.1016/j.jmrt.2013.10.007.

267. T. Rajmohan, K. Palanikumar, and S. Prakash, *Grey-fuzzy algorithm to optimise machining parameters in drilling of hybrid metal matrix composites.* Composites Part B: Engineering, **2013**. 50: p. **297-308**.DOI: https://doi.org/10.1016/j.compositesb.2013.02.030.
268. M Muthuvel and G Ranganath, *Optimization of machining parameters in milling of composite materials.* International Journal of Mechanical Engineering and Robotic Research, **2012**. 1(2).
269. C. C. Tsao and H. Hocheng, *Evaluation of thrust force and surface roughness in drilling composite material using Taguchi analysis and neural network.* Journal of Materials Processing Technology, **2008**. 203(1): p. **342-348**.DOI: https://doi.org/10.1016/j.jmatprotec.2006.04.126.
270. Zohir Tabet, Ahmed Belaadi, Messaouda Boumaaza, and Mostefa Bourchak, *Drilling of a bidirectional jute fibre and cork-reinforced polymer biosandwich structure: ANN and RSM approaches for modelling and optimization.* The International Journal of Advanced Manufacturing Technology, **2021**. 117(11): p. **3819-3839**.DOI: 10.1007/s00170-021-07679-y.
271. Amirhossein Lotfi, Huaizhong Li, and Dzung Viet Dao, *Drilling Behavior of Flax/Poly(Lactic Acid) Bio-Composite Laminates: An Experimental Investigation.* Journal of Natural Fibers, **2020**. 17(9): p. **1264-1280**.DOI: 10.1080/15440478.2018.1558158.
272. Şenol Bayraktar and Yakup Turgut, *Determination of delamination in drilling of carbon fiber reinforced carbon matrix composites/Al 6013-T651 stacks.* Measurement, **2020**. 154: p. **107493**.DOI: https://doi.org/10.1016/j.measurement.2020.107493.
273. Ugur Koklu, Sezer Morkavuk, Carol Featherston, Malik Haddad, David Sanders, Muhammad Aamir, Danil Yu Pimenov, and Khaled Giasin, *The effect of cryogenic machining of S2 glass fibre composite on the hole form and dimensional tolerances.* The International Journal of Advanced Manufacturing Technology, **2021**. 115(1): p. **125-140**.DOI: 10.1007/s00170-021-07150-y.
274. Mohammad Baraheni, Mohammad Reza Shabgard, and Saeid Amini, *Evaluating the hole quality produced by vibratory drilling: additive manufactured PLA+*. The International Journal of Advanced Manufacturing Technology, **2021**. 117(3): p. **785-794**.DOI: 10.1007/s00170-021-07750-8.
275. M. A. Moghaddas, A. Y. Yi, and K. F. Graff, *Temperature measurement in the ultrasonic-assisted drilling process.* The International Journal of Advanced Manufacturing Technology, **2019**. 103(1): p. **187-199**.DOI: 10.1007/s00170-019-03487-7.
276. Jinyang Xu, Chao Li, Mohamed El Mansori, Gongyu Liu, and Ming Chen, *Study on the Frictional Heat at Tool-Work Interface when Drilling CFRP Composites.* Procedia Manufacturing, **2018**. 26: p. **415-423**.DOI: https://doi.org/10.1016/j.promfg.2018.07.049.
277. S. Alizadeh Ashrafi, S. Sharif, A. Akhavan Farid, and M. Y. Yahya, *Performance evaluation of carbide tools in drilling CFRP-Al stacks.* Journal of Composite Materials, **2013**. 48(17): p. **2071-2084**.DOI: 10.1177/0021998313494429.
278. Imed Boughdiri, Khaled Giasin, Tarek Mabrouki, and Redouane Zitoune, *Effect of cutting parameters on thrust force, torque, hole quality and dust generation during drilling of GLARE 2B laminates.* Composite Structures, **2021**. 261: p. **113562**.DOI: https://doi.org/10.1016/j.compstruct.2021.113562.
279. A. Rivero, G. Aramendi, S. Herranz, and L. N. López de Lacalle, *An experimental investigation of the effect of coatings and cutting parameters on the dry drilling performance of aluminium alloys.* The International Journal of Advanced Manufacturing Technology, **2006**. 28(1): p. **1-11**.DOI: 10.1007/s00170-004-2349-3.
280. Shusheng Bi and Jie Liang, *Experimental studies and optimization of process parameters for burrs in dry drilling of stacked metal materials.* The International Journal of Advanced Manufacturing Technology, **2011**. 53(9): p. **867-876**.DOI: 10.1007/s00170-010-2877-y.

281. B. Suresh Kumar, N. Baskar, and K. Rajaguru, *Drilling operation: A review.* Materials Today: Proceedings, **2020**. 21: p. **926-933**.DOI: https://doi.org/10.1016/j.matpr.2019.08.160.
282. Farzad Pashmforoush, Reza Farshbaf Zinati, and Davoud Maleki, *Investigation of ultrasonic vibration on thrust force, surface integrity, and geometrical tolerances during drilling of natural filler reinforced composites.* Proceedings of the Institution of Mechanical Engineers, Part C: Journal of Mechanical Engineering Science, **2020**. 234(20): p. **4041-4055**.DOI: 10.1177/0954406220920320.
283. A. Krishnamoorthy, S. Rajendra Boopathy, K. Palanikumar, and J. Paulo Davim, *Application of grey fuzzy logic for the optimization of drilling parameters for CFRP composites with multiple performance characteristics.* Measurement, **2012**. 45(5): p. **1286-1296**.DOI: https://doi.org/10.1016/j.measurement.2012.01.008.
284. Juan Carlos Campos Rubio, Leandro José da Silva, Wanderson de Oliveira Leite, Tulio Hallak Panzera, Sergio Luiz Moni Ribeiro Filho, and João Paulo Davim, *Investigations on the drilling process of unreinforced and reinforced polyamides using Taguchi method.* Composites Part B: Engineering, **2013**. 55: p. **338-344**.DOI: https://doi.org/10.1016/j.compositesb.2013.06.042.
285. Scott Menard, *Coefficients of Determination for Multiple Logistic Regression Analysis.* The American Statistician, **2000**. 54(1): p. **17-24**.DOI: 10.1080/00031305.2000.10474502.
286. Muhammad Shahbaz, Syed A. Taqvi, Adrian Chun Minh Loy, Abrar Inayat, Fahim Uddin, Awais Bokhari, and Salman Raza Naqvi, *Artificial neural network approach for the steam gasification of palm oil waste using bottom ash and CaO.* Renewable Energy, **2019**. 132: p. **243-254**.DOI: https://doi.org/10.1016/j.renene.2018.07.142.
287. Adewale George Adeniyi, Joshua O. Ighalo, and Gonçalo Marques, *Utilisation of machine learning algorithms for the prediction of syngas composition from biomass bio-oil steam reforming.* International Journal of Sustainable Energy, **2021**. 40(4): p. **310-325**.DOI: 10.1080/14786451.2020.1803862.
288. Joshua O. Ighalo, Chinenye Adaobi Igwegbe, Adewale George Adeniyi, and Sulyman A. Abdulkareem, *Artificial Neural Network Modeling of the Water Absorption Behavior of Plantain Peel and Bamboo Fibers Reinforced Polystyrene Composites.* Journal of Macromolecular Science, Part B, **2021**. 60(7): p. **472-484**.DOI: 10.1080/00222348.2020.1866282.
289. Barshan Dev, Md Ashikur Rahman, Md Jahidul Islam, Md Zillur Rahman, and Deju Zhu, *Properties prediction of composites based on machine learning models: A focus on statistical index approaches.* Materials Today Communications, **2024**. 38: p. **107659**.DOI: https://doi.org/10.1016/j.mtcomm.2023.107659.
290. Yeping Peng, Usama Khaled, Abdullah A. A. A. Al-Rashed, Rashid Meer, Marjan Goodarzi, and M. M. Sarafraz, *Potential application of Response Surface Methodology (RSM) for the prediction and optimization of thermal conductivity of aqueous CuO (II) nanofluid: A statistical approach and experimental validation.* Physica A: Statistical Mechanics and its Applications, **2020**. 554: p. **124353**.DOI: https://doi.org/10.1016/j.physa.2020.124353.
291. N. Senthilkumar, T. Tamizharasan, and S. Gobikannan, *Application of Response Surface Methodology and Firefly Algorithm for Optimizing Multiple Responses in Turning AISI 1045 Steel.* Arabian Journal for Science and Engineering, **2014**. 39(11): p. **8015-8030**.DOI: 10.1007/s13369-014-1320-3.
292. Kanak Kalita, Ishwer Shivakoti, and Ranjan Kumar Ghadai, *Optimizing process parameters for laser beam micro-marking using genetic algorithm and particle swarm optimization.* Materials and Manufacturing Processes, **2017**. 32(10): p. **1101-1108**.DOI: 10.1080/10426914.2017.1303156.

293. Azzedine Makhlouf, Ahmed Belaadi, Messaouda Boumaaza, Lakhdar Mansouri, Mostefa Bourchak, and Mohammad Jawaid, *Water Absorption Behavior of Jute Fibers Reinforced HDPE Biocomposites: Prediction Using RSM and ANN Modeling.* Journal of Natural Fibers, **2022**. 19(16): p. **14014-14031**.DOI: 10.1080/15440478.2022.2114976.
294. Abdelaziz Lekrine, Ahmed Belaadi, Messaouda Boumaaza, Hassan Alshahrani, and Mostefa Bourchak, *Water absorption of industrial high-density polyethylene biocomposites reinforced with Washingtonia filifera fibers: optimization using Fick's, RSM, and ANN models.* **2022**.DOI: https://doi.org/10.21203/rs.3.rs-1538795/v1.
295. N. Venkateshwaran and A. ElayaPerumal, *Hole quality evaluation of natural fiber composite using image analysis technique.* Journal of Reinforced Plastics and Composites, **2013**. 32(16): p. **1188-1197**.DOI: 10.1177/0731684413486847.
296. M. Y. Noordin, V. C. Venkatesh, S. Sharif, S. Elting, and A. Abdullah, *Application of response surface methodology in describing the performance of coated carbide tools when turning AISI 1045 steel.* Journal of Materials Processing Technology, **2004**. 145(1): p. **46-58**.DOI: https://doi.org/10.1016/S0924-0136(03)00861-6.
297. Ahmed Belaadi, Messaouda Boumaaza, Salah Amroune, and Mostefa Bourchak, *Mechanical characterization and optimization of delamination factor in drilling bidirectional jute fibre-reinforced polymer biocomposites.* The International Journal of Advanced Manufacturing Technology, **2020**. 111(7): p. **2073-2094**.DOI: 10.1007/s00170-020-06217-6.
298. Suman Kant and CS Jawalkar, *Mechanical properties and delamination factor evaluation of cellulose (nettle) fiber reinforced polymer composites using RSM.* **2021**.
299. Ahmed Belaadi, Hamdi Laouici, and Mostefa Bourchak, *Mechanical and drilling performance of short jute fibre-reinforced polymer biocomposites: statistical approach.* The International Journal of Advanced Manufacturing Technology, **2020**. 106(5): p. **1989-2006**.DOI: 10.1007/s00170-019-04761-4.
300. Rohan Munjal, Sohaib Arif, Frank Wendler, and Olfa Kanoun *Comparative Study of Machine-Learning Frameworks for the Elaboration of Feed-Forward Neural Networks by Varying the Complexity of Impedimetric Datasets Synthesized Using Eddy Current Sensors for the Characterization of Bi-Metallic Coins*. Sensors, 2022. 22, DOI: 10.3390/s22041312.
301. Efosa Charles Igodan and Kingsley Chiwuike Ukaoha, *Architecture Optimization Model for the Deep Neural Network for Binary Classification Problems.* i-Manager's Journal on Software Engineering, **2019**. 14(2): p. **18**.DOI: DOI:10.26634/jse.14.2.17162.
302. S. R. Karnik, V. N. Gaitonde, and J. P. Davim, *A comparative study of the ANN and RSM modeling approaches for predicting burr size in drilling.* The International Journal of Advanced Manufacturing Technology, **2008**. 38(9): p. **868-883**.DOI: 10.1007/s00170-007-1140-7.
303. Bakthavachalu Balamugundan and Loganathan Karthikeyan, *Optimization of Process Parameters during Milling of Friction Stir Processed GFRP Composites.* Advanced Materials Research, **2014**. 984-985: p. **297-303**.DOI: 10.4028/www.scientific.net/AMR.984-985.297.
304. S. Ragunath, Meenakshi L. Rathod, K. G. Saravanan, N. Rakesh, and Melkamu Kifetew, *Optimization of Machining Parameters of Natural/Glass Fiber with Nanoclay Polymer Composite Using Response Surface Methodology.* Journal of Nanomaterials, **2023**. 2023: p. **9485769**.DOI: 10.1155/2023/9485769.
305. Junjie Feng, Guansheng Yin, Hongliang Tuo, and Zhiqiang Niu, *Parameter optimization and regression analysis for multi-index of hybrid fiber-reinforced recycled coarse aggregate concrete using orthogonal experimental design.* Construction and Building Materials, **2021**. 267: p. **121013**.DOI: https://doi.org/10.1016/j.conbuildmat.2020.121013.

306. Giorgio Marrubini, Stefano Dugheri, Giovanni Cappelli, Giulio Arcangeli, Nicola Mucci, Patrik Appelblad, Camillo Melzi, and Andrea Speltini, *Experimental designs for solid-phase microextraction method development in bioanalysis: A review.* Analytica Chimica Acta, **2020**. 1119: p. **77-100**.DOI: https://doi.org/10.1016/j.aca.2020.04.012.
307. Mohammad Neaz Morshed, Md Nahid Pervez, Nemeshwaree Behary, Nabil Bouazizi, Jinping Guan, and Vincent A. Nierstrasz, *Statistical modeling and optimization of heterogeneous Fenton-like removal of organic pollutant using fibrous catalysts: a full factorial design.* Scientific Reports, **2020**. 10(1): p. **16133**.DOI: 10.1038/s41598-020-72401-z.
308. Farooq Ahmed, Ji Hyeon Byeon, Ki Moon Park, and Tae Jo Ko, *The Optimization of Ball End-Milling Parameters on the Surface Roughness of STD61 Steel using the Taguchi Method.* Journal of the Korean Society of Manufacturing Process Engineers, **2017**. 16(4): p. **153-158**.
309. Achyut K Pandaa and R Singhb, *Optimization of Process Parameters by Taguchi Method: Catalytic degradation of polypropylene to liquid fuel.* Int J Multidiscip Curr Res, **2013**. 4: p. **50-54**.
310. Nianqi Cui, Xiuni Gan, Sufang Huang, Zhe Chu, Dandan Chen, Yuping Zhang, Meijuan Lan, and Jingfen Jin, *Values and preferences of health care professionals, policy-makers, patients and family members regarding recommendations of adapted physical restraint guidelines in critical care: A survey research.* Nursing in Critical Care, **2023**. 28(6): p. **957-966**.DOI: https://doi.org/10.1111/nicc.12955.

Published scientific papers

JOURNAL OF MATERIALS RESEARCH AND TECHNOLOGY 2022;21:131–152

Available online at www.sciencedirect.com

jmr&t Journal of Materials Research and Technology

journal homepage: www.elsevier.com/locate/jmrt

Original Article

Assessment of induced delamination drilling of natural fiber reinforced composites: a statistical analysis

Riyadh Benyettou [a,b], *Salah Amroune* [a,b], *Mohamed Slamani* [a,b], *Yasemin Seki* [c], *Alain Dufresne* [d], *Mohammad Jawaid* [e,*], *Salman Alamery* [f]

[a] *Department of Mechanical Engineering, Faculty of Technology, University of M'sila, Algeria*
[b] *Materials and Structural Mechanics Laboratory (LMMS) University of M'sila Algeria*
[c] *Department of Textile Engineering, Dokuz Eylul University, Buca, Izmir, Turkey*
[d] *Univ. Grenoble Alpes, CNRS, Grenoble INP, LGP2, F-38000, France*
[e] *Laboratory of Bio Composite Technology, Institute of Tropical Forestry and Forest Products (INTROP), Universiti Putra Malaysia, 43400 Serdang, Selangor, Malaysia*
[f] *Department of Biochemistry, College of Science, King Saud University, PO Box 22452, Riyadh, 11451, Saudi Arabia*

ARTICLE INFO

Article history:
Received 23 June 2022
Accepted 29 August 2022
Available online 10 September 2022

Keywords:
Bio composite
Palm fiber
Cylindricity
Circularity
ANOVA
RSM
CMM

ABSTRACT

This work focuses on the study of the drilling performance of bio composites reinforced with date palm fibers (CDPF). It is a new fiber that is characterized in terms of piercing behavior for the first time. The experimental study was carried out with three types of drills, with a diameter of 10 mm and feed and spindle speeds of the order of (40, 80 and 200 mm/min) and (560, 1120 and 2240 rpm), respectively. The drilling performance was assessed in terms of delamination and surface quality, such as circularity and cylindricity of the drilled holes. Using the CMM machine, the value of the delamination factor was determined using Image J software. The results showed that the value of the latter increased with the increase in feed rate and decreased with the increase in spindle speed. The delamination factor has maximum and minimum values of approximately 1.98 and 1.01 respectively. For the first time, RSM and ANOVA were used to assess the influence and interaction of input parameters (cutting conditions) on the output parameters (delamination factor F_d) during drilling of CDPF. The results obtained help manufacturers, to choose the most appropriate machining conditions to achieve better machinability for other newly developed NFRCs in the aeronautical and defense industry where the substitution of the synthetic fibers by the natural fibers becomes inevitable for economic reasons.

© 2022 The Author(s). Published by Elsevier B.V. This is an open access article under the CC BY-NC-ND license (http://creativecommons.org/licenses/by-nc-nd/4.0/).

* Corresponding author.
E-mail address: jawaid_md@yahoo.co.in (M. Jawaid).
https://doi.org/10.1016/j.jmrt.2022.08.161
2238-7854/© 2022 The Author(s). Published by Elsevier B.V. This is an open access article under the CC BY-NC-ND license (http://creativecommons.org/licenses/by-nc-nd/4.0/).

JOURNAL OF NATURAL FIBERS
2022, VOL. 19, NO. 17, 15902–15918
https://doi.org/10.1080/15440478.2022.2136323

Taylor & Francis
Taylor & Francis Group

Check for updates

Experimental Investigation of the Absorption Behavior of Date Palm Fiber Reinforced Iso-Polyester Composites: Artificial Neuron Network (ANN) Modeling

Riyadh Benyettou[a,b], Salah Amroune[a,b], Slamani Mohamed[a,b], Yasemin Seki[c], and Alain Dufresne[d]

[a]Department of Mechanical Engineering, Faculty of Technology, University of M'sila, M'sila, Algeria; [b]Materials and Structural Mechanics Laboratory (LMMS), University of M'sila Algeria, M'sila, Algeria; [c]Department of Textile Engineering, Dokuz Eylul University, Izmir, Turkey; [d]CNRS, Grenoble INP, LGP2, Univ. Grenoble Alpes, Grenoble, France

ABSTRACT

The present article attempts to study absorption properties of bio-composites reinforced with date palm fibers. The effect of fiber loading on water absorption at room temperature 25°C was investigated. The weight gain was measured of bio-composites immersed in distilled water, seawater and rainwater, for more than 670 hours, until reaching the saturation with a measurement interval between 24 and 48 hours. To understand absorption phenomenon, scanning electron microscopy was used. Porosity rate was determined using image J software. It was noted the water absorption rate of the bio composites reached 16.20%, 16.33%, 21.94%, 41.99% for seawater, 16.41%, 16.52%, 20.84%, 30.08% for distilled water, and 14.00%, 14.04%, 19.30%, 36.94% for rainwater, respectively. The absorption increases when increasing fiber content. The diffusion coefficient of bio-composites has minimum and maximum values of about 1.94×10^{-6}mm^2/s and 3.99×10^{-6}mm^2/s, respectively. Palm fibers are highly porous. The porosity value was higher than 51%. To predict the absorption rate, artificial neural network method was used. The ANN models obtained are very well correlated with the experimental data where the values of the correlation coefficient of the datasets are all beyond 0.99 and the average error value was estimated at 3×10^{-5}.

摘要

本文试图研究椰枣纤维增强生物复合材料的吸附性能. 研究了室温25°C下纤维负载对吸水率的影响. 将生物复合材料浸泡在蒸馏水、海水和雨水中670小时以上, 直到达到饱和, 测量间隔为24至48小时. 为了了解吸收现象, 使用了扫描电子显微镜. 利用image J软件测定孔隙率. 生物复合材料的吸水率分别为海水16.20%、16.33%、21.94%、41.99%, 蒸馏水16.41%、16.52%、20.84%、30.08%, 雨水14.00%、14.04%、19.30%、36.94%. 随着纤维含量的增加, 吸收率增加. 生物复合材料的扩散系数最小值约为1.94 × 10-6 mm2/s, 最大值约为3.99 × 10-6mmm2/s. 棕榈纤维具有高度的多孔性. 孔隙度值高于51%. 为了预测吸收率, 采用了ANN方法. 获得的ANN模型与实验数据有很好的相关性, 其中数据集的相关系数均超过0.99, 平均误差估计为3 × 10-5.

KEYWORDS
Bio composite; water absorption; diffusion; ANN; date palm fiber; 生物复合材料

关键词
生物复合材料; 吸水率; 扩散; 椰枣纤维; 多孔性

Introduction

Nowadays, composites are constantly evolving toward products that are either the cheapest possible, or the most efficient, and ideally both. In this context, plant fiber composites are among the most widely used reinforced materials in the industry, due to several factors such as their wide range of applications, recyclability, the possibility of processing with different polymers and environmentally health. (Adeniyi,

CONTACT Yasemin Seki yasemin.seki@deu.edu.tr Department of Textile Engineering, Dokuz Eylul University, Buca, Izmir, Turkey

© 2022 Taylor & Francis

ACADEMIC JOURNAL OF MANUFACTURING ENGINEERING, VOL.21, ISSUE 1/2023

INVESTIGATION OF MACHINABILITY OF BIOCOMPOSITES: MODELING AND ANN OPTIMIZATION

Riyadh BENYETTOU[1, 2], Salah AMROUNE[1, 2], Mohamed SLAMANI[1,2], Ali KILIÇ[3]

[1]*Department of Mechanical Engineering, Faculty of Technology, University of M'sila, Algeria.*

[2] *Materials and Structural Mechanics Laboratory (LMMS). University of M'sila. Algeria*

[3]*TEMAG Labs, Faculty of Textile Technologies and Design, Istanbul Technical University, Istanbul, Turkey*

E-mail: riyadh.benyettou@univ-msila.dz. salah.amroune@univ-msila.dz. mohamed.slamani@univ-msila.dz

alikilic@itu.edu.tr

***ABSTRACT**: This work studies the drilling performance of bio composites reinforced with cellulosic fibres. The drilling was carried out at three spindle speeds and at three feed rates using three dissimilar drills namely: HSS-TITAN, HSS-CARBIDE, and HSS-SUPER. The drilling performance was evaluated in terms of the delamination factor which was determined using the free software image J. The results showed that the value of this factor decreased with increasing spindle speed and increased with increasing feed rate. On the other hand, the HSS-SUPER drill causes less delamination than the other two drills. To predict the delamination value, the artificial neural network (ANN) method was used. The best hole quality was obtained when using the HSS-SUPER drill, with a spindle speed of 2200 rpm and a feed rate of 40 mm/rev. The worst case was brought when using an HSS-carbide drill, with a spindle speed of 500 rpm and a feed rate of 120 mm/ rev.*

***KEYWORDS:** Bio composite; Drilling; Palm fiber; Delamination; ANN.*

1 INTRODUCTION

Recently, composites have continued to develop towards products that are the least expensive and the most efficient. In this context, composites based on vegetable fibers such as kenaf, jute, hemp, sisal, coconut (Nayak and Satapathy 2021; Pujari, Ramakrishna, and Balaram Padal 2017; Wang et al. 2022; Archana, Jagannatha Reddy, and Paruti 2022; Norhasnan et al. 2021) are of great interest to researchers and manufacturers, especially in the automotive, aviation, steamship, and spacecraft industries, because they are ecological, recyclable, less expensive and light, and thanks to these features. It is necessary to study the techniques for their manufacture, and the most important of these techniques is drilling (Mohammed and Wolla 2022; Slamani et al. 2021; Sherwani et al. 2021; Benyettou, Amroune, Mohamed, et al. 2022).

In the manufacturing industry. Drilling is one of the most essential machining processes in the final assembly of parts, where this process is exposed to several problems, the most significant of which is delamination, and in order to reduce this problem. Several research works have focused on this phenomenon among which: (Yallew, Kumar, and Singh 2015) have studied the effect of drilling process parameters namely: the spindle speed of 900, 1800, 2800 rpm, the feed rate of 0.05, 0.12, 0.19 mm/rev and drill tip geometry (twist drill, Jo drill and parabolic CARBIDE drill at 118° angle

Alexandria Engineering Journal 79 (2023) 545–555

Contents lists available at ScienceDirect

Alexandria Engineering Journal

journal homepage: www.elsevier.com/locate/aej

Original Article

Modelling and optimization of the absorption rate of date palm fiber reinforced composite using response surface methodology

Riyadh Benyettou [a,b], Salah Amroune [a,b], Mohamed Slamani [a,b], Khalissa Saada [a,b], Hassan Fouad [c,*], Mohammad Jawaid [d,*], S. Sikdar [e]

[a] Department of Mechanical Engineering, Faculty of Technology, University of M'sila, Algeria
[b] Materials and Structural Mechanics Laboratory (LMMS), University of M'sila, Algeria
[c] Department of Applied Medical Science, Community College, King Saud University, PO Box 10219, Riyadh 11433, Saudi Arabia
[d] Laboratory of Bio Composite Technology, Institute of Tropical Forestry and Forest Products (INTROP), University Putra Malaysia, 43400 Serdang, Selangor, Malaysia
[e] Department of Engineering and Technology, School of Computing and Engineering, University of Huddersfield, HD1 3DH, United Kingdom

ARTICLE INFO

Keywords:
Bio composite
Natural fibers
Absorption
ANOVA
RSM

ABSTRACT

The aim of this work to explore the absorption behavior of bio composites reinforced with date palm fibers. RSM and ANOVA were utilized to evaluate the impact and interdependence of input variables (Time: from 24 h to 672 h, Fiber content: 15 %, 20 %, and 25 %, and types of water: seawater, distilled water, and rainwater) on the output variables (Mass of CDPF) during a water absorption process that lasted more than 670 h at 23 °C. The findings revealed that the bio composites with the above-mentioned filler content absorbed more water as the amount of fibers increased, with absorption rates of 14.03 %, 19.39 %, 30.94 % for seawater, 15.42 %, 20.64 %, and 36.08 % for distilled water, and 16.37 %, 21.98 %, and 42.10 % for rainwater, respectively. Additionally, the study measured the diffusion coefficient of bio composites, which had a minimum value of about $2.11 \times 10^{-6}mm^2/s$ and a maximum value of about $3.99 \times 10^{-6}mm^2/s$. The results of RSM model analysis showed that this model is accurate and reliable. Where the values of R^2 and adjusted R^2 coefficients for the Mass of CDPF were 99.63 % and 99.61 %, respectively, indicating an ideal match between experimental and predicted values. These findings provide valuable information for engineers interested in incorporating date palm fiber bio composites during development and implementation.

1. Introduction

Recently, most researchers have focused on studying the properties of bio composites because they have many advantages over traditional materials such as fiberglass-based composites or metallic materials. They are generally lighter, easier to produce and use, and have a lower environmental impact. Bio composite materials can also be made from renewable sources and are generally biodegradable, making them more environmentally friendly [1–3]. Bio composites are used in a wide variety of applications, from construction and packaging to automobiles, planes and ships [4–7]. As these bio composites come into direct contact with weather elements like rain, and humidity, it is crucial to examine their water absorption behavior. Therefore, this current work focuses on studying and analyzing the water absorption behavior of palm fiber reinforced composites.

As mentioned earlier, in contemporary times, bio composites enriched with plant fibers such as kenaf, jute, coir, hemp, sisal, ramie, flax, sugarcane, coffee, rice and palm [8–19] fibers are receiving great attention as an alternative to synthetic fibers. Where many studies have focused on the phenomenon of absorption of bio-composite materials reinforced with cellulosic fibers, among these studies: Tezara et al. [20] examine the mechanical properties and water absorption behavior of epoxy composites reinforced by jute-ramie hybridization. The results showed that the hybrid composite had better performance compared to the pure jute composites, despite a reduction in mechanical properties after exposure to water. They indicated that the appropriate stacking sequence and material selection are crucial factors that affect the properties of the composite, The highest percentage increase in weight was observed in the following order (where R represents Ramie and J represents Jute): Jute had the highest percentage gain weight (8.10 %), followed by RJJJR (8.02 %), JRRRJ (8.01 %), JRJRJ (7.93 %), RJRJR (7.90 %), and RJRJ (7.57 %). More recently. The study on the

* Corresponding authors.
E-mail addresses: menhfef@ksu.edu.sa (H. Fouad), jawaid@upm.edu.my (M. Jawaid).

https://doi.org/10.1016/j.aej.2023.08.042
Received 30 May 2023; Received in revised form 30 July 2023; Accepted 13 August 2023
Available online 22 August 2023
1110-0168/© 2023 THE AUTHORS. Published by Elsevier BV on behalf of Faculty of Engineering, Alexandria University. This is an open access article under the CC BY-NC-ND license (http://creativecommons.org/licenses/by-nc-nd/4.0/).